3.3 General Considerations

3.3.1 Evaluation by Analysis

The MFFP is analytically evaluated in accordance with 10 CFR 71[11] and Regulatory Guide 7.8[12] for all applicable NCT and HAC thermal loads. Table 3.3-1 summarizes the design basis conditions considered in these evaluations. The load conditions are defined as follows:

- *NCT Hot:* An ambient temperature of 100 °F is used to evaluate the maximum temperatures within the package with maximum decay heat and 10 CFR §71.71(c)(1) prescribed insolation (see Table 3.3-2).
- *NCT Hot (no solar):* Same as NCT Hot, but without insolation. This case serves as the basis for evaluation of the maximum temperature at the accessible surfaces of the package in accordance with 10 CFR §71.43(g). 10 CFR §71.43(g) stipulates that for non-exclusive use packages, the maximum accessible surface temperature must not exceed 122 °F for this condition. This case is also used as an initial condition for the HAC fire (hot) condition.
- *NCT Cold:* An ambient temperature of -20 °F is used to evaluate the temperatures within the package with maximum decay heat and no insolation. The steady-state results are used as initial conditions for the HAC fire (cold) described below.
- *NCT Cold (no heat):* A -40 °F steady-state ambient temperature without decay heat. This is an analytically trivial case in that no analysis is required to determine that the package and its contents will reach -40 °F under steady-state conditions. The case addresses the minimum material temperatures that may occur.
- *HAC Fire (hot):* Thermal conditions are evaluated as a steady-state ambient temperature of 100 °F with maximum decay heat and zero insolation prior to the event, followed by a thirty-minute transient with an ambient temperature of 1,475 °F with maximum decay heat and zero insolation, and then back to a steady-state ambient temperature of 100 °F with maximum decay heat and maximum insolation per 10 CFR §71.71(c)(1). This load case evaluates the peak temperature achieved for the various packaging components under the HAC fire event and the associated thermal stresses.
- *HAC Fire (cold):* The evaluation involves a steady-state initial condition with an ambient temperature of -20 °F with maximum decay heat and zero insolation, followed by a 30-minute transient with an ambient temperature of 1,475 °F with maximum decay heat, and then back to a steady-state ambient temperature of -20 °F with maximum decay heat and zero insolation. This thermal condition may be evaluated either as an alternative to, or in addition to, the HAC fire (hot) condition above.

The primary heat transfer mechanisms utilized in the thermal analyses are conduction, convection, and radiation within the MFFP packaging, and convection and radiation from the exterior of the packaging

---

[11] Title 10, Code of Federal Regulations, Part 71 (10 CFR 71), *Packaging and Transportation of Radioactive Material*, Final Rule, 01-26-04.

[12] Regulatory Guide 7.8, *Load Combinations for the Structural Analysis of Shipping Casks for Radioactive Material*, Revision 1, U. S. Nuclear Regulatory Commission, March 1989.

to the ambient environment. The steady-state and transient heat transfer analyses are performed using the thermal network analyzer computer programs SINDA/FLUINT [13] with Thermal Desktop® [14].

3.3.1.1 NCT Analytical Model

The NCT analytical thermal model of the MFFP is developed for use with the Thermal Desktop® and SINDA/FLUINT computer programs. These programs are designed to function together to build, exercise, and post-process a thermal model. The Thermal Desktop® computer program is used to provide graphical input and output display function, as well as computing the radiation exchange conductors for the defined geometry and optical properties. Thermal Desktop® is designed to run as an AutoCAD® application. As such, all of the CAD tools available for generating geometry within AutoCAD® can be used for generating a thermal model. In addition, the use of the AutoCAD® layers tool presents a convenient means of segregating the thermal model into its various elements.

The SINDA/FLUINT computer program is a general purpose code suitable for either finite difference or finite-element models. The code can be used to compute the steady-state and transient behavior of the modeled system. SINDA/FLUINT has been validated for simulating the thermal response of spent fuel packages and has been used in the safety analysis of numerous packages for both spent nuclear fuel and nuclear material.

The thermal model of the MFFP represents a 180° model of the package between the closure end of the package and the mid-point of the body cavity (i.e., a 1/4-symmetry model). Symmetry planes are assumed along the package's vertical axis and at the mid-point in the body cavity. This level of modeling is acceptable since symmetry conditions will exist across the vertical axis of the normally horizontal package and since the upper and lower impact limiters are essentially identical. Given that the closure lid end of the package contains the thermally sensitive butyl rubber O-rings, it was chosen for modeling. While in actual practice the active length of the MOX FAs will be located closer to the lower end of the package, this modeling conservatively assumes that the active length of the FAs are centered about the mid-plane of the body cavity. This modeling approach conserves the 1/4-symmetry in the decay heat loading and yields conservative temperatures for the O-ring containment seals, and closure lid end of the model.

Figure 3.3-1 presents a 'solid' view of the general layout of the thermal model used to simulate the thermal performance of the MFFP under NCT conditions. As seen, the thermal model provides an accurate representation of the geometry of the package and its internal structure. Specific modeling is included for the structure internal to the closure lid, the doubler and at the attachment lugs for the impact limiter, and the clamp arm structures used to secure the MOX FAs to the strongback structure.

Figure 3.3-2 presents a 'solid' view of the backside for the thermal model. The accurate representation of the impact limiter attachment lugs and bolts can be seen. Approximately 6,800 thermal nodes, 4,050 planar elements, 40 surfaces, and 3,060 solids are used to represent the various components of the MFFP and its MOX FAs. The model assumes temperature dependant thermal properties for all of the package's steel and aluminum (e.g., boral) components, as well as

[13] SINDA/FLUINT, *Systems Improved Numerical Differencing Analyzer and Fluid Integrator*, Version 4.5 & 5.1, Cullimore & Ring Technologies, Inc., Littleton, CO, 2002 & 2007.

[14] Thermal Desktop®, Version 4.5 & 5.1, Cullimore & Ring Technologies, Inc., Littleton, CO, 2002 & 2007.

the air within the package cavity. Given that the polyurethane foam material properties change little over the NCT temperature range of interest, constant thermal property values are used for the polyurethane foam used in the impact limiter and the body collar.

Figure 3.3-3 illustrates the solids model of the body shell, the body collar, the doubler plate, impact limiter lugs, and the impact limiter attachment bolts. Approximately 700 nodes and 300 solids are used to provide geometric and thermal resolution over the 180° thermal representation of body shell.

Figure 3.3-4 and Figure 3.3-5 illustrate the solids model of the closure lid. As seen, the interior structure of the lid is accurately captured. Approximately 520 nodes, 230 solids, and 16 plate type elements are used to provide the geometric and thermal resolution over the 180° thermal representation of the closure lid. Heat transfer within the lid structure is modeled as a combination of conduction through the solids and radiation and closed-cell convection across the void spaces.

Figure 3.3-6 illustrates the thermal modeling of the 1/4-inch thick angles of the strongback structure, the 1/8-inch thick enclosing surfaces of the fuel control structures (FCSs), and the attachment blocks used to attach the strongback angle plates. The hinges and channel stiffening members of the FCS are omitted from the thermal model. Approximately 700 nodes, 300 solids, and 540 plate type elements are used to provide the geometric and thermal resolution over the 180° thermal representation of the strongback structure.

Figure 3.3-7 illustrates the thermal modeling of the 11-gauge (0.12-inch) thick boral plates used to provide neutron absorption along the surfaces of the strongback and the FCSs. Approximately 400 nodes and 7 plate type elements are used to provide the geometric and thermal resolution. The layout of the thermal modeling for the boral plates is similar to that used for the associated strongback structure. Heat transfer between the boral plates and the strongback plates is assumed to be via conduction and radiation across a nominal 0.02 inch air gap. This modeling approach conservatively bounds the thermal resistance between the two surfaces which, due to variations in flatness and contact pressure, may not be in direct contact over their entire surface area.

Figure 3.3-8 illustrates a combined view of the strongback structure, clamp arm, and top plate. Each clamp arm structure has been simplified to two (2) 3/8-inch thick plates for the purposes of the thermal modeling. This modeling approach captures the principal heat transfer paths and the 'blocking' effect that the clamp arms provide for radiation exchange along the length of the body cavity. While the 'push blocks' have not specifically been modeled, contact conductance is included between the clamp arms and the outer surfaces of the FCSs.

Figure 3.3-9 illustrates the solid elements used to simulate the MOX FAs and the surrounding air space between the edges of the FAs and the inner surfaces of the FCSs. As explained in Section 3.2, *Material Properties and Component Specifications*, rather than include the details of the fuel geometry in the thermal model, the entire region within each FCS is represented as homogenous solid with a uniform volumetric heat load and anisotropic thermal properties. The thermal properties are based on a detailed model of the fuel assembly geometry (see Appendix 3.6.2, *Thermal Model Details*). A volumetric heat load is applied to the solids based on a volume representing an 8.887 inch × 8.887 inch area within the inner surfaces of the FCSs and the 144-inch active length of the fuel. The 8.887 inch dimension, based on a preliminary design of the FCS, is 3/16 inches larger than the actual 8.7 inch inside dimension of the FCS. The additional thermal resistance within the FAs associated with the assumed larger dimension is insignificant, but conservatively bounds (i.e., is higher than) the value associated with the actual 8.7 inch dimension. Further, in the actual design, the start of the active length of the fuel will rest closer to

the bottom end of the package than the distance between the end of the active fuel region and the closure end of the package. However, for conservatism, this analysis assumes that half of the active fuel length (i.e., 72 inches) is within the modeled section. This assumption places the heat generating region of the FAs closer to the closure seals than will occur in the actual package. The remaining 7.145 inches of fuel length required to raise the top of each FA to within approximately 3.8 inches of the inner surface of the closure lid (i.e., the same distance as the actual FA is expected to reach) is assumed to be 'inactive' fuel. The same thermal conductivity properties are applied over this 'inactive' length, but the volumetric heating is set to zero. Table 3.2-4 presents the effective, anisotropic thermal properties for the homogenized fuel region.

Due to the non-uniform composition and geometry of the boral/aluminum composite plates and the FAs with direction, anisotropic thermal conductivity properties are used for these materials. Material orientators are used within the model to specify which thermal properties are associated with each direction of heat flow.

Figure 3.3-10 illustrates the solid model used for the impact limiter shell and polyurethane foam. Approximately 1,750 nodes, 1,030 solids, and 660 plate type elements are used to provide the geometric and thermal resolution over the 180° thermal representation of the impact limiter.

3.3.1.2 HAC Analytical Model

The analytical thermal model of the MFFP used for HAC conditions is a modified version of the NCT model described in Section 3.3.1.1, *NCT Analytical Model*. The primary modifications to the model consist of the following:

- Simulated the worst-case HAC free and puncture drop damage consisting of a 30-foot side drop on the closure lid end and subsequent puncture damage to the impact limiter outer sheet,
- Increased the emissivity of all external surfaces of the body shell and the impact limiters to 0.8 to account for possible soot accumulation on the surfaces during the HAC event,
- Increased the emissivity of the inner surfaces of the body shell and the impact limiter to 0.6 to account for possible oxidation of the XM-19 and Type 304 stainless steels during the HAC event,
- Simulated the charring and ablation of the polyurethane surfaces that may occur (see Section 3.5.2.2, *Performance of Rigid Polyurethane Foam Under HAC Fire Conditions*),
- Application of convection heat transfer coefficients between the package and the ambient that are appropriate for gas velocities of 32 to 50 ft/sec (10 to 15 m/sec)[15,16] during the 30-minute fire event,
- Used convection coefficients based on still air are assumed following the 30-minute fire event,
- Used variable ambient conditions to simulate the elevated temperature of the fire for

[15] Schneider, M.E and Kent, L.A., *Measurements of Gas Velocities And Temperatures In A Large Open Pool Fire, Heat and Mass Transfer in Fire* - HTD Vol. 73, 1987, ASME, New York, NY.

[16] Advisory Material For The IAEA Regulations For The Safe Transport Of Radioactive Material, Safety Series No. 37, Third Edition, Amended 1990, International Atomic Energy Agency, Vienna, 1990.

convective and radiation heat transfer and then re-set to the pre-fire ambient condition, with the addition of ambient heating due to insolation.

Discussion of the HAC thermal analysis is provided in Section 3.5, *Thermal Evaluation Under Hypothetical Accident Conditions.*

3.3.2 Evaluation by Test

This section is not applicable since evaluation by test was not performed for the MFFP.

3.3.3 Margins of Safety

A summary of the maximum temperatures, with their respective temperature margins, for both NCT and HAC are provided in Table 3.3-3. As shown by this table, the minimum temperature margin is 61 °F for the closure lid O-ring seal under HAC. From Section 3.1.4, *Summary of Maximum Pressures*, the maximum normal operating pressure (MNOP) is 10 psig. Therefore, the margin of safety (MS) for the 25-psig design pressure is:

$$MS = \frac{25}{10} - 1.0 = +1.50$$

From Section 3.1.4, *Summary of Maximum Pressures*, the maximum pressure for HAC is 127.7 psig. Structural evaluation of the MFFP for this maximum pressure at temperature is provided in Section 2.7.4.3, *Stress Calculations*. As shown in that section, the margin of safety (MS) for the 127.7 psig pressure is +2.06.

Thermally-induced stresses in the MFFP are discussed in Section 3.4.3, *Maximum Thermal Stresses* for NCT.

Table 3.3-1 – MFFP Package Design Basis Thermal Load Conditions

Condition	Description	Applicable Conditions				
		Ambient Temperature (°F)	Insolation		Decay Heat	
			Max.[1]	Zero	Max.	Zero
1	NCT Hot[2]	100	×		×	
2	NCT Hot (no solar)[2,3,6]	100		×	×	
3	NCT Cold[2,3]	-20		×	×	
4	NCT Cold Environment (no heat)[4,5]	-40		×		×
5	HAC Fire (hot)[3]	100 / 1475 / 100	- / - /×	×/ × / -	×	
6	HAC Fire (cold)[3]	-20 / 1475 / -20		×	×	

Notes:

(1) Insolation in accordance with 10 CFR §71.71(c)(1).

(2) Thermal conditions used to evaluate thermal acceptance criteria and for structural load combinations.

(3) For the HAC fire event, a transient consisting of an initial steady-state initial condition (i.e., case 2 or case 3), followed by a 30-minute fire event, and concluded with a post-fire transient analysis to establish the peak temperatures. Insolation can be ignored prior to and during the fire, but must be included following the fire.

(4) NCT Cold Environment load condition is evaluated without decay heat to establish minimum material temperatures for material compatibility.

(5) NCT Cold Environment condition evaluated with maximum decay heat to establish the worst-case thermal gradients.

(6) NCT Hot (no solar) used to assure compliance with 10 CFR §71.43(g) criteria for accessible surface temperature.

Table 3.3-2 – Insolation Data per 10 CFR §71.71(c)(1)

Form and Location of Surface	Total Insolation for a 12-hour Period (g cal/cm^2)[1]
Flat surfaces transported horizontally; base surface	None
Flat surfaces transported horizontally; all other surfaces	800
Flat surfaces not transported horizontally	200
Curved surfaces	400

Notes: (1) The 12-hour period covers the daylight hours. Insolation for the remaining 12 hours (nights) is zero. The total insolation values are averaged over a 12-hour period vs. 24 hours for evaluation of package temperatures since the relatively low thermal mass of the package will lead to faster response to the daily variation in insolation levels.

Table 3.3-3 –Summary of Thermal Margins for NCT and HAC Thermal Analyses (°F)

Item	Hot NCT	Peak HAC	Maximum Allowable		Minimum Temperature Margin[1]
			NCT	HAC	
Peak MOX FA	**221**	551	**392**	1,337	171
Avg. MOX FA	**190**	298	**392**	1,337	202
Poison On Strongback	178	**525**	850	**1,000**	475
Poison On FCS	177	**713**	850	**1,000**	287
Strongback Structure	178	**646**	800	**800**	154
Body Shell	**159**	1,407	**800**	2,500	641
Body Collar	149	**432**	800	**1,000**	568
Closure Lid	**147**	311	**800**	1,000	653
Impact Limiter Lugs	**154**	1,330	**800**	2,500	646
Impact Limiter					
• Max. Foam	149	N/A	**300**	N/A	151
• Bulk Avg. Foam	145	N/A	**300**	N/A	155
• Skin	**149**	1,474	**800**	2,500	651
Impact Limiter Bolts					
• Bolt Head	**154**	1,319	**800**	2,500	646
• Bolt Shaft	**144**	961	**800**	2,500	656
• Bolt Threads	**144**	306	**800**	2,500	656
O-ring Seals					
• Closure Lid	159	**352**	225	**400**	48 °F
• Vent/Sampling Port	**146**	305	**225**	400	79 °F

Note: (1) Minimum temperature margin based on **bold** temperatures.

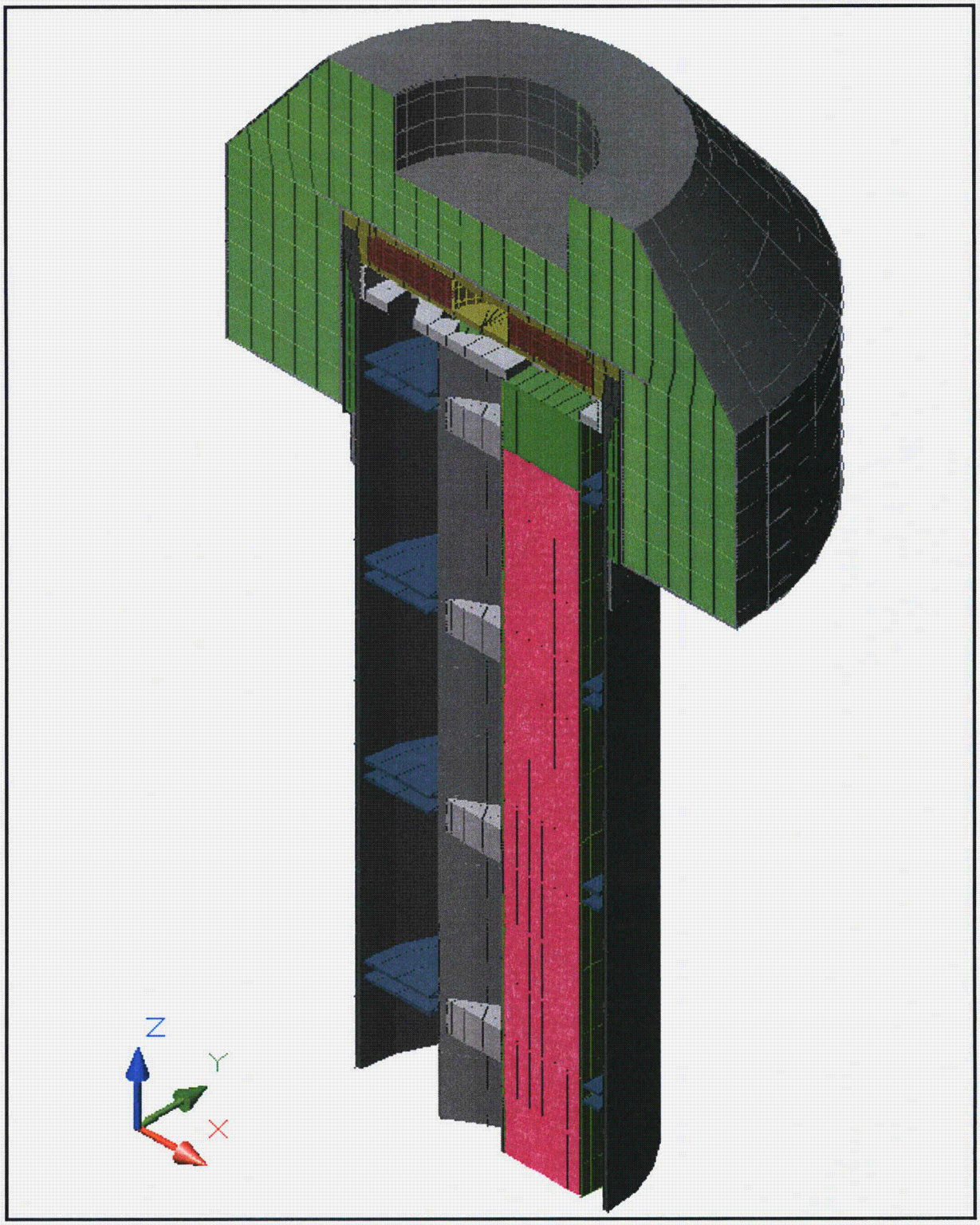

(Note: the positive z-axis is oriented the length of the package and the positive x-axis towards the bottom of the normally horizontal package)

Figure 3.3-1 – Solid View of NCT Thermal Model

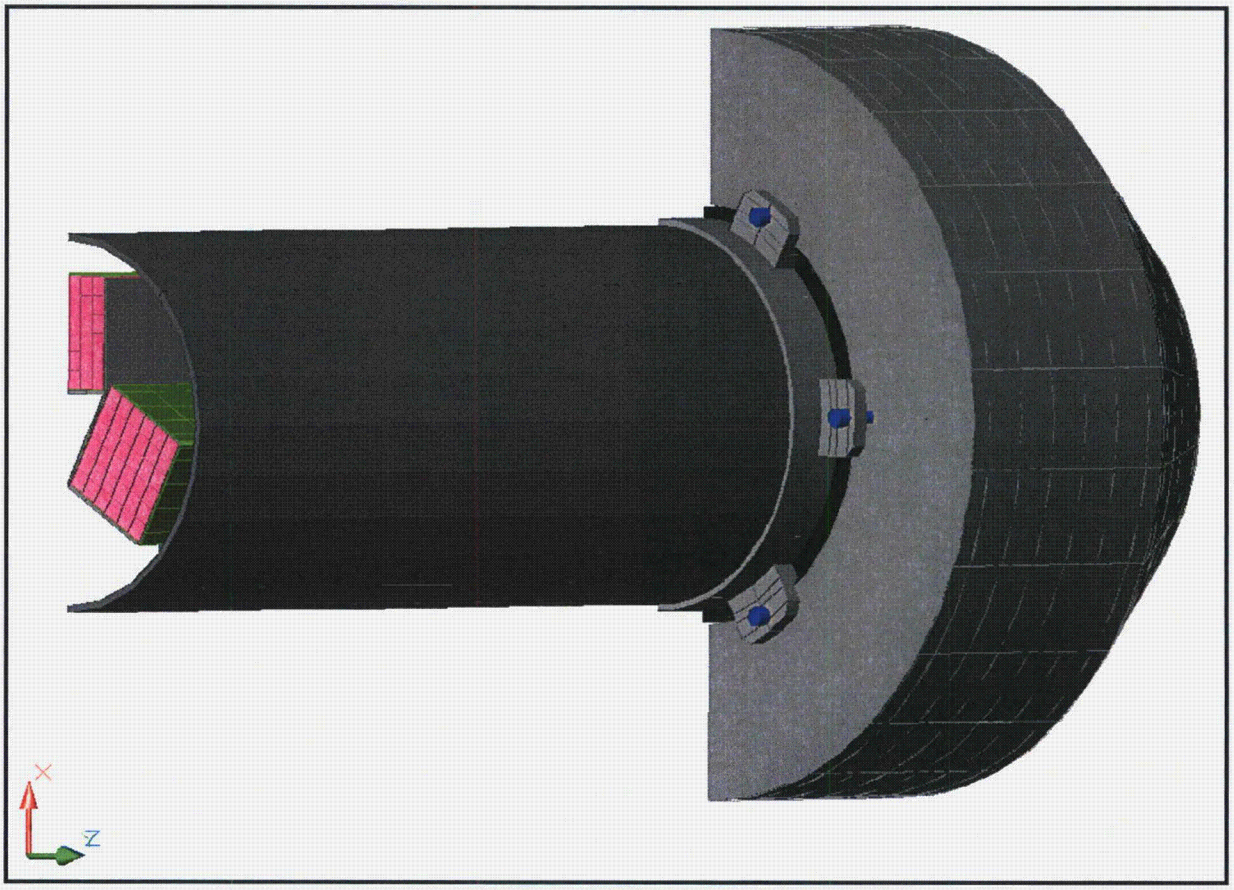

(Note: the positive z-axis is oriented the length of the package and the positive x-axis towards the bottom of the normally horizontal package)

Figure 3.3-2 – Solid View of 'Backside' of NCT Thermal Model

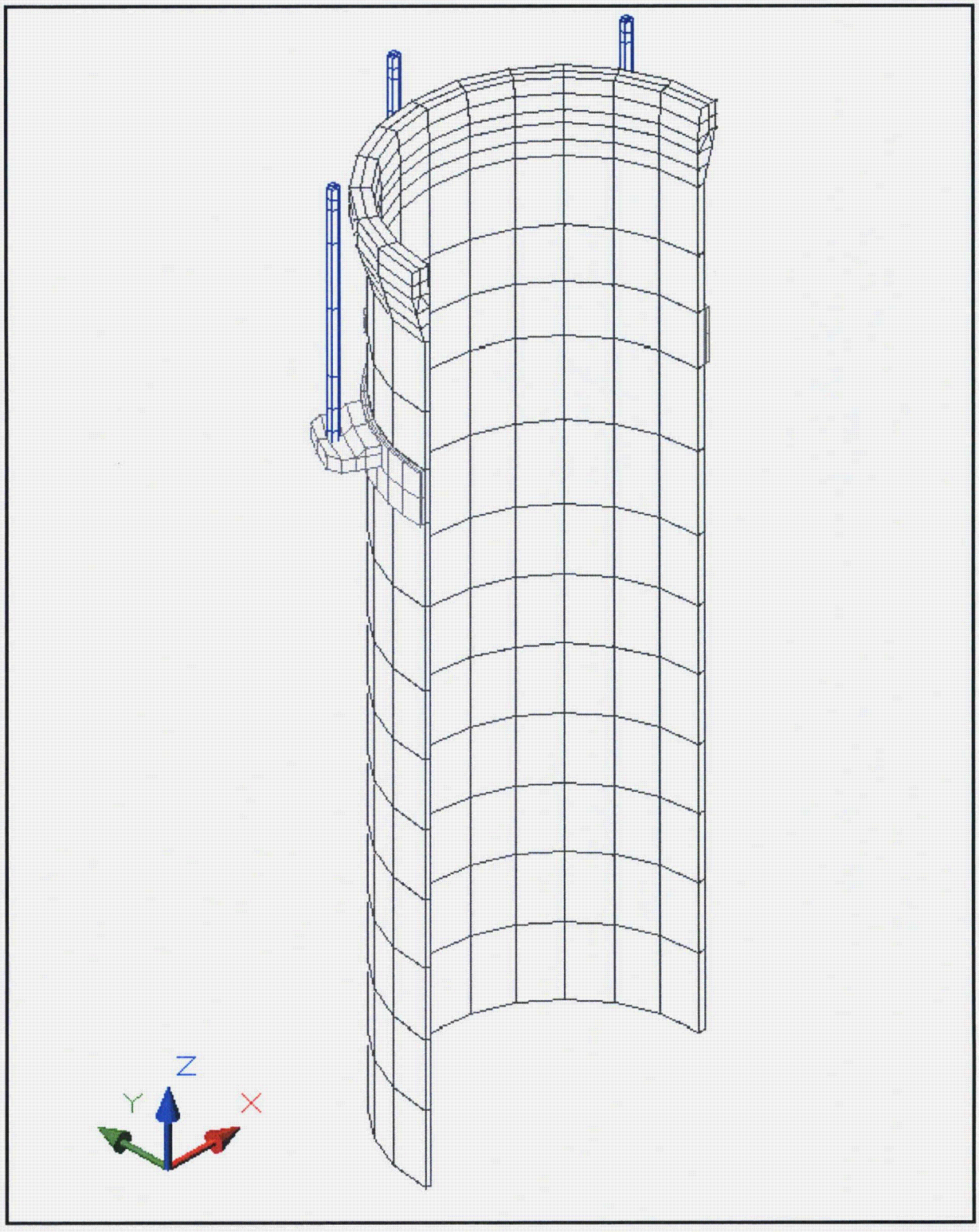

(Note: the positive z-axis is oriented the length of the package and the positive x-axis towards the bottom of the normally horizontal package)

Figure 3.3-3 – Perspective View of Solid Model for Body Shell

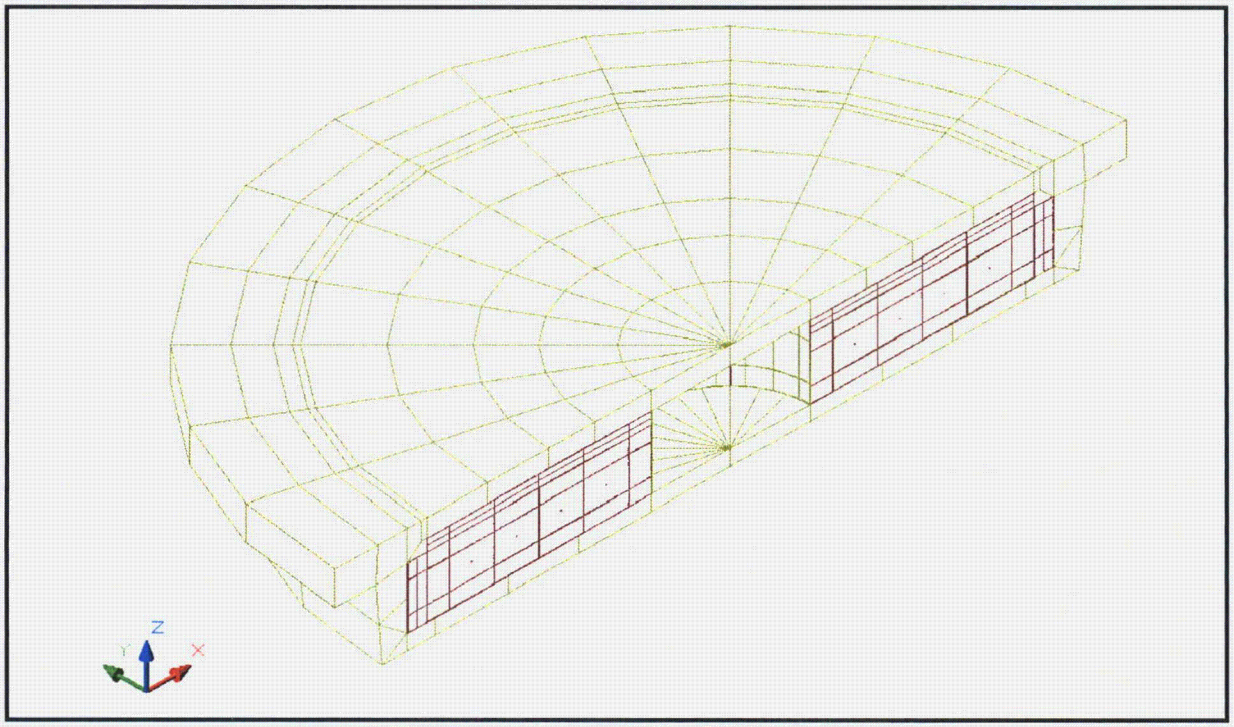

(Note: the positive z-axis is oriented the length of the package and the positive x-axis towards the bottom of the normally horizontal package)

Figure 3.3-4 – Perspective View of Solid Model for Closure Lid

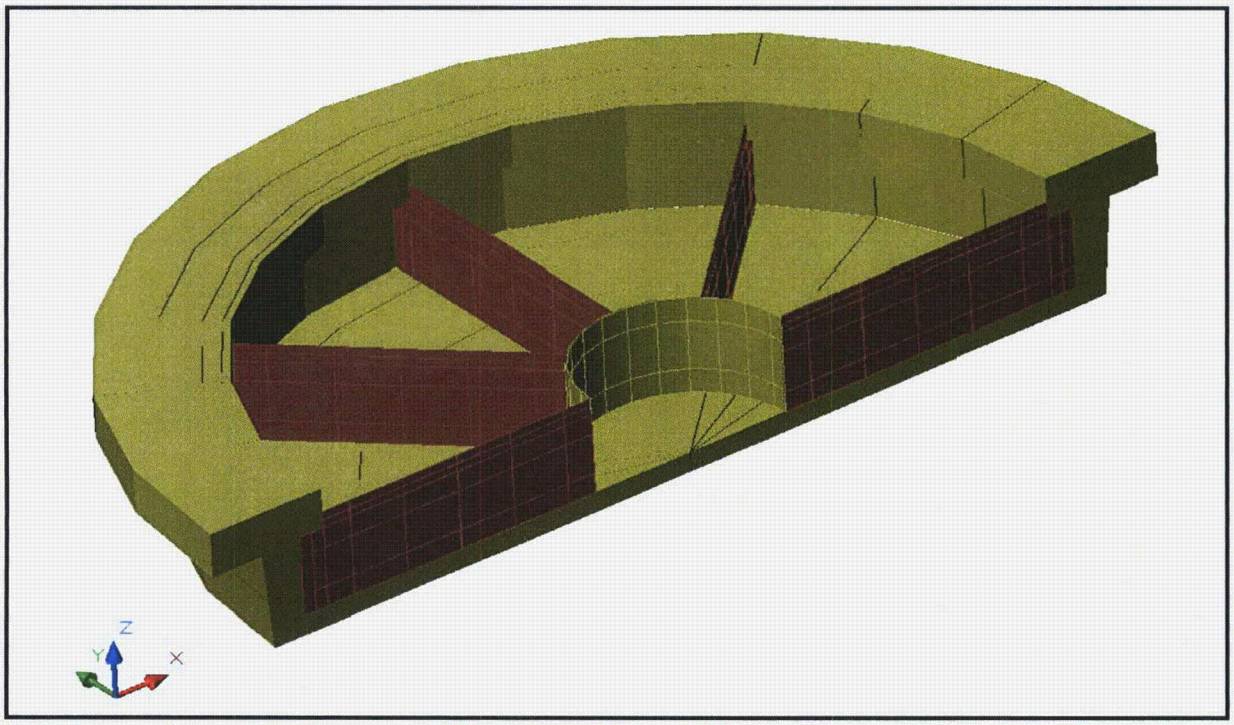

(Note: the positive z-axis is oriented the length of the package and the positive x-axis towards the bottom of the normally horizontal package)

Figure 3.3-5 – Perspective View of Solid Closure Lid Model (Top Cover not shown for Clarity)

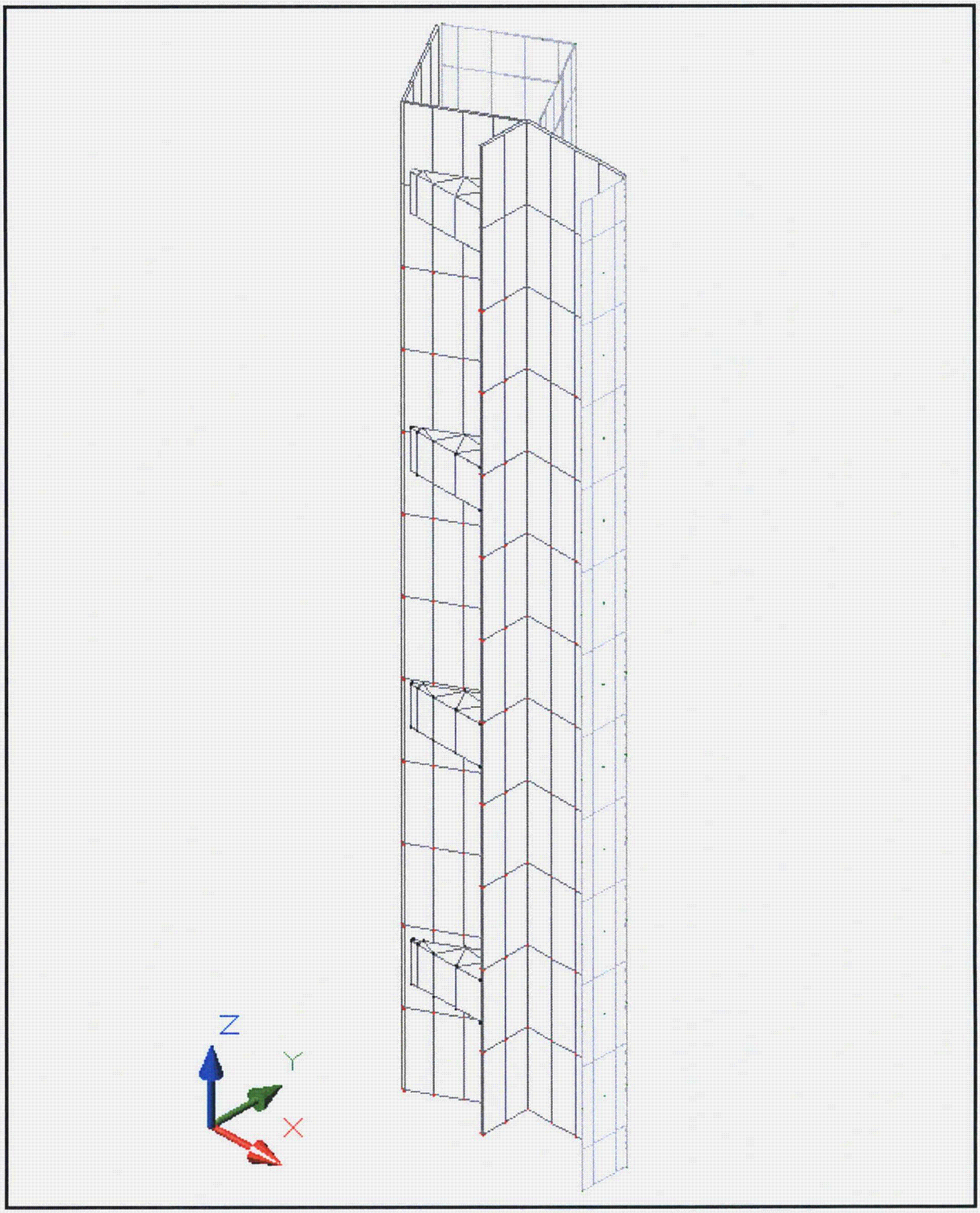

(Note: the positive z-axis is oriented the length of the package and the positive x-axis towards the bottom of the normally horizontal package)

Figure 3.3-6 – Solid View of Strongback Structure

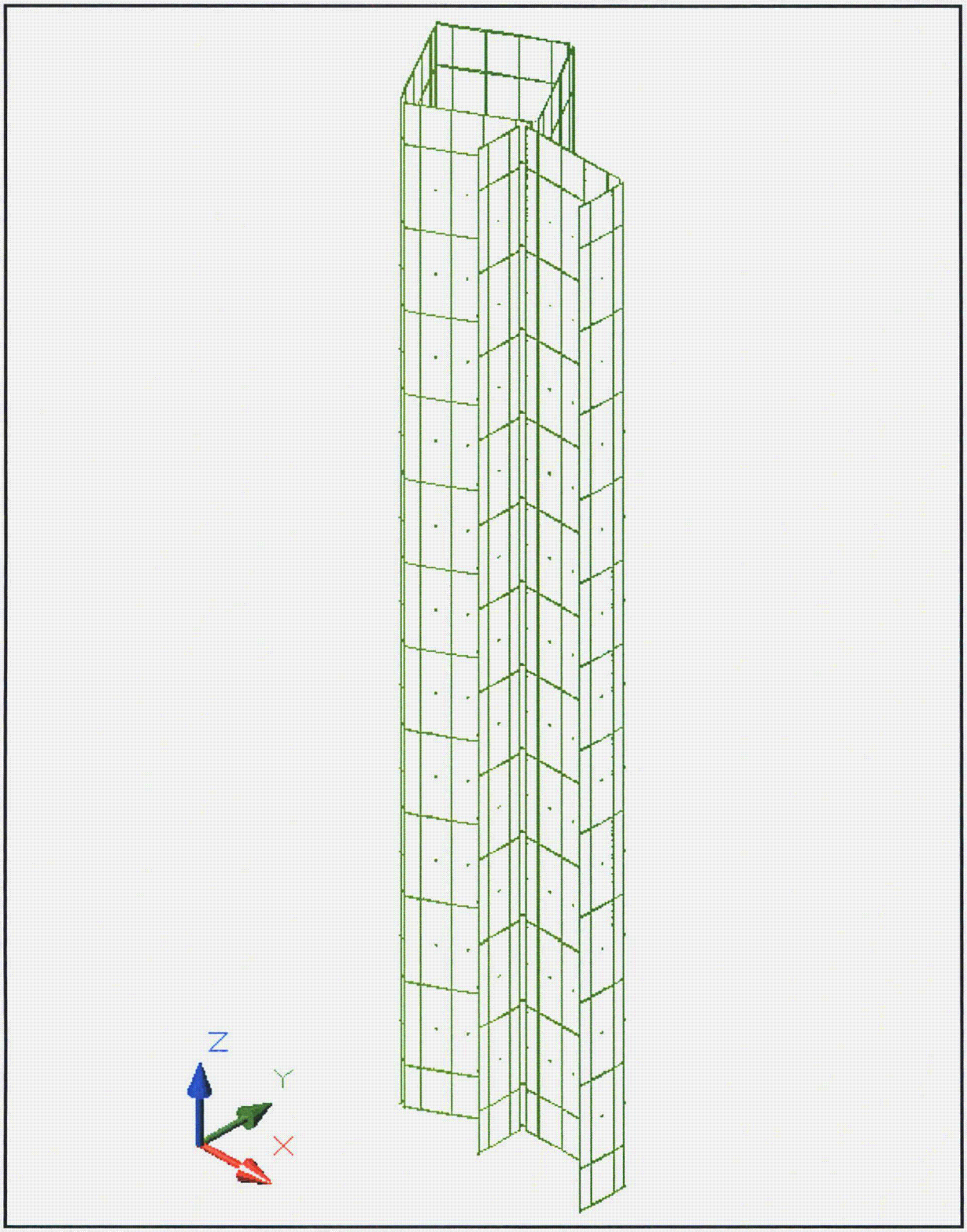

(Note: the positive z-axis is oriented the length of the package and the positive x-axis towards the bottom of the normally horizontal package)

Figure 3.3-7 – Solid View of Boral Neutron Absorber Plates

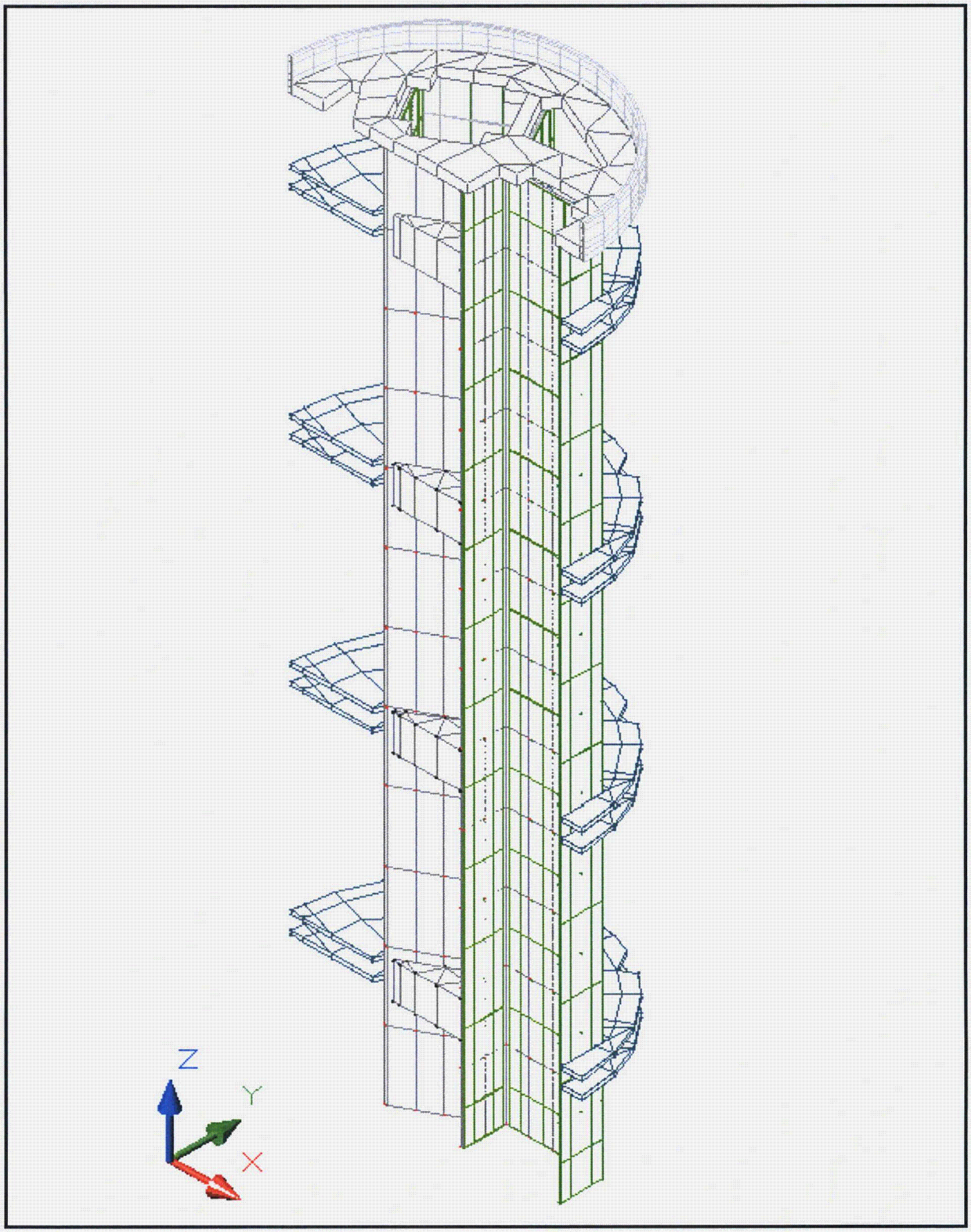

(Note: the positive z-axis is oriented the length of the package and the positive x-axis towards the bottom of the normally horizontal package)

Figure 3.3-8 – Solid View of Strongback Structure

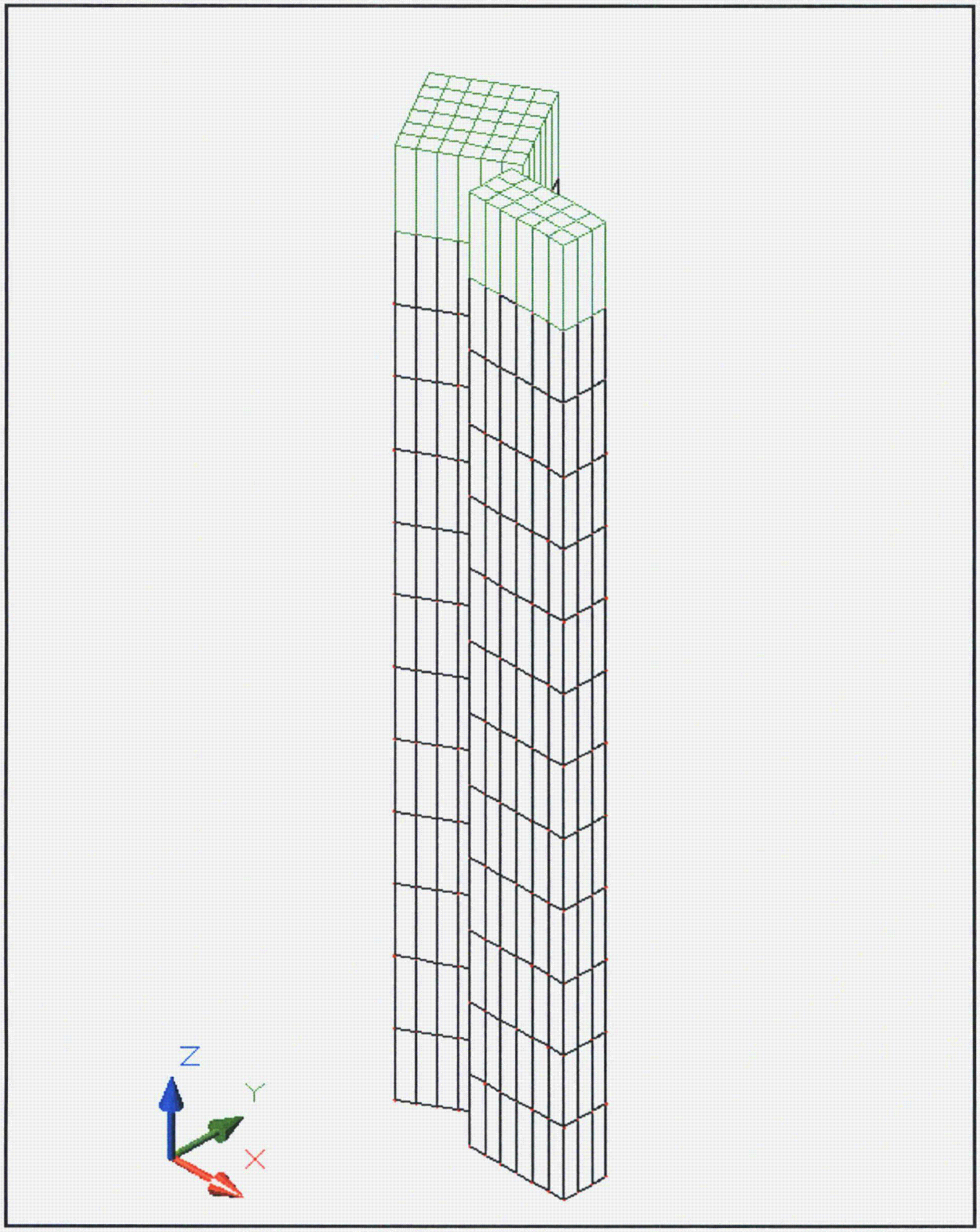

(Note: the positive z-axis is oriented the length of the package and the positive x-axis towards the bottom of the normally horizontal package)

Figure 3.3-9 – Solid View of 'Homogenized' Regions Representing MOX FAs

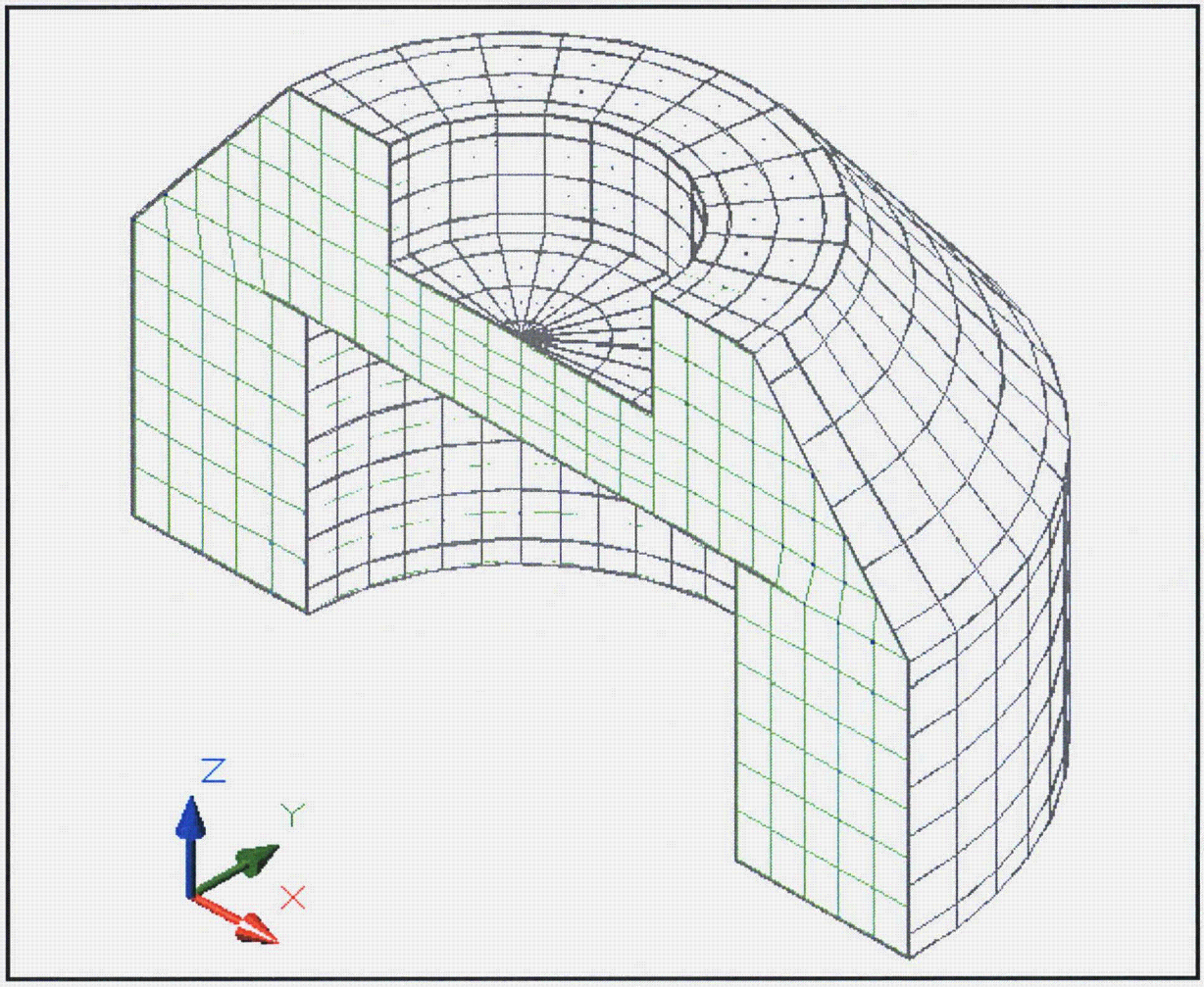

(Note: the positive z-axis is oriented the length of the package and the positive x-axis towards the bottom of the normally horizontal package)

Figure 3.3-10 – Solid View of Impact Limiter Model

3.4 Thermal Evaluation for Normal Conditions of Transport

This section presents the thermal analysis methodology and the evaluation of the thermal performance for the Mixed Oxide Fresh Fuel Package (MFFP) under NCT conditions to demonstrate compliance with the requirements of 10 CFR §71.43(g)[1] and §71.71. The thermal evaluations are performed using conservative analytical techniques to assure that all materials are maintained within their applicable minimum and maximum allowable temperature during all modes of operation.

The thermal loading on the MFFP during NCT arises from insolation on the outer surfaces of the package and from the decay heat of the payload. The thermal conditions that are considered for NCT are those specified in 10 CFR §71.71(c)(1). Accordingly, an ambient temperature of 100 °F with the following insolation values are used for heat input to the exterior package surfaces. Note that since the package is normally transported horizontally, the ends of the impact limiter are treated as 'flat surfaces not transported horizontally' with an insolation value of 200 gcal/cm^2.

Form and Location of Surface	Total Insolation for a 12-Hour Period (gcal/cm2)
Flat surfaces transported horizontally: • Base • Other surfaces	 None 800
Flat surfaces not transported horizontally	200
Curved surfaces	400

These values represent the total insolation over a 12-hour period. The NCT evaluations applied these insolation values averaged over a 12-hour period as a steady-state heat loading on the package surfaces.

3.4.1 Heat and Cold

3.4.1.1 Heat

Table 3.4-1 presents a summary of the temperatures determined for the major components of the MFFP packaging normal conditions of transportation (NCT). The steady-state thermal analysis results demonstrate that the MOX FA, strongback structure, body shell, containment O-ring seals, and impact limiter components of the MFFP are all within their respective allowable material temperatures under the evaluated NCT conditions and for the design decay heat loading. Additionally, the minimum material temperatures under the NCT cold condition with zero decay heat also comply with the material specifications. The analysis also demonstrates that all accessible package surfaces remain below 122 °F when transported in an ambient temperature of 100 °F and without insolation, as stipulated by 10 CFR §71.43(g).

The maximum temperatures for the MFFP are determined for operation in a constant 100 °F ambient air temperature with and without the regulatory insolation. These NCT thermal load cases are

[1] Title 10, Code of Federal Regulations, Part 71 (10 CFR 71), *Packaging and Transportation of Radioactive Material*, Final Rule, 01-26-04.

described in Section 3.3.1, *Evaluation by Analysis,* (i.e., Load Conditions 1 and 2). As seen from the summary of the temperature results presented in Table 3.4-1, the peak temperatures determined for the MFFP components and the MOX FAs are well within their allowable temperature limits, as established in Section 3.2, *Material Properties and Components Specifications.*

Delrin® plastic is used as a bearing surface between the body shell and the strongback assembly at the circumference of the top and base plates. At this location the Delrin® plastic will reach a temperature level that is between that of the top plate and the body shell in the same location. Examination of the temperature distributions in Figure 3.4-2 and Figure 3.4-5 indicates this temperature level to be between 150 and 164 °F. As such, the Delrin® plastic is shown to remain within its continuous operational temperature limit of 180 °F and well below the allowable 250 °F limit for intermittent operation.

Neoprene pads are used throughout the strongback structure to cushion the interface between various components. As such, the peak temperature reached by the neoprene pads will be equivalent to the peak temperature of the strongback structure. The peak temperature of 178.4 °F level achieved for the poison surfaces on the strongback structure under the NCT Hot condition is within the allowable maximum service temperature of 180 °F established for the neoprene rubber in Section 3.2, *Material Properties and Components Specifications.*

In compliance with 10 CFR §71.43(g), the maximum temperature of any accessible outer surface is limited to 122 °F or less under NCT conditions when insolation is not present. Since, as demonstrated in Table 3.4-1, the maximum temperature of the accessible surfaces under load Case 2 (i.e., 100 °F and no insolation) is 110 °F or lower, compliance with 10 CFR §71.43(g) is demonstrated.

Figure 3.4-1 through Figure 3.4-5 illustrate the temperature distribution within the MFFP for the NCT Hot condition. The overall temperature distribution within the MFFP is illustrated in Figure 3.4-1. As expected from the low decay heat loading applicable to this design, only a relatively small temperature differential exists within the package. The distribution of the active fuel length within the model can be noted from the figure.

Figure 3.4-2 illustrates the temperature distribution within the body shell. Again, only a relatively small temperature differential exists along the length of the shell, with the minimum temperature occurring at the closure lid. Figure 3.4-3 and Figure 3.4-4 present the associated temperature distributions within the closure lid and the impact limiter, respectively. The temperature distribution within the impact limiter illustrated in Figure 3.4-4 reflects the conservative assumptions of a 12-hour average insolation loading applied to the entire surface of the impact limiter. In reality, due to the insulation quality of the polyurethane foam, the temperature distribution within the limiter would be more accurately a function of a 24-hour average insolation loading. Further, self shading will limit the insolation loading on the lower surfaces of the impact limiter. As such, the actual peak temperatures to be expected within the impact limiter are conservatively bounded by this analysis.

Figure 3.4-5 presents the predicted temperature distribution within the strongback structure. As seen from the figure, the relatively high thermal conductivity of the boral neutron poison plates, combined with the low decay heat loading and its uniform distribution over the active fuel length, results in uniform temperature levels over much of the strongback structure.

3.4.1.2 Cold

The minimum temperature distribution for the MFFP packaging occurs with a zero decay heat load and an ambient air temperature of -40 °F per 10 CFR §71.71(c)(2). The steady-state analysis of this condition represents a trivial case that requires no thermal calculations be performed. Instead, it is assumed that all package components achieve the -40 °F temperature under steady-state conditions. As discussed in Section 3.2.2, *Component Specifications*, the -40 °F temperature is within the allowable range of all of the MFFP packaging components.

As a potential initial condition for all normal or accident events, a minimum uniform temperature of -20 °F and no insolation must be considered per 10 CFR §71.71(b) and §71.73(b) (i.e., Load Condition 3, Table 3.3-1). Table 3.4-1 presents a summary of the resulting temperatures with the design MOX FA decay heat load. All of the assumed conditions for minimum temperatures yield component temperature levels that are within the allowable temperature limits.

Figure 3.4-6 illustrates the temperature distribution within the MFFP packaging for the NCT Cold condition of -20 °F and no insolation.

3.4.2 Maximum Normal Operating Pressure

The maximum normal operating pressure (MNOP) for NCT is presented in Table 3.4-2. The MNOP is based on an initial cavity backfill of air at atmospheric pressure at 70 °F (294 K), an assumed failure rate of 3% of the fuel rods[1], and heat up of the gases in internal cavity under the design decay heat loading and the respective ambient condition. For the purpose of rod pressure determination, the only significant gas contributor is the initial helium backfill as no fission products will exist within the un-irradiated FAs.

The bulk average gas temperature for each condition is determined by the SINDA/FLUINT thermal model. The body cavity is assumed to have a free volume of approximately 80,073 cubic inches. The free volume in the body cavity is based on a cavity 28.5 inches in diameter and 165.25[2] inches long, a displacement volume of 4,685 cubic inches for each FA, and a displacement volume of 11,292 cubic inches for the strongback assembly. The strongback displacement is computed based on a total weight of 2,900 pounds, of which 160 pounds is from the neutron poison plates (density = 0.0917 lb_m/in^3, per Table 3.2-2) and the remaining 2,740 pounds is assumed to be Type 304 stainless steel (density = 0.287 lb_m/ in^3, per Table 3.2-1).

The total moles of helium fill gas within each fuel assembly depend on the assembly specific fuel rod total free volume and the fill gas pressure. Since the rods are backfilled during fabrication and prior to irradiation or exposure to elevated temperatures, the nominal rod dimensions are used. The ideal gas law applies for determination of fuel rod fill gas moles:

$$N_{Rod} = \frac{P_{Fill} V_{rod}}{RT}$$

[1] U. S. Nuclear Regulatory Commission, NUREG-1617, Table 4-1, *Standard Review Plan for Transportation Packages for Spent Fuel*, March 2000.

[2] Correct value is 165.45 inches; value used is conservative.

where:

P_{Fill} = Rod fill gas pressure (atm)

V_{rod} = Fuel assembly rod internal free volume (liters)

R = Ideal Gas Constant = 0.0821 atm-liter/gmole-K

T = Temperature at rod backfill = 294 K (70 °F)

There are 264 fuel rods in a 17 × 17 MOX FA, and 24 burnable poison assembly rods (BPRAs). Each fuel rod and BPRA has an initial helium fill pressure between 200 to 300 psig, and 400 to 600 psig, respectively. For conservatism, the initial helium fill pressure will be assumed to be 300 psig for the fuel rods and 600 psig for the BPRAs. The free volume for a fuel rod or BPRA is 1.67 in^3 (0.0274 liters). Based on the equation above, there would be 7.55 g-moles of helium fill gas in each MOX FA, or a total of $N_{MOX\ Fill\ Gas}$ = 22.64 g-moles for three assemblies.

The initial gas in the internal cavity at the time of closure is calculated as follows:

$$N_{fill} = \frac{1\,atm \times V_{free}}{R \times T_{fill}}$$

The maximum NCT pressure is then calculated as follows:

$$P_{NCT\ Max} = \frac{N_{package} R T_{NCT}}{V_{free}}$$

$$N_{package} = N_{fill} + Rod\ Failure\ Rate \times N_{MOX\ fill\ gas} + N_{outgassing}$$

where:

$N_{package}$ = total moles of gas in internal cavity

N_{fill} = moles air within internal cavity at time of package closure

Rod Failure Rate = assumed number of failed rods within each MOX FA. A 3% failure rate, which matches the regulatory failure rate for NCT of spent nuclear fuel, will conservatively bound the expected failure rate for a fresh FA.

$N_{MOX\ fill\ gas}$ = moles of rod fill gas within package cavity

$N_{outgassing}$ = moles gas generated by outgassing from component material within package cavity

= 0 (NCT temperatures are within long-term temperature limits for the materials)

R = Ideal gas constant (0.0821 atm-liter/gmole-K)

V_{free} = Internal cavity free volume

= Gross cavity volume minus displacement volumes for FAs and strongback

= 105,420 – [(3 × 4,685) + 11,292], in^3 = 80,073 in^3 (1,312 liters)

T_{NCT} = Bulk average gas temperature within package (K) at the specific condition

The computed maximum NCT pressure from Table 3.4-2 is seen to be 17.6 psia (2.9 psig). For conservatism, the MNOP is assumed to be 24.7 psia (10 psig). Significant margin exists between the MNOP and the MFFP's design pressure limit of 39.7 psia (25 psig).

3.4.3 Maximum Thermal Stresses

Maximum thermal stresses for NCT are determined using the temperature results from Section 3.4.1.1, *Heat*, and Section 3.4.1.2, *Cold*. NCT thermal stresses are discussed in Section 2.6.1, *Heat*, and Section 2.6.2, *Cold*.

3.4.4 Evaluation of Package Performance for Normal Conditions of Transport

The steady-state thermal analysis results demonstrate that the MOX FA, strongback structure, body shell, containment seals, and impact limiter components of the MFFP are all within their respective allowable material temperatures under the evaluated NCT conditions and for the design decay heat loading. Additionally, the minimum material temperatures under the NCT cold condition with zero decay heat also comply with the material specifications. The analysis also demonstrates that all accessible package surfaces remain below 122 °F when transported in an ambient temperature of 100 °F and without insolation, as stipulated by 10 CFR §71.43(g).

The MNOP resulting from the NCT Hot condition and conservative assumptions is within the package's maximum design pressure limit.

Therefore, the MFFP is found to comply with all of the thermal requirements specified in 10 CFR §71.71.

Table 3.4-1 – NCT Temperatures

Location	Temperature (°F)			
	NCT Hot	NCT Hot w/o Solar	NCT Cold	Maximum Allowable (1)
Peak MOX FA	221	179	77	392
Avg. MOX FA	190	130	37	392
Poison On Strongback	178	134	22	850
Poison On Fuel Box Enclosure	177	133	21	850
Strongback Structure	178	134	22	800
Body Shell	159	110	-9	800
Body Collar	149	109	-9	800
Closure Lid	147	109	-9	800
Impact Limiter Lugs	154	108	-10	800
Impact Limiter				
• Max. Foam	149	107	-11	300
• Bulk Avg. Foam	145	101	-11	300
• Skin	149	107	-11	800
Impact Limiter Bolts				
• Bolt Head	154	107	-12	800
• Bolt Shaft	144	106	-13	800
• Bolt Threads	144	107	-11	800
Seals				
• Closure Seal	159	110	-10	225
• Vent/Sampling Port	146	108	-10	225
Bulk Avg. Fill Gas	166	121	5	--

Notes: (1) See Section 3.2, *Material Properties and Component Specifications* for basis for 'Maximum Allowable' temperatures.

Table 3.4-2 – Package NCT Internal Pressures

Parameter	NCT Hot	NCT Hot w/o Solar	NCT Cold
Bulk Avg. Fill Gas Temperature	166 °F	121 °F	5 °F
Quantity of Package Fill Gas	54.3 g-moles	54.3 g-moles	54.3 g-moles
Gas From Failed FA Rods	0.68 g-moles	0.68 g-moles	0.68 g-moles
Gas From Component Outgassing	0 g-moles	0 g-moles	0 g-moles
Internal Cavity Pressure	17.6 psia (2.9 psig)	16.3 psia (1.6 psig)	13.1 psia (-1.6 psig)

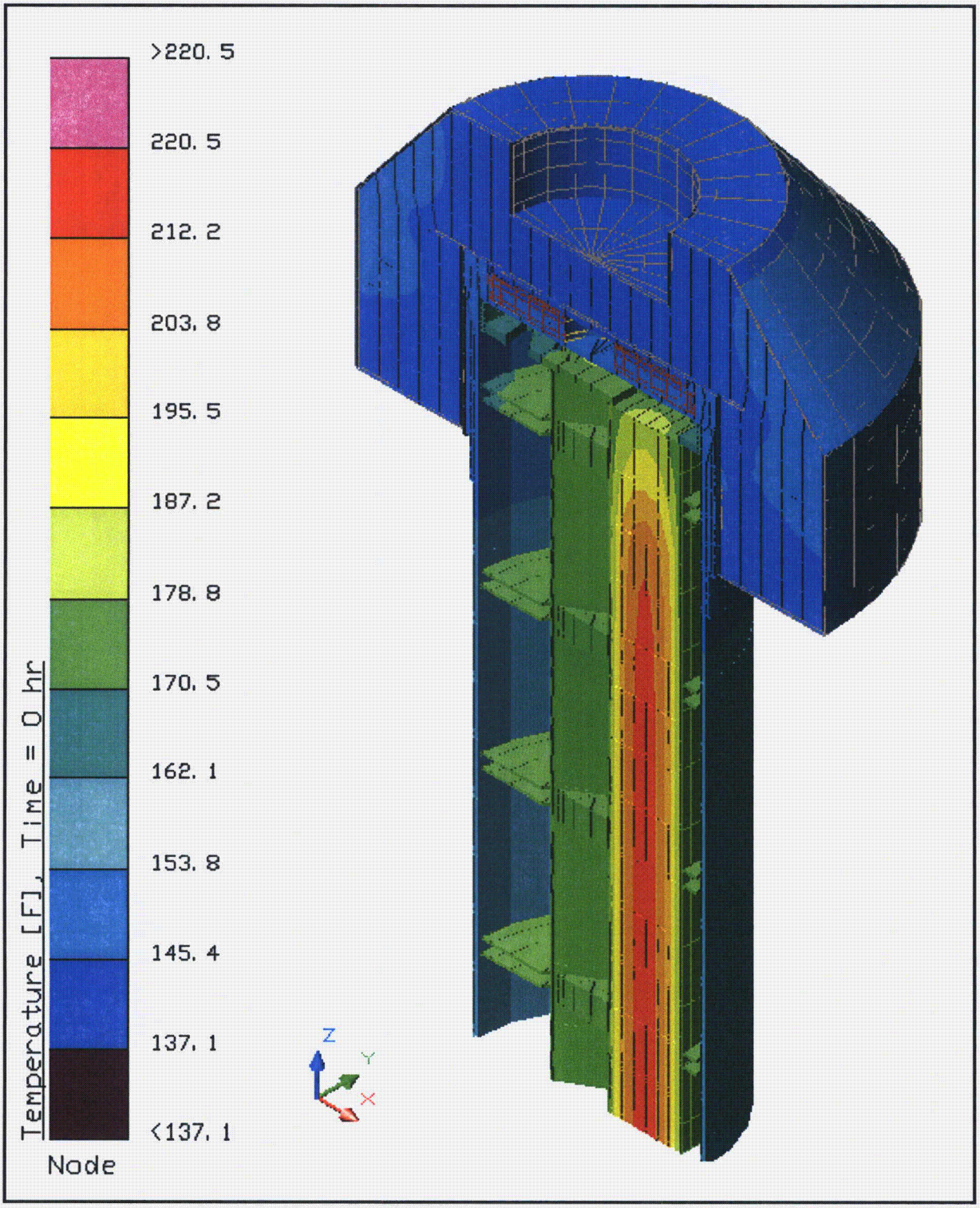

(Note: the positive z-axis is oriented the length of the package and the positive x-axis towards the bottom of the normally horizontal package)

Figure 3.4-1 – Temperature Distribution within MFFP for NCT Hot Condition

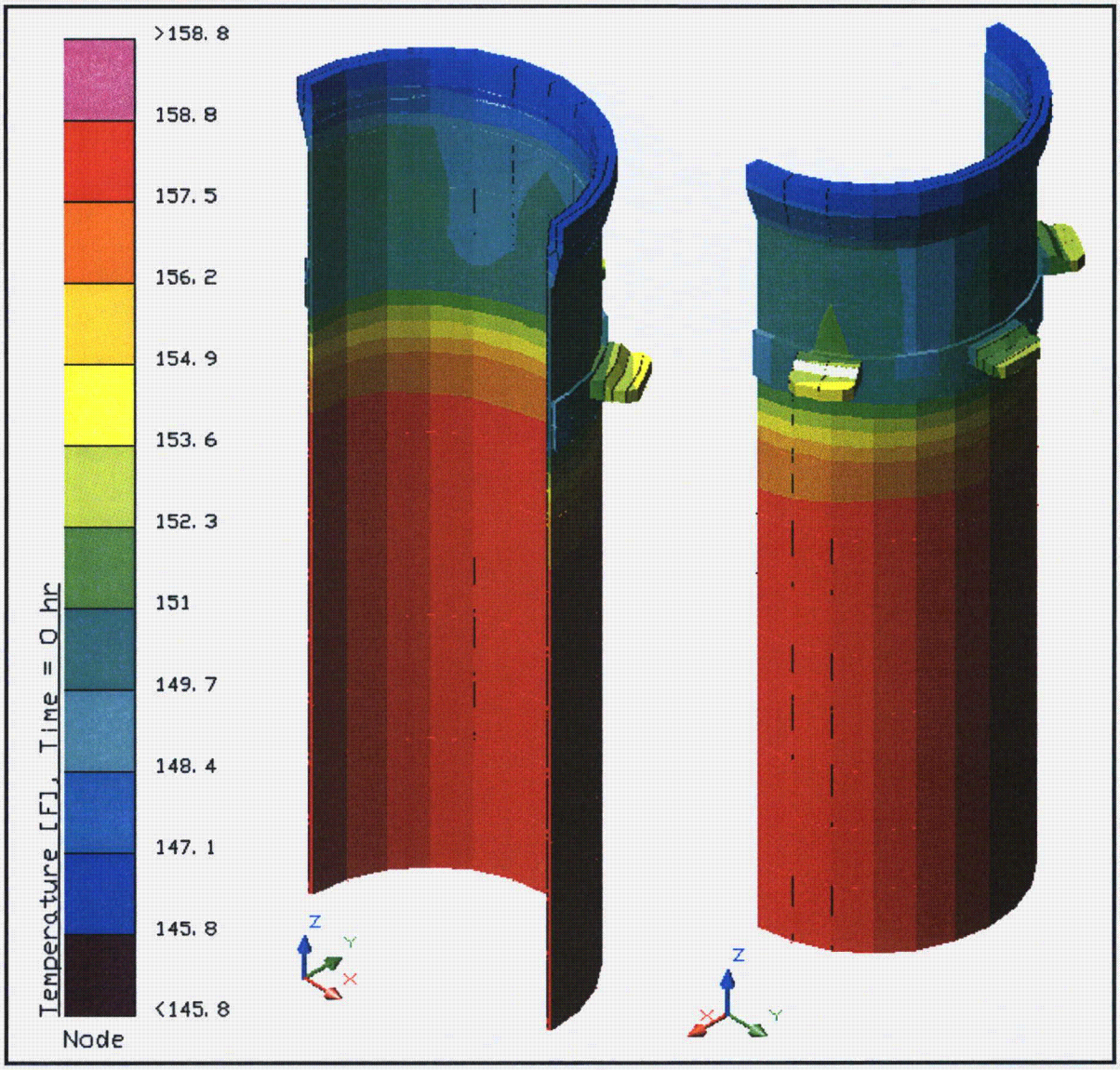

(Note: the positive z-axis is oriented the length of the package and the positive x-axis towards the bottom of the normally horizontal package)

Figure 3.4-2 – Temperature Distribution within Body Shell for NCT Hot Condition

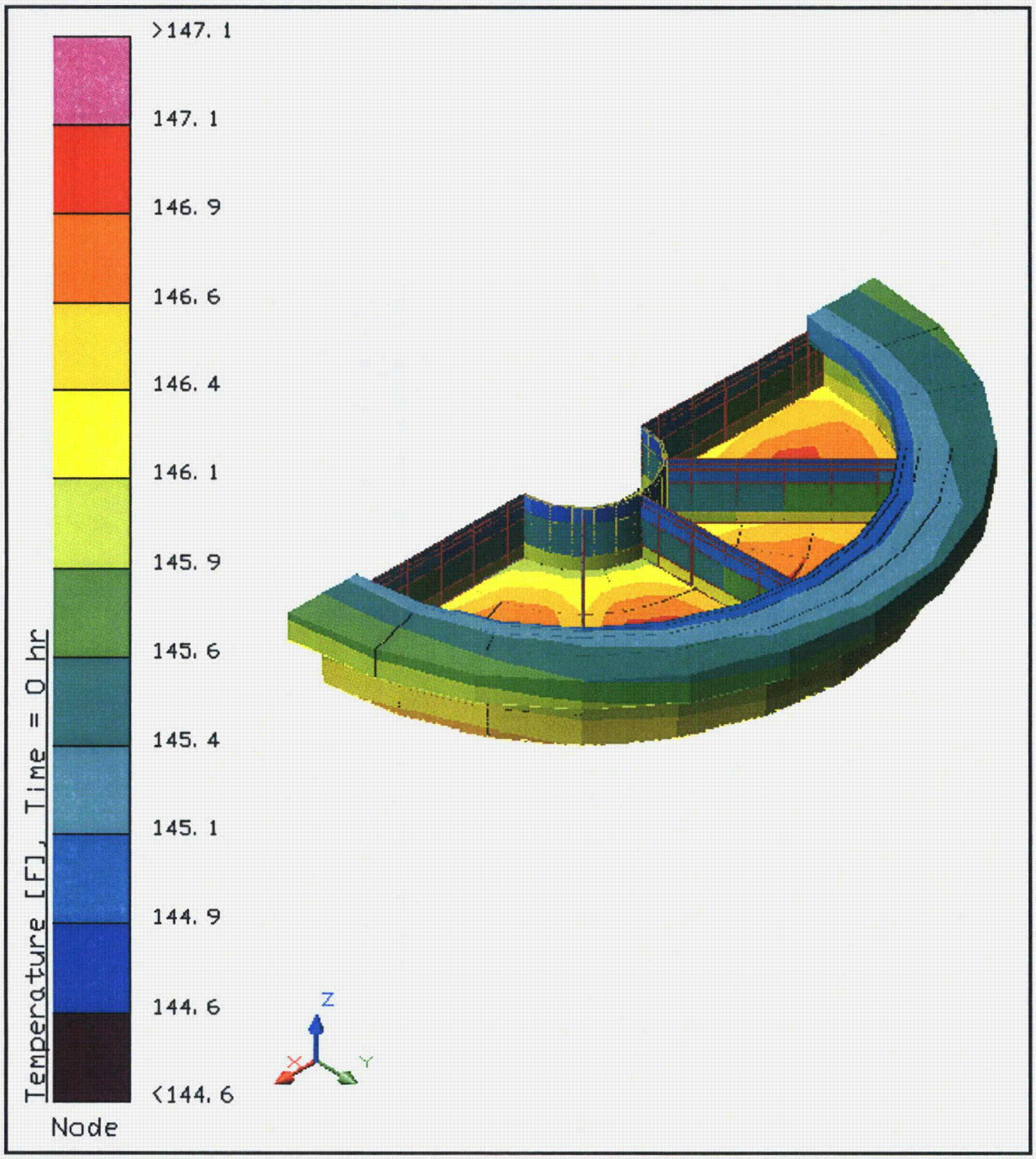

(Note: the positive z-axis is oriented the length of the package and the positive x-axis towards the bottom of the normally horizontal package)

Figure 3.4-3 – Temperature Distribution within Closure Lid for NCT Hot Condition

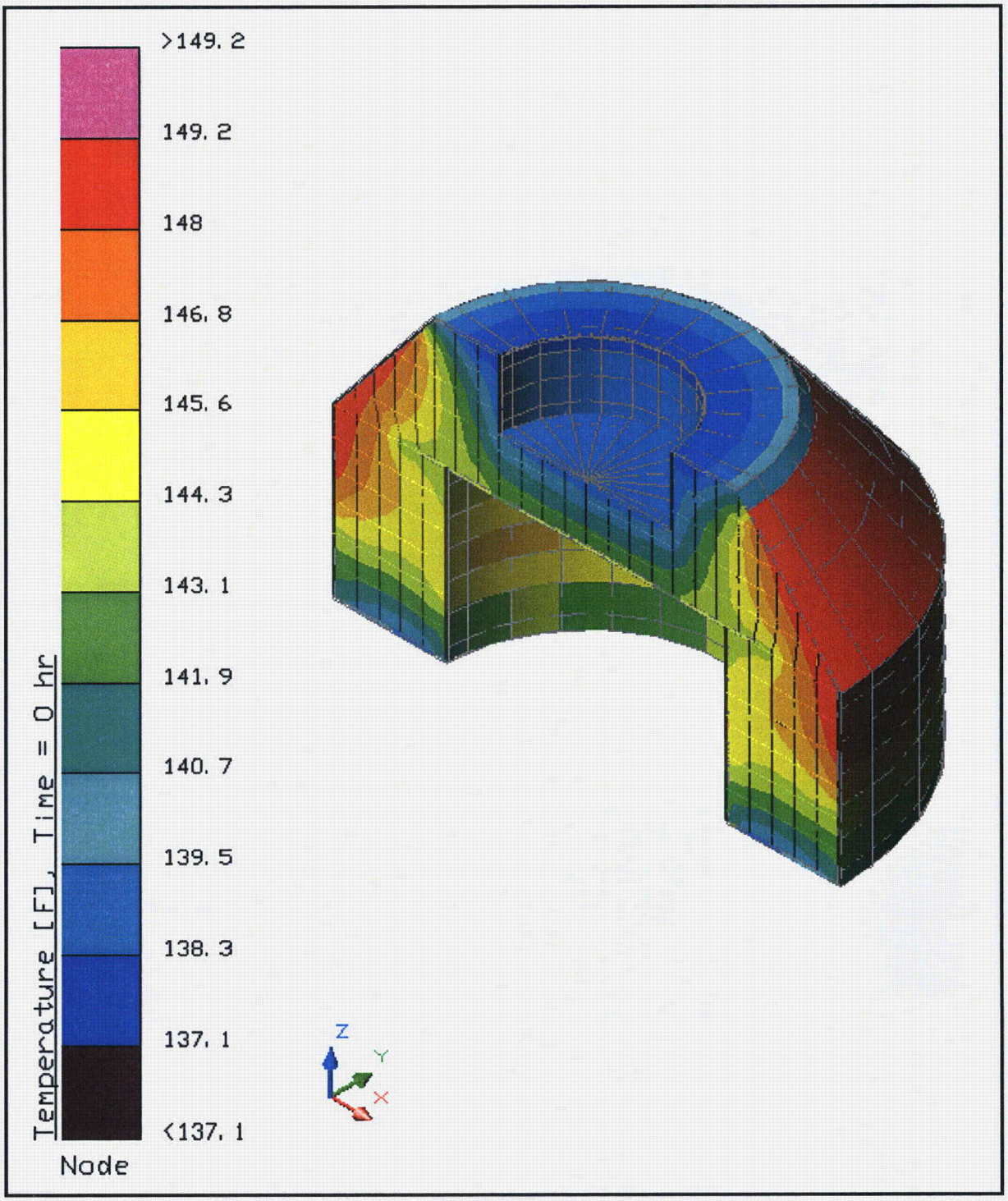

(Note: the positive z-axis is oriented the length of the package and the positive x-axis towards the bottom of the normally horizontal package)

Figure 3.4-4 – Temperature Distribution within Impact Limiter for NCT Hot Condition

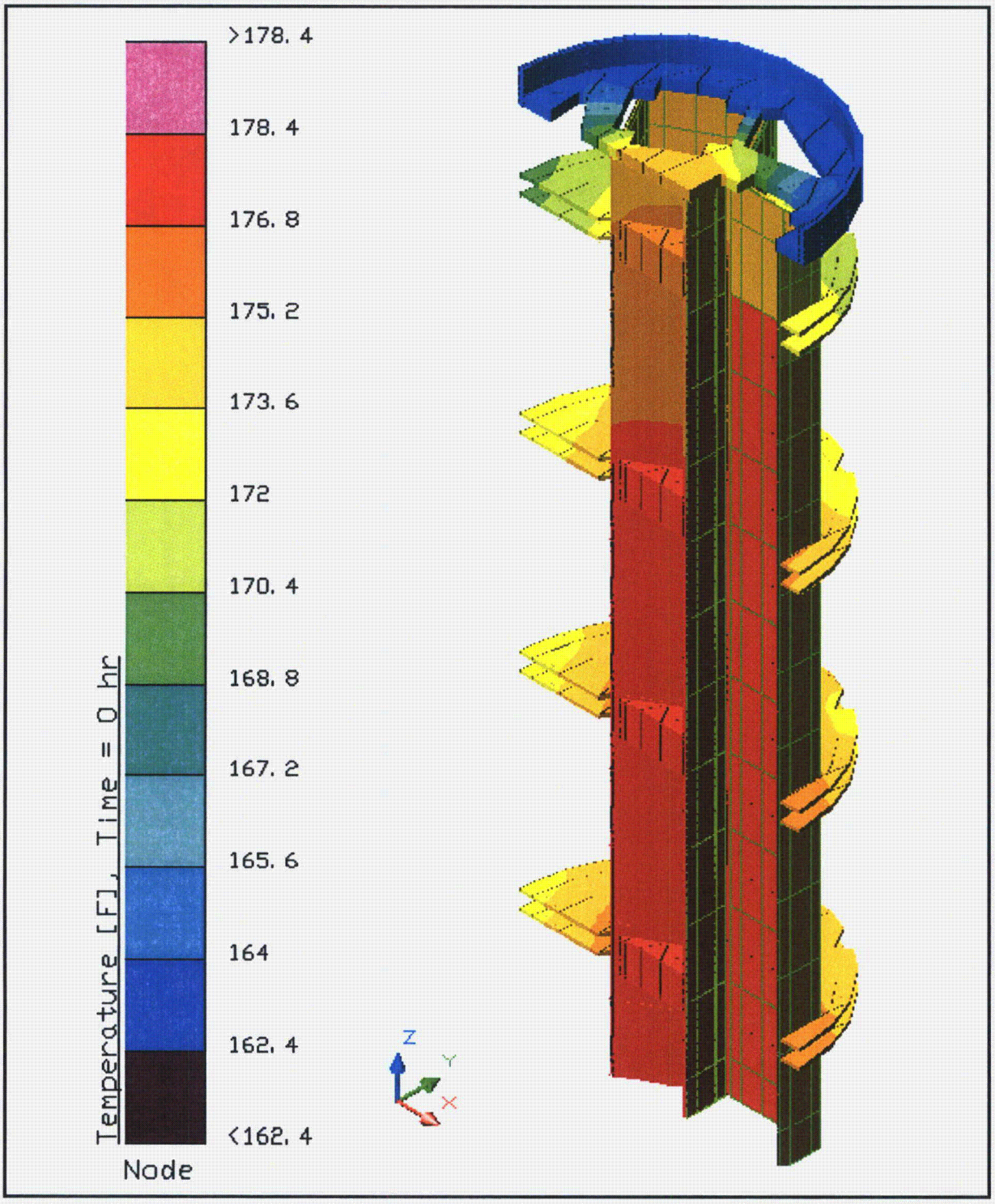

(Note: the positive z-axis is oriented the length of the package and the positive x-axis towards the bottom of the normally horizontal package)

Figure 3.4-5 – Temperature Distribution within Strongback Structure for NCT Hot Condition

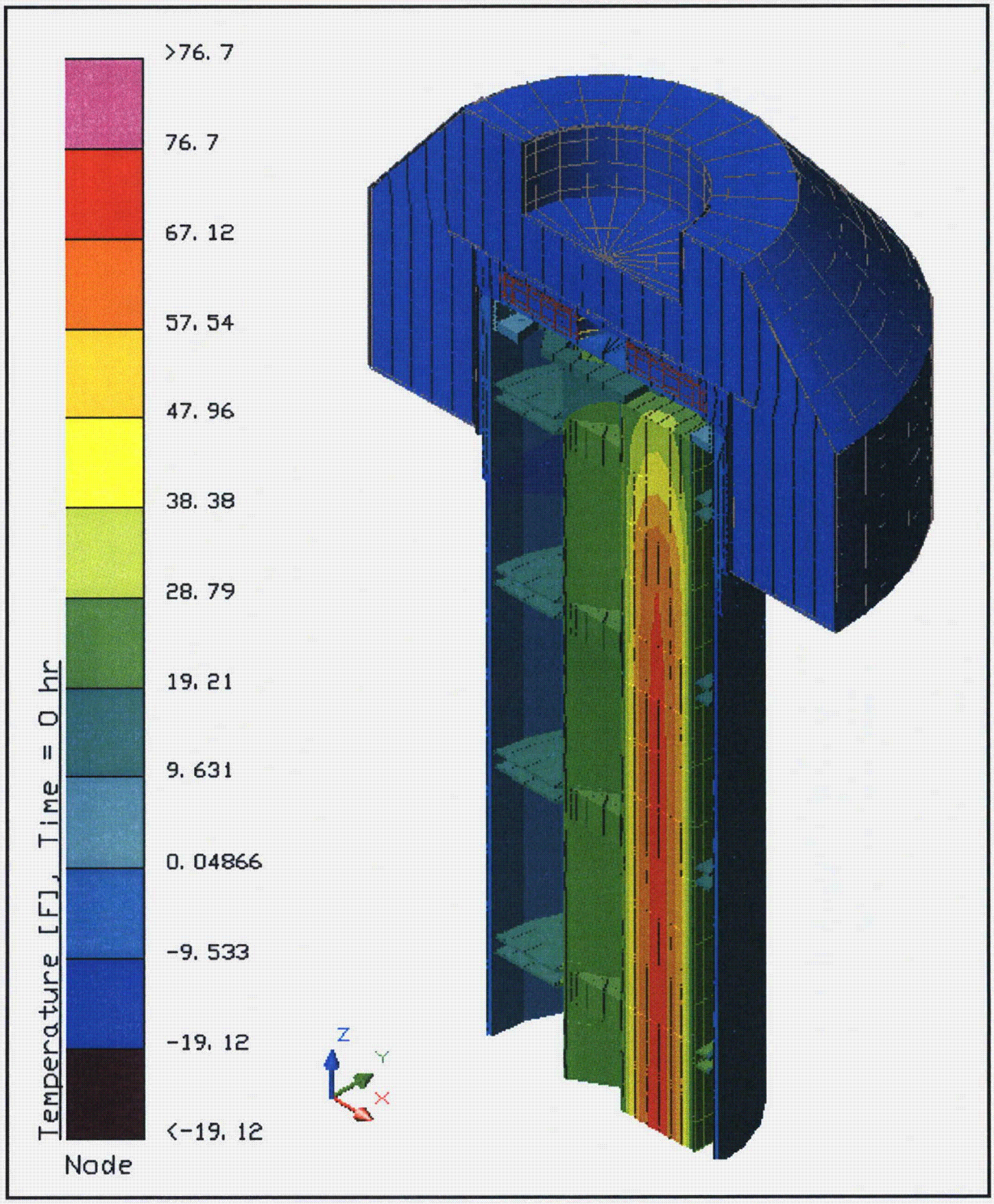

(Note: the positive z-axis is oriented the length of the package and the positive x-axis towards the bottom of the normally horizontal package)

Figure 3.4-6 – Temperature Distribution within MFFP for NCT Cold Condition

3.5 Thermal Evaluation Under Hypothetical Accident Conditions

This section presents the results of the MFFP thermal analysis for the hypothetical accident condition (HAC) specified in 10 CFR §71.73(c)(4)[1].

3.5.1 Initial Conditions

The initial temperature distribution in the package prior to the HAC fire event is taken from the steady state conditions determined in Section 3.4.1.1, *Heat*, with 100 °F, the design decay heat loading, and no insolation. The absence of insolation prior to the HAC event is consistent with the *Summary and Resolution of Public Comments* relating to §71.73, which states, "*...the effects of solar radiation may be neglected before and during the thermal test...*". Insolation is included after the end of the 30 minute fire for computing the thermal response of the package during cool down.

To determine the effect of a HAC fire event, the damaged MFFP described in Section 3.3.1.2, *HAC Analytical Model*, is exposed to a convective and radiative heat flux associated with a fully engulfing fire with a flame temperature of 1,475 °F and an effective emissivity of 1.0. This value of emissivity is conservatively greater than the value of 0.9 specified by §71.73. The duration of the HAC fire event is 30 minutes, after which time the thermal boundary conditions are returned to the original ambient temperature of 100 °F. Following the end of the HAC fire event, the thermal transient analysis is continued for a sufficient time to determine the maximum temperatures for all components. Consistent with the requirements of 10 CFR §71.73(c)(4), the surface absorptivity of all external surfaces is set to 0.8.

3.5.2 Fire Test Conditions

3.5.2.1 Analytical Model

The analytical model used for the evaluation of the thermal performance of the MFFP design under HAC conditions is the same as that described in Section 3.3.1.1, *NCT Analytical Model*, for all but the impact limiters. The presence of the impact limiters provides significant thermal protection to the MFFP, even after accounting for the potential damage arising from the free drop and puncture drop accidents. However, due to the potential free drop and puncture drop damage and the potential degradation of the polyurethane foam under the elevated temperatures resulting from the HAC fire, both the geometry and the thermal properties of the impact limiter components will be significantly different from those used to compute the NCT performance. The following paragraphs address the modeling changes to the impact limiter to account for the free drop damage, the physical changes occurring in the foam material exposed to elevated temperatures, and the potential damage related to the puncture drop.

To bound the potential damage to the MFFP from the pre-fire accidents, the results from a series of free drop tests on a full-scale prototypic certification test unit (CTU) were examined for potential damage affects on the package. The drop tests covered a range of hypothetical drop orientations (i.e., side drop, C.G.-over-corner, and slapdown free drop tests, plus a series of

[1] Title 10, Code of Federal Regulations, Part 71 (10 CFR 71), *Packaging and Transportation of Radioactive Material*, Final Rule, 01-26-04.

puncture drop tests). Of the evaluated drop scenarios, the side free drop with a subsequent puncture bar attack to the impact limiter at the same damaged area is determined to have the potential for inflicting the most damage to the thermally sensitive area of the package (i.e., the closure and/or vent/sampling port seals).

Appendix 2.12.3, *Certification Test Results*, describes the setup and damage resulting from a side free drop test on the CTU and presents photos that illustrate the level of damage incurred (see Figure 3.5-1). An approximate inward crush of 4.4 inches was observed during the free drop with a resultant final crush depth of approximately 3.5 inches after springback. In addition to the inward crush, the weld joint on the outer edge of the lid end impact limiter was split for an approximate length of 28 inches, as shown in Appendix 2.12.3, *Certification Test Results*. No other weld joint failure was noted on the remainder of the impact limiter. The actual weld joint design for the MFFP impact limiter will not fail, as discussed in Appendix 2.12.7, *Impact Limiter Weld Joint Test Results*. However, the CTU weld joint damage is included in the thermal evaluation to provide additional conservatism in the thermal model for the HAC condition.

Since the drop tests were conducted for simulated cold weather operations, the extent of damage needed to be extrapolated to the higher temperature levels within the polyurethane foam under NCT hot conditions. Figure 3.5-2 illustrates the differences in the predicted crushed depths, with the depth of the crush doubling from approximately 3.5 inches to approximately 7 inches for operations under NCT hot conditions. The foam crush is modeled explicitly by modifying the geometry of the impact limiter prior to the initiation of the HAC event to capture the extent of foam compaction associated with the flattening of the limiter. Figure 3.5-3 illustrates the revised geometry of the thermal model for the impact limiter shell to simulate the side free drop hot damage. The increase in apparent foam density in the damaged region is conservatively ignored and the thermal conductivity of the foam changes only slightly with density.

Although this assumed crush for the NCT hot condition is less that the maximum dynamic crush deflection identified in Table 2.12.1-8 of Appendix 2.12.1, *Impact Limiter Evaluation*, the assumed damage plus the additional foam loss due to the assumed weld joint failure bounds the potential increased crush distance identified in Table 2.12.1-8 of Appendix 2.12.1, *Impact Limiter Evaluation*, without weld joint failure.

The second area in which the thermal model of the impact limiter was modified addressed the physical change to the outer layer of the foam material when exposed to the elevated temperatures of the HAC event. As discussed in Section 3.5.2.2, *Performance of Rigid Polyurethane Foam Under HAC Fire Conditions*), the LAST-A-FOAM® FR-3700 material undergoes a non-linear thermal response when exposed to elevated temperatures. Little or no decomposition occurs at temperatures below 400 °F, but decomposition increases non-linearly with temperature until only about 5% of the original mass is left when a temperature of 1,500 °F is reached. However, despite this weight loss, the material does not typically 'burn away', but instead develops a char layer that has a similar thickness and which acts thermally like a layer of still gas with multiple layers of radiation planes. By modeling this layer as a pseudo 'void' space, the thermal model not only captures the thermal conductivity of the layer, it conservatively estimates the level of radiation heat transfer occurring across the depth of the char layer. This modeling approach also conservatively accounts for possibility that, under limited situations, a portion of the foam material may be carried outside of the impact limiter skin by the force of the outgas flow. Since the modeled 'void' space is actually filled with char material, neither free nor forced convection will occur.

To bound the extent of the foam material impacted by the elevated temperatures and the potential loss due to ablation of the char layer, the modeling assumes that the outer 4-inch layer of foam at the circumference of the impact limiter and a 3-inch layer of foam at the flat faces of the impact limiter are lost at the beginning of the HAC event. Figure 3.5-4 illustrates the changes to the geometry of the polyurethane foam within the impact limiter to simulate both the side free drop damage and the potential degradation of the foam under the elevated temperatures from the HAC fire event. See the discussion in Section 3.5.2.2, *Performance of Rigid Polyurethane Foam Under HAC Fire Conditions*, for additional information regarding the basis for this modeling approach..

The third type of modeling change made to the impact limiter thermal model for the HAC event captured the potential damage due to the puncture bar drop. The puncture bar drop tests demonstrated that no serious damage to the impact limiter would occur from any of the drop orientations, except for the puncture bar attack on the recessed end of the limiter (see Figure 2.12.3-11) where a tear in the plate was noted. In the event that this puncture bar damage was combined with the weld split noted from the side drop, there would be the potential for developing a 'chimney' flow of hot gases through the impact limiter during the HAC fire event. Such a scenario would further require an orientation of the impact limiter during the fire event to be such that the weld split and puncture bar tear were vertically aligned. Further, the two damaged regions would need to be located in approximately the same circumferential location on the limiter. While such a scenario is highly improbable, the thermal modeling for the HAC event evaluated the potential impact on the thermal performance of the MFFP by simulating a local region of foam lost due to ablation in the region of the 'chimney flow'. This 'chimney flow' region is simulated as an additional loss of foam over a semi-circular shaped region in the vicinity of the side impact damage (see right side of Figure 3.5-2) which leaves only approximately 1 inch of foam remaining at its apex. While in reality, this damaged area will develop over the duration of the 30-minute fire, the thermal model conservatively assumes it forms instantaneously when the fire event commences.

The scenarios for developing a chimney flow within the impact limiter with the package in the horizontal orientation were evaluated and dismissed as not being credible events. The puncture drop tests demonstrated that the puncture bar would not cause a failure in the side weld joint (see Figure 2.12.3-13) or would tear a hole in the side of the impact limiter. The opening of the meltable plugs during the fire is not sufficient to create a chimney flow based on full-scale burn tests of other NRC-licensed packages. As such, the modeling addressed the only scenario deemed plausible which would create the upper/lower openings required to initiate the formation of a chimney. Again, it should be noted that the type of weld joint failure conservatively assumed for this thermal modeling will not occur for the actual weld joint design for the MFFP impact limiter, as discussed in Appendix 2.12.7, *Impact Limiter Weld Joint Test Results.*

3.5.2.2 Performance of Rigid Polyurethane Foam Under HAC Fire Conditions

The General Plastics LAST-A-FOAM® FR-3700 polyurethane foam used in the impact limiters has been used in more than 25 radioactive materials (RAM) packages over the last 20 years. The FR-3700 formulation is specially designed to allow predictable impact-absorption performance under dynamic loading, while also providing an intumescent char layer that insulates and protects hazardous materials, even when exposed to pool-fire conditions. Upon exposure of this proprietary rigid polyurethane foam to fire temperatures, the foam degrades into an intumescent char that swells and tends to fill voids or gaps in the impact limiters created by free drop or puncture bar damage. The resultant char layer is structurally strong and will shield the underlying undamaged foam from further direct exposure to the

external high temperatures. This behavior has been observed in full-scale fire tests of other RAM packages, such as TRUPACT-II[2] and HalfPACT[3] packages.

Since the degradation of the foam under elevated temperatures is an endothermic process, the foam is self-extinguishing and will not support a flame once the external fire is removed. However, the gases generated by the degradation process are combustible and will burn under piloted conditions. Further, a portion of these generated gases could remain trapped within the charred layer of the foam for a period after the cessation of the HAC fire event and would be available to support further combustion, but at a much reduced level, until sufficient time has passed for their depletion from the cell structure.

Since the mechanisms behind the observed variations in the thermal properties and behavior of the FR-3700 foam at elevated temperatures are varied and complex, and because only a limited amount of research has occurred in this area, no definitive analytical model of the foam properties under HAC conditions exists. As such, a combination of empirical data and modeling conservatism is used to simulate the thermal performance of the LAST-A-FOAM® FR-3700 polyurethane foam for this application.

The FR-3700 product literature[4] describes the setup and results of a series of fire tests conducted on a series of 5-gallon paint cans filled with FR-3700 foam at densities from 8 to 24 pounds per cubic foot. One end of the test articles (i.e., the "hot face" surface) was subjected to an open diesel fueled burner flame at temperatures of 1,800 to 2,200 °F for 45 minutes. This flame duration is 15 minutes longer than the 30 minute HAC fire event required by 10 CFR §71.73(c)(3). A thermal shield prevented direct exposure to the burner flame by any surface of the test article other than the hot face. Each of the three test articles was instrumented with nine thermocouples. In addition, samples of the foam were subjected to thermal decomposition testing in a radiant oven. The exposure temperatures for the tests varied from 70 to 1,500 °F, and were conducted in both air and nitrogen atmospheres. A thermogravimetric analysis (TGA) was conducted to evaluate the sample weight loss as a function of temperature. These test results indicate that the following steps occur in the thermal breakdown of the foam during the HAC fire event:

- Below 500 °F, the variation in foam thermal properties with temperature are slight and reversible. As such, fixed values for specific heat and thermal conductivity are appropriate.
- Irreversible thermal degradation of the foam begins as the temperature rises above 500 °F and increases non-linearly with temperature. This degradation is accompanied by vigorous out-gassing from the foam and an indeterminate amount of internal heat generation. The internal heat generation arises from the gases generated by the degradation process that are combustible under piloted conditions. However, since the decomposition process is exothermic, the foam will not support combustion indefinitely and further, the out-gassing process removes a significant amount of heat itself via mass transport.

---

[2] U.S Department of Energy (DOE), *Safety Analysis Report for the TRUPACT-II Shipping Package*, USNRC Docket No. 71-9218, U.S. Department of Energy, Carlsbad Field Office, Carlsbad, New Mexico.

[3] U.S Department of Energy (DOE), *Safety Analysis Report for the HalfPACT Shipping Package*, USNRC Docket No. 71-9279, U.S. Department of Energy, Carlsbad Field Office, Carlsbad, New Mexico.

[4] *LAST-A-FOAM FR-3700 for Crash and Fire Protection of Nuclear Material Shipping Containers,* General Plastics Manufacturing Company, Tacoma, WA.

- The weight loss due to out-gassing not only has direct affect on the heat flux into the remaining virgin foam, but changes the composition of the resulting foam char since the foam constituents are lost at different rates. This change in composition affects both the specific heat and the thermal conductivity of the foam char layer.
- As temperature continues to rise, the developing char layer begins to take on the characteristics of a gas-filled cellular structure where radiative interchange from one cell surface to another becomes a significant portion of the overall heat transfer mechanism. This change in the dominant heat transfer mechanism causes the apparent heat conductivity to take on a highly non-linear relationship with temperature.
- Finally, at temperatures above 1,250 °F, the thermal breakdown of the foam is essentially completed and only about 5 to 10% of the original mass is left. In the absence of direct exposure to a flame or erosion by the channeling of the outgas products through the foam, the char layer will be the same or slightly thicker than the original foam depth. This char layer will continue to provide radiative shielding to the underlying foam material.

Given the observed non-linear variations in the thermal properties and behavior of the FR-3700 foam at elevated temperatures, a thermal modeling method was devised to conservatively simulate the decomposition behavior of the foam during the HAC fire event. As discussed above, the foam begins an irreversible decomposition process at approximately 500 °F, and reaches a stable char at temperatures in excess of 1,250 °F. The decomposition wave front begins at the outer layer and progresses inward with time. The final depth of the char is a function of the foam density and the fire temperature and duration. This decomposition process is conservatively modeled by transforming a thickness of foam equal to the expected final char depth into still air at the beginning of the fire and simulating conduction and radiation across this air-filled 'void' from the hot impact limiter shell to the remaining foam surface. Since the char material would normally completely fill this void and severely restrict the radiative heat transfer mode (the dominant mode at fire temperatures), this approach is conservative.

The depth of the final char thickness which can be expected for the 10 lb_m/ft^3 density foam used in the top end impact limiter is estimated from a table provided in the FR-3700 product literature[4], under the section entitled *Fire Protection*, which lists the temperatures obtained from laboratory fire tests. The test specimen was a 5-gallon metal pail filled with the foam material at various densities, and instrumented with thermocouples at specified depths from the top surface. The pail was completely filled with foam and fitted with a metal lid and a burner flame was applied to the lid end of the pail (i.e., the *hot face* or H.F.). The top three rows of the table lists the temperatures achieved at various depths in the foam for 8, 16, and 24 lb_m/ft^3 density after an elapsed time of 30 minutes[5], and the maximum temperature reached at each depth. As can be noted from the temperatures achieved at the hot face, the flame temperatures in the tests are considerably hotter than the regulatory fire temperature of 1,475 °F. Therefore, in order to render the data in the table consistent with a regulatory flame temperature of 1,475 °F, the test results were proportionately reduced as a function of depth and an assumed hot face temperature of 1,475 °F. For example, for 8 lb_m/ft^3 foam at zero depth (i.e., the hot face), the temperature was reduced to 1,475 °F, while at the 1-inch depth the temperature after 30 minutes was reduced to

[5] The lower three rows present data for foam with a cover layer of ceramic fiber insulation which is not used in this application and, therefore, not included this discussion.

960 °F. Repeating this process at increasing depths, the temperature was reduced by lesser amounts, until at a depth of 6 inches (where there was no temperature response after 30 minutes) the correction is zero.

The resulting predicted thermal response of the foam for regulatory fire conditions is illustrated in Figure 3.5-5. The figure illustrates the estimated corrected curves for the regulatory flame temperature of 1,475 °F for 8 and 16 lb_m/ft^3 density foam. Curves for 10, 12, and 14 lb_m/ft^3 density foams are found by linear interpolation. It should also be noted that this procedure conservatively ignores the non-linear effect of radiation heat transfer wherein the rate of heat transfer to the hot face from the flame would not scale linearly as assumed here, but would scale with the absolute temperature to the fourth power. As such, had this effect been properly accounted for, the actual foam temperatures would be even lower since the heat available to decompose the foam would be significantly lower that assumed by this approach.

Based on the results presented in Figure 3.5-5, the 10 lb_m/ft^3 foam is predicted to reach approximately 500 °F at a depth of 3 inches after 30 minutes and that the foam temperature at a depth of approximately 4.5 inches would not have responded at all. Given that a temperature of 500 °F represents the point where irreversible foam decomposition occurs, the result indicates that the char depth for 10 lb_m/ft^3 foam would be 3 inches after 30 minutes of exposure to a 1,475 °F regulatory fire.

Therefore, the performance of the LAST-A-FOAM® FR-3700 during the HAC event is analytically simulated for this application by reducing the depth of foam at each location to conservatively bound the potential loss of the foam from any of the various mechanisms described above. The heat transfer across the resultant void space is then computed based on conduction and radiation across an equivalent air space, despite the fact that the affected foam will typically be simply decomposed to a char layer as opposed to being lost altogether. By removing the foam at the start of the HAC fire transient and by treating the affected foam as a void space for the purposes of computing the radiation heat transfer across the char layer, the modeling conservatively bounds the temperature response of the package to the transient loss of the foam over the time period of the HAC event and the potential loss of a portion of the char layer due to ablation. Specifically, the modeling assumes that the outer 4-inch layer of foam at the circumference of the impact limiter and a 3-inch layer of foam at the flat faces of the impact limiter are lost at the beginning of the HAC event.

3.5.3 Maximum Temperatures and Pressures

3.5.3.1 Maximum Temperatures

Table 3.5-1 provides a summary of pre-fire, steady-state temperatures, the temperatures at the end of the 30-minute fire event, and the peak temperatures achieved during the subsequent package cooldown. Figure 3.5-6 illustrates the associated temperature distribution within the MFFP at the end of the 30-minute fire. As noted from Table 3.5-1, the peak temperatures for the critical components (e.g., closure and vent port O-ring seals, peak MOX FAs, boral, etc.) are all within their respective allowable limits.

The peak MOX FA temperature achieved during the HAC event is 786 °F below the allowable short-term limit of 1,337 °F. The strongback and the FCSs effectively shield the FAs from direct exposure to the hot surfaces of the body shell. The peak temperature of 713 °F noted for the boral neutron absorbing material is well below the allowable short-term limit of 1,000 °F.

Although the body shell temperature reaches a peak temperature of 1,407 °F during the HAC event, the time at temperature levels over 1,000 °F is less than 30 minutes (see Figure 3.5-9). As such, no significant permanent loss in material structural properties is expected. In contrast, the body collar and closure lid, which are shielded by the impact limiter structure despite the assumed damage conditions, remain below 500 °F throughout the HAC transient. Figure 3.5-7 illustrates the temperature distribution in the body shell at the end of the 30-minute fire when the peak shell temperature is achieved, while Figure 3.5-8 illustrates the temperature distribution in the shell approximately 2 hours after the end of the 30-minute fire when the peak temperatures at the closure lid bolts is reached.

The peak butyl O-ring seal temperature of 352 °F seen for the closure seal is below the conservatively established short-term limit of 400 °F for exposures of 8 hours or less. The peak vent/sampling port O-ring temperatures are predicted to be 305 °F. As the temperature trends presented in Figure 3.5-10 illustrates, not only are the peak O-ring seal temperatures below the allowable short-term limit of 400 °F, but the transient O-ring seal temperatures demonstrate that the temperature trend for the material complies with the time at temperature limitations defined in Section 3.2, *Material Properties and Component Specifications.*

Figure 3.5-9 and Figure 3.5-10 illustrate the transient temperature response during the simulated HAC event for selected package components.

3.5.3.2 Maximum Pressures

With the exception of the consideration for potential out-gassing from components within the body cavity and an assumed 100% failure rate[6] for the MOX fuel rods, the maximum pressure attained for HAC conditions is determined in the same manner as described in Section 3.4.2, *Maximum Normal Operating Pressure*. While the MFFP is designed to protect the MOX FA from catastrophic failure during the pre-fire free and puncture drops and the subsequent 30-minute fire event, this analysis conservatively assumes that the cladding boundary on all fuel rods and poison rods within the MOX FA have been breached. As determined in Section 3.4.2, *Maximum Normal Operating Pressure*, a total of 22.64 g-moles of helium gas exists within the fuel rods of the three (3) MOX FAs within the package.

Further, it is conservatively assumed that the entire mass of the neoprene rubber and the Delrin® plastic pads have been volatized under the elevated temperatures reached within the body cavity during the HAC event. There are approximately 7 pounds of neoprene rubber and 2.3 pounds of Delrin® plastic in the body cavity. Volatizing this entire mass would create approximately 143.1 g-moles of gas within the cavity.

Table 3.5-2 presents the predicted pressure within the body cavity prior to the HAC fire, at the end of the 30-minute fire, and 9.5 hours after the end of the fire. As seen, the peak pressure generated within the package cavity is estimated to be 142.4 psia at the end of the fire when the peak cavity gas temperature is reached. The pressure will then decrease as the package cools, reaching 76.9 psia 9.5 hours after the end of the fire.

---

[6] U. S. Nuclear Regulatory Commission, NUREG-1617, Table 4-1, *Standard Review Plan for Transportation Packages for Spent Fuel*, March 2000.

3.5.4 Accident Conditions for Fissile Material Packages for Air Transport

This section does not apply for the MFFP, since air transport is not claimed.

3.5.5 Evaluation of Package Performance for Accident Conditions of Transport

The evaluation of the package performance under HAC conditions demonstrates that the packaging will have sufficient thermal protection remaining after the hypothetical drop and puncture bar damage to protect the thermally sensitive areas of the packaging. All package components are seen as remaining within their associated maximum temperature limits.

Table 3.5-1 - HAC Temperatures

Location	Temperature (°F)			
	Pre-fire Steady-state	End Of 30 Minute Fire	HAC Peaks	Maximum Allowable
Peak MOX FA	179	468	551	1,337
Avg. MOX FA	130	250	298	1,337
Poison On Strongback	134	438	525	1,000
Poison On Fuel Box Enclosure	133	703	713	1,000
Strongback Structure	134	617	646	800
Body Shell	110	1,407	1,407	2,500
Body Collar	109	341	432	1,000
Closure Lid	109	181	311	1,000
Impact Limiter Lugs	108	1,330	1,330	2,500
Impact Limiter				
• Max. Foam	107	N/A	N/A	N/A
• Bulk Avg. Foam	101	N/A	N/A	N/A
• Skin	107	1,474	1,474	2,500
Impact Limiter Bolts				
• Bolt Head	107	1,319	1,319	2,500
• Bolt Shaft	106	961	961	2,500
• Bolt Threads	107	238	306	2,500
O-ring Seals				
• Closure Lid	110	208	352	400
• Vent/Sampling Port	108	150	305	400
Bulk Avg. Fill Gas	121	807	807	--

Notes:

① Pre-fire steady-state conditions taken from Table 3.4-1 for 'NCT Hot without Insolation'.

② See Section 3.2, *Material Properties and Component Specifications*, for basis for 'Maximum Allowable' temperatures.

Table 3.5-2 – Package HAC Internal Pressures

Parameter	Pre-fire Steady-State	End Of 30-Minute Fire	9.5 Hours After Fire
Bulk Avg. Fill Gas Temperature	121 °F	807 °F	225 °F
Quantity of Package Fill Gas	54.3 g-moles	54.3 g-moles	54.3 g-moles
Gas From Failed FA Rods	0.68 g-moles	22.64 g-moles	22.64 g-moles
Gas From Component Outgassing	0 g-moles	143.1 g-moles	143.1 g-moles
Internal Cavity Pressure	16.3 psia (1.6 psig)	142.4 psia (127.7 psig)	76.9 psia (62.2 psig)

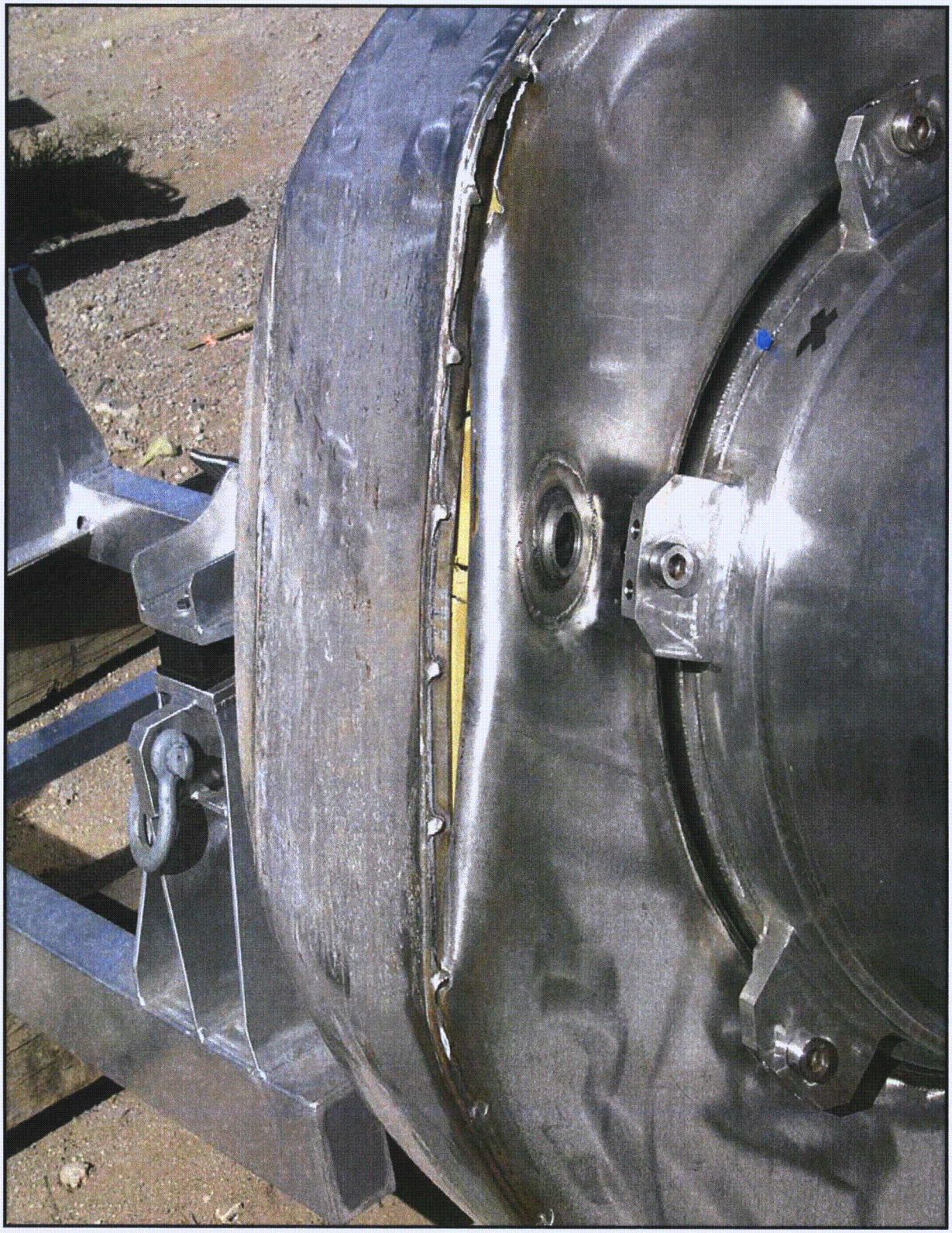

Figure 3.5-1 – CTU Impact Limiter Damage from Full-Scale Side 30-ft Free Drop Test

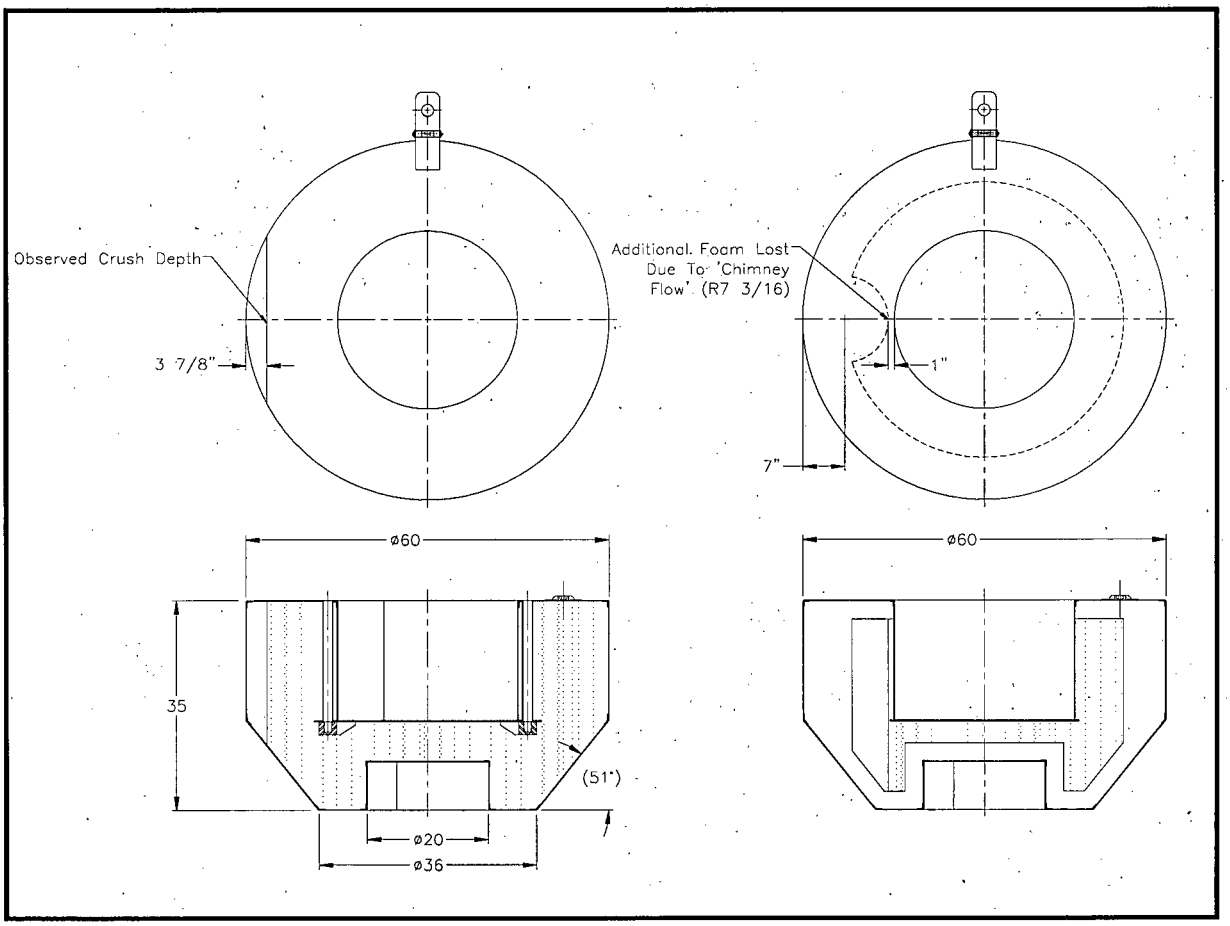

(Note: Observed impact limiter damage from drop test on left and simulated damaged impact limiter for warm weather conditions on right)

Figure 3.5-2 – Projected Side Drop Damage to Impact Limiter

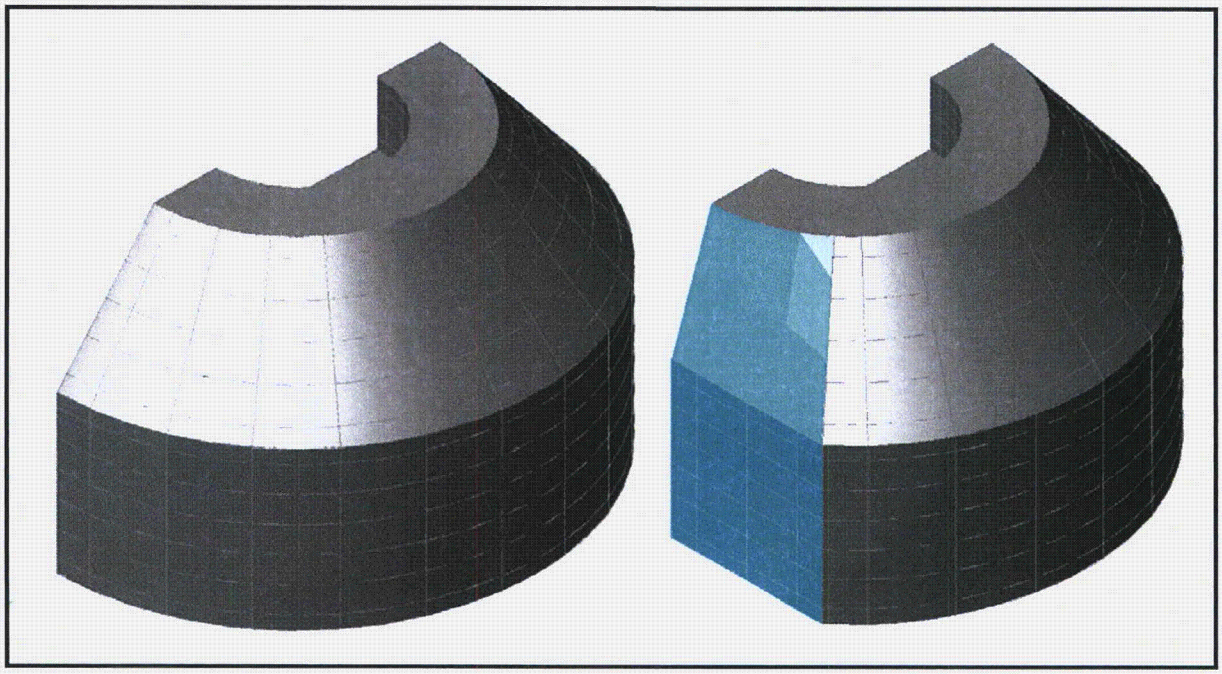

(Note: Undamaged impact limiter from NCT model on left and simulated damaged impact limiter for HAC modeling on right)

Figure 3.5-3 – Illustration of Modification to Impact Limiter Geometry to Reflect Side Drop Damage

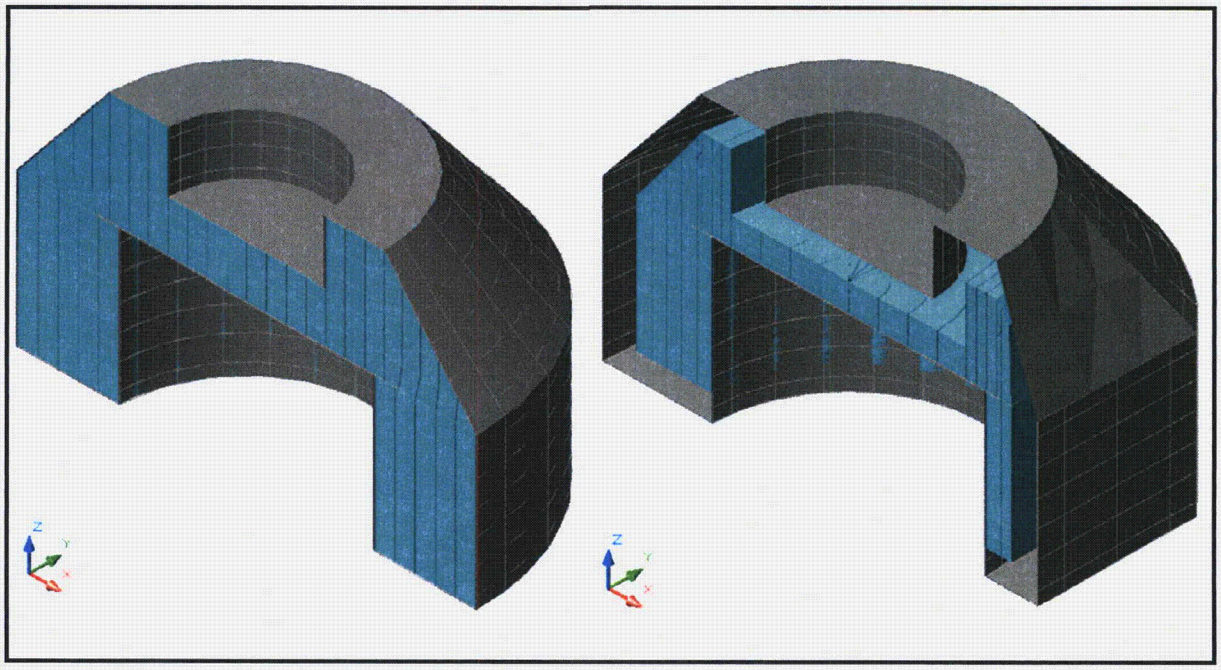

(Note: Undamaged foam geometry from NCT model on left and simulated damaged foam geometry for HAC modeling on right)

Figure 3.5-4 – Illustration of Foam Geometry Modification to Reflect Potential Loss During HAC Event

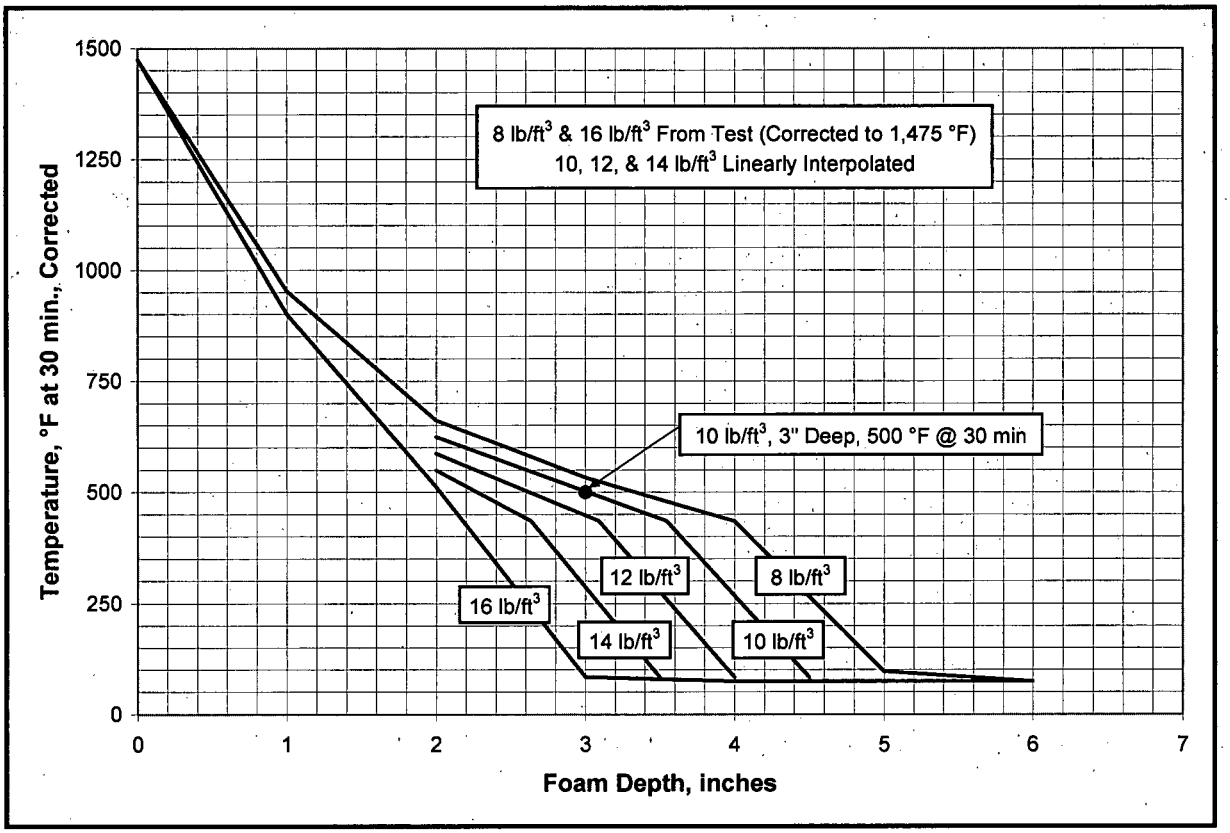

Figure 3.5-5 – Predicted Foam Temperature Response to Regulatory Fire After 30 Minutes

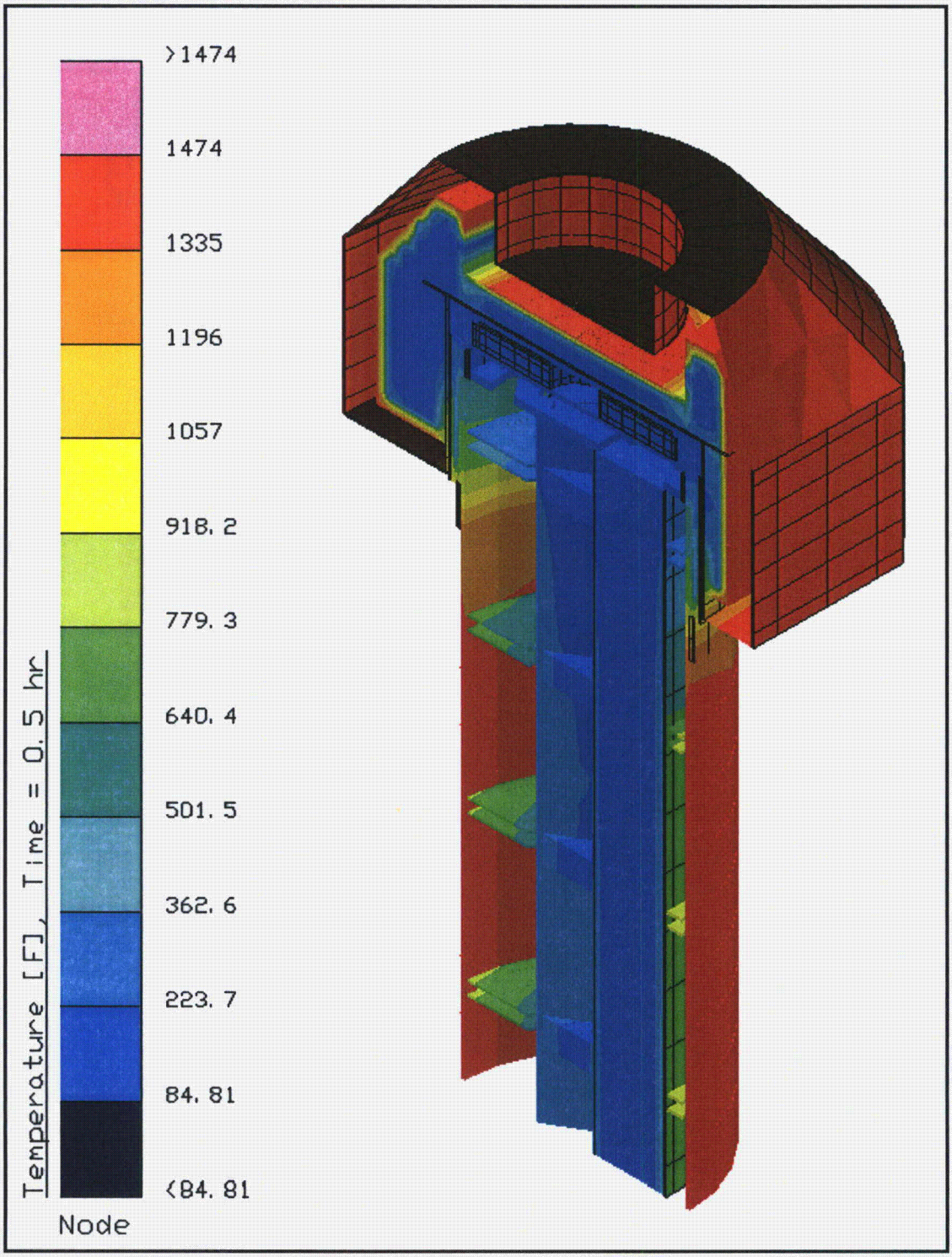

Figure 3.5-6 – Temperature Distribution within MFFP at End of 30-Minute Fire Event

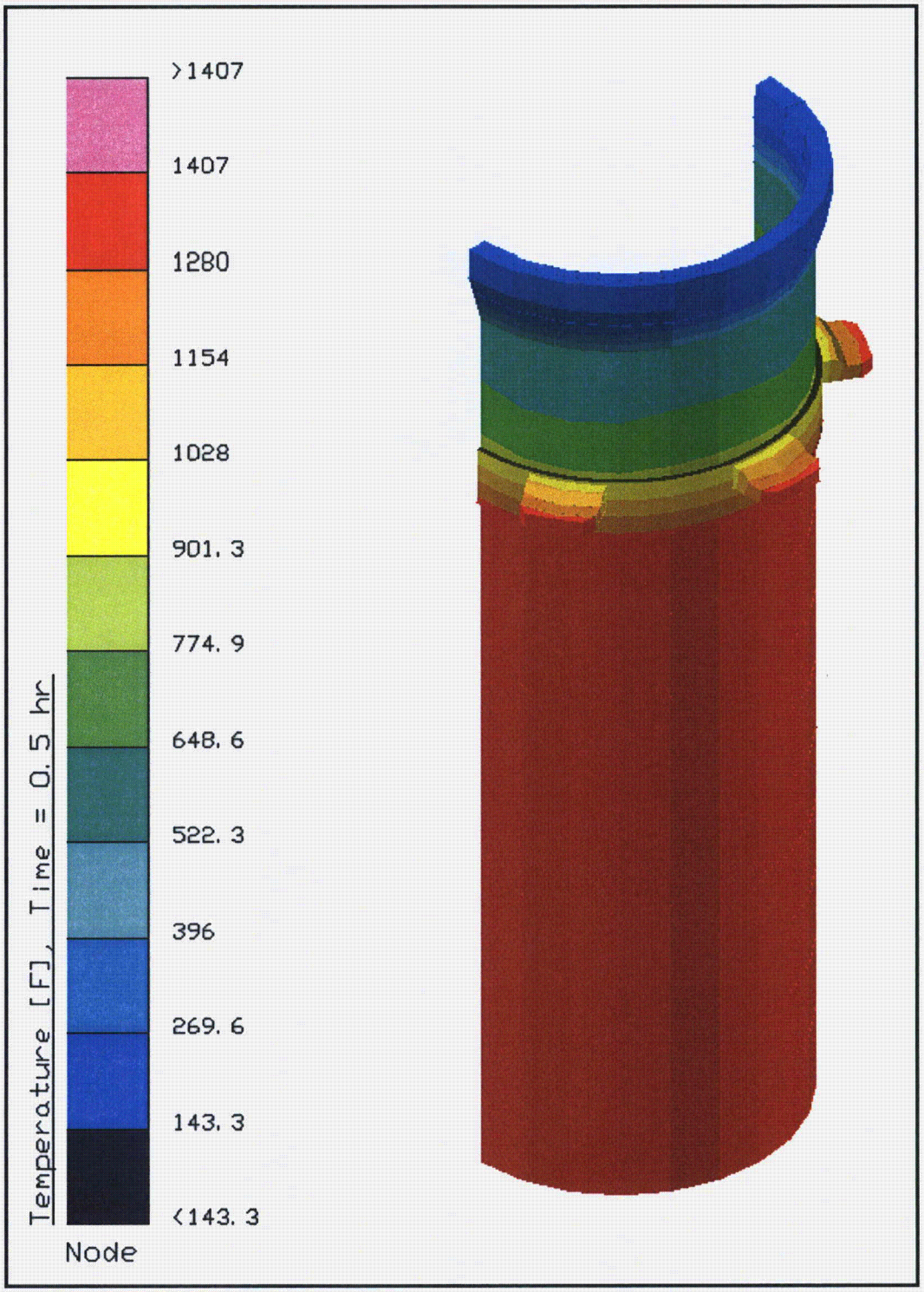

Figure 3.5-7 – Body Shell Temperature Distribution at End of 30-Minute Fire Event

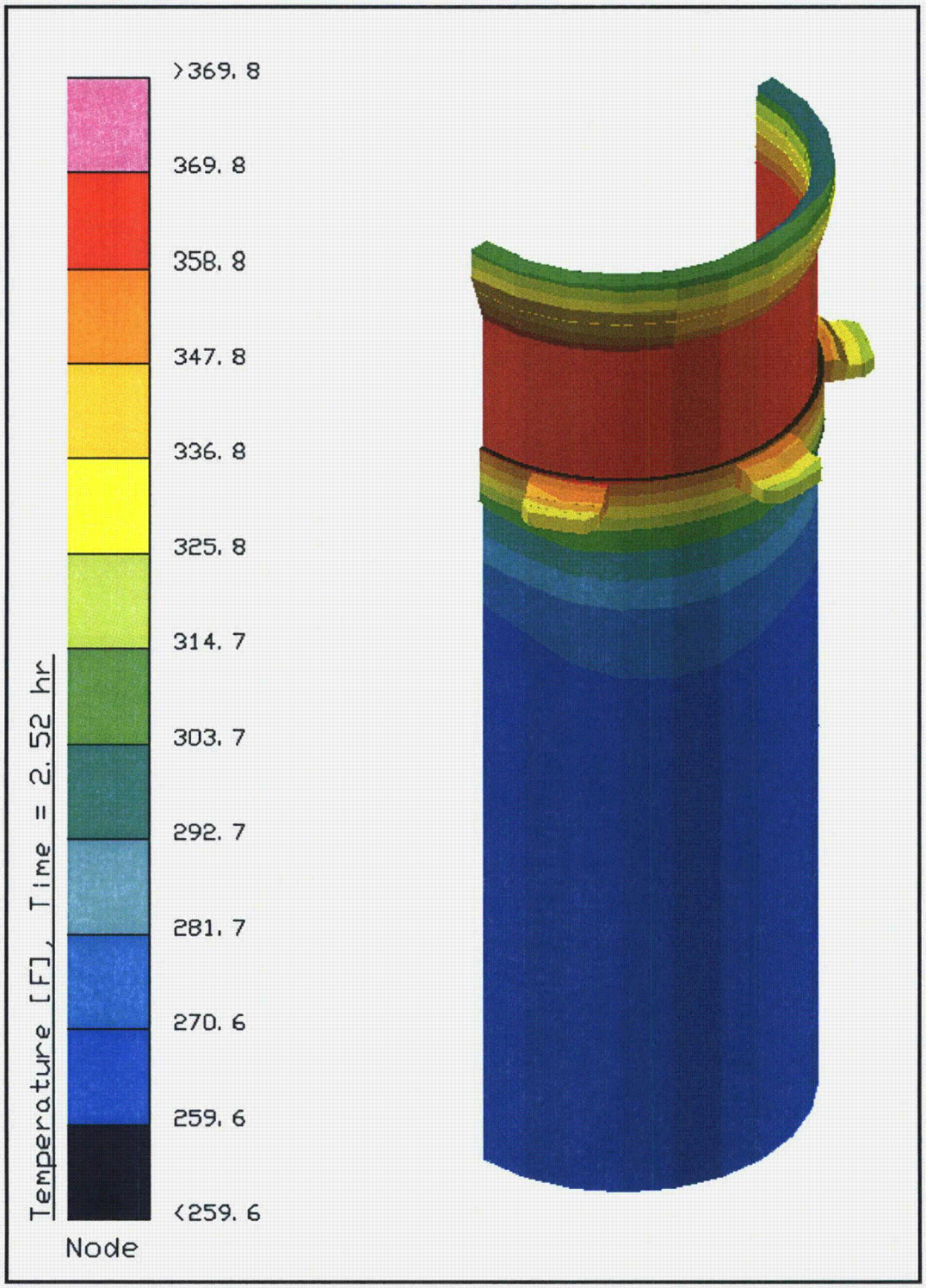

Figure 3.5-8 – Body Shell Temperature Distribution 2 Hours After End of Fire Event

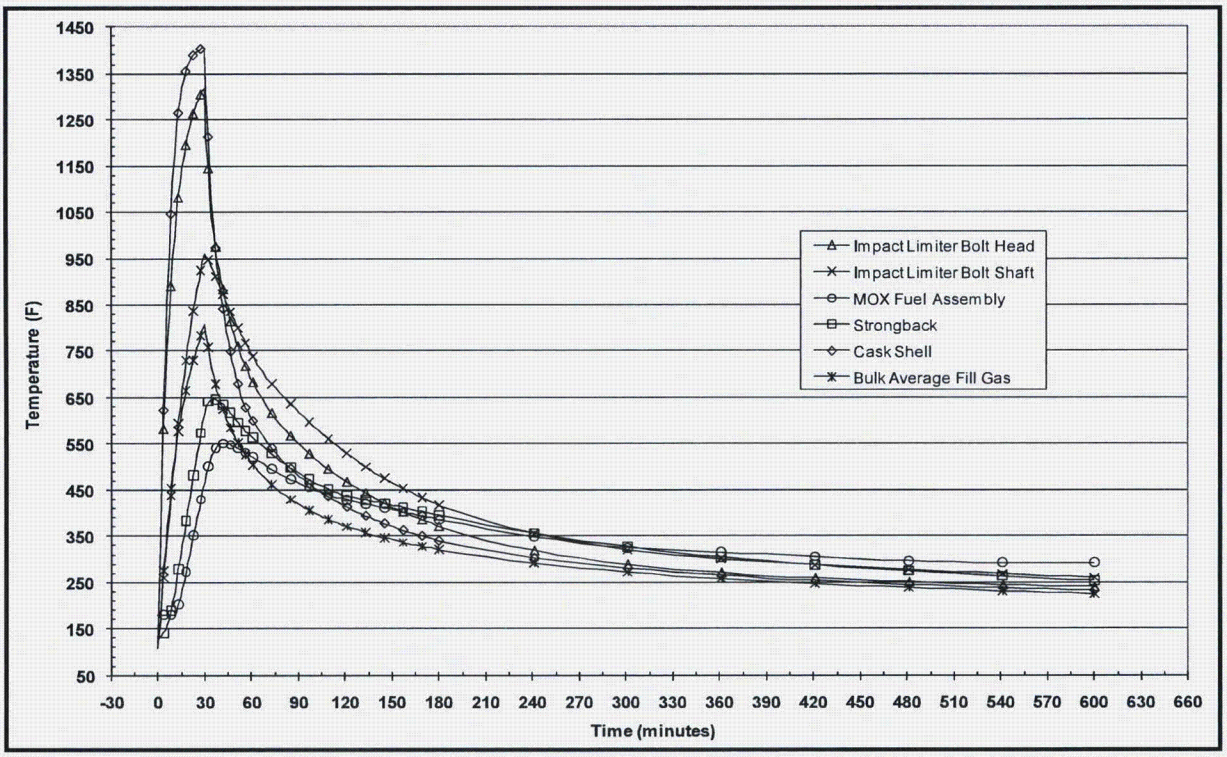

Figure 3.5-9 – HAC Temperature Transient for Selected MFFP Components

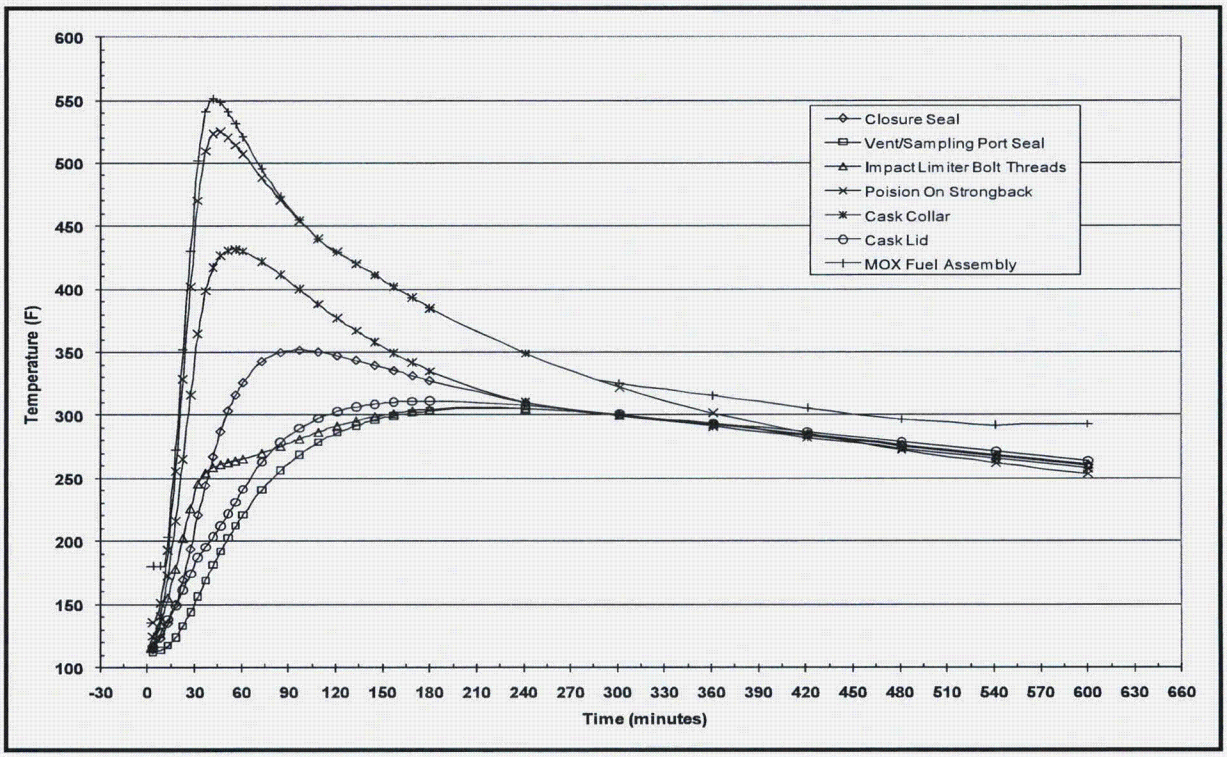

Figure 3.5-10 – HAC Temperature Transient for Additional MFFP Components

3.6 Appendices

3.6.1 Computer Analysis Results

3.6.2 Thermal Model Details

This page intentionally left blank.

3.6.1 Computer Analysis Results

Due to the size and number of the output files associated with each analyzed condition, results from the computer analysis are provided on a CD-ROM.

This page left intentionally blank.

3.6.2 Thermal Model Details

3.6.2.1 Convection Coefficient Calculation

The evaluation of the thermal performance of the MFFP over the wide range of potential operating conditions encountered during NCT and HAC conditions is based on semi-empirical relationships for convection heat transfer. The convective heat transfer coefficient, h_c, has a form of:

$$h_c = Nu\frac{k}{L}$$

where k is the thermal conductivity of the gas at the mean film temperature and L is the characteristic length of the vertical or horizontal surface. These semi-empirical relationships are chosen to account for the variation in convection heat transfer rates between laminar and turbulent operating conditions and for the shape and orientation of the specific surface experiencing convective heat transfer. The specific relationships used for this analysis are discussed below. Rohsenow, Hartnett, and Ganic, *Handbook of Heat Transfer Fundamentals*, 2nd edition, McGraw-Hill Publishers, 1973.

Natural convection from vertical surfaces is computed using Equations 6-39 to 6-42 of Rohsenow, et. al.[26], where the characteristic length is the height of the surface. These equations, which are applicable over the range of Rayleigh number (Ra) between 1 and 10^{12}, are as follows:

$$Nu^T = \overline{C}_L Ra^{1/4}$$

$$\overline{C}_l = \frac{4}{3}\left[\frac{0.503}{\left(1+(0.492/Pr)^{9/16}\right)^{4/9}}\right]$$

$$Nu_L = \frac{2.8}{\ln\left(1+2.8/Nu^T\right)}$$

$$Nu_t = C_t^V Ra^{1/3}$$

$$C_t^V = \frac{0.13\,Pr^{0.22}}{\left(1+0.61\,Pr^{0.81}\right)^{0.42}}$$

$$Nu = \frac{h_c L}{k} = \left[(Nu_L)^6 + (Nu_t)^6\right]^{1/6}$$

$$Ra_L = \frac{\rho^2 g_c \beta L^3 \Delta T}{\mu^2} \times Pr$$

where:

h_c = convection coefficient Nu = Nusselt number

[26] Rohsenow, Hartnett, and Ganic, *Handbook of Heat Transfer Fundamentals*, 2nd edition, McGraw-Hill Publishers, 1973.

g_c = gravitational acceleration
ΔT = temperature difference
μ = dynamic viscosity
L = characteristic length
Ra = Rayleigh number
β = coefficient of thermal expansion
ρ = density of air at the film temperature
Pr = Prandtl number
k = thermal conductivity of air at the mean film temperature
h_c = convection coefficient

Note that k, c_p, and μ are each a function of air temperature as taken from Table 3.2-6. Values for ρ are computed using the ideal gas law, β for an ideal gas is simply the inverse of the absolute temperature of the gas, and Pr is computed using the values for k, c_p, and μ from Table 3.2-6. Unit conversion factors are used as required to reconcile the units for the various properties used.

Calculation of the convection coefficient between horizontal, cylinders (i.e., the body shell and portions of the impact limiter) and the ambient environment is computed using Equation 3-43, Chapter 1, from Guyer[27]. The characteristic length, D, is the outer diameter of the cylinder. This equation, applicable for $10^{-5} < Ra < 10^{12}$, is as follows:

$$Nu = \frac{h_c D}{k} = \left\{ 0.60 + \frac{0.387 Ra_D^{1/6}}{\left[1 + (0.559/Pr)^{9/16}\right]^{8/27}} \right\}^2$$

Natural convection from horizontal surfaces is computed from Equations 4.39 and 4.40 of Rohsenow, et. al.[28] where the characteristic dimension (L) is equal to the plate surface area divided by the plate perimeter. For a heated surface facing upwards or a cooled surface facing downwards and Ra > 1:

$$Nu = \frac{h_c L}{k} = \left[(Nu_L)^{10} + (Nu_t)^{10} \right]^{1/10}$$

$$Nu_L = \frac{1.4}{\ln\left(1 + 1.677/\left(\overline{C_L} Ra^{1/4}\right)\right)}$$

$$\overline{C_L} = \frac{0.671}{\left[1 + (0.492/Pr)^{9/16}\right]^{4/9}}$$

$$Nu_t = 0.14 Ra^{1/3}$$

For a heated surface facing downwards or a cooled surface facing upwards and $10^3 < Ra < 10^{10}$, the correlation is as follows:

$$Nu = Nu_L = \frac{2.5}{\ln\left(1 + 2.5/Nu^T\right)} \qquad Nu^T = \frac{0.527}{\left(1 + (1.9/Pr)^{9/10}\right)^{2/9}} Ra^{1/5}$$

[27] Guyer, E.C., *Handbook of Applied Thermal Design*, McGraw-Hill, Inc., 1989.

[28] Rohsenow, Hartnett, and Choi, *Handbook of Heat Transfer*, 3rd edition, McGraw-Hill Publishers, 1998.

3.6.2.2 Effective Thermal Conductivity of MOX Fuel Assemblies

3.6.2.2.1 Purpose

The thermal analysis of the MFFP presented in Sections 3.4, *Thermal Evaluation for Normal Conditions of Transport*, and 3.5, *Thermal Evaluation Under Hypothetical Accident Conditions* models the zirconium alloy clad fuel assemblies as homogeneous solid regions with uniform internal heat generation. In order to accurately predict the temperature rise from the enclosing walls of the strongback assembly to the peak rod location within each fuel assembly using this type of modeling the effective thermal conductivity of the homogeneous solid region must be determined. The effective thermal conductivity calculation accounts for the actual geometry of the fuel assembly and the fact that the heat generation occurs only within the fuel rods.

3.6.2.2.2 Assumptions

1. Table 3.6-1 presents a summary of the relevant design information for the MOX FAs, including portions extracted from Table 1.2-1 of Section 1.2.3, *Contents of Packaging*, and Table 6.2-1 and Table 6.2-3 of Section 6.2, *Fissile Material Contents*.
2. The fuel assemblies are centered within each strongback enclosure.
3. The zirconium alloy cladding is assumed to have a conservatively low emissivity value[29] of 0.16.
4. Per Section 3.2, *Material Properties and Component Specifications*, the boral surfaces within fuel control structures (FCSs) around the fuel assemblies have an emissivity of 0.15, while the stainless steel surfaces have an emissivity of 0.2.
5. A decay heat loading of 80 watts is uniformly distributed over the 144-inch active fuel length.
6. Heat transfer from the assembly to the guide sleeve is via radiation and conduction only.
7. The dimension between the inner surfaces of the FCSs is assumed to be 8.887 inch dimension, based on a preliminary design of the FCS. Although this dimension is 3/16 inches larger than the actual 8.7 inch inside dimension of the FCS, the additional thermal resistance within the FAs associated with the larger dimension is insignificant, but conservatively bounds (i.e., is higher than) the value associated with the actual 8.7-inch dimension.

3.6.2.2.3 Methodology

The analysis methodology used for this calculation is based on the calculation approach outlined in Section 3.2.2 of Report BBA000000-01717-5705-00010[30]. One quarter of the MOX FA and the surrounding strongback walls are modeled. The boundaries formed by the strongback enclosure

---

[29] Murphy, E. V. and Havelock, F., *Emissivity of Zirconium Alloys In Air In The Temperature Range 100-400 °C*, Journal of Nuclear Materials, Volume 60, 1976, pp. 167-176.

[30] "*Spent Nuclear Fuel Effective Thermal Conductivity Report*", prepared TRW Environmental Safety Systems, Inc. for DOE Civilian Radioactive Waste Management System (CRWMS), Report BBA000000-01717-5705-00010, Rev. 0, July 1996.

are set to specified temperature levels for the purposes of this calculation, while symmetry conditions are assumed at the remaining two boundaries. The Thermal Desktop®[31] and SINDA/FLUINT[32] computer programs were used to develop and exercise this detailed thermal model of the fuel assembly. Figure 3.6-1 presents a perspective view of the modeled fuel assembly and strongback wall segment, while Figure 3.6-2 illustrates the finite element modeling used.

The interior of the MFFP is to be filled with air with heat transfer across the interior void volume of the MOX FA via radiation and conduction. Heat transfer across the interiors of the various fuel rods is via conduction through the MOX pellet. While a gap may exist between the cladding and the fuel pellet, the associated ΔT is assumed to be negligible since the size of the gap is small and since the level of decay heat is also low. Further, other analyses have shown the resistance due to this gap has an insignificant effect on the radial heat transfer within the fuel assembly.

Table 3.6-2 presents the component thermal conductivity values assumed for the thermal modeling. Since the analysis is conducted using a series of steady-state simulations, values for density and specific heat are not required.

The design volumetric heat loading used for the MOX FA is as follows:

$$\text{Design volumetric heat load} = \left[\frac{(\text{Decay Heat per Assembly}) \times (\text{Peaking Factor})}{(\text{No. of fuel rods}) \times (\text{Volume per rod})} \right]$$

$$\begin{aligned}\text{Volume per rod} &= \text{Active Fuel Length} \times \pi \times (\text{Fuel rod OD} - 2 \times \text{Cladding Thickness})^2 / 4 \\ &= 144" \times \pi \times (0.374 - 2 \times 0.0225)^2 / 4 \\ &= 12.241769 \text{ in}^3\end{aligned}$$

$$\begin{aligned}\text{Design volumetric heat load w/ 80 W} &= \left[\frac{(80 \text{ watts}) \times (1.00)}{(264) \times (12.241769 \text{ in}^3)} \right] \\ &= 0.0247538 \text{ watts/in}^3\end{aligned}$$

3.6.2.2.4 Effective Thermal Conductivity Calculations

The thermal model described above was exercised for boundary temperature levels (i.e., -40, 0, 50, 100, 150, 200, 275, 350, 425, 500, 575, 650, and 725°F). Figure 3.6-3 presents a representative illustration of the computed temperature distribution within the MOX FA, with the illustrated case being for a boundary temperature of 150 °F. The resulting peak temperatures computed for the fuel assembly are presented in Table 3.6-3. In accordance with the development of the equation for effective conductivity of the SAND90-2406 report[33] (i.e., see page II-127 and equation 6.1-5), the effective thermal conductivity is computed as:

---

[31] Thermal Desktop®, Version 4.5 & 5.1, Cullimore & Ring Technologies, Inc., Littleton, CO, 2002 and 2007.

[32] SINDA/FLUINT, Systems Improved Numerical Differencing Analyzer and Fluid Integrator, Version 4.5 & 5.1, Cullimore & Ring Technologies, Inc., Littleton, CO, 2002 & 2007.

[33] SAND90-2406, Sanders, T. L., et al., *A Method for Determining the Spent-Fuel Contribution to Transport Cask Containment Requirements*, TTC-1019, UC-820, November 1992.

$$k_{effective} = \left[\frac{0.29468 \times \text{Volumetric Heat Generation Based On Assembly Width} \times \left(\frac{\text{Assembly Width}}{2} \right)^2}{(T_{peak} - T_{sleeve})} \right]$$

This equation can be restated as:

$$k_{effective} = \left[\frac{0.29468 \times \text{Decay Heat Loading For Modeled Section} \times 4}{4 \times \text{Length of Modeled Segment} \times (T_{peak} - T_{sleeve})} \right]$$

The decay heat loading computed from the model, the length of the modeled segment (i.e., 1.0 inches high), and the noted peak temperature and boundary sleeve temperature are substituted to yield the computed effective thermal conductivity. Table 3.6-3 presents the computed effective thermal conductivity for the MOX FA heat load and boundary temperature. As expected, the Report BBA000000-01717-5705-00010 values, which assume a fuel cladding emissivity of 0.8, are close to those predicted for the MOX FA at low temperatures where conduction dominates, but diverge from the computed MOX effective conductivity values at high temperatures where heat transfer via radiation dominates.

For use in finite element modeling, Section 6.2.2 of Report BBA000000-01717-5705-00010[30] recommends that the effective thermal conductivity values be made a function of the mean assembly temperature, or $(T_{peak} - T_{sleeve})/2$. Figure 3.6-4 illustrates the correlation between the computed effective thermal conductivity and the median assembly temperature.

The axial heat transfer within the fuel assembly is assumed to be limited to that which will occur within the cladding of the fuel rods only. This approach is based on the conservative assumption that gaps between the individual fuel pellets will limit the axial heat transfer rate between the individual pellets. The axial thermal conductivity values presented in Table 3.2-4 use the fuel rod geometry and number of fuel rods for MOX FA and the cross-sectional area of the fuel region to account for the fact that the fuel assemblies are treated as homogenized regions within this modeling. For example, at a temperature of 260 °F, the effective axial conductivity is computed as:

$$k_{axial\ direction} = 264\ pins \times \frac{\pi}{4}\left(0.374"^2 - (0.374" - 2 \times 0.0225")^2\right) \times 0.2255 \frac{Btu}{hr - in - {}^{o}F} \div (8.887" \times 8.887")$$

$$k_{axial\ direction} = 0.01873 \frac{Btu}{hr - in - {}^{o}F} @ 260^{\circ}F$$

Table 3.6-1 – Summary of Design Data for MOX FA

Parameter	Value
Number of fuel rods	264
Number of guide tubes	24
Number of instrument tubes	1
Parameter	**Inches**
Pellet diameter	0.3225
Active fuel length	144
Cladding thickness	0.023
Fuel rod OD	0.374
Fuel rod pitch	0.496
Poison rod tube OD	0.381
Poison rod tube thickness	0.0255
Guide tube OD	0.482
Guide tube thickness	0.016

Table 3.6-2 – Thermal Properties for Effective Fuel Conductivity Calculation

Temperature (°F)	Conductivity (BTU/hr-in-°F)
Zirconium Alloy Cladding[34,35,36]	
32	0.8442
100	0.8404
200	0.8373
300	0.8380
400	0.8421
500	0.8500
600	0.8609
700	0.8756
800	0.8940
1000	0.9407
MOX Pellet[37]	
46	0.2559
80	0.2552
260	0.2255
440	0.2027
620	0.1846
800	0.1709
980	0.1628
1160	0.1597
Type 304 Stainless Steel - See Table 3.2-1	
Air - See Table 3.2-6	

[34] Peletsky V. E. and Musayeva, Z. A., *Effect Of Oxidation On Transport Properties of Zirconium - 1% Niobium Alloy*, International Journal Of Thermophysics, Vol. 16, Number 6, 1995, pp 1481 –1487.

[35] Peletsky V. E. and Petrova, I. L., *Investigation Of The Thermophysical Properties of The Alloy Zr - 1% NbBy A Subsecond Pulse Heating Technique*, High Temperatures - High Pressures, 1997, Volume 29, pp 373 –378.

[36] Lusternik, V. E., Peletsky V. E., and Petrova, I. L., *High Temperature Calorimetric Measurements of Zr - 1% Nb Alloy At Various Rates Of Heating*, High Temperatures - High Pressures, 1993, Volume 25, pp 539 –543.

[37] Van Craeynest, J. C. and Stora, J. P. *Effet del la porosite' sur la variation de la conductibilite' thermique de bioxyde d'uranium en foncitionde la temperature*, Journal of Nuclear Materials, Volume 37, 1970, pp. 153-158.

Table 3.6-3 – Computed MOX Effective Thermal Conductivity

Decay Heat (W)	Sleeve Temperature (°F)	Peak Temperature (°F)	Medium Assembly Temperature (°F)	Effective Thermal Conductivity (Btu/hr-in-°F)
80	-40	17.5	-11.3	0.00237
	0	53.1	26.6	0.00256
	50	98.4	74.2	0.00281
	100	144.5	122.3	0.00306
	150	191	170.5	0.00332
	200	238	219.0	0.00358
	275	309.1	292.1	0.00399
	350	380.8	365.4	0.00442
	425	452.9	439.0	0.00488
	575	598.2	586.6	0.00587
	650	671.2	660.6	0.00642
	725	744.4	734.7	0.00701

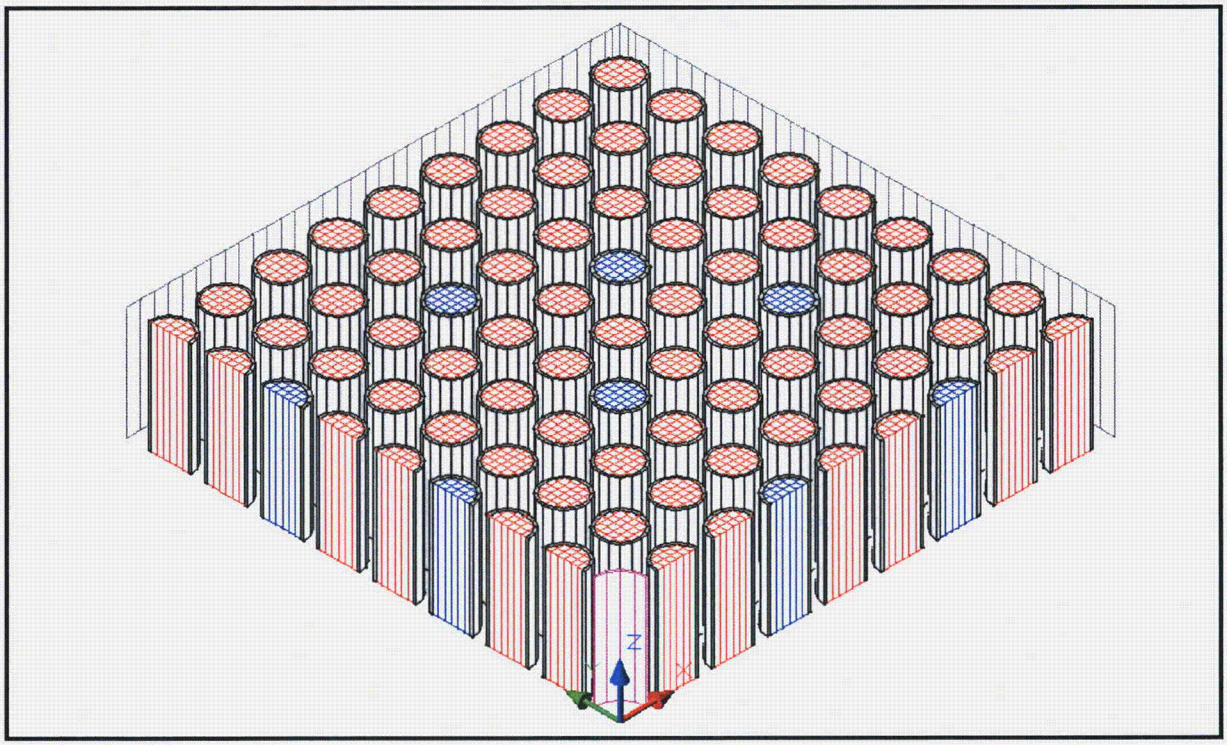

Figure 3.6-1 – Perspective View of MOX Thermal Model (1/4-Segment)

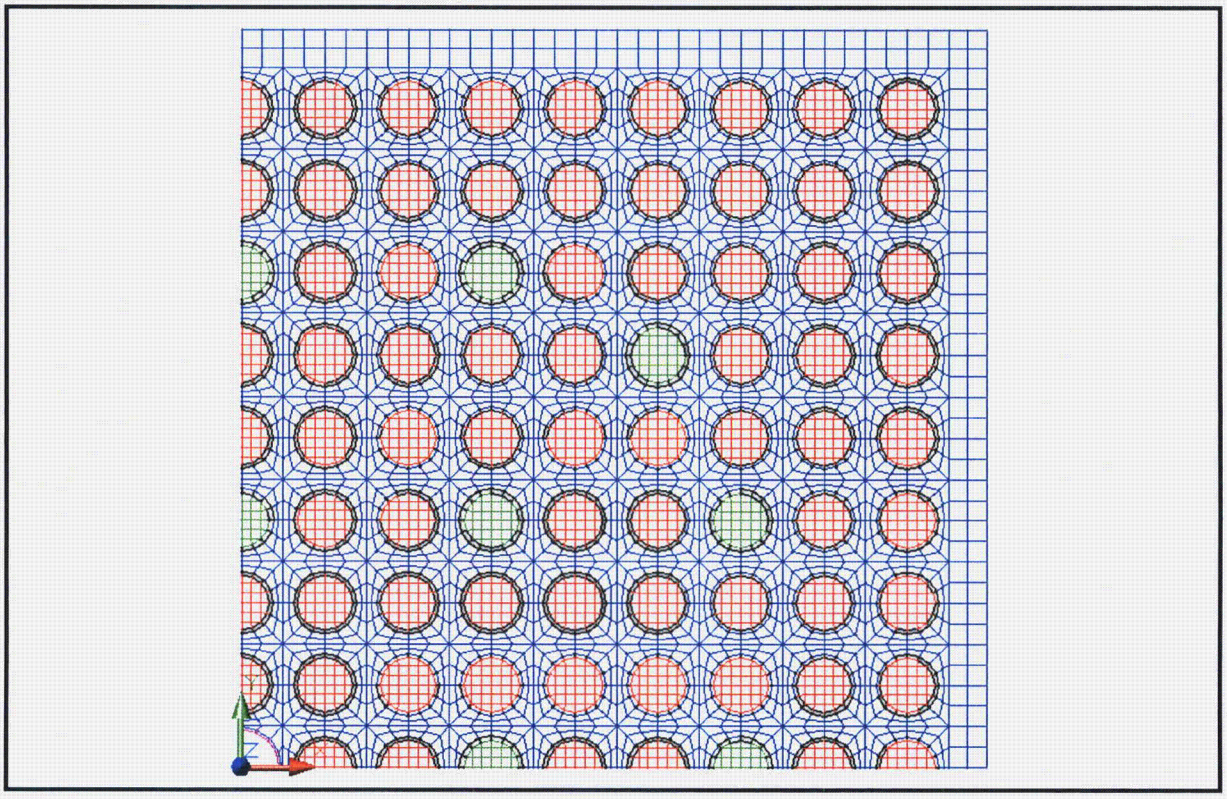

Figure 3.6-2 – Finite Element Modeling of 1/4-Segment MOX Assembly

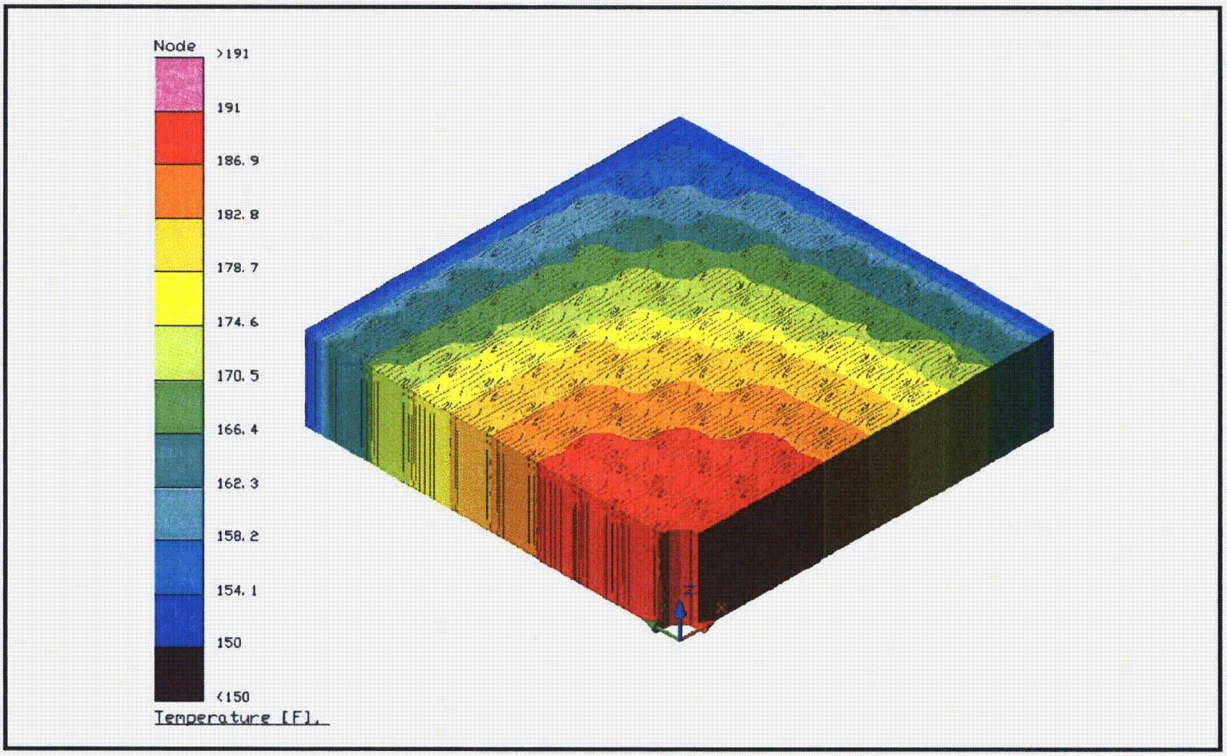

Figure 3.6-3 – Representative Temperature Distribution within 1/4-Segment MOX Assembly

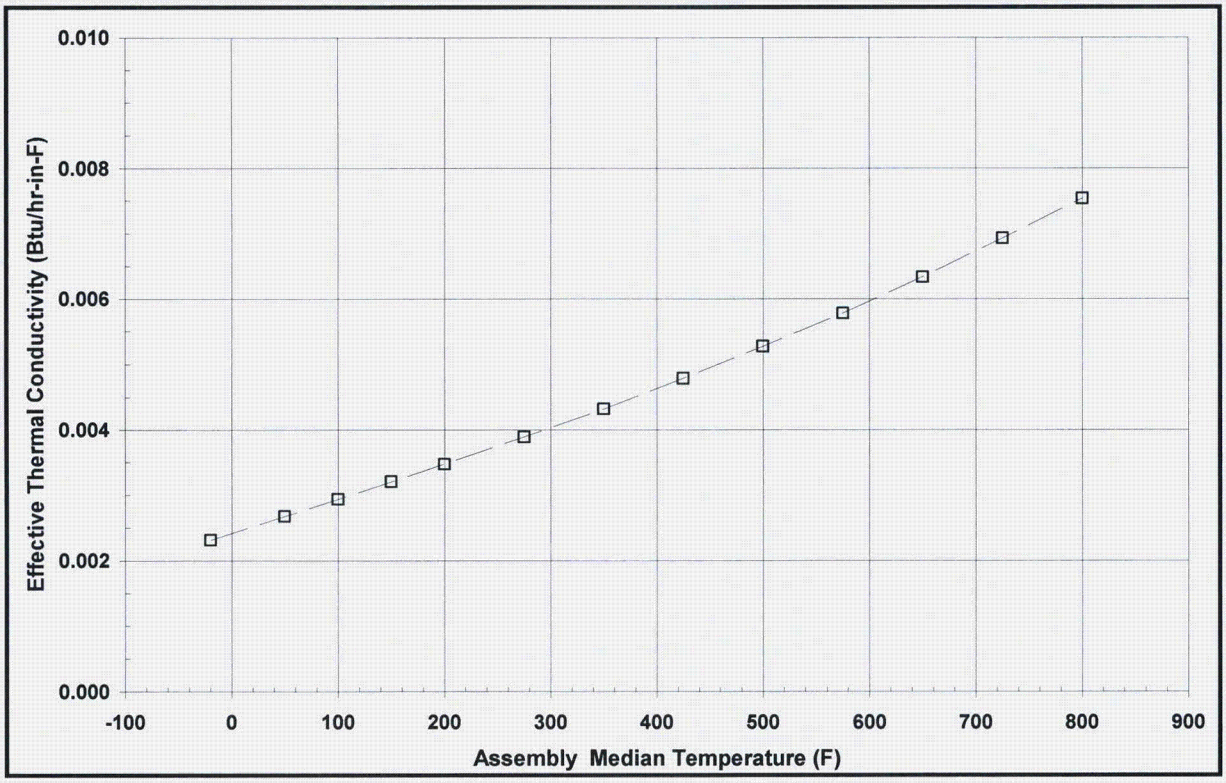

Figure 3.6-4 – Effective Radial Thermal Conductivity for MOX FAs

4.0 CONTAINMENT

4.1 Description of the Containment System

4.1.1 Containment Boundary

A single level of containment is provided for the fresh MOX fuel payload by the MFFP. In general, all containment components are fabricated from Type XM-19 austenitic stainless steel, with exceptions noted in the following detailed description.

The containment boundary for the MFFP consists of the 9/16-inch thick cylindrical shell, the 1½-inch thick bottom plate, the 5/8-inch inner closure lid plate, the closure lid seal forging, and the upper forging on the body. The non-stainless steel components included in the containment boundary are the center butyl O-ring seal for the closure lid, the ASTM A564, 630 (H1100), nickel plated alloy steel closure bolts, the ASTM B16 brass vent and fill port plugs, and their associated butyl rubber sealing elements.

4.1.1.1 Containment Penetrations

The only penetrations into the containment boundary are the vent port, fill port, and closure lid. Each penetration is designed to demonstrate "leaktight" sealing integrity, i.e., a leakage rate not to exceed 1×10^{-7} standard cubic centimeters per second (scc/s), air, per ANSI N14.5[1].

4.1.1.2 Closure

With reference to Figure 1.1-2 in Chapter 1.0, *General Information*, the closure lid is secured to the body via twenty-four (24), 3/4-inch × 3-inch long socket head cap screws (SHCS). The installation of the closure lid consists of four main steps:

1. As an option, lightly lubricate the O-ring seals with vacuum grease; install the O-ring seals into their respective O-ring seal grooves located in the closure lid.
2. Align the closure lid with the body.
3. Install the closure lid.
4. Install twenty-four (24), 3/4-inch SHCS through the closure lid and into the lid end forging on the body.

4.1.1.3 Seals

The elastomeric portion of the containment boundary is comprised of a nominally 3/8-inch diameter, O-ring bore seal in the center groove of the closure lid, and stat-o-seal sealing elements (an O-ring integrated with a stainless steel washer) for the vent and fill port plugs.

The elastomeric containment O-ring seals and stat-o-seals are fabricated of a butyl compound, suitable for normal conditions of transport (NCT) ranging from a low temperature of -65 °F to a high

[1] ANSI N14.5-1997, *American National Standard for Radioactive Materials - Leakage Test on Packages for Shipment*, American National Standard Institute, Inc. (ANSI).

temperature of 225 °F for long durations. Further, the butyl compound is capable of a hypothetical accident condition (HAC) high temperature of 400 °F for a short duration (8 hours). Details of the containment vessel and associated penetrations are provided in the drawings in Section 1.4.2, *Packaging General Arrangement Drawings*. Further discussion of the thermal performance capabilities of the butyl rubber O-ring seals is provided in Section 3.2.2, *Component Specifications*.

Three nearly identical O-ring seals are provided on the outer diameter of the closure lid. The center O-ring seal comprises the containment seal, whereas the outer O-ring seal serves to create an annular test cavity for verification of the center seal integrity via leakage rate testing. The inner O-ring seal serves to create a fill cavity for the test gas. For leakage rate testing of the closure lid containment O-ring seal using a helium mass spectrometer leak detector (MSLD) or other leak test equipment, the fill cavity is purged and backfilled with helium gas, and the seal test cavity is evacuated and tested using a MSLD (or other leak test equipment). Upon successfully performing the closure lid main O-ring seal leakage rate test, the MSLD (or other leak test equipment) is moved to the vent and fill ports to verify sealing integrity, since these penetrations form part of the package's containment boundary.

4.1.1.4 Welds

All containment vessel body welds are full penetration welds that have been radiographed to ensure structural and containment integrity. Non-radiographed, safety related welds, such as those that attach the impact limiter mounting lugs to the cylindrical shell, are examined using liquid penetrant testing on the final pass or both the root and final passes, as applicable. All containment boundary welds are confirmed to be leaktight as delineated in Section 8.1.4, *Fabrication Leakage Rate Tests*.

4.1.2 Special Requirements for Plutonium

The MFFP is designed to contain and transport payloads in excess of 20 Ci of plutonium in solid form (i.e., fuel assemblies). Therefore, the requirements of 10 CFR §71.63[2] are satisfied.

[2] Title 10, Code of Federal Regulations, Part 71 (10 CFR 71), *Packaging and Transportation of Radioactive Material*, Final Rule, 01-26-04.

4.2 General Considerations

4.2.1 Type A Fissile Package

This section does not apply for the MFFP, since the package is a Type B fissile package.

4.2.2 Type B Packages

The MFFP is designed with a "leaktight" containment boundary, as defined by ANSI N14.5[1], to contain the MOX FA payload. Leak tightness of the containment boundary has been demonstrated by full-scale structural testing, as presented in Appendix 2.12.3, *Certification Test Results*, that demonstrated no release of radioactive materials per the "leaktight" definition of ANSI N14.5 under any of the normal conditions of transport tests and the hypothetical accident condition tests described in 10 CFR §71.71[2] and §71.73, respectively. The full-scale structural tests included leakage rate tests of the containment metallic boundary and elastomeric seals. These leakage rate tests are specified for the MFFP in Section 8.1.4, *Fabrication Leakage Rate Tests*.

[1] ANSI N14.5-1997, *American National Standard for Radioactive Materials – Leakage Tests on Packages for Shipment,* American National Standards Institute, Inc. (ANSI).

[2] Title 10, Code of Federal Regulations, Part 71 (10 CFR 71), *Packaging and Transportation of Radioactive Material*, Final Rule, 01-26-04.

This page left intentionally blank.

4.3 Containment Requirements for Normal Conditions of Transport

4.3.1 Containment of Radioactive Material

The results of the normal conditions of transport (NCT) structural and thermal evaluations presented in Sections 2.6, *Normal Conditions of Transport*, and 3.4, *Thermal Evaluation Under Normal Conditions of Transport*, respectively, and the results of the full-scale structural testing presented in Appendix 2.12.3, *Certification Test Results*, demonstrate that there is no release of radioactive materials per the "leaktight" definition of ANSI N14.5[1] under any of the normal conditions of transport tests described in 10 CFR §71.71[2].

4.3.2 Pressurization of the Containment Vessel

The maximum normal operating pressure (MNOP) of the MFFP is 10 psig per Section 3.4.2, *Maximum Normal Operating Pressure*. The design pressure of the MFFP is 25 psig. Based on the structural analyses presented in Section 2.0, *Structural Evaluation*, pressure increases to 25 psig will not reduce the effectiveness of the MFFP in maintaining containment integrity per Section 4.3.1, *Containment of Radioactive Material.*

4.3.3 Containment Criterion

At the completion of fabrication, the MFFP shall be leakage rate tested as described in Section 4.5.1, *Fabrication Leakage Rate Tests*. For annual maintenance, the MFFP shall be leakage rate tested as described in Section 4.5.2, *Maintenance/Periodic Leakage Rate Tests*. In addition, at the time of seal replacement if other than during routine maintenance (e.g., if damage during assembly necessitates seal replacement), maintenance/periodic leakage rate testing shall be performed for that seal. For verification of proper assembly prior to shipment, the MFFP shall be leakage rate tested as described in Section 4.5.3, *Preshipment Leakage Rate Tests.*

---

[1] ANSI N14.5-1997, *American National Standard for Radioactive Materials – Leakage Tests on Packages for Shipment,* American National Standards Institute, Inc. (ANSI).

[2] Title 10, Code of Federal Regulations, Part 71 (10 CFR 71), *Packaging and Transportation of Radioactive Material*, Final Rule, 01-26-04.

This page left intentionally blank.

4.4 Containment Requirements for Hypothetical Accident Conditions

4.4.1 Fission Gas Products

Although there are no fission gas products in the MOX FAs, the pressures for hypothetical accident conditions (HAC) are calculated assuming 100% of fill gas is released from all of the fuel rods in the three fuel assemblies inside the package, as presented in Section 3.5.3, *Maximum Temperatures and Pressures*.

4.4.2 Containment of Radioactive Material

The results of the hypothetical accident condition (HAC) structural and thermal evaluations performed in Sections 2.7, *Hypothetical Accident Conditions*, and 3.5, *Thermal Evaluation Under Hypothetical Accident Conditions*, respectively, and the results of the full-scale structural testing presented in Appendix 2.12.3, *Certification Test Results*, demonstrate that there is no release of radioactive materials per the "leaktight" definition of ANSI N14.5[1] under any of the hypothetical accident condition tests described in 10 CFR §71.73[2].

4.4.3 Containment Criteria

The MFFP is leakage rate tested as described in Section 4.1.1.3, *Seals*, to demonstrate the leaktight containment criterion of ANSI N14.5.

---

[1] ANSI N14.5-1997, *American National Standard for Radioactive Materials – Leakage Tests on Packages for Shipment,* American National Standards Institute, Inc. (ANSI).

[2] Title 10, Code of Federal Regulations, Part 71 (10 CFR 71), *Packaging and Transportation of Radioactive Materials*, United States Nuclear Regulatory Commission (USNRC), Final Rule, 01-26-04.

This page left intentionally blank.

4.5 Leakage Rate Tests for Type B Packages

The MFFP is designed with a "leaktight" containment boundary, as defined in ANSI N14.5[1], to transport the MOX FAs. Demonstration of the leaktight capabilities of the MFFP are accomplished by performing leakage rate tests of the metallic and elastomeric containment boundary. A summary of these leakage rate tests prior to first use, during routine maintenance, and upon assembly for transport is described in the following sections.

4.5.1 Fabrication Leakage Rate Tests

During fabrication and following the pressure testing per Section 8.1.3.2, *Pressure Testing*, the containment boundary is tested per the leakage rate test delineated in Section 8.1.4, *Fabrication Leakage Rate Tests*. The fabrication leakage rate tests are consistent with the guidelines of Section 7.3 of ANSI N14.5. These leakage rate tests verify the containment integrity of each penetration and the metallic boundary of the MFFP to a leakage rate not to exceed 1×10^{-7} scc/s, air, following fabrication of the package.

4.5.2 Maintenance/Periodic Leakage Rate Tests

Annually, or at the time of damaged containment seal replacement or sealing surface repair, the O-ring seals shall be leakage rate tested as delineated in Section 8.2.2, *Maintenance/Periodic Leakage Rate Tests*. The maintenance/periodic leakage rate tests are consistent with the guidelines of Sections 7.4 and 7.5 of ANSI N14.5. This test verifies the integrity of each O-ring seal to a leakage rate not to exceed 1×10^{-7} scc/s, air.

4.5.3 Preshipment Leakage Rate Tests

Prior to shipment of a loaded MFFP, the center O-ring seal, the vent port stat-o-seal and the fill port stat-o-seal shall be leak tested per Section 7.4, *Preshipment Leakage Rate Tests*. The preshipment leakage rate tests are consistent with the guidelines of Section 7.6 of ANSI N14.5. This test verifies the sealing integrity of the closure lid, vent port, and fill port seals to a leakage rate sensitivity of 1×10^{-3} scc/s, air.

The maintenance/periodic leakage rate tests, delineated in Section 8.2.2, *Maintenance/Periodic Leakage Rate Tests*, may be performed as an option, in lieu of the preshipment leakage rate tests.

---

[1] ANSI N14.5-1997, *American National Standard for Radioactive Materials – Leakage Tests on Packages for Shipment,* American National Standards Institute, Inc. (ANSI).

This page left intentionally blank.

5.0 SHIELDING EVALUATION

The compliance of the MFFP packaging with respect to the dose rate limits established by 10 CFR §71.47[1] for normal conditions of transport (NCT) or 10 CFR §71.51(a)(2) for hypothetical accident conditions (HAC) are satisfied when limiting the MFFP package to three (3) Mixed Oxide (MOX) fresh fuel assemblies (FAs) having a radioisotope content listed in Table 1.2-2.

Under these conditions, the maximum surface dose rate will be less than the limit of 200 mrem/hr for NCT and verified by measurement. This dose rate limit is for payload packages prior to addition of any lead, steel or other shielding material for *as-low-as-reasonably-achievable* (ALARA) dose reduction purposes during non-transport handling operations.

Prior to transport, the MFFP package shall be monitored for both gamma and neutron radiation to demonstrate compliance with 10 CFR §71.47. As noted in Section 2.6.7, *Free Drop*, the MFFP package is not significantly deformed under NCT free drop conditions. Therefore, the package will meet the dose rate limits for NCT if the measurements demonstrate compliance with the allowable dose rate levels in 10 CFR §71.47 (200 mrem/hr). The transport index, as defined in 10 CFR §71.4, will be determined by measuring the dose rate a distance of one meter from the package surface per the requirements of 49 CFR §173.403[2].

Shielding materials are not specifically provided by the MFFP package, and none are permitted within the package to meet the dose rate limits of 10 CFR §71.47 for NCT. Since significant fuel deformation or package deformation does not occur under HAC, the HAC surface dose rates and 1-meter dose rates will not be significantly different from the NCT dose rates. This result ensures that the post-HAC, allowable dose rate of 1 rem/hr a distance of one meter from the package surface per 10 CFR §71.51(a)(2) will be met because the surface dose rate will remain below the 200 mrem/hr limit.

[1] Title 10, Code of Federal Regulations, Part 71 (10 CFR 71), *Packaging and Transportation of Radioactive Material*, Final Rule, 01-26-04.

[2] Title 49, Code of Federal Regulations, Part 173 (49 CFR 173), *Shippers - General Requirements for Shipments and Packagings*, Final Rule, 01-26-04.

This page left intentionally blank.

6.0 CRITICALITY EVALUATION

The following analyses demonstrate that the MFFP complies with the requirements of 10 CFR §71.55[1] and §71.59. The analyses presented herein show that the criticality requirements are satisfied when limiting the MFFP package to a maximum of three pressurized water reactor (PWR) mixed-oxide (MOX) fresh fuel assemblies (FAs) as described in Section 1.2.3, *Contents of Packaging.*

6.1 Description of Criticality Design

6.1.1 Design Features Important for Criticality

A comprehensive description of the MFFP package is provided in Section 1.2, *Packaging Description*, and in the drawings in Appendix 1.4.2, *Packaging General Arrangement Drawings.* This section summarizes those design features important for criticality.

The primary design feature used to ensure criticality safety is the use of neutron poison plates (boral) with a minimum B-10 areal density of 0.035 g/cm^2. The neutron poison plates surround each fuel assembly on all four sides. Neutron poison plates that span the active fuel length are fastened to the radial and tangential strongback angles. The remaining two sides of each assembly are constrained by fuel control structures (FCSs), which are hinged angles placed between the clamp arms. Neutron poison plates (boral) are bolted to the exterior surface of each FCS.

Criticality safety is also ensured by the structural design of the MFFP. The stainless steel strongback angles and clamp arms firmly secure the FAs to the package. The FCS provides additional support in the event of an accident and prevents unrestrained pitch expansion of the fuel. Finally, the stainless steel shell of the package itself provides separation from adjacent packages and provides a leaktight containment boundary that excludes water from the package.

6.1.2 Summary Table of Criticality Evaluation

The upper subcritical limit (USL) for ensuring that the MFFP (package or package array) is acceptably subcritical, as determined in Section 6.8, *Benchmark Evaluations*, is:

$$USL = 0.9288$$

The package is considered to be acceptably subcritical if the computed k_{safe} (k_s), which is defined as $k_{effective}$ (k_{eff}) plus twice the statistical uncertainty (σ), is less than the USL, or:

$$k_s = k_{eff} + 2\sigma < USL$$

The USL is determined on the basis of a benchmark analysis and incorporates the combined effects of code computational bias, the uncertainty in the bias based on both benchmark-model and computational uncertainties, and an administrative margin. The results of the benchmark analyses indicate that the USL is adequate to ensure subcriticality of the MFFP.

[1] Title 10, Code of Federal Regulations, Part 71 (10 CFR 71), *Packaging and Transportation of Radioactive Material*, Final Rule, 01-26-04.

The results of the criticality calculations are summarized in Table 6.1-1. The maximum calculated k_s is 0.9037 which occurs for the HAC infinite array case with fully moderated internal region and void external region. Under NCT, the maximum calculated k_s is 0.6039 for the array case.

The NCT cases assume no moderation. This assumption is credible because of the leaktight performance of the MFFP under both NCT and HAC. Consequently, NCT reactivities are negligibly low.

For HAC, water is assumed to be present in the containment system. Reactivity increases monotonically as water density is increased to a maximum of 100% water density. For the HAC cases, the pitch is also allowed to expand to the maximum possible extent allowed by the FCS to simulate possible fuel assembly damage. Reactivity is a maximum when the pitch is the maximum allowed by the FCS, indicating that the system is undermoderated.

6.1.3 Criticality Safety Index

For both NCT and HAC, an infinite number of MFFPs are evaluated in a close-packed hexagonal array. Therefore, "N" is infinite, and in accordance with 10 CFR §71.59 the criticality safety index (CSI) is 50/N = 0.

Table 6.1-1 – Summary of Criticality Analysis Results

Normal Conditions of Transport (NCT)			
Case	**k_{eff}**	**σ**	**k_s**
Single Unit Maximum k_s	0.2858	0.0008	0.2874
Infinite Array Maximum k_s	0.6027	0.0006	0.6039
Hypothetical Accident Conditions (HAC)			
Case	**k_{eff}**	**σ**	**k_s**
Single Unit Maximum k_s	0.8981	0.0010	0.9001
Infinite Array Maximum k_s	0.9017	0.0010	0.9037
USL	0.9288		

6.2 Fissile Material Contents

The payload cavity of an MFFP can accommodate one triangular strongback assembly containing up to three mixed-oxide (MOX) fresh fuel assemblies (FAs). The overall arrangement of the fuel within the package is provided in Figure 6.3-1. Because MCNP utilizes metric inputs, metric values are also specified here and in other tables in this chapter. The physical design parameters of a MOX FA are given in Table 6.2-1 and Table 6.2-2. The nucleonic MOX FA design parameters are given in Table 6.2-3.

As discussed in Table 6.2-3, the actual MOX FAs may contain zoned fuel regions, although in the criticality analysis all fuel pins are conservatively assumed to be at the maximum Pu loading. In addition, the fuel assemblies may contain burnable poison rods, although in the criticality analysis burnable poison rods are conservatively ignored.

Table 6.2-1 – MOX PWR Fuel Assembly Physical Design Parameters

Parameter	English Value	Metric Value
Configuration	17 × 17	
Number of Fuel Rods	264	
Number of Guide Tubes	24	
Number of Instrument Tubes	1	
Length (top of leaf spring to bottom nozzle)	161.61 inches	410.49 cm
Width, top nozzle	8.406 inches	21.351 cm
Width, bottom nozzle	8.425 inches	21.400 cm
Width, overall assembly	8.565 inches maximum	21.755 cm maximum
Weight of UO_2/PuO_2 per assembly (95% theoretical density)	1,157 pounds	525 kg
Weight of Heavy Metals per assembly (95% theoretical density)	1,020 pounds	463 kg
Fuel Rod Pitch	0.496 ± 0.006 inches	1.2598 ± 0.015 cm
Guide Thimble OD	0.482 inches	1.224 cm
Guide Thimble ID	0.450 inches	1.143 cm

Table 6.2-2 – MOX Fuel Rod Physical Parameters

Parameter	English Value	Metric Value
Cladding Material	Zirconium-Based M5 Alloy	
Outside Diameter	0.374 inches	0.950cm
Inside Diameter	0.329 inches	0.836 cm
Overall Length	152.4 inches	387.1 cm
Active Fuel Length	144.00 inches	365.76 cm
Weight	5.33 pounds	2.42 kg
Weight of UO_2/PuO_2	4.384 pounds	1.989 kg
Upper End Cap Length	0.515 inches	1.308 cm
Lower End Cap Length	0.575 inches	1.461 cm

Table 6.2-3 – Nucleonic Design Parameters

Parameter	English Value	Metric Value
Pellet Diameter	0.3225 inches	0.8192 cm
Pellet Density	--	10.44 g/cc (95% theoretical density) 10.99 g/cc (100% theoretical density)
Effective Pellet Density (homogenized pellet stack accounting for dish and chamfer, used in MCNP models)	--	10.31 g/cc (95% theoretical density) 10.85 g/cc (100% theoretical density)
Concentration Ranges* ($^w/_o$) (average per assembly) * The maximum Pu loading of 6.0% applies to both the assembly average and individual fuel rods. The rods may either vary (such as the use of high, medium, and low enriched zones within the assembly), or be constant.	Total Uranium 94.0$^w/_o$ or greater of which: ^{234}U: 0 to 0.05 $^w/_o$ ^{235}U: 0 to 0.30 $^w/_o$ ^{238}U: 99.65 to 100 $^w/_o$ Total Plutonium up to 6.0$^w/_o$ of which: ^{238}Pu: 0 to 0.05 $^w/_o$ ^{239}Pu: 90 to 95 $^w/_o$ ^{240}Pu: 5 to 9 $^w/_o$ ^{241}Pu: 0 to 1 $^w/_o$ ^{242}Pu: 0 to 0.1 $^w/_o$	

6.3 General Considerations

Criticality calculations for the MFFP package are performed using the three-dimensional Monte Carlo computer code MCNP5[1]. Descriptions of the fuel assembly geometric models are given in Section 6.3.1, *Model Configuration.* The material properties for all materials used in the models are provided in Section 6.3.2, *Material Properties.* The computer code and cross section libraries used are provided in Section 6.3.3, *Computer Codes and Cross-Section Libraries.* Finally, the most reactive configuration for each case is provided in Section 6.3.4, *Demonstration of Maximum Reactivity.*

6.3.1 Model Configuration

6.3.1.1 Contents Model

The MFFP contents are represented by a conservative model of the MOX fresh fuel assembly. The model contains fuel loading that exceeds the designs currently being considered. In addition, the fuel assembly model conservatively:

- Neglects fuel rod zoning
- Assumes the maximum fuel loading, including fissile isotope distribution, possible
- Ignores any effect of burnable poison fuel assemblies, even if present.

Table 6.2-1, Table 6.2-2, and Table 6.2-3 contain the significant parameters used in the contents model. The contents model uses nominal dimensions with the exception of the pitch, which is optimized to maximize reactivity.

Each fuel pin is modeled explicitly, including the top and bottom end plugs, plenum, and pellet/cladding gap. The 24 empty guide thimbles are modeled explicitly, and the center instrument tube is assumed to be the same as a guide thimble. The grid straps are conservatively ignored, as well as the top and bottom nozzles, which are modeled as variable density water. The fuel pin pellet-cladding gap is also filled with variable density water to match the moderation assumed in the package cavity. The HAC models also consider the reactivity effects of the fuel pins shifting axially.

6.3.1.2 Packaging Model

A comprehensive description of the MFFP packaging is provided in Section 1.2, *Packaging Description,* and in the packaging drawings in Appendix 1.4.2, *Packaging General Arrangement Drawings.* The packaging includes a containment vessel, an internal strongback assembly, and impact limiters. The impact limiters cover each end of the body and are steel shells filled with polyurethane form.

The packaging is lightweight due to the weight constraints built into the design. For modeling simplicity, the impact limiters are neglected for both NCT and HAC models. Ignoring the impact limiters conservatively:

[1] MCNP5, "*MCNP – A General Monte Carlo N-Particle Transport Code, Version 5; Volume II: User's Guide,*" LA-CP-03-0245, Los Alamos National Laboratory, April, 2003.

- Allows for greater reflection in the single package cases (because the reflector is closer to the contents).
- Accounts for any HAC damage to the limiters (due to crush during impact).
- Conservatively places packages closer together for the array calculations (because the impact limiters would provide additional spacing and reduce moderation or reflection).

Because the containment shell sustains only localized puncture damage during HAC (refer to Figure 2.12.3-35 for puncture damage) and because minor variations in the package dimensions have little effect on the criticality calculations, nominal packaging dimensions are used for both the basic NCT and HAC models.

Details of the packaging model are provided in the following figures. Figures are presented to scale and are generated from the MCNP input files. The packaging model represents geometrically significant structural and poison materials. Key dimensions used in the MCNP models are provided in Table 6.3-1. Notations are made in the table when the model dimensions differ from the final design. The model is more conservative than the final design because the FCS poison plates as modeled are smaller than actual size.

Figure 6.3-1 shows the model geometry through a planar slice of the package for the NCT case. The strongback is modeled as a simplified triangular shaped structure. Because the design allows for easy water migration through the strongback, any water moderation is modeled to completely fill all void spaces. Water reflector (12 inches) surrounds the package on all sides. Figure 6.3-2 shows an axial view of the NCT geometry.

Figure 6.3-3 and Figure 6.3-4 present a close-up view of the lower fuel assembly at different axial elevations with labels on all major components. Each fuel assembly is completely surrounded on all four sides to restrict movement. As shown in Figure 6.3-3, the top and right boundary of the assembly is bounded by the strongback. Borated aluminum (boral) neutron poison plates are bolted to the strongback between the strongback and neutron poison cover plates.

The strongback and strongback boral are continuous pieces, while the neutron poison cover plates are segmented and are located only opposite each clamp arm. Steel bolts are explicitly modeled in the strongback boral to reduce the boron loading. As shown in Figure 6.3-3, the left and bottom boundary of each assembly is supported by eight clamp arms and seven fuel control structures (FCSs). Each FCS segment has neutron poison plates attached on the outer surface of the FCS. For simplicity, the clamp arms and strongback support triangles are not explicitly modeled, although the seven steel segments that form the FCS are modeled as one continuous piece because the steel clamp arms will be present between the segments. The impact of including the clamp arms and strongback triangles is assessed in additional calculations in which these components are homogenized into the water region.

The FCS neutron poison plates are modeled as discrete segments. The FCS neutron poison plates are not modeled with bolt holes as with the strongback boral, although the FCS neutron poison plates are modeled conservatively short to minimize the amount of boral.

Figure 6.3-5 shows a close-up view of the model corner. Note that the neutron poison plate is explicitly modeled as a B_4C-Al matrix clad on each side by aluminum.

Figure 6.3-6 and Figure 6.3-7 show the top and bottom of the package. Note that the top and bottom nozzles are modeled as variable density water. Also, these figures explicitly show the

fuel pin end caps and plenum regions. Figure 6.3-8 and Figure 6.3-9 show the strongback and FCS poison plates and the extent to which they overlap the active fuel region.

6.3.2 Material Properties

All material compositions used in the models are representative of the actual materials used in the MFFP. The compositions and densities of all packaging materials as input to MCNP are provided in Table 6.3-2 through Table 6.3-6. Note that most materials (Type 304, XM-19, fuel) are input with weight fractions on the material card and gram density on the cell card. The boral is input with number densities on the material card and total number density on the cell card.

As fuel isotopics are provided as ranges in Table 6.2-3, the fuel isotopics selected for the criticality model are chosen to maximize reactivity. As Pu-241 is more reactive than Pu-239 for moderated systems (which are the most reactive cases for the MFFP), the Pu-241 content is maximized. As Pu-240 acts as a poison, the Pu-240 content is minimized. The balance of Pu is assumed to be Pu-239. The U-235 content is conservatively assumed to be at the maximum value. The fuel isotopics utilized are provided in Table 6.3-2.

The effective density of the fuel is computed to be 10.31 g/cm^3 based on the mass of fuel in a pin (95% theoretical density), pellet diameter, and active fuel length, as shown in Table 6.3-2. The fuel density assuming 100% theoretical density is 10.85 g/cm^3.

Type 304 stainless steel is used for the strongback angles and poison cover plates; its composition and density are provided in Table 6.3-3.

Most of the models used in the analysis assume M5 fuel cladding, end caps, and thimble tubes; M5 composition and density are provided in Table 6.3-4. Final runs were made with a more generic zirconium-based material with niobium in the range 0 to 3%.

Type XM-19 stainless steel is used for the MFFP structural shell; its composition and density are provided in Table 6.3-5.

The neutron poison plates have a minimum B-10 areal density of 0.035 g/cm^2. Only 75% credit is taken for the B-10 number density. The number densities of the B_4C-Al boral matrix are provided in Table 6.3-6. The boral is clad with aluminum assumed to be pure and with a density of 2.713 g/cm^3.

Water used in the models is assumed to be pure; density is case dependent.

6.3.3 Computer Codes and Cross-Section Libraries

The Monte Carlo computer program MCNP5 is used for this criticality analysis and has been verified for proper operation on the machine(s) on which it is installed. MCNP5 and its predecessor codes (MCNP4C, MCNP4B, etc.) have been an industry standard for neutron transport and criticality analysis for several decades.

MCNP5 primarily uses continuous energy ENDF/B-VI cross sections at room temperature, although ENDF/B-V cross sections are used when ENDF/B-VI cross sections are not available (i.e., iron, chromium, and nickel). A summary of the neutron cross sections utilized are provided in Table 6.3-7. Note that these cross sections are the default cross sections utilized by the program when no particular cross section set is specified. The S(α,β) card [LWTR.01t] is used to simulate hydrogen in room temperature water.

The NCT cases are run with 500 generations and 1,000 particles per generation. These files converge quickly because of the absence of moderating material. The HAC cases are run with 500 generations and 2,000 particles per generation. All cases use the SDEF card to distribute the starting neutrons over the length of every fuel pin. This ensures a uniform starting distribution and stable convergence. A 1-σ standard deviation of approximately 0.001 is considered acceptable for the results.

6.3.4 Demonstration of Maximum Reactivity

6.3.4.1 Single Package

The most reactive single package model is for the HAC case max_hac_single_su1. To ensure this is the most reactive case, the following parameters have been investigated:

- The internal moderation is varied from 0 to 1.0 g/cm^3. The water in the pellet-cladding gap is also assumed to vary with the internal moderation. The most reactive condition is for full-density water.
- The pitch is varied from the "nominal-minus-tolerance" value to the maximum pitch such that the fuel assembly completely fills the space constrained by the FCS. The pitch is expanded uniformly over all three assemblies. Note that in the fully expanded position, the steel neutron poison cover plates that hold the borated aluminum to the strongback are artificially removed from the package model to allow room for this expansion. The case with a maximum pitch is the most reactive.
- The package is reflected with steel, which is shown to be slightly more reactive than either water or lead reflectors.
- Miscellaneous minor steel components in the package are homogenized into the water region for the most reactive case. This addition of steel further raises the reactivity slightly.
- The zirconium based alloy cladding has no niobium content, which is shown to be slightly more reactive than with niobium present.
- The fuel pellets are assumed to be 100% dense.
- The most reactive number of fuel pins are allowed to shift either up or down to the maximum possible extent.
- The most reactive single package therefore has full density moderator inside the package and the pellet-cladding gap, maximum pitch, steel reflector, homogenized minor steel components, pure-zirconium cladding, 100% dense fuel pellets, and axially shifted fuel pins.

6.3.4.2 Arrays of Undamaged Packages

The most reactive NCT array case is max_nct_array. An infinite hexagonal array is assumed. Because the MFFP is leaktight under NCT conditions, the package cavity is assumed to be dry. In the absence of moderation, the reactivity is very low and only one pitch is investigated. The only parameter investigated is the external water density, which is allowed to vary over the range 0 to 1.0 g/cm^3. The fuel pellets are assumed to be 100% dense and the zirconium based alloy cladding has no niobium content. Maximum reactivity is obtained with no water between the packages.

6.3.4.3 Arrays of Damaged Packages

The most reactive HAC array case is max_hac_array_sd2. An infinite hexagonal array is assumed. To ensure this is the most reactive case, the following parameters have been investigated:

- The internal moderation is varied from 0 to 1.0 g/cm^3. The water in the pellet-cladding gap is also assumed to vary with the internal moderation. The most reactive condition is for full-density water.
- The external moderation is varied from 0 to 1.0 g/cm^3. The most reactive condition is for no external moderation.
- The pitch is varied from the "nominal minus tolerance" value to the maximum pitch such that the fuel assembly completely fills the space constrained by the FCS. The pitch is expanded uniformly over all three assemblies. Note that in the fully expanded position, the steel neutron poison cover plates that hold the borated aluminum to the strongback are artificially removed from the package model to allow room for this expansion. The case with a maximum pitch is the most reactive.
- Miscellaneous minor steel components in the package are homogenized into the water region for the most reactive case. This addition of steel further raises the reactivity slightly.
- The zirconium based alloy cladding has no niobium content, which is shown to be slightly more reactive than with niobium present.
- The fuel pellets are assumed to be 100% dense.
- The most reactive number of fuel pins are allowed to shift either up or down to the maximum possible extent.
- The most reactive package array therefore has full density moderator inside the package and the pellet-cladding gap, no external moderation, maximum pitch, homogenized minor steel components, pure-zirconium cladding, 100% dense fuel pellets, and axially shifted fuel pins.

Table 6.3-1 – Key Packaging Model Dimensions

Description	English Value (in)	Metric Value (cm)
Total package length	171.3	435.2
Body shell OD	29.625	75.248
Body shell ID	28.50	72.39
Bottom end thickness	1.50	3.81
Closure lid thickness (total)	4.38	11.13
Closure lid upper plate thickness	0.75	1.91
Closure lid lower plate thickness	0.63	1.60
Length of "tangential" strongback angle	8.30	21.08
Length of "radial" strongback angle	9.07	23.04
Strongback thickness	0.25	0.64
Strongback length (excluding top/bottom plate assemblies)	160.11	406.68
Radial poison plate hole diameter (same as tangential) (0.4 inches on SAR drawing, negligible impact on results)	0.375	0.953
Radial poison plate hole axial location (same as tangential)	Refer to drawings in §1.4.2	Refer to drawings in §1.4.2
Radial poison plate width (same as tangential)	8.43	21.41
Radial poison plate, radial distance between bolt holes (used for all pairs) (4.7 inches on SAR drawing, negligible impact on results)	4.352	11.054
Radial poison plate, axial distance between bolt holes (used for all pairs, same as tangential) (2.8 inches on SAR drawing, negligible impact on results)	2.848	7.234
Radial poison plate, distance from inner hole to edge of plate (2.2 inches on SAR drawing, negligible impact on results)	2.12	5.39
Tangential poison plate, radial distance between bolt holes (used for all pairs)	5.50	13.97
Tangential poison plate, distance from inner hole to edge of plate (1.0 inches on SAR drawing, negligible impact on results)	0.97	2.46
Poison cover plate thickness	0.1874 (7-gauge)	0.4760
Poison cover plate width	8.43	21.41
Poison cover plate height (Note: used for both radial and tangential)	4.25	10.80
End poison cover plate height (Note: modeled as 1.25 inches at the top for simplicity)	1.0	2.54
Middle triangle base length (also used for upper triangle)	7.36	18.69

Table 6.3-1 – Key Packaging Model Dimensions (con't)

Description	English Value (in)	Metric Value (cm)
Middle triangle height (also used for upper triangle)	6.38	16.21
Middle triangle plate thickness	0.50	1.27
Middle triangle, 3-in. Sch 40 pipe OD	3.50	8.89
Middle triangle, 3-in. Sch 40 pipe ID	3.068	7.793
Middle triangle pipe height	2.85	7.24
Upper triangle height	2.00	5.08
Upper triangle hole ID (minimum)	2.032	5.161
Maximum Al cladding thickness for boral	0.017	0.043
Maximum boral thickness	0.085	0.216
Thickness of FCS steel (0.125 inches on SAR drawing, negligible impact on results)	0.187	0.475
Width of radial FCS arm (assumed, value not on SAR drawing)	8.63	21.92
Width of tangential FCS arm (assumed, value not on SAR drawing)	8.88	22.56
Width of radial FCS Boral® (8.14 inches on SAR drawing, model is conservative)	7.75	19.69
Width of tangential FCS Boral® (8.56 inches on SAR drawing, model is conservative)	8.00	20.32
Distance from surface of strongback boral to inner surface of FCS (maximum area for FA expansion) (8.7 inches on SAR drawing, model is conservative)	8.8	22.4
Height of bottom FCS Boral® segment (21.12 inches on SAR drawing, model is conservative)	20.30	51.56
Height of standard length FCS Boral® segments (17.5 inches on SAR drawing, model is conservative)	17.0	43.18

Table 6.3-2 – Fuel Composition

Component	Wt.% in U or Pu	Wt.% in U or Pu Assumed for Models	Wt.% in Total Mixture
Total U/(U+Pu) = 94.0 wt.%			
U-234	≤ 0.05	0	0
U-235	≤ 0.3	0.3	0.249
U-238	99.65 - 100	99.7	82.615
Total Pu/(U+Pu) = 6.0 wt.%			
Pu-238	≤ 0.05	0	0
Pu-239	90.0 – 95.0	94	4.972
Pu-240	5.0 – 9.0	5	0.264
Pu-241	≤ 1.0	1	0.053
Pu-242	≤ 0.1	0	0
O	--	--	11.847
Total	--	--	100.0

Table 6.3-3 – Type 304 Stainless Steel Composition

Component	Wt.%
C	0.08
Si	1.0
P	0.045
Cr	19.0
Mn	2.0
Fe	68.375
Ni	9.5
Density = 7.94 g/cm^3	

Table 6.3-4 – Zirconium- M5 Alloy Composition

Component	Wt.%
Zr	Balance
Nb	1.2
Density = 6.50 g/cm^3	

Table 6.3-5 – XM-19 Austenitic Stainless Steel Composition

Component	Wt.%
C	0.06
N	0.4
Si	0.75
P	0.04
S	0.03
V	0.3
Cr	23.5
Mn	6.0
Ni	13.5
Nb	0.3
Mo	3.0
Fe	52.12
Density = 7.94 g/cm^3	

Note: Maximum values used, balance is Fe.

Table 6.3-6 – Boral Composition (0.035 g/cm^2 B-10)

Component	Number Density (atoms/b-cm)
B-10	7.3123E-03
B-11	3.9244E-02
C	1.2248E-02
Al	3.3439E-02
Total	9.2244E-02

Note: Boral thickness is 0.085 inches. The number density of B-10 has been reduced to 75% of the minimum value corresponding to an areal density of 0.035 g/cm^2; remaining elements unchanged. Neutron poison plates consist of B_4C mixed with aluminum; B_4C theoretical density is 2.51 g/cm^3.

Table 6.3-7 – MCNP5 Neutron Cross Sections

Isotope/Element	Cross Section Label
1001.62c	1-h-1 at 293.6K from endf-vi.8 njoy99.50
7014.62c	7-n-14 at 293.6K from endf-vi.8 njoy99.50
8016.62c	8-o-16 at 293.6K from endf-vi.8 njoy99.50
13027.62c	13-al-27 at 293.6K from endf-vi.8 njoy99.50
16032.62c	16-s-32 at 293.6K from endf/b-vi.8 njoy99.50
23000.62c	23-v-0 at 293.6K from endf/b-vi.8 njoy99.50
25055.62c	25-mn-55 at 293.6K from endf/b-vi.8 njoy99.50
5010.66c	5-b-10 at 293.6K from endf-vi.1 njoy99.50
5011.66c	5-b-11 at 293.6K from endf-vi.0 (MOD) njoy99.50
6000.66c	6-c-0 at 293.6K from endf-vi.6 njoy99.50
15031.66c	15-p-31 at 293.6K from endf-vi.6 njoy99.50
14000.60c	14-si-nat from endf/b-vi
24000.50c	njoy
26000.55c	njoy
28000.50c	njoy
40000.66c	40-zr-0 at 293.6K from endf-vi.1 njoy99.50
41093.66c	41-nb-93 at 293.6K from endf-vi.6 njoy99.50
42000.66c	42-mo-0 at 293.6K from endf-vi.0 njoy99.50
92235.66c	92-u-235 at 293.6K from endf-vi.5 njoy99.50
92238.66c	92-u-238 at 293.6K from endf-vi.5 njoy99.50
94239.66c	94-pu-239 at 293.6K from endf-vi.5 njoy99.50
94240.66c	94-pu-240 at 293.6K from endf-vi.2 njoy99.50
94241.66c	94-pu-241 at 293.6K from endf-vi.3 njoy99.50

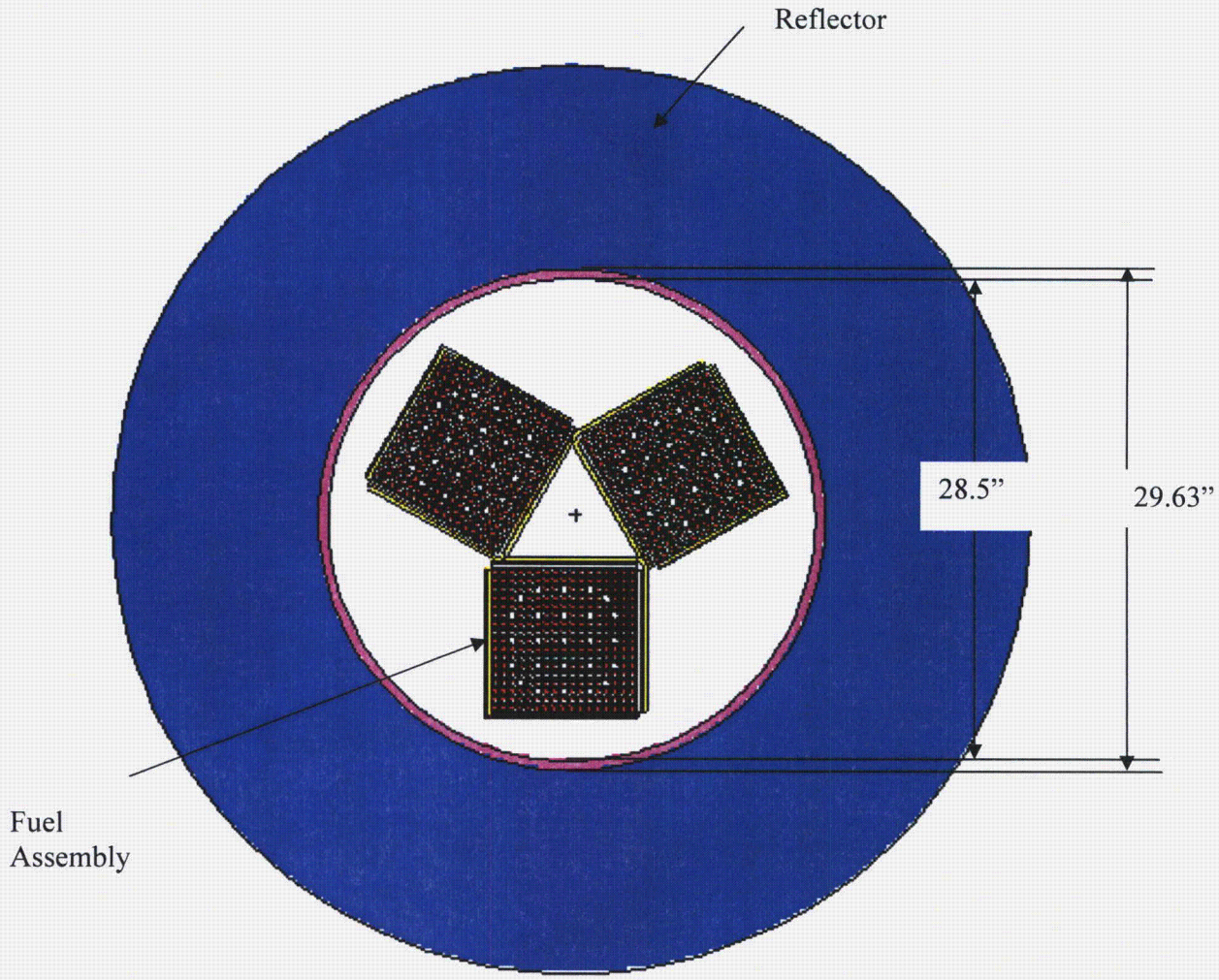

Figure 6.3-1 – NCT Model Geometry, Planar View

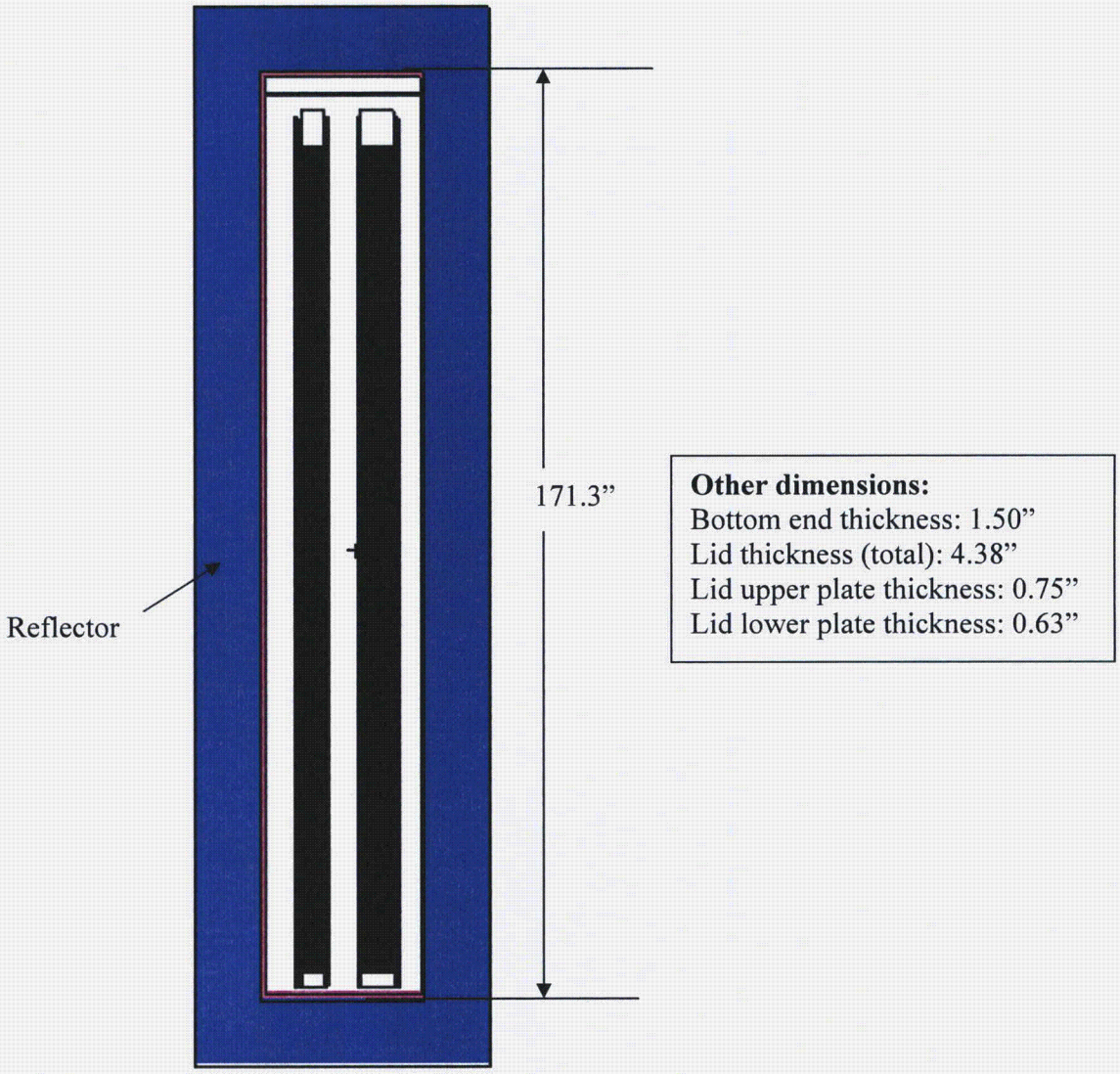

Figure 6.3-2 – NCT Model Geometry, Axial View

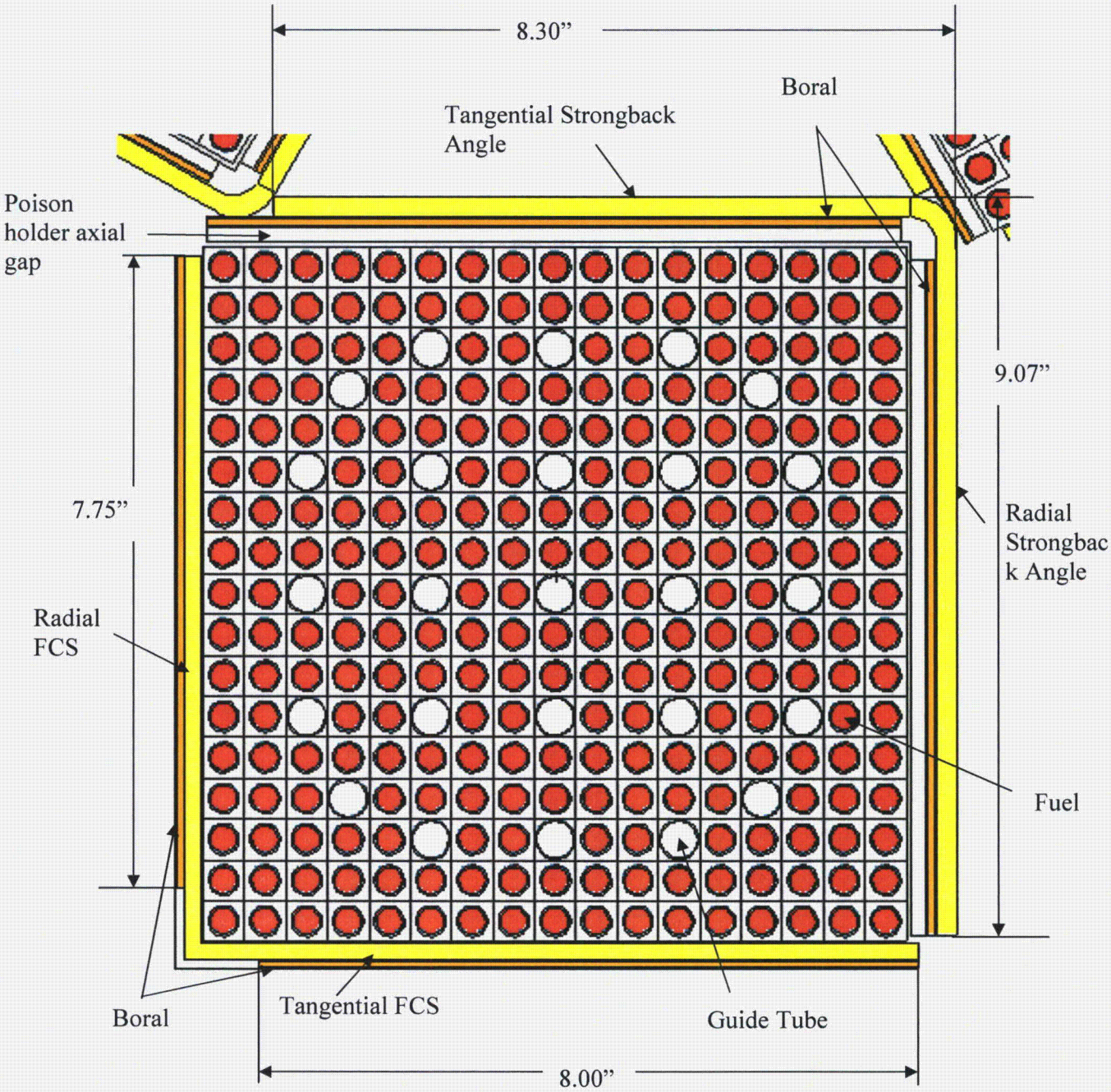

Other dimensions:

Max. height of boral FCS pieces:	20.3” for bottom segment
	17” for remaining segments

Figure 6.3-3 – NCT Model Geometry (Close-up through FCS Neutron Poison Cover Plates)

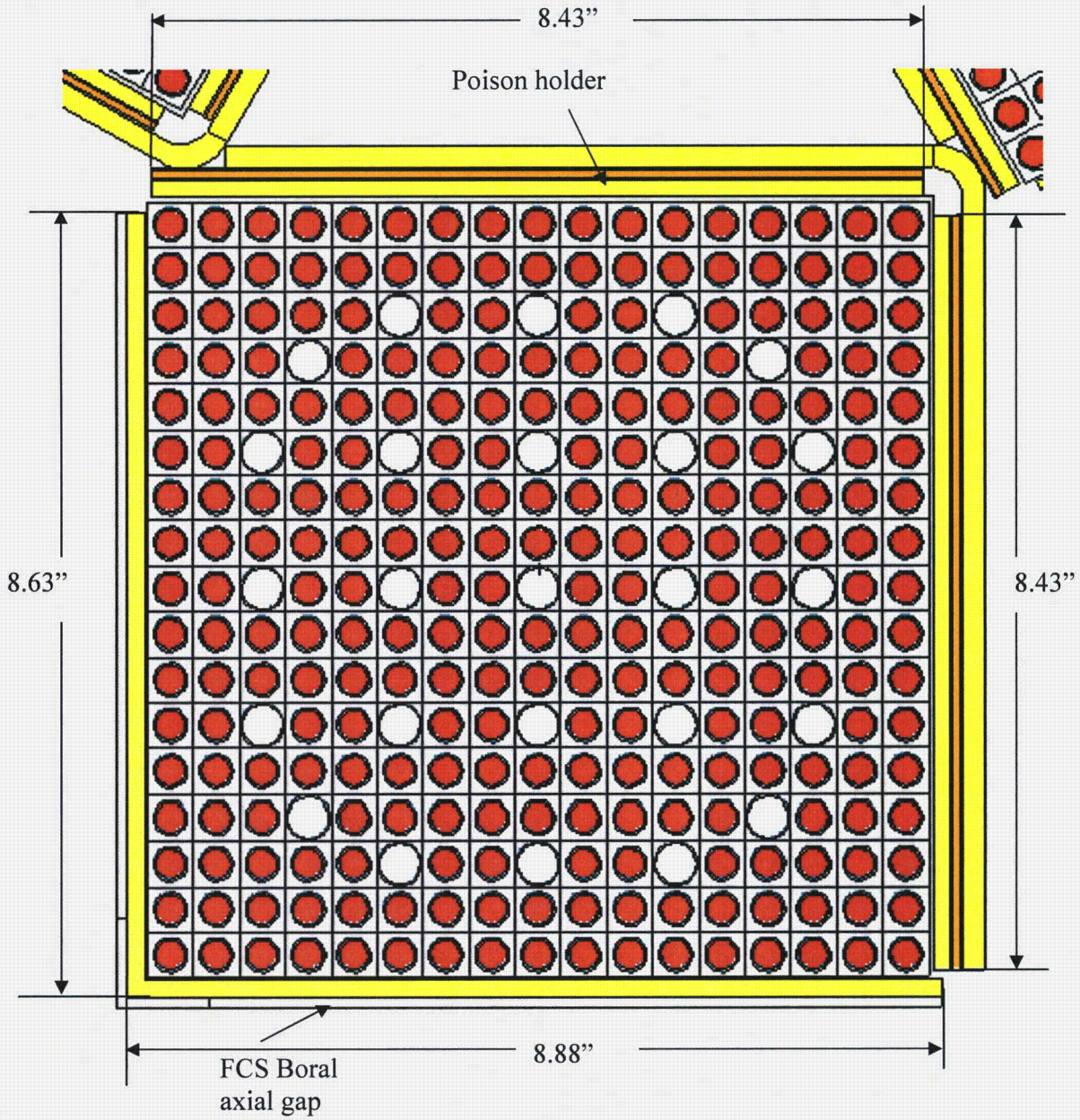

Other dimensions:
Thickness of FCS Sheet: 0.1874”
Poison holder height (except end): 4.25”
End poison holder height: 1.25”
Poison holder thickness: 0.1874”
Guide thimble OD: 0.482”
Guide thimble ID: 0.450”

Figure 6.3-4 – NCT Model Geometry (Close-up through Neutron Poison Cover Plate)

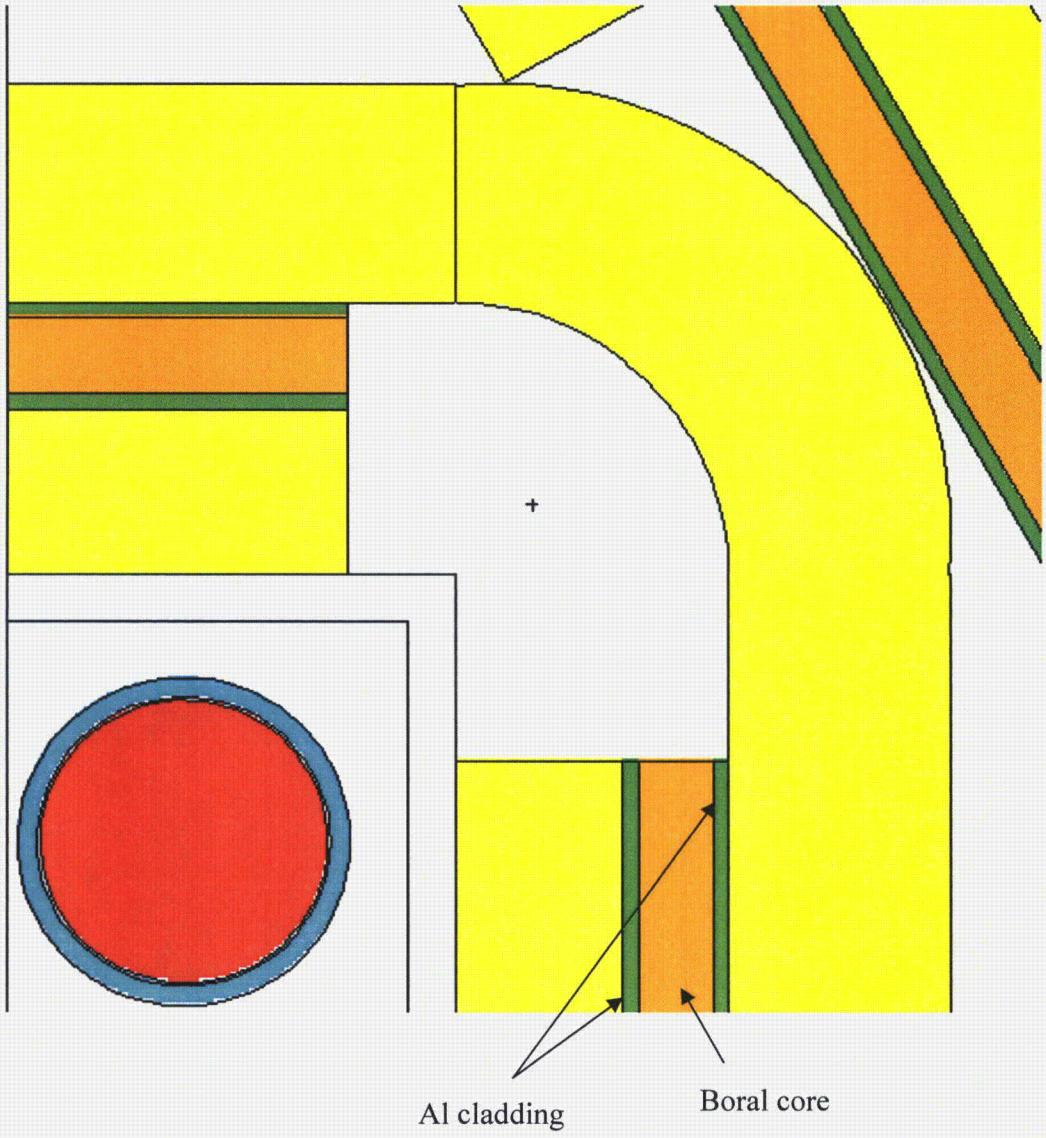

Other dimensions:
Fuel pellet OD: 0.3225”
Cladding OD: 0.374”
Cladding ID: 0.329”
Boral cladding thickness: 0.017”
Boral thickness: 0.085”
Strongback thickness: 0.25”
Strongback length: 160.11”

Figure 6.3-5 – NCT Model Geometry (Close-up of Corner)

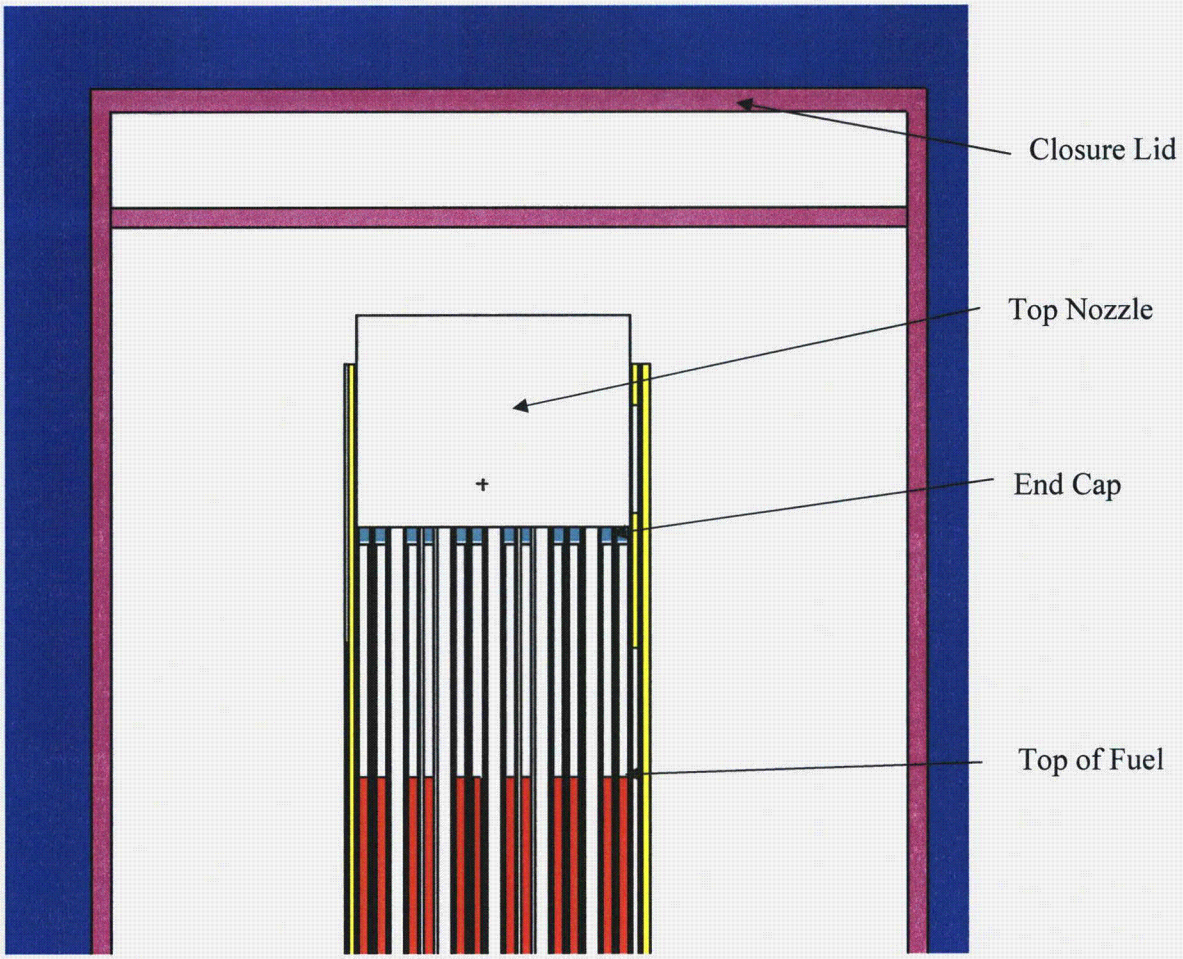

Other dimensions:
Overall fuel assembly length: 161.61"
Overall fuel rod length: 152.4"
Active fuel length: 144.0"

Figure 6.3-6 – NCT Model Geometry (Axial Close-up of Top)

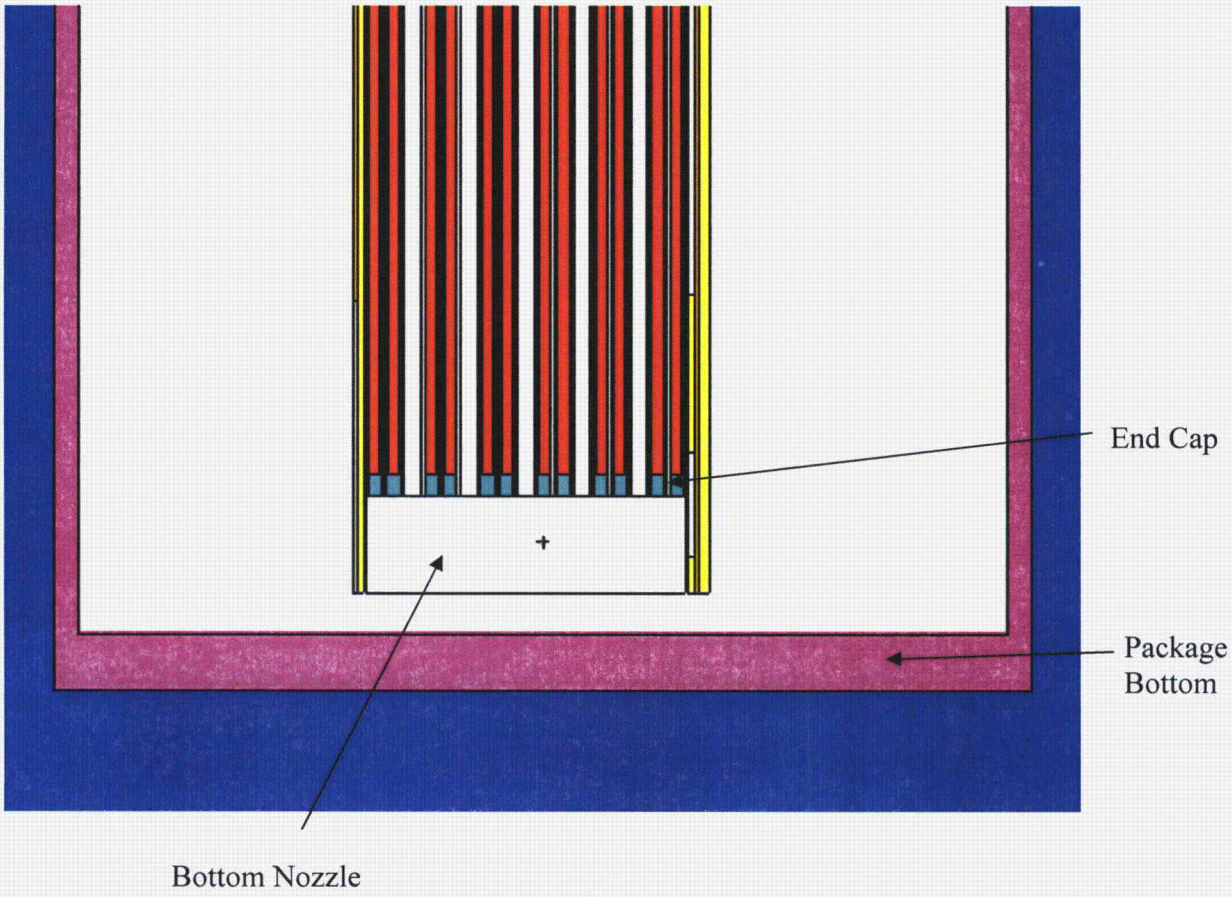

Figure 6.3-7 – NCT Model Geometry (Axial Close-up of Bottom)

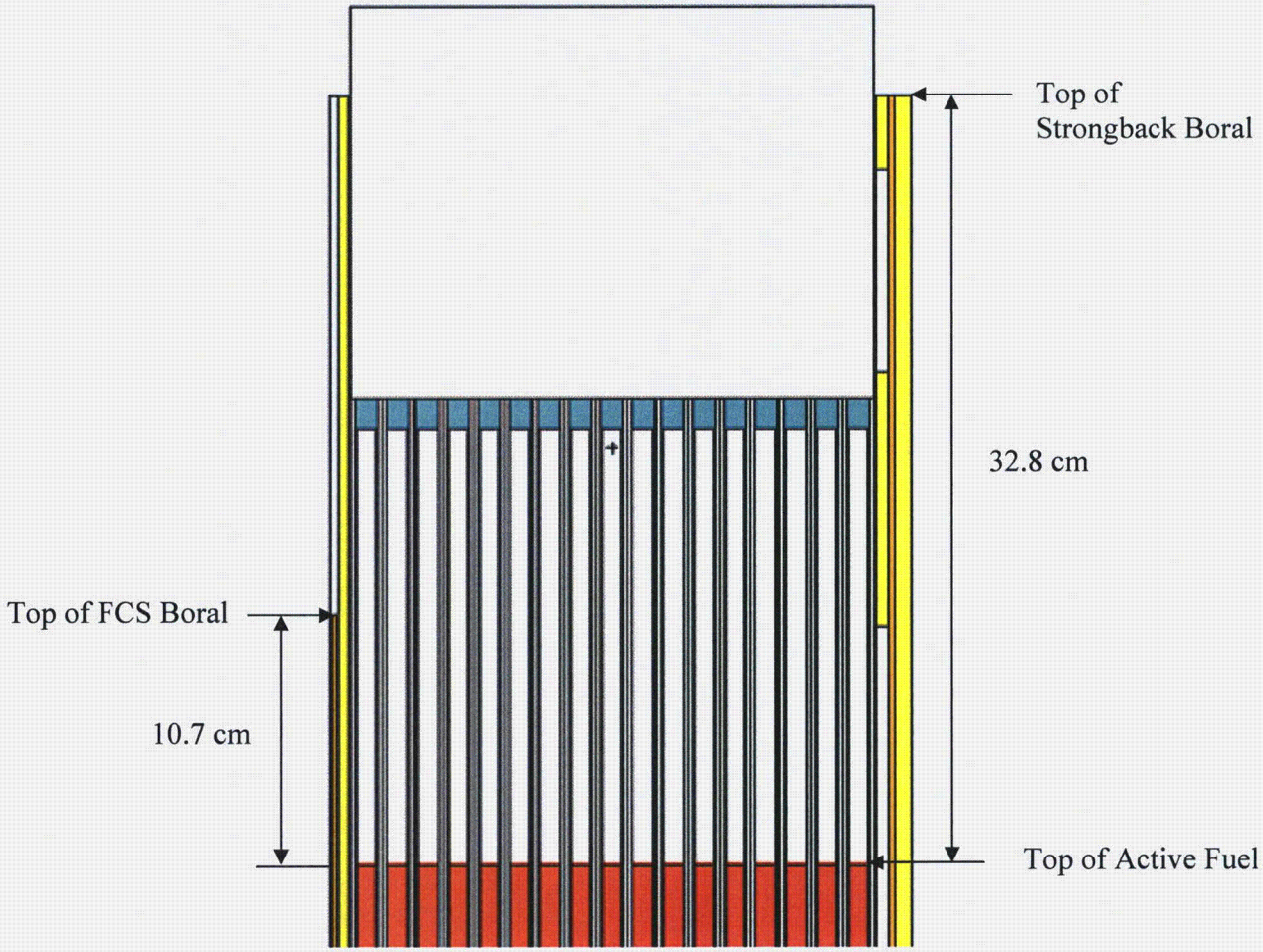

Figure 6.3-8 – NCT Model Geometry (Top Poison Coverage)

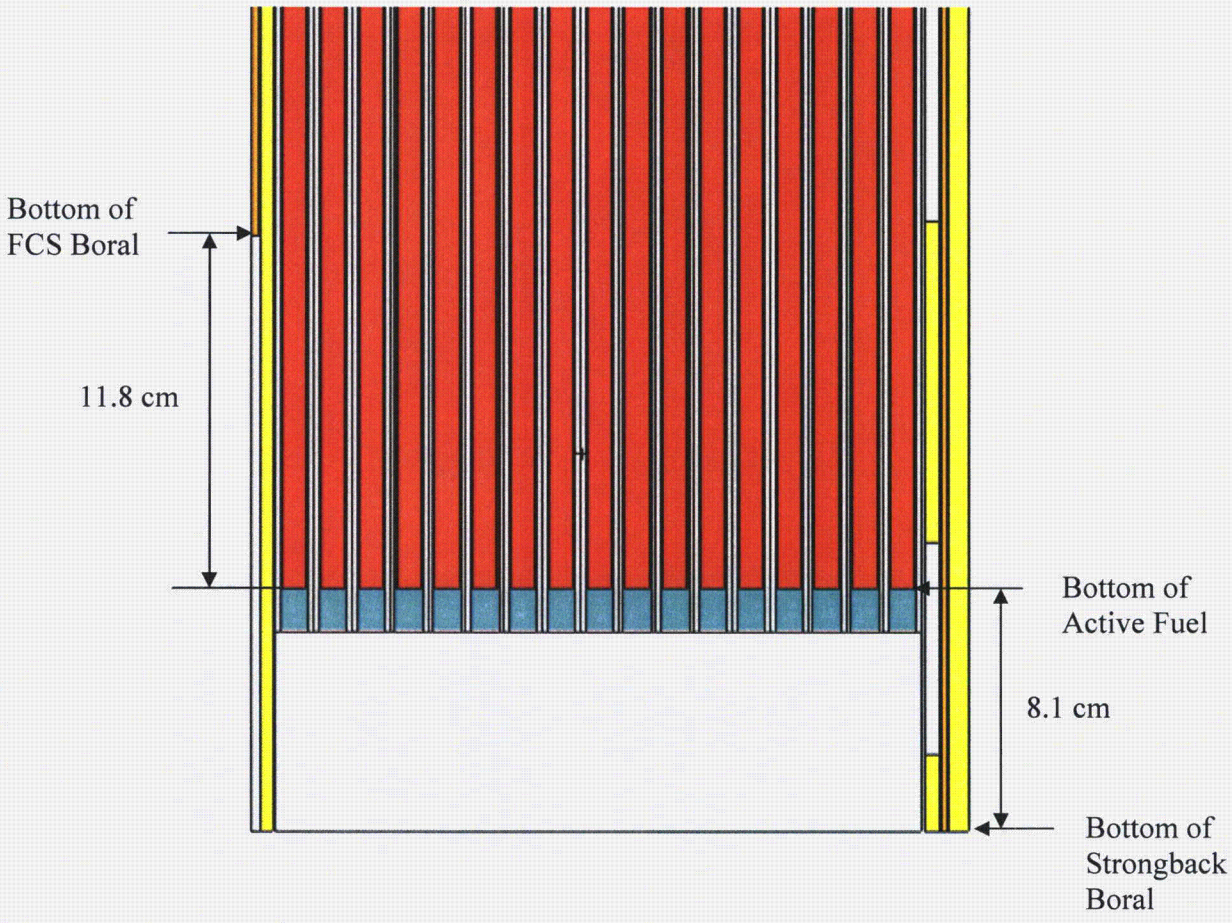

Figure 6.3-9 – NCT Model Geometry (Bottom Poison Coverage)

This page left intentionally blank.

6.4 Single Package Evaluation

Compliance with the requirements of 10 CFR §71.55 is demonstrated by analyzing optimally moderated damaged and undamaged, single-unit MFFP packages. The figures and descriptions provided in Section 6.3.1, *Model Configuration*, describe the basic geometry of the single-unit models.

6.4.1 Single Package Configuration

Because the engineering drop tests show no measurable change in the package external dimensions but expansion of the assembly pitch, the NCT and HAC models are the same, except (1) optimized internal water (within voids inside containment) is included in the HAC calculations, (2) the HAC cases allow for pitch expansion up to the maximum allowed extent, and (3) the HAC cases consider axial shifting of the fuel pins.

Each of the three FAs are radially symmetric about the origin. The model is constructed by building the lower assembly in the correct geometrical location using the MCNP LATTICE feature and then simply rotating copies of this assembly counterclockwise to build the other two assemblies. To simplify model preparation, the strongback assembly and outer FCS are modeled in separate MCNP "universes" and then inserted into the primary universe by use of the MCNP FILL command. This allows for simple rotation of these components to generate the complete model.

6.4.1.1 NCT Configuration

The largest allowable pin pitch in the undamaged condition is assumed (0.502 inches, 1.2751 cm). The package is reflected on all sides with 12 inches of three common reflectors: water, steel, and lead (cases nct_single_b35pnomplustol, nct_single_b35pnomplustol_Rsteel, nct_single_b35pnomplustol_Rlead). The lead reflector case is the most reactive of the three reflectors analyzed. Other reflectors might yield slightly higher results, although in the absence of internal moderation, the reactivity is extremely low (<0.3) and no further analysis is warranted. Because no water is present within the package for the NCT cases and the reactivity is low, parametric studies on the pitch are not warranted.

All cases except the final maximum case (max_nct_single) are run with a pellet density of 10.31 g/cm^3 and M5 cladding. To bound possible future fluctuations in the pellet density and cladding composition, the lead reflector case is run with a pellet density of 10.85 g/cm^3 and pure-zirconium cladding. It is shown in Section 6.6.3, *Impact of Niobium Content in the Cladding*, that pure zirconium cladding is slightly more reactive than cladding containing niobium.

6.4.1.2 HAC Configuration

The FCS limits the expansion of the fuel assemblies to a maximum of 8.8 inches. This dimension of 8.8 inches is defined from the surface of the strongback boral to the inner surface of the FCS, see Figure 6.4-1. In the HAC single package models, the pitch is allowed to range from a minimum value of nominal minus tolerance (0.490 inches) to a maximum value such that the OD of the outer fuel pins fill a region 8.8 inches square (0.5266 inches). In the MCNP models, the steel poison cover plates are "sliced off" to allow for this pin expansion. The various pitches used in the analysis, along with the nomenclature utilized, are provided in Table 6.4-1.

For the HAC single package model, it is assumed that water has completely flooded the package internals, including the pellet-cladding gap. The package is reflected with 12 inches of water on all sides. Note that reactivity increases with increasing pitch, indicating that the system is under moderated. The maximum reactivity is calculated for the maximum pitch expansion.

Using this model with maximum pitch and 12 inches water reflector, a further series of cases are run to investigate the effects of reduced internal moderation by reducing the internal water density. Because water is free to flow throughout the internals of the package, it is assumed that all internal water densities are uniformly reduced. As expected for an under moderated system, the reactivity decreases with decreasing water density.

The worst-case pitch geometry is also run with full-water moderation and both steel and lead reflectors. The increase in k_s with these reflectors is small (only a few mk), and the system is most reactive with a steel reflector. Because the difference in k_s between the three reflectors studied is small (~3 mk), analysis of other reflectors is not warranted.

Because the high-density steel and lead reflector cases (cases hac_single_b35pmax2_Rsteel, hac_single_b35pmax2_Rlead) are slightly more reactive than the water reflectors, additional cases (denoted with _hsteel in case name) are run to investigate the effect of including minor steel components that have been ignored in the model, namely, the clamp arms and the strongback triangles. The clamp arms are steel structures that weigh approximately 36 pounds each and secure the fuel assembly to the strongback. The strongback triangles fit into the triangular region between the strongbacks and provide support. The top and bottom triangles are primarily solid steel, while the triangle pieces in the central regions are fabricated from 1/2-inch thick steel plate and are mostly void.

For simplicity, this additional steel is not modeled explicitly but is homogenized into the water surrounding the assemblies. Water between the fuel pins remains unchanged and does not contain the homogenized steel. The triangle steel represents approximately 5.8% (by volume) of the region between the strongbacks, while the clamp arm steel represents approximately 3.2% (by volume) of the region between the fuel and the body shell wall. To maximize the amount of steel within the model, 5.8% steel is assumed for both regions. The reactivity for this case is slightly higher than the case without the homogenized steel, although the increase is within the statistical uncertainty of the calculations.

All cases except the final maximum cases (beginning max_hac_single) are run with a pellet density of 10.31 g/cm^3 and M5 cladding. To bound possible future fluctuations in the pellet density and cladding composition, the case with a steel reflector and homogenized minor steel components is run with a pellet density of 10.85 g/cm^3 and pure-zirconium cladding. It is shown in Section 6.6.3, *Impact of Niobium Content in the Cladding*, that pure zirconium cladding is slightly more reactive than cladding containing niobium.

The last set of calculations allows axial shifting of the fuel pins. These models use a pellet density of 10.85 g/cm^3 and pure-zirconium cladding. Approximately 8 fuel pins shifted upward through the holes in the top nozzle during the drop tests. In order to bound any potential axial displacement of the fuel pins, models are developed in which pins are allowed to shift up to the top lid or down to the bottom of the package. Models are developed with 8, 24, 60, and 116 pins shifted either up or down in a regular pattern, see Figure 6.4-2. Pins are shifted every other row to increase moderation between pins at the ends. To approximate the actual test results, models are also developed with only 10 or 20 randomly selected rods shifting either up or down. Cases are also developed in which all of the rods displace either up or down.

Pins are assumed to shift either up or down within a model, as the direction of shift will be dependent upon the package orientation upon impact. It is not possible for the some pins to shift up and other pins to shift down as a result of the same accident.

The relation of fuel to the top and bottom of the strongback for the nominal (unshifted) geometry is shown in Figure 6.3-6 and Figure 6.3-7, respectively. Fuel pins shifted up and down are shown in Figure 6.4-3 and Figure 6.4-4, respectively. Note that the top and bottom nozzles, as well as elements of the strongback, are necessarily ignored to allow the pins to shift in this fashion. Such extreme shifting would likely be incredible and was not observed in the drop tests.

6.4.2 Single Package Results

Criticality results for the NCT single package analysis is provided in Table 6.4-2. For the NCT case, the maximum $k_s = 0.2874$ is below the USL and is obtained for the case with a lead reflector, a pellet density of 10.85 g/cm^3, and pure zirconium cladding.

Criticality results for the HAC single package analysis without and with axially shifted fuel pins are provided in Table 6.4-3 and Table 6.4-4, respectively. For the HAC case, the maximum $k_s = 0.9001$ is below the USL and is obtained for the case with full-density water (with homogenized minor steel components) in the package cavity, maximum pin pitch, a steel reflector, a pellet density of 10.85 g/cm^3, pure zirconium cladding, and shifted fuel pins. The maximum $k_s = 0.9001$ occurs for two different cases, 20 fuel pins randomly shifted down, and 8 fuel pins shifted up. Allowing various combinations of fuel pins to shift axially has a small, positive effect on the reactivity, although the effect is in typically within the uncertainty of the Monte Carlo method.

NCT cases are run with 1,000 particles per generation, 530 generations, with 30 generations skipped. HAC cases are run with 2,000 particles per generation, 530 generations, with 30 generations skipped. MCNP5 performs statistical checks on k-collision, k-absorption, and k-track length. These cycle values should be normally distributed at the 99% confidence level or below. All of the reported results meet this convergence criteria. Convergence plots for the limiting NCT and HAC cases are provided in Figure 6.4-5 and Figure 6.4-6, respectively.

This page left intentionally blank.

Table 6.4-1 – Summary of Fuel Pin Pitch Nomenclature and Dimensions

Fuel Pin Pitch	Case label abbreviation	Pin Pitch (cm)	Pin Pitch (inches)
Nominal minus the tolerance	pnomminustol	1.2446	0.4900
Nominal	pnom	1.2598	0.4960
Nominal plus the tolerance	pnomplustol	1.2751	0.5020
Mid-point value	pmid	1.2952	0.5099
Maximum	pmax	1.3150	0.5177
Maximum with removal of poison cover plates	pmax2	1.3376	0.5266

Table 6.4-2 – Criticality Results for NCT Single Package

Case Identifier	Internal Water Density (g/cm^3)	EALF (MeV)	H/ ($^{239}Pu+^{235}U$)	V^m/V^f	^{239}Pu/ (U+Pu)	k_{eff}	σ	k_s ($k_{eff}+2\sigma$)
max_nct_single	**0**	**3.62E-01**	**0**	**1.740**	**0.056**	**0.2858**	**0.0008**	**0.2874**
nct_single_b35pnomplustol_Rsteel	0	2.66E-01	0	1.740	0.056	0.2627	0.0008	0.2642
nct_single_b35pnomplustol_Rlead	0	3.52E-01	0	1.740	0.056	0.2766	0.0008	0.2781
nct_single_b35pnomplustol	0	1.03E-01	0	1.740	0.056	0.2076	0.0005	0.2086

Table 6.4-3 – Criticality Results for HAC Single Package (no shifted pins)

Case Identifier	Internal Water Density (g/cm^3)	EALF (MeV)	H/ ($^{239}Pu+^{235}U$)	V^m/V^f	^{239}Pu/ (U+Pu)	k_{eff}	σ	k_s ($k_{eff}+2\sigma$)
max_hac_single_0Nb	1	7.32E-7	96.044	2.050	0.056	0.8958	0.0009	0.8976
hac_single_b35pmax2_Rsteel_hsteel	1	6.59E-07	101.074	2.050	0.056	0.8910	0.0010	0.8930
hac_single_b35pmax2_Rlead_hsteel	1	6.66E-07	101.074	2.050	0.056	0.8902	0.0010	0.8921
hac_single_b35pmax2_Rsteel	1	6.53E-07	101.074	2.050	0.056	0.8880	0.0010	0.8900
hac_single_b35pmax2_Rlead	1	6.68E-07	101.074	2.050	0.056	0.8860	0.0009	0.8879
hac_single_b35pmax2	1	6.60E-07	101.074	2.050	0.056	0.8854	0.0009	0.8872
hac_single_b35pmax	1	7.23E-07	95.466	1.936	0.056	0.8752	0.0010	0.8771
hac_single_b35pmid	1	7.82E-07	90.631	1.838	0.056	0.8626	0.0010	0.8646
hac_single_b35pnomplustol	1	8.45E-07	85.793	1.740	0.056	0.8511	0.0010	0.8532
hac_single_b35pnom	1	9.11E-07	82.179	1.667	0.056	0.8448	0.0010	0.8468
hac_single_b35pnomminustol	1	9.76E-07	78.609	1.594	0.056	0.8335	0.0010	0.8354
hac_single_b35pmax2_i95	0.95	7.49E-07	96.021	2.050	0.056	0.8621	0.0009	0.8640
hac_single_b35pmax2_i90	0.9	8.61E-07	90.967	2.050	0.056	0.8347	0.0010	0.8367
hac_single_b35pmax2_i75	0.75	1.41E-06	75.806	2.050	0.056	0.7527	0.0009	0.7546
hac_single_b35pmax2_i50	0.5	5.51E-06	50.537	2.050	0.056	0.5873	0.0008	0.5890
hac_single_b35pmax2_i25	0.25	9.77E-05	25.269	2.050	0.056	0.3993	0.0007	0.4007
hac_single_b35pmax2_i10	0.1	3.04E-03	10.107	2.050	0.056	0.2838	0.0005	0.2847
hac_single_b35pmax2_i0	0	9.90E-02	0.000	2.050	0.056	0.2064	0.0004	0.2071

Table 6.4-4 – Criticality Results for HAC Single Package (with shifted pins)

Case Identifier	Internal Water Density (g/cm^3)	Shifted Pins	EALF (MeV)	H/ ($^{239}Pu+^{235}U$)	V^m/V^f	^{239}Pu/ (U+Pu)	k_{eff}	σ	k_s ($k_{eff}+2\sigma$)
max_hac_single_srnddn10	1	10 down random	7.28E-07	96.044	2.050	0.056	0.8970	0.0009	0.8988
max_hac_single_srnddn20	**1**	**20 down random**	**7.15E-07**	**96.044**	**2.050**	**0.056**	**0.8983**	**0.0009**	**0.9001**
max_hac_single_sd1	1	8 down	7.22E-07	96.044	2.050	0.056	0.8957	0.0010	0.8976
max_hac_single_sd2	1	24 down	7.19E-07	96.044	2.050	0.056	0.8958	0.0010	0.8977
max_hac_single_sd3	1	60 down	7.17E-07	96.044	2.050	0.056	0.8960	0.0009	0.8978
max_hac_single_sd4	1	116 down	7.22E-07	96.044	2.050	0.056	0.8956	0.0010	0.8976
max_hac_single_salldn	1	All down	7.30E-07	96.044	2.050	0.056	0.8963	0.0010	0.8983
max_hac_single_srndup10	1	10 up random	7.14E-07	96.044	2.050	0.056	0.8968	0.0010	0.8987
max_hac_single_srndup20	1	20 up random	7.26E-07	96.044	2.050	0.056	0.8964	0.0010	0.8983
max_hac_single_su1	**1**	**8 up**	**7.24E-07**	**96.044**	**2.050**	**0.056**	**0.8981**	**0.0010**	**0.9001**
max_hac_single_su2	1	24 up	7.25E-07	96.044	2.050	0.056	0.8958	0.0010	0.8979
max_hac_single_su3	1	60 up	7.08E-07	96.044	2.050	0.056	0.8962	0.0009	0.8981
max_hac_single_su4	1	116 up	7.13E-07	96.044	2.050	0.056	0.8964	0.0010	0.8985
max_hac_single_sallup	1	All up	7.26E-07	96.044	2.050	0.056	0.8953	0.0009	0.8972

This page left intentionally blank.

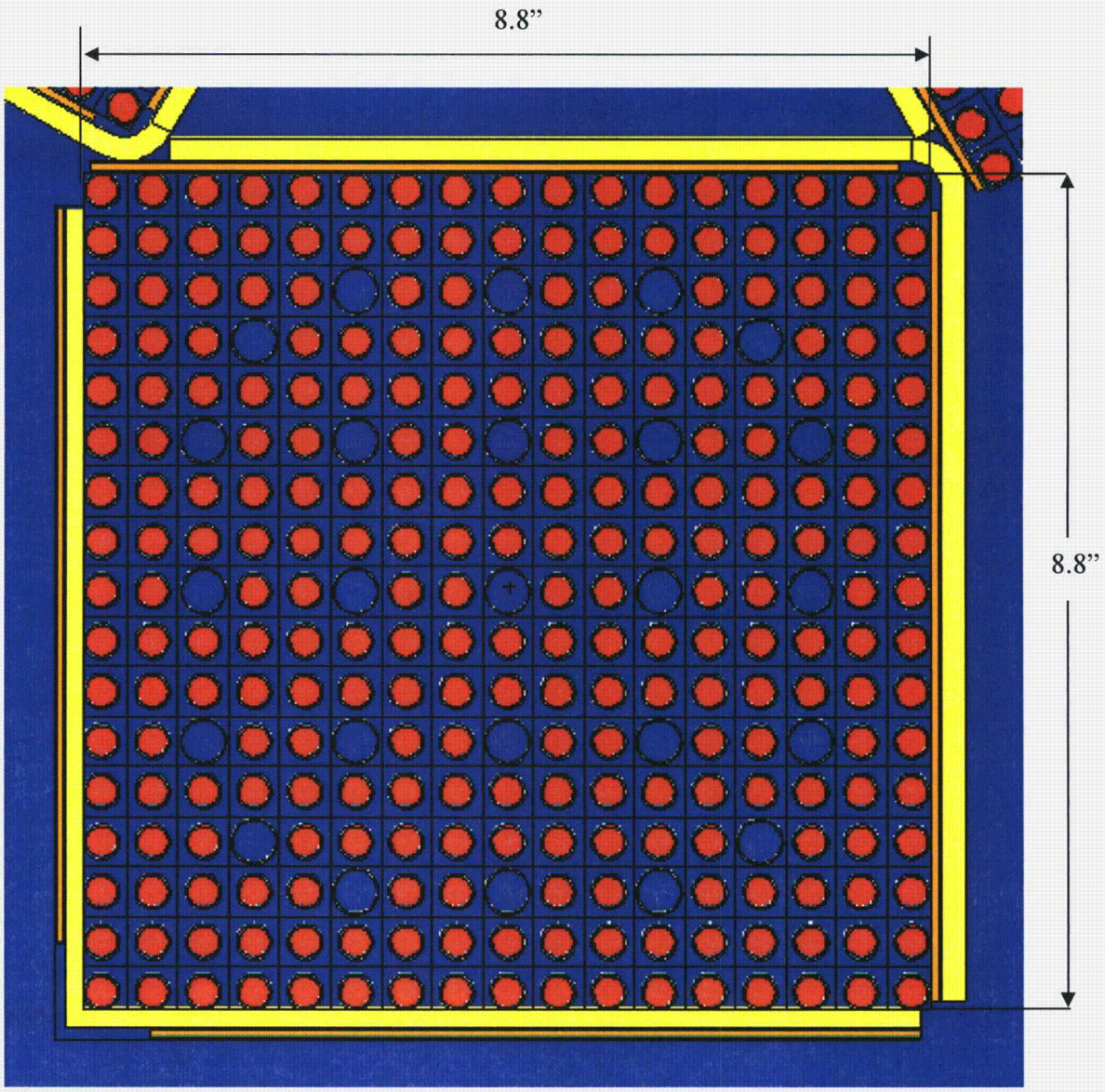

Note that the pitch has expanded to the maximum possible extent (8.8-inch square) and that the poison holders have been "sliced off" to allow for this expansion.

Figure 6.4-1 – HAC Model Geometry, Worst-Case Pitch

10 randomly shifted pins

1	1	1	1	1	1	1	1	1	1	1	1	1	1	1	1	1
1	1	1	1	1	1	1	1	1	1	1	1	1	1	1	1	1
1	1	1	1	1	4	1	1	4	1	1	4	1	1	1	1	1
1	1	1	4	1	3	1	1	1	1	1	1	1	4	1	1	1
1	1	1	1	1	1	1	1	1	1	1	3	1	1	1	1	1
1	1	4	1	1	4	1	1	4	1	1	4	1	1	4	1	1
1	1	1	3	1	1	3	1	1	1	1	1	1	1	1	1	1
1	1	1	1	1	1	1	1	1	1	1	1	1	3	1	1	1
1	1	4	1	1	4	1	1	4	1	3	4	1	1	4	1	1
1	1	1	1	1	1	3	1	1	1	1	1	1	1	1	1	1
1	1	1	1	1	1	1	1	1	1	1	1	1	3	1	1	1
1	1	4	1	1	4	1	1	4	1	1	4	1	1	4	1	1
1	1	1	1	1	1	1	1	1	1	3	1	1	1	1	1	1
1	1	1	4	1	1	3	1	1	1	1	1	1	4	1	1	1
1	1	1	1	1	4	1	1	4	1	1	4	1	1	1	1	1
1	1	1	1	1	1	1	1	1	1	1	1	1	1	1	1	1
1	1	1	1	1	1	1	1	1	1	1	1	1	1	1	1	1

20 randomly shifted pins

1	1	1	1	1	1	1	1	1	1	1	1	1	1	1	1	1
1	1	1	1	1	1	1	1	1	1	1	1	1	1	1	1	1
1	1	1	1	1	4	1	1	4	1	1	4	1	1	1	1	1
1	1	1	4	1	3	1	1	1	1	1	1	1	4	1	1	1
1	1	1	1	1	1	1	3	1	1	1	3	1	1	1	1	1
1	1	4	1	1	4	1	1	4	1	1	4	1	1	4	1	1
1	1	1	3	1	1	3	1	1	1	3	1	1	1	1	1	1
1	1	1	1	1	1	1	3	1	1	1	1	1	3	1	1	1
1	1	4	1	1	4	1	1	4	1	3	4	1	1	4	1	1
1	1	1	3	1	1	3	1	1	3	1	1	1	1	1	1	1
1	1	1	1	1	1	1	1	1	1	3	1	1	3	1	1	1
1	1	4	3	1	4	1	3	4	1	1	4	1	1	4	1	1
1	1	1	1	1	1	1	1	1	1	3	1	1	1	1	1	1
1	1	1	4	1	1	3	1	1	3	1	1	3	4	1	1	1
1	1	1	1	1	4	1	1	4	1	1	4	1	1	1	1	1
1	1	1	1	1	1	1	1	1	1	1	1	1	1	1	1	1
1	1	1	1	1	1	1	1	1	1	1	1	1	1	1	1	1

1 is a fuel pin in the standard axial position

3 is a shifted fuel pin (either up or down)

4 is a guide thimble

Figure 6.4-2 – Fuel Pin Loading Patterns for Axially Shifted Fuel

8 shifted pins

1	1	1	1	1	1	1	1	1	1	1	1	1	1	1	1	1
1	1	1	1	1	1	1	1	1	1	1	1	1	1	1	1	1
1	1	1	1	1	4	1	1	4	1	1	4	1	1	1	1	1
1	1	1	4	1	1	1	1	1	1	1	1	1	4	1	1	1
1	1	1	1	1	1	1	1	1	1	1	1	1	1	1	1	1
1	1	4	1	1	4	1	1	4	1	1	4	1	1	4	1	1
1	1	1	1	1	1	1	1	1	1	1	1	1	1	1	1	1
1	1	1	1	1	1	1	3	3	3	1	1	1	1	1	1	1
1	1	4	1	1	4	1	3	4	3	1	4	1	1	4	1	1
1	1	1	1	1	1	1	3	3	3	1	1	1	1	1	1	1
1	1	1	1	1	1	1	1	1	1	1	1	1	1	1	1	1
1	1	4	1	1	4	1	1	4	1	1	4	1	1	4	1	1
1	1	1	1	1	1	1	1	1	1	1	1	1	1	1	1	1
1	1	1	4	1	1	1	1	1	1	1	1	1	4	1	1	1
1	1	1	1	1	4	1	1	4	1	1	4	1	1	1	1	1
1	1	1	1	1	1	1	1	1	1	1	1	1	1	1	1	1
1	1	1	1	1	1	1	1	1	1	1	1	1	1	1	1	1

24 shifted pins

1	1	1	1	1	1	1	1	1	1	1	1	1	1	1	1	1
1	1	1	1	1	1	1	1	1	1	1	1	1	1	1	1	1
1	1	1	1	1	4	1	1	4	1	1	4	1	1	1	1	1
1	1	1	4	1	1	1	1	1	1	1	1	1	4	1	1	1
1	1	1	1	1	1	1	1	1	1	1	1	1	1	1	1	1
1	1	4	1	1	4	3	3	4	3	3	4	1	1	4	1	1
1	1	1	1	1	3	1	1	1	1	1	3	1	1	1	1	1
1	1	1	1	1	3	1	3	3	3	1	3	1	1	1	1	1
1	1	4	1	1	4	1	3	4	3	1	4	1	1	4	1	1
1	1	1	1	1	3	1	3	3	3	1	3	1	1	1	1	1
1	1	1	1	1	3	1	1	1	1	1	3	1	1	1	1	1
1	1	4	1	1	4	3	3	4	3	3	4	1	1	4	1	1
1	1	1	1	1	1	1	1	1	1	1	1	1	1	1	1	1
1	1	1	4	1	1	1	1	1	1	1	1	1	4	1	1	1
1	1	1	1	1	4	1	1	4	1	1	4	1	1	1	1	1
1	1	1	1	1	1	1	1	1	1	1	1	1	1	1	1	1
1	1	1	1	1	1	1	1	1	1	1	1	1	1	1	1	1

1 is a fuel pin in the standard axial position

3 is a shifted fuel pin (either up or down)

4 is a guide thimble

Figure 6.4-2 – Fuel Pin Loading Patterns for Axially Shifted Fuel (2/3)

60 shifted pins

1	1	1	1	1	1	1	1	1	1	1	1	1	1	1	1	1
1	1	1	1	1	1	1	1	1	1	1	1	1	1	1	1	1
1	1	1	1	1	4	1	1	4	1	1	4	1	1	1	1	1
1	1	1	4	3	3	3	3	3	3	3	3	3	4	1	1	1
1	1	1	3	1	1	1	1	1	1	1	1	1	3	1	1	1
1	1	4	3	1	4	3	3	4	3	3	4	1	3	4	1	1
1	1	1	3	1	3	1	1	1	1	1	3	1	3	1	1	1
1	1	1	3	1	3	1	3	3	3	1	3	1	3	1	1	1
1	1	4	3	1	4	1	3	4	3	1	4	1	3	4	1	1
1	1	1	3	1	3	1	3	3	3	1	3	1	3	1	1	1
1	1	1	3	1	3	1	1	1	1	1	3	1	3	1	1	1
1	1	4	3	1	4	3	3	4	3	3	4	1	3	4	1	1
1	1	1	3	1	1	1	1	1	1	1	1	1	3	1	1	1
1	1	1	4	3	3	3	3	3	3	3	3	3	4	1	1	1
1	1	1	1	1	4	1	1	4	1	1	4	1	1	1	1	1
1	1	1	1	1	1	1	1	1	1	1	1	1	1	1	1	1
1	1	1	1	1	1	1	1	1	1	1	1	1	1	1	1	1

116 shifted pins

1	1	1	1	1	1	1	1	1	1	1	1	1	1	1	1	1
1	3	3	3	3	3	3	3	3	3	3	3	3	3	3	3	1
1	3	1	1	1	4	1	1	4	1	1	4	1	1	1	3	1
1	3	1	4	3	3	3	3	3	3	3	3	3	4	1	3	1
1	3	1	3	1	1	1	1	1	1	1	1	1	3	1	3	1
1	3	4	3	1	4	3	3	4	3	3	4	1	3	4	3	1
1	3	1	3	1	3	1	1	1	1	1	3	1	3	1	3	1
1	3	1	3	1	3	1	3	3	3	1	3	1	3	1	3	1
1	3	4	3	1	4	1	3	4	3	1	4	1	3	4	3	1
1	3	1	3	1	3	1	3	3	3	1	3	1	3	1	3	1
1	3	1	3	1	3	1	1	1	1	1	3	1	3	1	3	1
1	3	4	3	1	4	3	3	4	3	3	4	1	3	4	3	1
1	3	1	3	1	1	1	1	1	1	1	1	1	3	1	3	1
1	3	1	4	3	3	3	3	3	3	3	3	3	4	1	3	1
1	3	1	1	1	4	1	1	4	1	1	4	1	1	1	3	1
1	3	3	3	3	3	3	3	3	3	3	3	3	3	3	3	1
1	1	1	1	1	1	1	1	1	1	1	1	1	1	1	1	1

1 is a fuel pin in the standard axial position

3 is a shifted fuel pin (either up or down)

4 is a guide thimble

Figure 6.4-2 – Fuel Pin Loading Patterns for Axially Shifted Fuel (3/3)

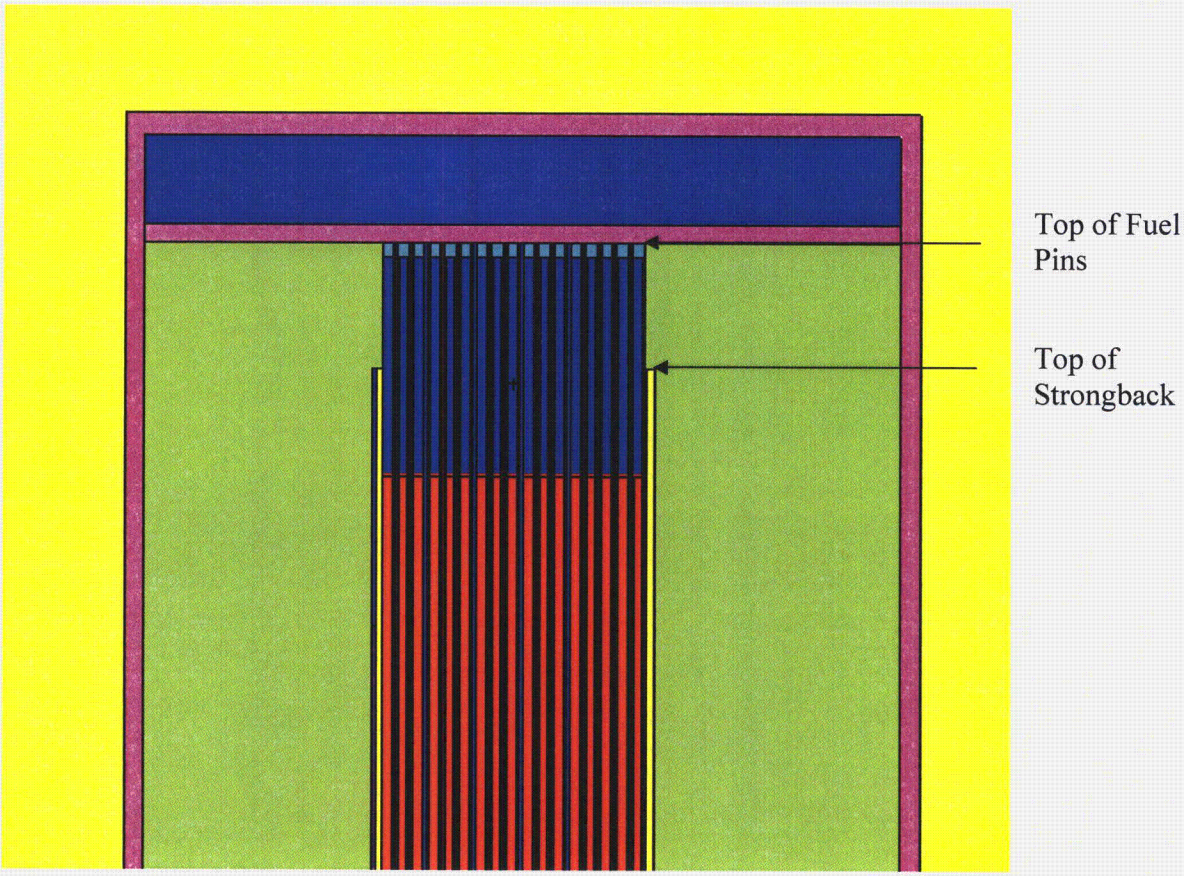

Figure 6.4-3 – HAC Model Geometry, Pins Shifted Up

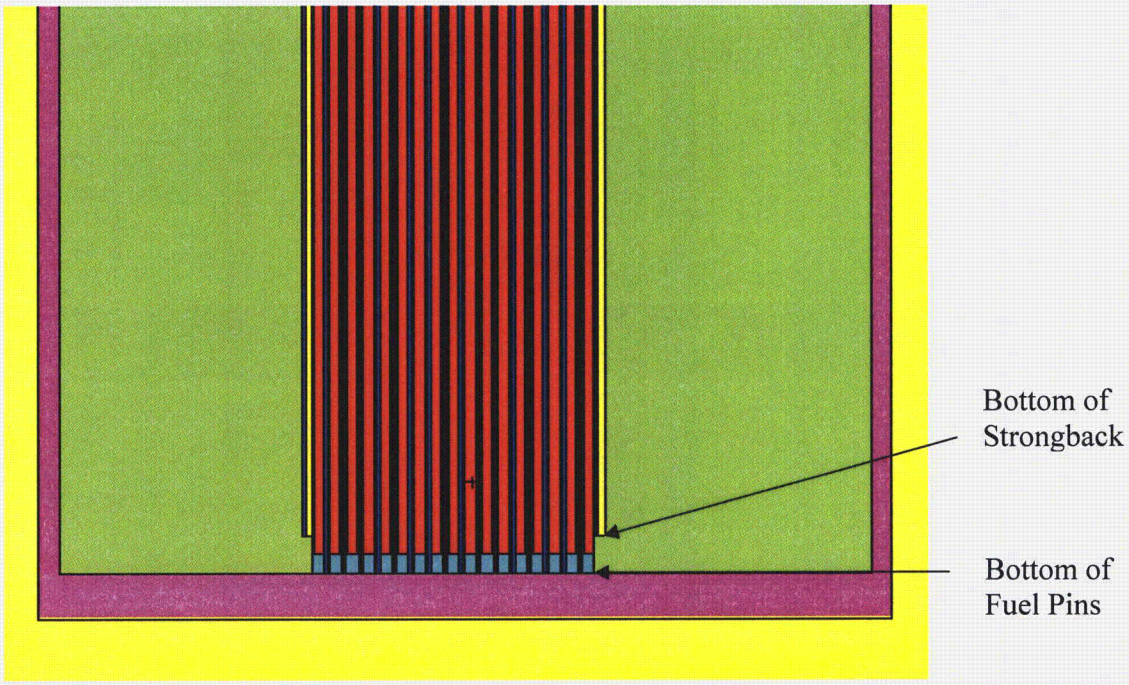

Figure 6.4-4 – HAC Model Geometry, Pins Shifted Down

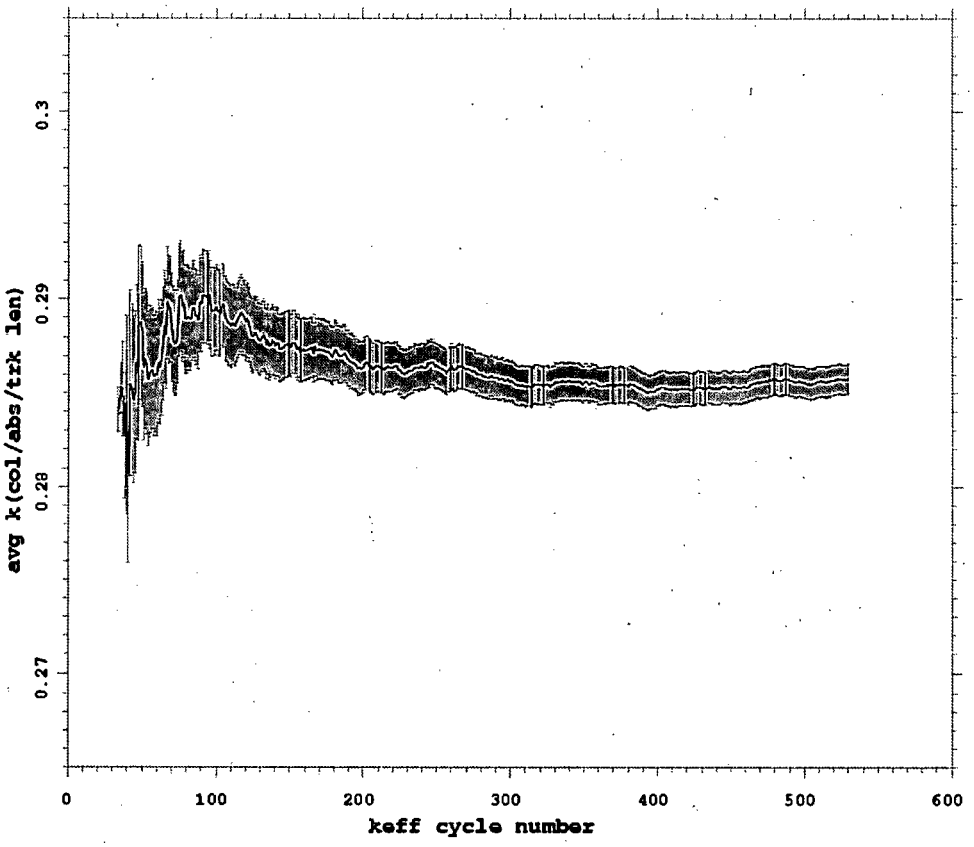

Figure 6.4-5 – Convergence of Maximum NCT Single Case (max_nct_single)

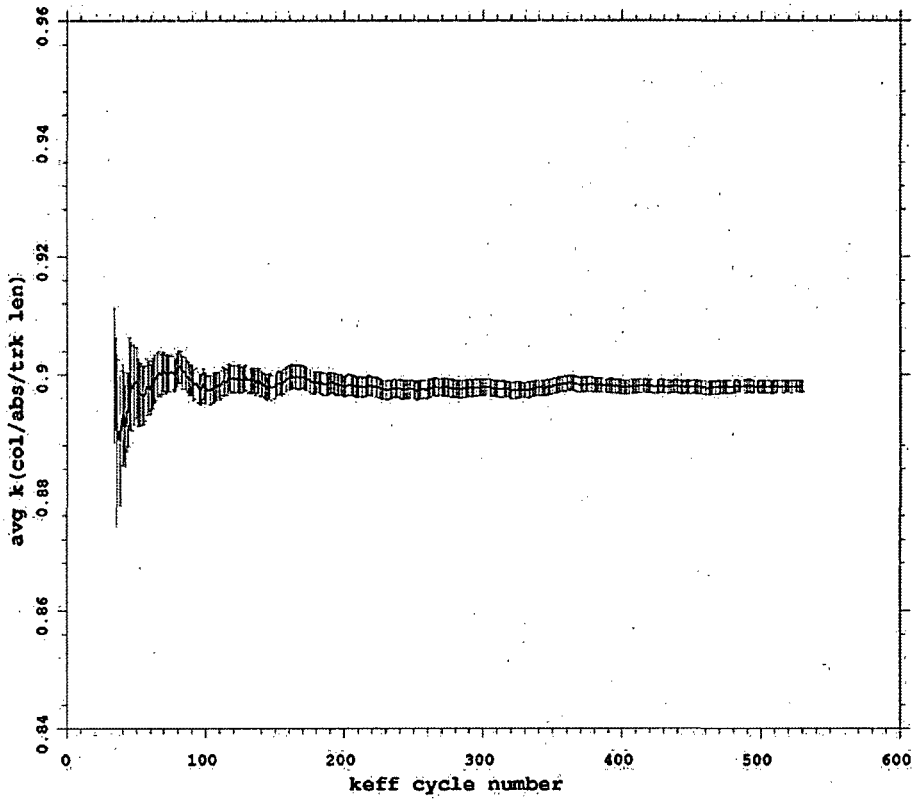

Figure 6.4-6 – Convergence of Maximum HAC Single Case (max_hac_single_su1)

6.5 Evaluation of Package Arrays Under Normal Conditions of Transport

6.5.1 NCT Array Configuration

The NCT array model is developed by assuming an infinite close-packed hexagonal array, see Figure 6.5-1. No water is assumed inside the package and the clamp arms and strongback triangles are ignored. Outside the package, water is assumed to vary between 0.0 and 1.0 g/cm^3. The worst-case is obtained for no water between the packages.

All cases except the final maximum case (max_nct_array) are run with a pellet density of 10.31 g/cm^3 and M5 cladding. To bound possible future fluctuations in the pellet density and cladding composition, the case with no external moderator is run with a pellet density of 10.85 g/cm^3 and pure-zirconium cladding. It is shown in Section 6.6.3, *Impact of Niobium Content in the Cladding*, that pure zirconium cladding is slightly more reactive than cladding containing niobium.

6.5.2 NCT Array Results

The maximum k_s = 0.6039 is below the USL and is obtained for the case with no external moderation, a pellet density of 10.85 g/cm^3, and a pure zirconium cladding. Criticality results for the NCT array cases are provided in Table 6.5-1.

Cases are run with 1,000 particles per generation, 530 generations, with 30 generations skipped. Convergence is well-behaved and the convergence plot as a function of generation for the limiting case is provided in Figure 6.5-2.

This page left intentionally blank.

Table 6.5-1 – Criticality Results for an Infinite Array of NCT Packages

Case Identifier	Water Density (g/cm^3)		EALF (MeV)	H/ ($^{239}Pu+^{235}U$)	V^m/V^f	$\frac{^{239}Pu}{(U+Pu)}$	k_{eff}	σ	k_s ($k_{eff}+2\sigma$)
	Internal	External							
Max_nct_array	**0**	**0**	**0.0977**	**0**	**1.740**	**0.056**	**0.6027**	**0.0006**	**0.6039**
nct_array_b35pnomplustol_o100	0	1.0	0.0273	0	1.740	0.056	0.3225	0.0006	0.3237
nct_array_b35pnomplustol_o95	0	0.95	0.0262	0	1.740	0.056	0.3273	0.0006	0.3285
nct_array_b35pnomplustol_o90	0	0.90	0.0255	0	1.740	0.056	0.3309	0.0006	0.3321
nct_array_b35pnomplustol_o75	0	0.75	0.0237	0	1.740	0.056	0.3464	0.0006	0.3476
nct_array_b35pnomplustol_o50	0	0.50	0.0199	0	1.740	0.056	0.3805	0.0007	0.3818
nct_array_b35pnomplustol_o25	0	0.25	0.0189	0	1.740	0.056	0.4523	0.0007	0.4536
nct_array_b35pnomplustol_o10	0	0.1	0.0262	0	1.740	0.056	0.5311	0.0007	0.5325
nct_array_b35pnomplustol_o05	0	0.05	0.0385	0	1.740	0.056	0.5664	0.0006	0.5677
nct_array_b35pnomplustol_o001	0	0.001	0.0947	0	1.740	0.056	0.5882	0.0006	0.5895
nct_array_b35pnomplustol_o0	0	0	0.0955	0	1.740	0.056	0.5887	0.0006	0.5898

This page left intentionally blank.

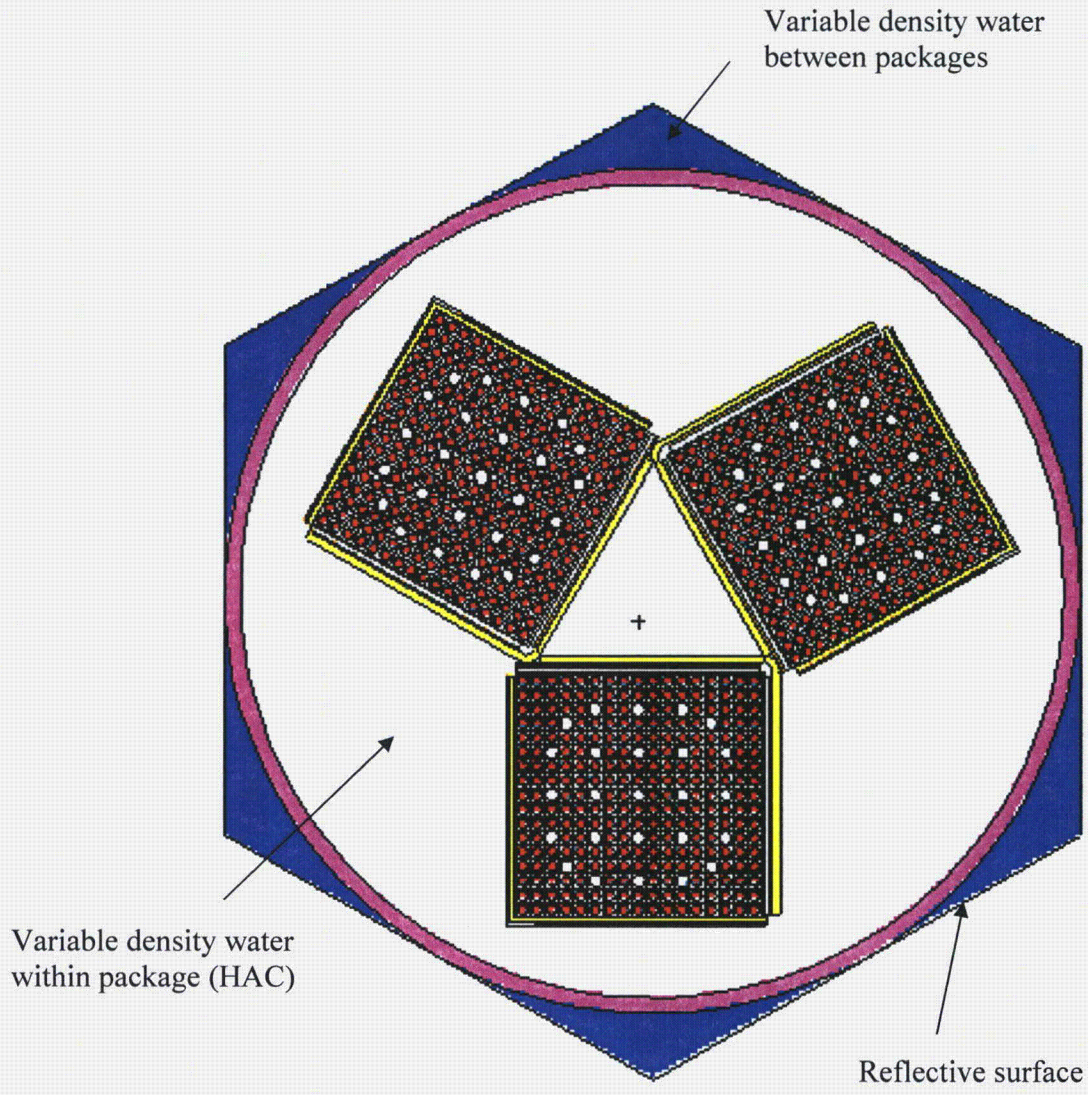

Figure 6.5-1 – Model Geometry, Infinite Array

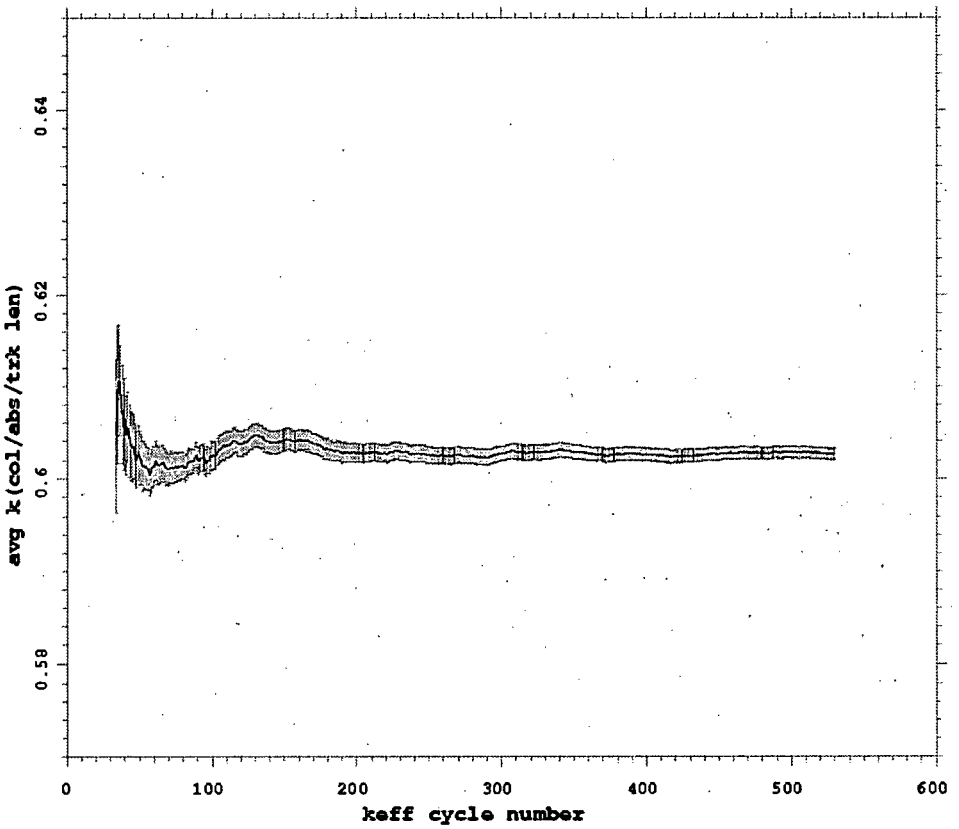

Figure 6.5-2 – Convergence of Maximum NCT Array Case (max_nct_array)

6.6 Package Arrays Under Hypothetical Accident Conditions

6.6.1 HAC Array Configuration

The HAC array models are developed in the same manner as the NCT array models. The worst-case pitch from the single package HAC case (0.5266 inches) is assumed for all models. Internal and external water densities are varied independently to obtain the most reactive configuration. Because water is free to flow throughout the internals of the package, it is assumed that all internal water densities are uniformly reduced. Initially, the clamp arms and strongback angles are ignored. The maximum reactivity for the cases without clamp arms or strongback angles is obtained for the case with full internal moderation and no moderation between packages.

Although full-density internal water results in the worst-case reactivity, water also serves to isolate the fuel assemblies from one another. Therefore, ignoring the minor steel components, such as the clamp arms and strongback triangles, is a small non-conservative assumption because neutrons pass easily through steel and thus steel within the package will increase reactivity. As with the HAC single package models, the effect of ignoring small amounts of steel (i.e., the clamp arms and strongback angles) is quantified by assuming 5.8% (by volume) steel is homogenized within the body (case hac_array_b35pmax2_i100o0_hsteel). The reactivity increase when including the homogenized steel is insignificant and is within the uncertainty of this calculation.

All cases except the final maximum cases (beginning max_hac_array) are run with a pellet density of 10.31 g/cm^3 and M5 cladding. To bound possible future fluctuations in the pellet density and cladding composition, the case with no external moderator, 100% internal moderator, and homogenized minor steel components is run with a pellet density of 10.85 g/cm^3 and pure-zirconium cladding. It is shown in Section 6.6.3, *Impact of Niobium Content in the Cladding*, that pure zirconium cladding is slightly more reactive than cladding containing niobium.

A final set of cases is run that allow the fuel pins to shift axially, as described in Section 6.4.1.2. These cases have a pellet density of 10.85 g/cm^3 and pure-zirconium cladding.

Because the MFFP may transport either one or two assemblies instead of the maximum of three, dummy assemblies are used to balance the package weight. These dummy assemblies are fabricated out of steel. To examine the impact on reactivity of the dummy assemblies, reference HAC array models are run with both one and two fuel assemblies and dummy "assemblies" of void, water, and steel. The reactivity drops in all cases, indicating that any dummy fuel assembly design is acceptable.

6.6.2 HAC Array Results

The maximum k_s = 0.9037 is below the USL and is obtained for full internal moderation, no moderation between packages, a homogenized steel/water mixture surrounding the assemblies, a pellet density of 10.85 g/cm^3, pure-zirconium cladding, and 24 fuel pins shifted down. This value is only ~4 mk higher than the single package HAC result, indicating that communication between the packages is minimal. Note that allowing various combinations of fuel pins to shift axially has a small, positive effect on the reactivity, although the effect is in typically within the uncertainty of the Monte Carlo method. The detailed results for a full (3 assembly) package

without and with shifted fuel pins are provided in Table 6.6-1 and Table 6.6-2, respectively. The detailed results for a partially filled package are provided in Table 6.6-3.

Cases are run with 2,000 particles per generation, 530 generations, with 30 generations skipped. Convergence is well-behaved and the convergence plot as a function of generation for the limiting case is provided in Figure 6.6-1.

6.6.3 Impact of Niobium Content in the Cladding

The importance of the niobium content in the fuel assembly cladding is evaluated for 0 and 3% niobium by weight. Niobium perturbation calculations (using the MCNP perturbation feature) for single and array HAC cases are evaluated to identify the most reactive niobium content in the cladding under flooded conditions. Both cases indicate that 0 wt% niobium is more reactive than the 3 wt% niobium in the cladding. The difference in the reactivity is on the order of 0.001, which is also the approximate magnitude of the convergence of the remaining calculations. Thus, ignoring the niobium in the cladding for the maximum criticality calculations will be a small conservatism.

For the HAC array case (max_hac_array_pertNb) the removal of the niobium (3% by weight) results in a 0.00110 ±0.00025 increase in the reactivity. The second order contribution of the perturbation is calculated as 0.00010 ±0.00004. The HAC single package case (max_hac_single_pertNb) gives an increase in the reactivity of 0.00065±0.00024 (with a second order term of 0.00004 ±0.00003) for the removal of 3% by weight niobium from the cladding. The perturbation reactivity values are not directly used for comparison to the USL and are used simply to identify the most reactive case to be evaluated. Due to the small change in k, statistical fluctuations can randomly exceed the effect seen from the niobium content variation.

Table 6.6-1 – Criticality Results for an Infinite Array of HAC Packages (no shifted pins)

Case Identifier	Water Density (g/cm³)		EALF (MeV)	H/ (^{239}Pu+^{235}U)	V^m/V^f	$\frac{^{239}Pu}{(U+Pu)}$	k_{eff}	σ	k_s (k_{eff}+2σ)
	Internal	External							
max_hac_array_rho_0Nb	1	0	7.26E-7	96.044	2.050	0.056	0.8996	0.0010	0.9016
hac_array_b35pmax2_i100o0_hsteel	1	0	6.61E-07	101.074	2.050	0.056	0.8951	0.0010	0.8971
hac_array_b35pmax2_i100o100	1	1.0	6.67E-07	101.074	2.050	0.056	0.8883	0.0010	0.8903
hac_array_b35pmax2_i100o50	1	0.5	6.60E-07	101.074	2.050	0.056	0.8893	0.0010	0.8913
hac_array_b35pmax2_i100o10	1	0.10	6.48E-07	101.074	2.050	0.056	0.8930	0.0009	0.8948
hac_array_b35pmax2_i100o05	1	0.05	6.57E-07	101.074	2.050	0.056	0.8909	0.0010	0.8929
hac_array_b35pmax2_i100o01	1	0.01	6.51E-07	101.074	2.050	0.056	0.8932	0.0010	0.8952
hac_array_b35pmax2_i100o001	1	0.001	6.55E-07	101.074	2.050	0.056	0.8919	0.0010	0.8938
hac_array_b35pmax2_i100o0	1	0	6.60E-07	101.074	2.050	0.056	0.8912	0.0010	0.8931
hac_array_b35pmax2_i95o0	0.95	0	7.43E-07	96.021	2.050	0.056	0.8683	0.0010	0.8702
hac_array_b35pmax2_i90o0	0.9	0	8.55E-07	90.967	2.050	0.056	0.8470	0.0010	0.8489
hac_array_b35pmax2_i75o0	0.75	0	1.39E-06	75.806	2.050	0.056	0.7662	0.0010	0.7682
hac_array_b35pmax2_i50o0	0.5	0	4.90E-06	50.537	2.050	0.056	0.6221	0.0009	0.6238
hac_array_b35pmax2_i25o0	0.25	0	5.19E-05	25.269	2.050	0.056	0.4926	0.0007	0.4940
hac_array_b35pmax2_i10o0	0.1	0	6.08E-04	10.107	2.050	0.056	0.4849	0.0006	0.4862
hac_array_b35pmax2_i0o100	0	1.0	2.47E-02	0	2.050	0.056	0.3270	0.0004	0.3278
hac_array_b35pmax2_i0o90	0	0.9	2.27E-02	0	2.050	0.056	0.3342	0.0005	0.3351
hac_array_b35pmax2_i0o50	0	0.5	1.82E-02	0	2.050	0.056	0.3847	0.0005	0.3856
hac_array_b35pmax2_i0o10	0	0.10	2.51E-02	0	2.050	0.056	0.5343	0.0005	0.5352
hac_array_b35pmax2_i0o01	0	0.01	7.55E-02	0	2.050	0.056	0.5880	0.0005	0.5889
hac_array_b35pmax2_i0o001	0	0.001	9.35E-02	0	2.050	0.056	0.5905	0.0004	0.5913
hac_array_b35pmax2_i0o0	0	0	9.76E-02	0	2.050	0.056	0.5917	0.0004	0.5926

Table 6.6-2 – Criticality Results for an Infinite Array of HAC Packages (with shifted pins)

Case Identifier	Water Density (g/cm^3)		Shifted Pins	EALF (MeV)	H/ ($^{239}Pu+^{235}U$)	V^m/V^f	$\frac{^{239}Pu}{(U+Pu)}$	k_{eff}	σ	k_s ($k_{eff}+2\sigma$)
	Internal	External								
max_hac_array_srnddn10	1	0	10 down random	7.18E-07	96.044	2.050	0.056	0.9004	0.0010	0.9025
max_hac_array_srnddn20	1	0	20 down random	7.23E-07	96.044	2.050	0.056	0.9002	0.0011	0.9023
max_hac_array_sd1	1	0	8 down	7.20E-07	96.044	2.050	0.056	0.9001	0.0010	0.9020
max_hac_array_sd2	**1**	**0**	**24 down**	**7.36E-07**	**96.044**	**2.050**	**0.056**	**0.9017**	**0.0010**	**0.9037**
max_hac_array_sd3	1	0	60 down	7.27E-07	96.044	2.050	0.056	0.8992	0.0010	0.9012
max_hac_array_sd4	1	0	116 down	7.02E-07	96.044	2.050	0.056	0.9008	0.0009	0.9026
max_hac_array_salldn	1	0	All down	7.21E-07	96.044	2.050	0.056	0.9001	0.0010	0.9020
max_hac_array_srndup10	1	0	10 up random	7.33E-07	96.044	2.050	0.056	0.8991	0.0009	0.9010
max_hac_array_srndup20	1	0	20 up random	7.14E-07	96.044	2.050	0.056	0.8998	0.0009	0.9016
max_hac_array_su1	1	0	8 up	7.30E-07	96.044	2.050	0.056	0.9004	0.0009	0.9023
max_hac_array_su2	1	0	24 up	7.10E-07	96.044	2.050	0.056	0.8999	0.0010	0.9020
max_hac_array_su3	1	0	60 up	7.13E-07	96.044	2.050	0.056	0.9003	0.0010	0.9022
max_hac_array_su4	1	0	116 up	7.01E-07	96.044	2.050	0.056	0.8979	0.0010	0.8998
max_hac_array_sallup	1	0	All up	7.30E-07	96.044	2.050	0.056	0.8997	0.0010	0.9016

Table 6.6-3 – Criticality Results for an Infinite Array of HAC Partially Filled Packages (no shifted pins)

Case Identifier	Number of Assemblies	Dummy Assembly Material	EALF (MeV)	H/ (^{239}Pu+^{235}U)	V^m/V^f	$\frac{^{239}Pu}{(U+Pu)}$	k_{eff}	σ	k_s ($k_{eff}+2\sigma$)
hac_array_b35pmax2_i100o0_hsteel	3	null	6.61E-07	101.074	2.050	0.056	0.8951	0.0010	0.8971
hac_array_b35pmax2_i100o0_hsteel_1asss	1	Steel	6.61E-07	101.074	2.050	0.056	0.8577	0.0010	0.8596
hac_array_b35pmax2_i100o0_hsteel_1assv	1	Void	6.70E-07	101.074	2.050	0.056	0.8548	0.0010	0.8568
hac_array_b35pmax2_i100o0_hsteel_1assw	1	Water	6.68E-07	101.074	2.050	0.056	0.8568	0.0010	0.8588
hac_array_b35pmax2_i100o0_hsteel_2asss	2	Steel	6.56E-07	101.074	2.050	0.056	0.8772	0.0009	0.8791
hac_array_b35pmax2_i100o0_hsteel_2assv	2	Void	6.73E-07	101.074	2.050	0.056	0.8753	0.0009	0.8771
hac_array_b35pmax2_i100o0_hsteel_2assw	2	Water	6.65E-07	101.074	2.050	0.056	0.8741	0.0010	0.8761

This page left intentionally blank.

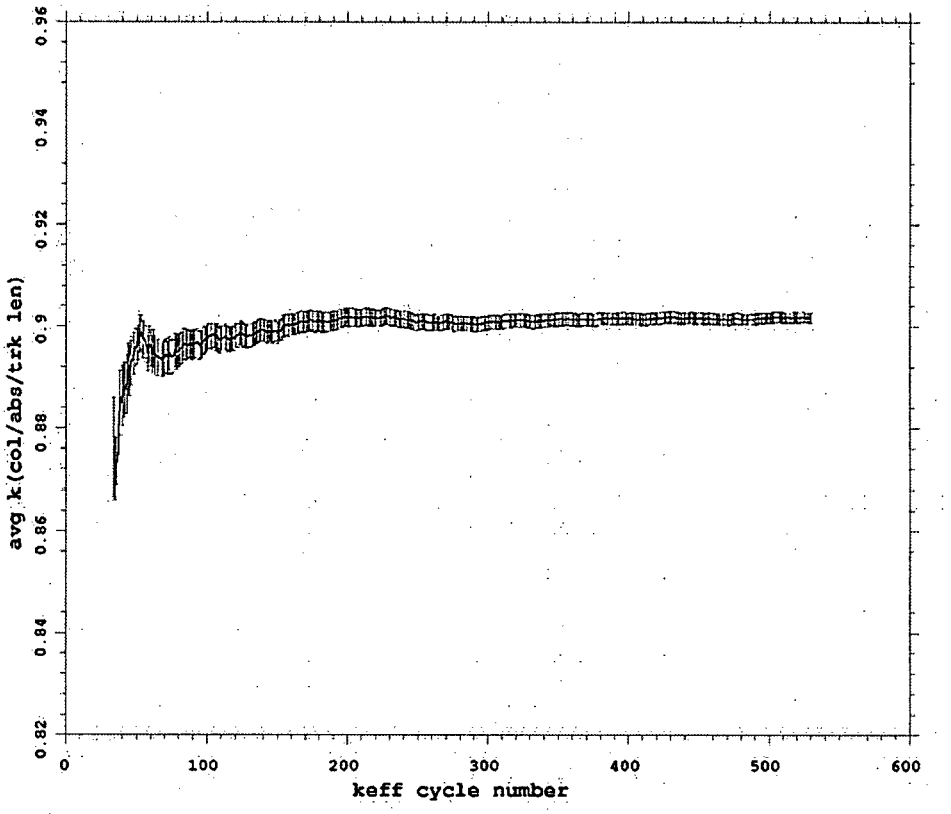

Figure 6.6-1 – Convergence of Maximum HAC Array Case (max_hac_array_sd2)

This page left intentionally blank.

6.7 Fissile Material Packages for Air Transport

This section does not apply for the MFFP, since air transport is not claimed.

This page left intentionally blank.

6.8 Benchmark Evaluations

The MCNP, Version 5, Monte Carlo computer code[1] with point-wise ENDF/B-V and -VI cross sections has been used extensively in criticality evaluations. This section justifies the validity of this computation tool and data library combination for application to the MFFP package criticality analysis and a bias factor is obtained from these calculations of the critical experiments.

The MCNP code uses room temperature continuous-energy (point-wise) cross sections that are thoroughly documented in Appendix G of the manual. These cross sections are defined with a high-energy resolution that describes each resolved cross section resonance for the isotope. All of the cross-sections used for these analyses were generated from the U.S. Evaluated Nuclear Data Files (ENDF/B).

The validation of the point-wise cross sections is conducted using 84 experimental criticality benchmarks applicable to the MFFP. The statistical analysis of the benchmark experiments results in a USL of 0.9288.

6.8.1 Applicability of Benchmark Experiments

The experimental benchmarks are taken from the OECD Nuclear Energy Agency's *International Handbook of Evaluated Criticality Safety Benchmark Experiments*[2]. This Handbook discusses each experiment in detail. It includes estimates of the uncertainty in the measurements, detailed information regarding dimensions and material compositions, comparisons between the multiplication factor calculated by various computer codes, and a list of input files that were used in their calculations. The only changes made to the input files involve changing to a consistent set of cross section libraries, as needed.

The critical experiment benchmarks are selected for use in this USL determination based upon their similarity to the MOX fresh fuel assembly. The important constituents of the MOX assembly are: mixed oxide fuel (plutonium with depleted uranium), borated absorber plates and a steel container and components. The nominal pin cell moderator volume to fuel volume ratio is 1.60 for MFFP fuel. Cases are selected based on plutonium being the dominant fissile material in a solid form (i.e., solutions were excluded). This first selection criteria identified critical experiments with composite mixed oxide fuel rods with uranium enrichments of less than 2%, greater than 1% Pu/(U+Pu) and moderator to fuel ratios of less than 20. This set of 145 experiments is filtered to remove those cases that contained cadmium and hafnium absorber materials which are not present in this analysis (leaving only boron as the accepted absorber material). The remaining 77 experiments have mixed plutonium/uranium fuel in a lattice with a thermal spectrum, similar to MOX fuel.

To provide benchmarks with harder neutron spectra, a second selection is performed over the metal fuel experiments with the same criteria. From this second search, 7 more critical benchmark experiments are identified. These later experiments use metal fuel in a graphite moderator/reflector.

---

[1] MCNP5, "*MCNP – A General Monte Carlo N-Particle Transport Code, Version 5; Volume II: User's Guide*," LA-CP-03-0245, Los Alamos National Laboratory, April, 2003.

[2] OECD Nuclear Energy Agency, *International Handbook of Evaluated Criticality Safety Benchmark Experiments*, NEA/NSC/DOC(95)03, September, 2003.

The overall selection of cases is weighted to the thermal spectra where calculated MOX assembly reactivity is highest. The critical experiments selected are listed in Table 6.8-1.

6.8.2 Bias Determination

The ORNL USLSTATS code[3], described in Appendix C of NUREG/CR-6361[4], is used to establish an upper subcritical limit (USL) for the analysis. Computed multiplication factors, k_{eff}, for the MOX package are deemed to be adequately subcritical if the computed value of k_{eff} plus two standard deviations is below the USL as follows:

$$k_s = k_{eff} + 2\sigma < USL$$

The USL includes the combined effects of code bias, uncertainty in the benchmark experiments, uncertainty in the computational evaluation of the benchmark experiments, and an administrative margin of subcriticality. The USL is determined using the confidence band with administrative margin technique (USLSTATS Method 1).

USLSTATS takes as input the k_{eff} as calculated by MCNP5, the total 1-σ uncertainty (combined benchmark and computational uncertainties), and a trending parameter. For the current analysis, four trending parameters have been selected (1) moderator to fuel volume ratio (v^m/v^f), (2) H/(Pu239+U235) ratio, (3) Pu239/(Pu+U), and (4) Energy of the Average Lethargy causing Fission (EALF). Parameters (1) and (2) are applied to only to the first 77 benchmarks because these parameters are not directly applicable to dry, non-lattice benchmarks. Parameters (3) and (4) are applied to all 84 benchmarks. The USL is computed by trending upon these variables and selecting the lowest USL.

The uncertainty value, σ_{tot}, assigned to each case is a combination of the benchmark-model uncertainty for each experiment, σ_{bench}, and the Monte Carlo uncertainty associated with the particular computational evaluation of the case, σ_{comp}, or:

$$\sigma_{tot} = (\sigma_{bench}^2 + \sigma_{comp}^2)^{1/2}$$

These values are input into the USLSTATS program in addition to the following parameters, which are the values suggested by the USLSTATS user's manual:

- P, proportion of population falling above lower tolerance level = 0.995
- 1-γ, confidence on fit = 0.95
- α, confidence on proportion P = 0.95
- Δk_m, administrative margin used to ensure subcriticality = 0.05.

[3] USLSTATS, "*USLSTATS: A Utility To Calculate Upper Subcritical Limits For Criticality Safety Applications,*" Version 1.3.6, Oak Ridge National Laboratory, December 15, 1998.

[4] J. J. Lichtenwalter, S. M. Bowman, M. D. DeHart, C. M. Hopper, *Criticality Benchmark Guide for Light-Water-Reactor Fuel in Transportation and Storage Packages*, NUREG/CR-6361, ORNL/TM-13211, March 1997.

This data is followed by triplets of trending parameter value, computed k_{eff}, and uncertainty for each case. The USL Method 1 performs a confidence band analysis on the data for the trending parameter. All benchmark data used as input to USLSTATS are reported in Table 6.8-2.

Note that USLSTATS assumes that all benchmark experiments have a $k_{eff} = 1.000$. However, some of the benchmark k_{eff} are greater or less than 1.000. The most accurate value for the model reactivity is used and the k_{eff} input into USLSTATS is normalized by dividing by the benchmark k_{eff}. The benchmark-model reactivity may be different than 1.000 due to experiments that were not exactly critical or due to model simplifications. For example, for experiments with fixed rod patterns, the addition of one more rod may bring the experiment from sub-critical to super-critical without the possibility of being exactly critical. Other known model assumptions may be evaluated with the experiment and may be included in the benchmark reactivity. Corrections may be based on analytical evaluation or measurements and the uncertainties in these adjustments are included in the benchmark's overall uncertainty. Typically the combined corrections are small and benchmark-model k_{eff} are close to 1.000.

The USL generated for each of the three trending parameters utilized is provided below.

Trending parameter	USL equation	Range of Applicability
v^m/v^f	USL1 = 0.9289 + (4.0398E-04)*X	1.1112 ≤ X ≤ 17.5
H/ (Pu239+U235)	USL1 = 0.9309 + (1.4706E-06)*X	51.000 ≤ X ≤ 1145.
Pu239/(U+Pu)	USL1 = 0.9297 + (1.0963E-02)*X (X < 0.709) = 0.9374 (X ≥ 0.709)	0.014 ≤ X ≤ 0.95
EALF	USL1 = 0.9288 + (3.6369E-02)*X (X < 0.20144) = 0.9362 (X ≥ 0.201)	8.07E-8 ≤ X ≤ 0.40 MeV

All of the trending parameters show little correlation, thus the use of a constant USL is appropriate. The MCNP results show an average negative bias (under prediction) in the reactivity for the selected benchmarks of about 0.007 ±0.006. The minimum USL value of 0.9288 is used which includes the bias, trend corrections, administrative margin (0.05) and the 95% confidence band width of the data.

Results for v^m/v^f

The volume ratio is equivalent to trending by pin pitch and was used as a selection criteria for the 77 lattice benchmark cases. The volume fractions are used to better represent the mixture of hexagonal and square lattice geometries used in the benchmarks. The USL1 value is a minimum at the minimum moderator to fuel volume ratio. As shown in Figure 6.8-1 there is little correlation with this variable and the calculated benchmark reactivity. The calculations for the MOX package have v^m/v^f ratios from about 1.6 to 2 with full density water. Not adjusting for the water density provides a trending that will be similar to trending on fuel pin pitch. The possible influence with water density is covered with the H/Pu+U ratio below.

Results for H/(Pu239+U235)

This parameter is utilized with the 77 lattice benchmark cases. Reactivity trend with respect to the ratio of the primary moderator (H) to the primary fissile isotopes (Pu239 and U235) within the pin cell was not significant. The smeared atom densities in the pin cells are used. For the

MOX package analyses, the H/(Pu239+U235) ratio ranges from 0 to 101. As shown on Figure 6.8-2, the benchmark data for low H/(Pu239+U235) ratios is sparse and variable. However, for this analysis the higher reactivity and more important cases occur with the larger H/(Pu239+U235) values (around 100) and in this range there is adequate benchmark data. The more important MFFP cases occur with more moderation which is also apparent in the EALF trending as discussed below.

Results for Pu239/(U+Pu)

This parameter is utilized with all 84 benchmark cases. The Pu239/(U+Pu) trending parameter was selected to identify any bias resulting from the selection of benchmark cases with different plutonium and uranium concentrations. The MOX package has a Pu239/(U+Pu) ratio of 0.056, which is within the range of applicability for the benchmark data as shown in Figure 6.8-3.

Results for EALF

This parameter is utilized with all 84 benchmark cases. The EALF comparison provides a means to observe neutron spectral dependencies or trends. The USL1 for the EALF parameter has a negligible increase with increasing EALF as shown in Figure 6.8-4 for the benchmark cases. The MOX analyses have EALF values from 6.5E-7 to 0.35 MeV. As shown in Figure 6.8-5 cases with a high EALF have a lower calculated reactivity. The MOX case with the peak reactivity has an EALF of 7.36E-7 MeV which is well represented by the benchmarks. Additional refinement of the benchmarks for high EALF values is not warranted due to the low calculated reactivity in this range, and thus large margin for safety.

Table 6.8-1 – Experimental Benchmarks

Used Y/N	Identification	Solid poison	EALF (eV)	Pu/(U+Pu) ratio	Pitch type	Pitch size (cm)
Y	MIX-COMP-THERM-001-001	null	1.07	0.2237	Square	0.9525
Y	MIX-COMP-THERM-001-002	null	0.292	0.2237	Square	1.258
Y	MIX-COMP-THERM-001-003	null	0.174	0.2237	Square	1.5342
Y	MIX-COMP-THERM-001-004	null	0.12	0.2237	Square	1.905
Y	MIX-COMP-THERM-002-001	null	0.581	0.0204	Square	1.778
Y	MIX-COMP-THERM-002-002	null	0.769	0.0204	Square	1.778
Y	MIX-COMP-THERM-002-003	null	0.197	0.0204	Square	2.20914
Y	MIX-COMP-THERM-002-004	null	0.288	0.0204	Square	2.20914
Y	MIX-COMP-THERM-002-005	null	0.142	0.0204	Square	2.51447
Y	MIX-COMP-THERM-002-006	null	0.188	0.0204	Square	2.51447
Y	MIX-COMP-THERM-003-001	null	0.922	0.0659	Square	1.3208
Y	MIX-COMP-THERM-003-002	null	0.559	0.0659	Square	1.4224
Y	MIX-COMP-THERM-003-003	null	0.663	0.0659	Square	1.4224
Y	MIX-COMP-THERM-003-004	null	0.192	0.0659	Square	1.8679
Y	MIX-COMP-THERM-003-005	null	0.159	0.0659	Square	2.01158
Y	MIX-COMP-THERM-003-006	null	0.103	0.0659	Square	2.6416
Y	MIX-COMP-THERM-004-001	null	0.149	0.03	Square	1.825
Y	MIX-COMP-THERM-004-002	null	0.148	0.0299	Square	1.825
Y	MIX-COMP-THERM-004-003	null	0.147	0.028	Square	1.825
Y	MIX-COMP-THERM-004-004	null	0.123	0.03	Square	1.956
Y	MIX-COMP-THERM-004-005	null	0.122	0.0299	Square	1.956
Y	MIX-COMP-THERM-004-006	null	0.121	0.0298	Square	1.956

Used Y/N	Identification	Solid poison	EALF (eV)	Pu/(U+Pu) ratio	Pitch type	Pitch size (cm)
Y	MIX-COMP-THERM-004-007	null	0.0951	0.03	Square	2.225
Y	MIX-COMP-THERM-004-008	null	0.0948	0.0299	Square	2.225
Y	MIX-COMP-THERM-004-009	null	0.0944	0.0298	Square	2.225
Y	MIX-COMP-THERM-004-010	null	0.082	0.03	Square	2.474
Y	MIX-COMP-THERM-004-011	null	0.0916	0.0299	Square	2.474
Y	MIX-COMP-THERM-005-001	null	0.399	0.0399	Hexagonal	2.159
Y	MIX-COMP-THERM-005-002	null	0.263	0.0399	Hexagonal	2.3622
Y	MIX-COMP-THERM-005-003	null	0.18	0.0399	Hexagonal	2.667
Y	MIX-COMP-THERM-005-004	null	0.15	0.0399	Hexagonal	2.90322
Y	MIX-COMP-THERM-005-005	null	0.111	0.0399	Hexagonal	3.52044
Y	MIX-COMP-THERM-005-006	null	0.0956	0.0399	Hexagonal	4.064
Y	MIX-COMP-THERM-005-007	null	0.0912	0.0399	Hexagonal	4.318
Y	MIX-COMP-THERM-006-001	null	0.383	0.0204	Hexagonal	2.032
Y	MIX-COMP-THERM-006-002	null	0.2	0.0204	Hexagonal	2.3622
Y	MIX-COMP-THERM-006-003	null	0.145	0.0204	Hexagonal	2.667
Y	MIX-COMP-THERM-006-004	null	0.123	0.0204	Hexagonal	2.90322
Y	MIX-COMP-THERM-006-005	null	0.101	0.0204	Hexagonal	3.3528
Y	MIX-COMP-THERM-006-006	null	0.0954	0.0204	Hexagonal	3.52044
Y	MIX-COMP-THERM-006-007	null	0.144	0.0204	Hexagonal	2.667
N	MIX-COMP-THERM-006-008	Hf	0.145	0.0204	Hexagonal	2.667
N	MIX-COMP-THERM-006-009	Hf	0.145	0.0204	Hexagonal	2.667
N	MIX-COMP-THERM-006-010	Hf	0.145	0.0204	Hexagonal	2.667
N	MIX-COMP-THERM-006-011	Hf	0.145	0.0204	Hexagonal	2.667
N	MIX-COMP-THERM-006-012	Hf	0.146	0.0204	Hexagonal	2.667
Y	MIX-COMP-THERM-006-013	Boron	0.145	0.0204	Hexagonal	2.667
Y	MIX-COMP-THERM-006-014	Boron	0.145	0.0204	Hexagonal	2.667
Y	MIX-COMP-THERM-006-015	Boron	0.145	0.0204	Hexagonal	2.667
Y	MIX-COMP-THERM-006-016	Boron	0.146	0.0204	Hexagonal	2.667
N	MIX-COMP-THERM-006-017	Cd	0.147	0.0204	Hexagonal	2.667
N	MIX-COMP-THERM-006-018	Cd + Hf	0.147	0.0204	Hexagonal	2.667
N	MIX-COMP-THERM-006-019	Cd + Hf	0.146	0.0204	Hexagonal	2.667
N	MIX-COMP-THERM-006-020	Cd + Hf	0.147	0.0204	Hexagonal	2.667
N	MIX-COMP-THERM-006-021	Cd + Hf	0.146	0.0204	Hexagonal	2.667
N	MIX-COMP-THERM-006-022	Cd + Hf	0.146	0.0204	Hexagonal	2.667
N	MIX-COMP-THERM-006-023	B + Cd	0.146	0.0204	Hexagonal	2.667
N	MIX-COMP-THERM-006-024	B + Cd	0.146	0.0204	Hexagonal	2.667
N	MIX-COMP-THERM-006-025	B + Cd	0.146	0.0204	Hexagonal	2.667
N	MIX-COMP-THERM-006-026	B + Cd	0.147	0.0204	Hexagonal	2.667
N	MIX-COMP-THERM-006-027	Cd	0.146	0.0204	Hexagonal	2.667
N	MIX-COMP-THERM-006-028	Cd	0.147	0.0204	Hexagonal	2.667
Y	MIX-COMP-THERM-006-029	null	0.101	0.0204	Hexagonal	3.3528
N	MIX-COMP-THERM-006-030	Hf	0.101	0.0204	Hexagonal	3.3528
N	MIX-COMP-THERM-006-031	Hf	0.101	0.0204	Hexagonal	3.3528
N	MIX-COMP-THERM-006-032	Hf	0.101	0.0204	Hexagonal	3.3528
N	MIX-COMP-THERM-006-033	Hf	0.101	0.0204	Hexagonal	3.3528
N	MIX-COMP-THERM-006-034	Hf	0.101	0.0204	Hexagonal	3.3528
Y	MIX-COMP-THERM-006-035	Boron	0.1	0.0204	Hexagonal	3.3528
Y	MIX-COMP-THERM-006-036	Boron	0.101	0.0204	Hexagonal	3.3528
Y	MIX-COMP-THERM-006-037	Boron	0.101	0.0204	Hexagonal	3.3528
Y	MIX-COMP-THERM-006-038	Boron	0.101	0.0204	Hexagonal	3.3528
N	MIX-COMP-THERM-006-039	Cd	0.101	0.0204	Hexagonal	3.3528

Used Y/N	Identification	Solid poison	EALF (eV)	Pu/(U+Pu) ratio	Pitch type	Pitch size (cm)
N	MIX-COMP-THERM-006-040	Cd + Hf	0.101	0.0204	Hexagonal	3.3528
N	MIX-COMP-THERM-006-041	Cd + Hf	0.101	0.0204	Hexagonal	3.3528
N	MIX-COMP-THERM-006-042	Cd + Hf	0.101	0.0204	Hexagonal	3.3528
N	MIX-COMP-THERM-006-043	Cd + Hf	0.101	0.0204	Hexagonal	3.3528
N	MIX-COMP-THERM-006-044	Cd + Hf	0.101	0.0204	Hexagonal	3.3528
N	MIX-COMP-THERM-006-045	B + Cd	0.101	0.0204	Hexagonal	3.3528
N	MIX-COMP-THERM-006-046	B + Cd	0.101	0.0204	Hexagonal	3.3528
N	MIX-COMP-THERM-006-047	B + Cd	0.101	0.0204	Hexagonal	3.3528
N	MIX-COMP-THERM-006-048	B + Cd	0.101	0.0204	Hexagonal	3.3528
N	MIX-COMP-THERM-006-049	Cd	0.101	0.0204	Hexagonal	3.3528
N	MIX-COMP-THERM-006-050	Cd	0.101	0.0204	Hexagonal	3.3528
Y	MIX-COMP-THERM-007-001	null	0.203	0.0199	Hexagonal	2.3622
Y	MIX-COMP-THERM-007-002	null	0.146	0.0199	Hexagonal	2.667
Y	MIX-COMP-THERM-007-003	null	0.123	0.0199	Hexagonal	2.9032
Y	MIX-COMP-THERM-007-004	null	0.1	0.0199	Hexagonal	3.3528
Y	MIX-COMP-THERM-007-005	null	0.0954	0.0199	Hexagonal	3.5204
Y	MIX-COMP-THERM-007-006	null	0.145	0.0199	Hexagonal	2.667
Y	MIX-COMP-THERM-007-007	Boron	0.146	0.0199	Hexagonal	2.667
Y	MIX-COMP-THERM-007-008	Boron	0.146	0.0199	Hexagonal	2.667
Y	MIX-COMP-THERM-007-009	Boron	0.146	0.0199	Hexagonal	2.667
Y	MIX-COMP-THERM-007-010	Boron	0.145	0.0199	Hexagonal	2.667
N	MIX-COMP-THERM-007-011	Hf	0.146	0.0199	Hexagonal	2.667
N	MIX-COMP-THERM-007-012	Hf	0.146	0.0199	Hexagonal	2.667
N	MIX-COMP-THERM-007-013	Hf	0.146	0.0199	Hexagonal	2.667
N	MIX-COMP-THERM-007-014	Hf	0.146	0.0199	Hexagonal	2.667
N	MIX-COMP-THERM-007-015	Hf	0.145	0.0199	Hexagonal	2.667
N	MIX-COMP-THERM-007-016	Cd	0.147	0.0199	Hexagonal	2.667
N	MIX-COMP-THERM-007-017	B + Cd	0.147	0.0199	Hexagonal	2.667
N	MIX-COMP-THERM-007-018	B + Cd	0.147	0.0199	Hexagonal	2.667
N	MIX-COMP-THERM-007-019	B + Cd	0.147	0.0199	Hexagonal	2.667
N	MIX-COMP-THERM-007-020	B + Cd	0.147	0.0199	Hexagonal	2.667
N	MIX-COMP-THERM-007-021	Cd + Hf	0.147	0.0199	Hexagonal	2.667
N	MIX-COMP-THERM-007-022	Cd + Hf	0.147	0.0199	Hexagonal	2.667
N	MIX-COMP-THERM-007-023	Cd + Hf	0.147	0.0199	Hexagonal	2.667
N	MIX-COMP-THERM-007-024	Cd + Hf	0.147	0.0199	Hexagonal	2.667
N	MIX-COMP-THERM-007-025	Cd + Hf	0.147	0.0199	Hexagonal	2.667
N	MIX-COMP-THERM-007-026	Cd	0.146	0.0199	Hexagonal	2.667
N	MIX-COMP-THERM-007-027	Cd	0.147	0.0199	Hexagonal	2.667
Y	MIX-COMP-THERM-008-001	null	0.408	0.02	Hexagonal	2.032
Y	MIX-COMP-THERM-008-002	null	0.205	0.02	Hexagonal	2.3622
Y	MIX-COMP-THERM-008-003	null	0.147	0.02	Hexagonal	2.667
Y	MIX-COMP-THERM-008-004	null	0.124	0.02	Hexagonal	2.9032
Y	MIX-COMP-THERM-008-005	null	0.101	0.02	Hexagonal	3.3528
Y	MIX-COMP-THERM-008-006	null	0.0952	0.02	Hexagonal	3.5204
Y	MIX-COMP-THERM-008-007	null	0.146	0.02	Hexagonal	2.667
N	MIX-COMP-THERM-008-008	Hf	0.146	0.02	Hexagonal	2.667
N	MIX-COMP-THERM-008-009	Hf	0.147	0.02	Hexagonal	2.667
N	MIX-COMP-THERM-008-010	Hf	0.147	0.02	Hexagonal	2.667
N	MIX-COMP-THERM-008-011	Hf	0.147	0.02	Hexagonal	2.667
N	MIX-COMP-THERM-008-012	Hf	0.147	0.02	Hexagonal	2.667
Y	MIX-COMP-THERM-008-013	Boron	0.146	0.02	Hexagonal	2.667

Used Y/N	Identification	Solid poison	EALF (eV)	Pu/(U+Pu) ratio	Pitch type	Pitch size (cm)
Y	MIX-COMP-THERM-008-014	Boron	0.147	0.02	Hexagonal	2.667
Y	MIX-COMP-THERM-008-015	Boron	0.147	0.02	Hexagonal	2.667
Y	MIX-COMP-THERM-008-016	Boron	0.147	0.02	Hexagonal	2.667
N	MIX-COMP-THERM-008-017	Cd	0.148	0.02	Hexagonal	2.667
N	MIX-COMP-THERM-008-018	Cd + Hf	0.147	0.02	Hexagonal	2.667
N	MIX-COMP-THERM-008-019	Cd + Hf	0.148	0.02	Hexagonal	2.667
N	MIX-COMP-THERM-008-020	Cd + Hf	0.148	0.02	Hexagonal	2.667
N	MIX-COMP-THERM-008-021	Cd + Hf	0.148	0.02	Hexagonal	2.667
N	MIX-COMP-THERM-008-022	Cd + Hf	0.148	0.02	Hexagonal	2.667
N	MIX-COMP-THERM-008-023	B + Cd	0.147	0.02	Hexagonal	2.667
N	MIX-COMP-THERM-008-024	B + Cd	0.148	0.02	Hexagonal	2.667
N	MIX-COMP-THERM-008-025	B + Cd	0.148	0.02	Hexagonal	2.667
N	MIX-COMP-THERM-008-026	B + Cd	0.148	0.02	Hexagonal	2.667
N	MIX-COMP-THERM-008-027	Cd	0.148	0.02	Hexagonal	2.667
N	MIX-COMP-THERM-008-028	Cd	0.148	0.02	Hexagonal	2.667
Y	MIX-COMP-THERM-009-001	null	0.537	0.015	Hexagonal	1.397
Y	MIX-COMP-THERM-009-002	null	0.304	0.015	Hexagonal	1.524
Y	MIX-COMP-THERM-009-003	null	0.158	0.015	Hexagonal	1.8034
Y	MIX-COMP-THERM-009-004	null	0.119	0.015	Hexagonal	2.032
Y	MIX-COMP-THERM-009-005	null	0.0972	0.015	Hexagonal	2.286
Y	MIX-COMP-THERM-009-006	null	0.093	0.015	Hexagonal	2.3622
Y	MIX-MET-INTER-001-001	null	36800	0.4525	null	null
Y	MIX-MET-FAST-008-002	null	347000	0.4525	null	null
Y	MIX-MET-FAST-008-003	null	83400	0.4525	null	null
Y	MIX-MET-FAST-008-004	null	186000	0.4525	null	null
Y	MIX-MET-FAST-008-005	null	285000	0.4525	null	null
Y	MIX-MET-INTER-001-006	null	26600	0.191	null	null
Y	PU-MET-FAST-033-001	null	422000	0.5255	null	null

This page left intentionally blank.

Table 6.8-2 – Benchmark k_{eff} Results

Case Name	EALF (MeV)	v_m/v_f	$\frac{^{239}Pu}{(U+Pu)}$	H/ (^{239}Pu + ^{235}U)	k_{ben}	σ_{bench}	k_{MCNP}	σ_{MCNP}	k_{MCNP} (normalized)	σ_{tot}
MIXCT1\mixct-001-c1	1.002E-06	3.335	0.193	51	1	0.0025	0.9919	0.0007	0.9919	0.0026
MIXCT1\mixct-001-c2	2.802E-07	6.868	0.193	106	1	0.0026	0.9931	0.0007	0.9931	0.0027
MIXCT1\mixct-001-c3	1.683E-07	10.881	0.193	168	1	0.0032	0.9908	0.0007	0.9908	0.0033
MIXCT1\mixct-001-c4	1.175E-07	17.534	0.193	271	1	0.0039	0.9944	0.0007	0.9944	0.0040
MIXCT2\mixct-002-pnl30	5.853E-07	1.195	0.019	147	1.001	0.0059	0.9926	0.0008	0.9916	0.0060
MIXCT2\mixct-002-pnl31	7.786E-07	1.195	0.019	147	1.0009	0.0045	0.9965	0.0009	0.9956	0.0046
MIXCT2\mixct-002-pnl32	1.962E-07	2.525	0.019	310	1.0024	0.0029	0.9959	0.0008	0.9936	0.0030
MIXCT2\mixct-002-pnl33	2.866E-07	2.525	0.019	310	1.0024	0.0021	1.0028	0.0008	1.0004	0.0023
MIXCT2\mixct-002-pnl34	1.407E-07	3.641	0.019	447	1.0038	0.0022	0.9978	0.0008	0.9940	0.0023
MIXCT2\mixct-002-pnl35	1.859E-07	3.641	0.019	447	1.0029	0.0024	1.0055	0.0008	1.0026	0.0025
MIXCT3\mixct-003-c1	8.994E-07	1.681	0.060	74	1	0.0071	0.9932	0.0009	0.9932	0.0072
MIXCT3\mixct-003-c2	5.499E-07	2.165	0.060	96	1	0.0057	0.9919	0.0009	0.9919	0.0058
MIXCT3\mixct-003-c3	6.544E-07	2.165	0.060	96	1	0.0052	0.9944	0.0009	0.9944	0.0053
MIXCT3\mixct-003-c4	1.898E-07	4.706	0.060	208	1	0.0028	0.9947	0.0009	0.9947	0.0029
MIXCT3\mixct-003-c5	1.571E-07	5.672	0.060	252	1	0.0024	0.9944	0.0009	0.9944	0.0026
MIXCT3\mixct-003-c6	1.017E-07	10.754	0.060	477	1	0.002	1.0000	0.0008	1.0000	0.0022
MIXCT4\mixct-004-c01	1.471E-07	2.420	0.021	438	1	0.0046	0.9909	0.0007	0.9909	0.0047
MIXCT4\mixct-004-c02	1.462E-07	2.420	0.021	438	1	0.0046	0.9929	0.0007	0.9929	0.0047
MIXCT4\mixct-004-c03	1.461E-07	2.420	0.021	438	1	0.0046	0.9924	0.0007	0.9924	0.0047
MIXCT4\mixct-004-c04	1.216E-07	2.976	0.021	538	1	0.0039	0.9934	0.0007	0.9934	0.0040
MIXCT4\mixct-004-c05	1.203E-07	2.976	0.021	538	1	0.0039	0.9883	0.0007	0.9883	0.0040
MIXCT4\mixct-004-c06	1.199E-07	2.976	0.021	538	1	0.0039	0.9949	0.0007	0.9949	0.0040
MIXCT4\mixct-004-c07	9.415E-08	4.239	0.021	767	1	0.004	0.9938	0.0007	0.9938	0.0041
MIXCT4\mixct-004-c08	9.387E-08	4.239	0.021	767	1	0.004	0.9948	0.0007	0.9948	0.0041

Case Name	EALF (MeV)	v_m/v_f	$\frac{^{239}Pu}{(U+Pu)}$	H/ (^{239}Pu + ^{235}U)	k_{ben}	σ_{bench}	k_{MCNP}	σ_{MCNP}	k_{MCNP} (normalized)	σ_{tot}
MIXCT4\mixct-004-c09	9.37E-08	4.239	0.021	767	1	0.004	0.9957	0.0007	0.9957	0.0041
MIXCT4\mixct-004-c10	8.083E-08	5.552	0.021	1005	1	0.0051	0.9952	0.0007	0.9952	0.0051
MIXCT4\mixct-004-c11	8.067E-08	5.552	0.021	1005	1	0.0051	0.9968	0.0007	0.9968	0.0051
MIXCT5\mixct-005-c1	3.957E-07	1.931	0.030	166	1.0008	0.0022	0.9936	0.0006	0.9928	0.0023
MIXCT5\mixct-005-c2	2.601E-07	2.566	0.030	220	1.0011	0.0026	0.9932	0.0006	0.9921	0.0027
MIXCT5\mixct-005-c3	1.787E-07	3.624	0.030	311	1.0016	0.0029	0.9995	0.0006	0.9979	0.0030
MIXCT5\mixct-005-c4	1.48E-07	4.533	0.030	389	1.0021	0.0028	0.9976	0.0006	0.9955	0.0029
MIXCT5\mixct-005-c5	1.092E-07	7.270	0.030	624	1.0026	0.0036	1.0024	0.0005	0.9998	0.0036
MIXCT5\mixct-005-c6	9.453E-08	10.117	0.030	868	1.0033	0.0042	1.0017	0.0005	0.9984	0.0042
MIXCT5\mixct-005-c7	9.029E-08	11.587	0.030	994	1.0035	0.0042	1.0034	0.0004	0.9999	0.0042
MIXCT6\mixct-006-c01	3.81E-07	1.515	0.019	186	1.0016	0.0051	0.9897	0.0006	0.9881	0.0051
MIXCT6\mixct-006-c02	1.98E-07	2.488	0.019	305	1.0017	0.0036	0.9951	0.0006	0.9934	0.0037
MIXCT6\mixct-006-c03	1.44E-07	3.515	0.019	431	1.0026	0.0036	0.9920	0.0006	0.9894	0.0037
MIXCT6\mixct-006-c04	1.22E-07	4.397	0.019	540	1.0051	0.0044	0.9985	0.0006	0.9934	0.0044
MIXCT6\mixct-006-c05	9.97E-08	6.282	0.019	771	1.004	0.0054	1.0008	0.0005	0.9968	0.0054
MIXCT6\mixct-006-c06	9.41E-08	7.054	0.019	866	1.0055	0.0051	0.9988	0.0005	0.9933	0.0051
MIXCT6\mixct-006-c07	1.43E-07	3.515	0.019	431	1.0024	0.0045	0.9899	0.0006	0.9875	0.0045
MIXCT6\mixct-006-c13	1.43E-07	3.515	0.019	431	1.0021	0.0044	0.9879	0.0006	0.9858	0.0044
MIXCT6\mixct-006-c14	1.44E-07	3.515	0.019	431	1.0026	0.0044	0.9869	0.0006	0.9843	0.0044
MIXCT6\mixct-006-c15	1.44E-07	3.515	0.019	431	1.0033	0.0044	0.9877	0.0006	0.9844	0.0044
MIXCT6\mixct-006-c16	1.44E-07	3.515	0.019	431	1.0035	0.0045	0.9868	0.0006	0.9833	0.0045
MIXCT6\mixct-006-c29	9.91E-08	6.282	0.019	771	1.004	0.0087	0.9948	0.0005	0.9908	0.0087
MIXCT6\mixct-006-c35	9.96E-08	6.282	0.019	771	1.0044	0.0087	0.9926	0.0005	0.9882	0.0087
MIXCT6\mixct-006-c36	9.95E-08	6.282	0.019	771	1.0036	0.0087	0.9929	0.0005	0.9893	0.0087
MIXCT6\mixct-006-c37	9.96E-08	6.282	0.019	771	1.0041	0.0087	0.9921	0.0005	0.9880	0.0087

Case Name	EALF (MeV)	v_m/v_f	$\frac{^{239}Pu}{(U+Pu)}$	H/ (^{239}Pu + ^{235}U)	k_{ben}	σ_{bench}	k_{MCNP}	σ_{MCNP}	k_{MCNP} (normalized)	σ_{tot}
MIXCT6\mixct-006-c38	9.98E-08	6.282	0.019	771	1.0044	0.0087	0.9915	0.0005	0.9872	0.0087
MIXCT7\mixct-007-c1	1.96E-07	2.488	0.016	337	1.0023	0.0035	0.9981	0.0005	0.9958	0.0035
MIXCT7\mixct-007-c2	1.418E-07	3.515	0.016	476	1.0024	0.0039	0.9949	0.0005	0.9926	0.0039
MIXCT7\mixct-007-c3	1.195E-07	4.397	0.016	596	1.0036	0.0046	0.9975	0.0005	0.9940	0.0046
MIXCT7\mixct-007-c4	9.755E-08	6.282	0.016	850	1.0037	0.0057	0.9973	0.0004	0.9936	0.0057
MIXCT7\mixct-007-c5	9.255E-08	7.054	0.016	955	1.0044	0.0061	0.9970	0.0004	0.9927	0.0061
MIXCT7\mixct-007-ca1	1.404E-07	3.515	0.016	476	1.0024	0.0045	0.9934	0.0005	0.9911	0.0045
MIXCT7\mixct-007-cb1	1.417E-07	3.515	0.016	476	1.0024	0.0044	0.9898	0.0005	0.9874	0.0044
MIXCT7\mixct-007-cb2	1.419E-07	3.515	0.016	476	1.0026	0.0044	0.9910	0.0005	0.9884	0.0044
MIXCT7\mixct-007-cb3	1.414E-07	3.515	0.016	476	1.0027	0.0044	0.9919	0.0005	0.9892	0.0044
MIXCT7\mixct-007-cb4	1.41E-07	3.515	0.016	476	1.0025	0.0044	0.9932	0.0005	0.9907	0.0044
MIXCT8\mixct-008-c1	4.028E-07	1.515	0.014	223	0.9997	0.0032	0.9909	0.0006	0.9912	0.0033
MIXCT8\mixct-008-c2	2.009E-07	2.488	0.014	366	1.0008	0.003	0.9938	0.0006	0.9930	0.0031
MIXCT8\mixct-008-c3	1.442E-07	3.515	0.014	517	1.0023	0.0038	0.9946	0.0006	0.9923	0.0038
MIXCT8\mixct-008-c4	1.211E-07	4.397	0.014	647	1.0015	0.0047	0.9979	0.0005	0.9964	0.0047
MIXCT8\mixct-008-c5	9.875E-08	6.282	0.014	924	1.0022	0.0056	0.9995	0.0005	0.9973	0.0056
MIXCT8\mixct-008-c6	9.344E-08	7.054	0.014	1038	1.0028	0.0065	0.9992	0.0005	0.9964	0.0065
MIXCT8\mixct-008-ca1	1.434E-07	3.515	0.014	517	1.0023	0.0039	0.9933	0.0006	0.9910	0.0039
MIXCT8\mixct-008-cb1	1.447E-07	3.515	0.014	517	1.0023	0.0039	0.9911	0.0005	0.9889	0.0039
MIXCT8\mixct-008-cb2	1.448E-07	3.515	0.014	517	1.0023	0.0039	0.9923	0.0006	0.9901	0.0039
MIXCT8\mixct-008-cb3	1.439E-07	3.515	0.014	517	1.0023	0.0039	0.9925	0.0006	0.9902	0.0039
MIXCT8\mixct-008-cb4	1.435E-07	3.515	0.014	517	1.0023	0.0039	0.9921	0.0006	0.9898	0.0039
MIXCT9\mixct-009-c1	5.586E-07	1.111	0.014	228	1.0003	0.0054	0.9938	0.0006	0.9935	0.0054
MIXCT9\mixct-009-c2	3.131E-07	1.569	0.014	321	1.002	0.0049	0.9904	0.0006	0.9884	0.0049
MIXCT9\mixct-009-c3	1.602E-07	2.718	0.014	556	1.0035	0.005	0.9923	0.0006	0.9888	0.0050

Case Name	EALF (MeV)	v_m/v_f	$\frac{^{239}Pu}{(U+Pu)}$	H/ (^{239}Pu + ^{235}U)	k_{ben}	σ_{bench}	k_{MCNP}	σ_{MCNP}	k_{MCNP} (normalized)	σ_{tot}
MIXCT9\mixct-009-c4	1.203E-07	3.800	0.014	778	1.0046	0.0062	0.9929	0.0005	0.9883	0.0062
MIXCT9\mixct-009-c5	9.804E-08	5.155	0.014	1055	1.0059	0.0074	0.9961	0.0005	0.9902	0.0074
MIXCT9\mixct-009-c6	9.336E-08	5.593	0.014	1145	1.0067	0.008	0.9974	0.0005	0.9908	0.0080
MIXFAST\mixmf-008-c1	0.03351	na	0.951	0	0.992	0.0063	1.0023	0.0011	1.0104	0.0064
MIXFAST\mixmf-008-c2	0.32584	na	0.951	0	1.001	0.0023	1.0147	0.0010	1.0137	0.0025
MIXFAST\mixmf-008-c3	0.084968	na	0.951	0	0.986	0.0044	0.9682	0.0010	0.9819	0.0045
MIXFAST\mixmf-008-c4	0.17542	na	0.951	0	0.973	0.0045	0.9830	0.0009	1.0103	0.0046
MIXFAST\mixmf-008-c5	0.27435	na	0.951	0	1.006	0.0069	0.9989	0.0009	0.9929	0.0070
MIXFAST\mixmf-008-c6	0.027577	na	0.223	0	0.971	0.0042	0.9744	0.0009	1.0035	0.0043
MIXFAST\pumf-033-c1	0.40279	na	0.493	0	0.9967	0.0026	0.9992	0.0005	1.0025	0.0026

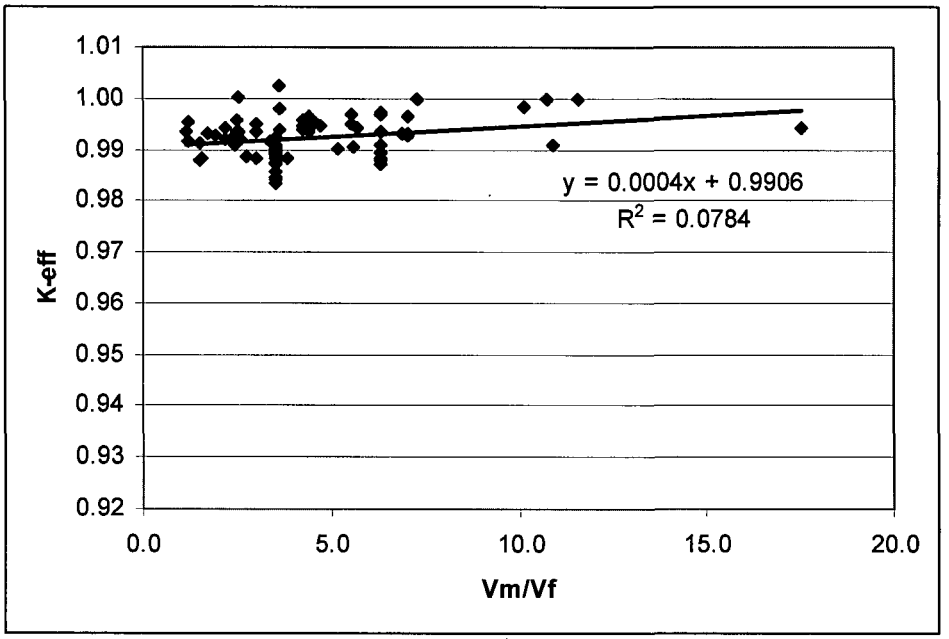

Figure 6.8-1 – Benchmark Data Trend for V_m/V_f

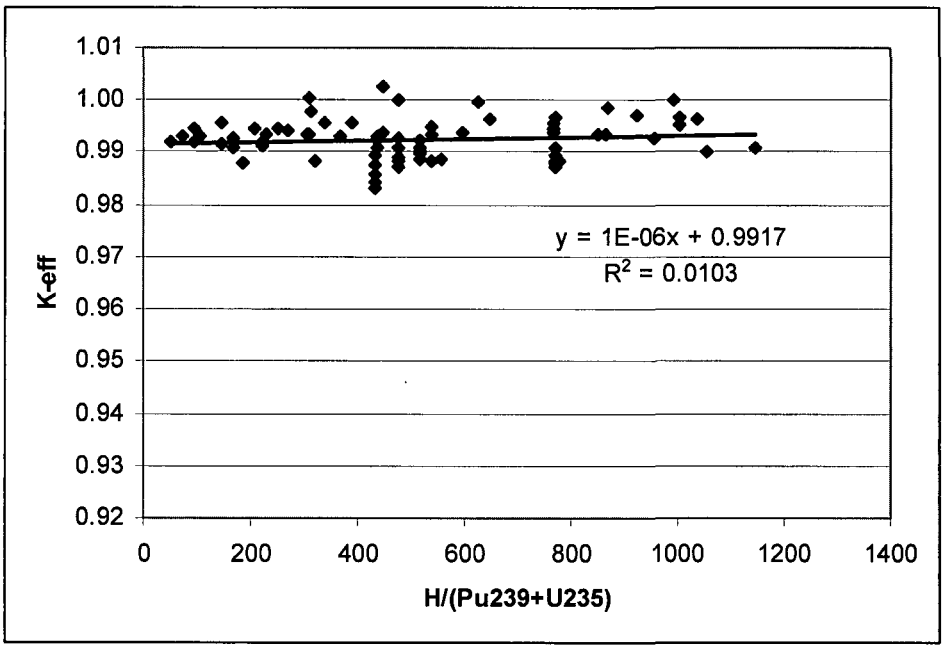

Figure 6.8-2 – Benchmark Data Trend for H/(Pu-239+U-235)

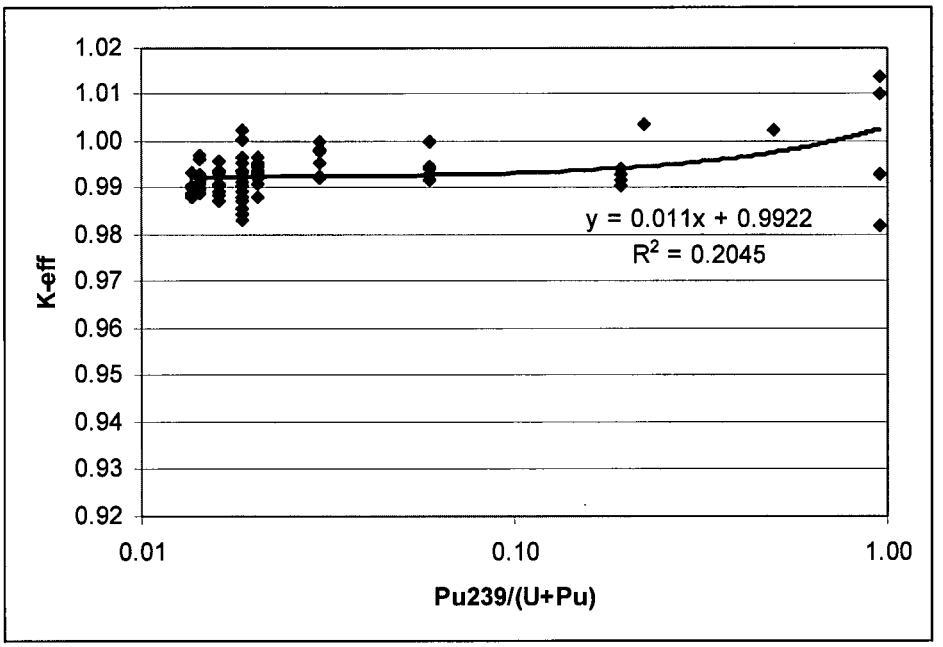

Figure 6.8-3 – Benchmark Data Trend for Pu-239/(U+Pu)

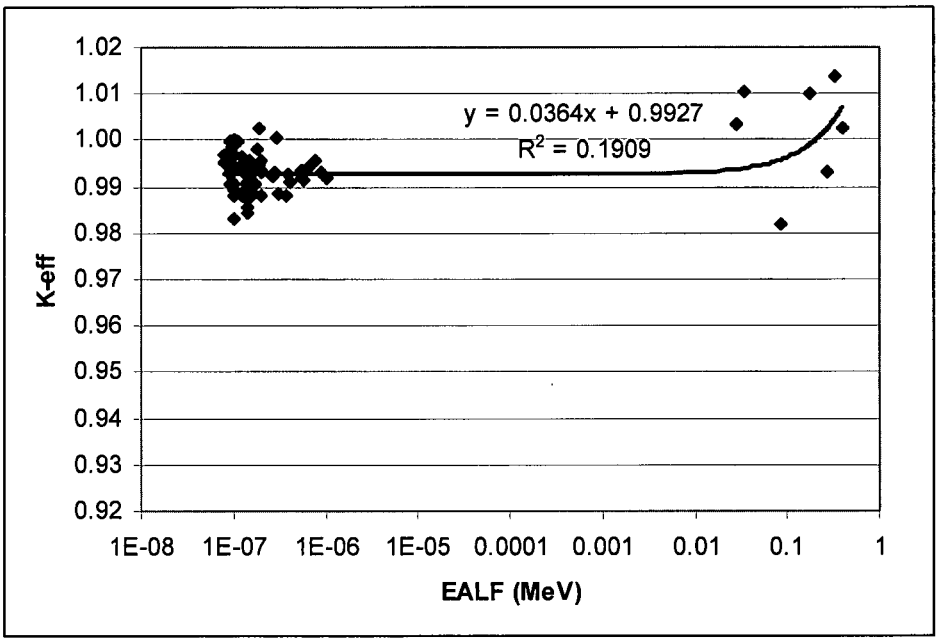

Figure 6.8-4 – Benchmark Data Trend for EALF

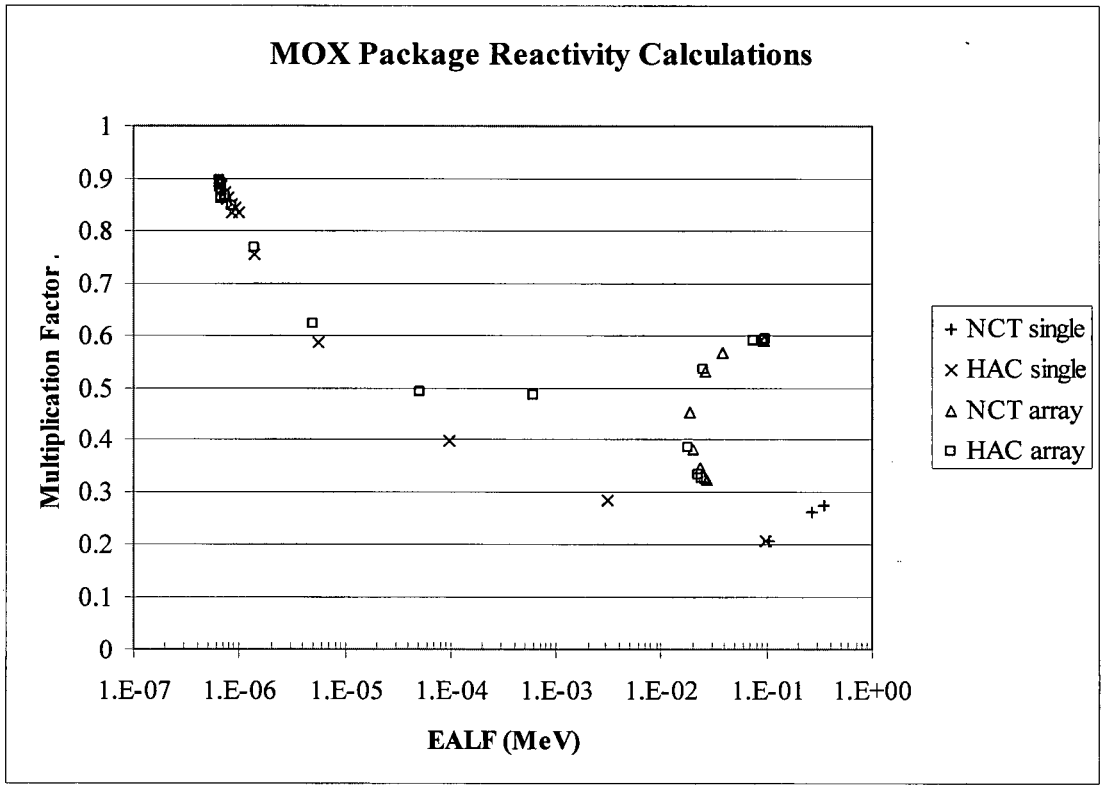

Figure 6.8-5 – Correlation of the MFFP Reactivity to EALF

This page left intentionally blank.

6.9 Appendices

Representative MCNP models are included in the following appendices:

6.9.1 Single Package Model

6.9.2 Infinite Array Model

This page left intentionally blank.

6.9.1 Single Package Model

This file is for the worst-case HAC model (max_hac_single_su1). Other files may be generated by adjusting the water density in the desired cells and modifying the pin pitch to the desired value.

```
MOX package max single conditions with 10.85 g/cc Fuel no Nb
c
c      ******Fuel Assembly*************
c     cells 1 to 3 transform the 3 assemblies to their locations
c 1      4 -1.0     -21  22 -23  24  -25   6            imp:n=1  $ top nozzle, void
c 2      4 -1.0     -21  22 -23  24  -7   26            imp:n=1  $ bottom nozzle, void
7      0          -21  22 -23  24   126  -25   fill=20  imp:n=1  $ pins
c
c 201    like 1 but trcl=53  $ assembly 2
c 202    like 2 but trcl=53
207    like 7 but trcl=53
c 220    like 1 but trcl=54  $ assembly 3
c 221    like 2 but trcl=54
222    like 7 but trcl=54
c
c -- "box" around fuel
c
301    0     (302 -303 300 -304 -906 26):
             (303 -305 300 -301 -906 26)   fill=30 imp:n=1   $ "box" cutout
302    like 301 but trcl=53
303    like 301 but trcl=54
c
c      perimeter containing strongback #1 in -y
50     0    (26 -906 902 -909 904 -910):
            (26 -906 909 -912 904 -901):
            (26 -906 912 904 -908):
            (26 -906 911 905 -904 -908):
            (26 -906 905 -900 903 -911) fill=7 imp:n=1
c      perimeter containing strongback #2
51     like 50 but trcl=53
c      perimeter containing strongback #3
52     like 50 but trcl=54
c
c     ******water beyond three units*****
131    9 -1.4  -61 -69  64    #7 #50 #51 #52 #301 #302 #303
                              #207 #222 imp:n=1
c      ******containment***************
141    5 -7.94  -62 -66  63 (61:65:-64)      imp:n=1           $ outer steel
143    5 -7.94  -61 -70  69                  imp:n=1           $ upper inner steel
145    4 -1.0  -61 -65  70                   imp:n=1           $ upper void
c      ******beyond containment********
195    6 -7.94 -72 -76  73  (62:66:-63)      imp:n=0.25        $ one foot refl
199    0                     (72:76:-73)     imp:n=0           $ outside world
c
c      Universe 20:  Fuel Lattice
c
200    4 -1.0   -12 11 -14 13 u=20 lat=1  trcl=30  fill=0:16 0:16 0:0
              1 1 1 1 1 1 1 1 1 1 1 1 1 1 1 1 1   $ row 17
              1 1 1 1 1 1 1 1 1 1 1 1 1 1 1 1 1   $ row 16
              1 1 1 1 1 4 1 1 4 1 1 4 1 1 1 1 1   $ row 15
              1 1 1 4 1 1 1 1 1 1 1 1 4 1 1 1 1   $ row 14
              1 1 1 1 1 1 1 1 1 1 1 1 1 1 1 1 1   $ row 13
              1 1 4 1 1 4 1 1 4 1 1 4 1 1 4 1 1   $ row 12
              1 1 1 1 1 1 1 1 1 1 1 1 1 1 1 1 1   $ row 11
              1 1 1 1 1 1 1 2 2 2 1 1 1 1 1 1 1   $ row 10
              1 1 4 1 1 4 1 2 4 2 1 4 1 1 4 1 1   $ row  9
              1 1 1 1 1 1 1 2 2 2 1 1 1 1 1 1 1   $ row  8
              1 1 1 1 1 1 1 1 1 1 1 1 1 1 1 1 1   $ row  7
              1 1 4 1 1 4 1 1 4 1 1 4 1 1 4 1 1   $ row  6
              1 1 1 1 1 1 1 1 1 1 1 1 1 1 1 1 1   $ row  5
              1 1 1 4 1 1 1 1 1 1 1 1 4 1 1 1 1   $ row  4
              1 1 1 1 1 4 1 1 4 1 1 4 1 1 1 1 1   $ row  3
              1 1 1 1 1 1 1 1 1 1 1 1 1 1 1 1 1   $ row  2
              1 1 1 1 1 1 1 1 1 1 1 1 1 1 1 1 1  imp:n=1     $ row  1 (top)
c
c      Universe 1:  Fuel pin in normal position
```

```
c
10     1 -10.85   -1       -4    5     u=1   imp:n=1   $ fuel
11     4 -1.0     -2   1   -4    5     u=1   imp:n=1   $ radial gap
12     7 -6.5     -3   2   -8    5     u=1   imp:n=1   $ clad
13     4 -1.0          3    7   -6     u=1   imp:n=1   $ radially beyond pin
14     4 -1.0     -2       -8    4     u=1   imp:n=1   $ above fuel void
15     7 -6.5     -3       -6    8     u=1   imp:n=1   $ top of fuel cap
16     7 -6.5     -3       -5    7     u=1   imp:n=1   $ bottom of fuel cap
17     4 -1.0               6         u=1   imp:n=1   $ top water to infinity
18     4 -1.0              -7         u=1   imp:n=1   $ bottom water to infinity
c
c      Universe 2:  Fuel pin shifted up
c
410     1 -10.85   -1       -4    5     trcl=(0 0 23.7109) u=2   imp:n=1   $ fuel
411     4 -1.0     -2   1   -4    5     trcl=(0 0 23.7109) u=2   imp:n=1   $ radial gap
412     7 -6.5     -3   2   -8    5     trcl=(0 0 23.7109) u=2   imp:n=1   $ clad
413     4 -1.0          3    7   -6     trcl=(0 0 23.7109) u=2   imp:n=1   $ radially beyond pin
414     4 -1.0     -2       -8    4     trcl=(0 0 23.7109) u=2   imp:n=1   $ above fuel void
415     7 -6.5     -3       -6    8     trcl=(0 0 23.7109) u=2   imp:n=1   $ top of fuel cap
416     7 -6.5     -3       -5    7     trcl=(0 0 23.7109) u=2   imp:n=1   $ bottom of fuel cap
417     4 -1.0               6         trcl=(0 0 23.7109) u=2   imp:n=1   $ top water to infinity
418     4 -1.0              -7         trcl=(0 0 23.7109) u=2   imp:n=1   $ bottom water to
infinity
c
c      Universe 3:  Fuel pin shifted down
c
420     1 -10.85   -1       -4    5   trcl=(0 0 -9.4361) u=3   imp:n=1   $ fuel
421     4 -1.0     -2   1   -4    5   trcl=(0 0 -9.4361) u=3   imp:n=1   $ radial gap
422     7 -6.5     -3   2   -8    5   trcl=(0 0 -9.4361) u=3   imp:n=1   $ clad
423     4 -1.0          3    7   -6   trcl=(0 0 -9.4361) u=3   imp:n=1   $ radially beyond pin
424     4 -1.0     -2       -8    4   trcl=(0 0 -9.4361) u=3   imp:n=1   $ above fuel void
425     7 -6.5     -3       -6    8   trcl=(0 0 -9.4361) u=3   imp:n=1   $ top of fuel cap
426     7 -6.5     -3       -5    7   trcl=(0 0 -9.4361) u=3   imp:n=1   $ bottom of fuel cap
427     4 -1.0               6       trcl=(0 0 -9.4361) u=3   imp:n=1   $ top water to infinity
428     4 -1.0              -7       trcl=(0 0 -9.4361) u=3   imp:n=1   $ bottom water to infinity
c
c      Universe 4:  Instrument/guide tube
c
41     4 -1.0      -18      5 -8              u=4   imp:n=1   $ inside
42     7 -6.5      -19  18  5 -8              u=4   imp:n=1   $ tube
43     4 -1.0       19      5 -8              u=4   imp:n=1   $ beyond tube
44     4 -1.0       8                         u=4   imp:n=1
45     4 -1.0      -5                         u=4   imp:n=1
c
c      Universe 14:  Water only
c
46     4 -1.0     -998                      u=14  imp:n=1
47     4 -1.0      998                      u=14  imp:n=1
c
c      Universe 7:  Strongback
c
700    6  -7.94      715 -710                  u=7  imp:n=1  $ tangential strongback
701    6  -7.94     (710 711 718):(-711 713)   u=7  imp:n=1  $ radial strongback+bend
702    2  -2.713     714 -719 -716             u=7  imp:n=1  $ tan Al clad
703    21  9.2244E-02 719 -720 -716
                    730 731 732 733 734 735 736 737 738
                    739 740 741 742 743 744 745 746 747
                    750 751 752 753 754 755 756 757 758
                    759 760 761 762 763 764 765 766 767 u=7  imp:n=1 $ tangential boral
704    2   -2.713     720 -715 -716               u=7  imp:n=1  $ tan Al clad
706    2   -2.713     712 -722 -717               u=7  imp:n=1  $ rad Al clad
707    21  9.2244E-02 722 -723 -717
                    770 771 772 773 774 775 776 777 778
                    779 780 781 782 783 784 785 786 787
                    790 791 792 793 794 795 796 797 798
                    799 800 801 802 803 804 805 806 807 u=7  imp:n=1 $ radial boral
708    2   -2.713     723 -713 -717                     u=7  imp:n=1 $ rad Al
710    4 -1.0        (710 711 -718):(716 -710 717 -715):
                     (710 -713 717 -711)                    u=7  imp:n=1
719    6 -7.94      ((-717 -712):(-716 -714 717))     -809  u=7  imp:n=1 $ poison holder
720    4 -1.0       ((-717 -712):(-716 -714 717)) 809 -810  u=7  imp:n=1
721    6 -7.94      ((-717 -712):(-716 -714 717)) 810 -811  u=7  imp:n=1
722    4 -1.0       ((-717 -712):(-716 -714 717)) 811 -812  u=7  imp:n=1
723    6 -7.94      ((-717 -712):(-716 -714 717)) 812 -813  u=7  imp:n=1
724    4 -1.0       ((-717 -712):(-716 -714 717)) 813 -814  u=7  imp:n=1
```

```
725     6 -7.94       ((-717 -712):(-716 -714 717)) 814 -815  u=7  imp:n=1
726     4 -1.0        ((-717 -712):(-716 -714 717)) 815 -816  u=7  imp:n=1
727     6 -7.94       ((-717 -712):(-716 -714 717)) 816 -817  u=7  imp:n=1
728     4 -1.0        ((-717 -712):(-716 -714 717)) 817 -818  u=7  imp:n=1
729     6 -7.94       ((-717 -712):(-716 -714 717)) 818 -819  u=7  imp:n=1
730     4 -1.0        ((-717 -712):(-716 -714 717)) 819 -820  u=7  imp:n=1
731     6 -7.94       ((-717 -712):(-716 -714 717)) 820 -821  u=7  imp:n=1
732     4 -1.0        ((-717 -712):(-716 -714 717)) 821 -822  u=7  imp:n=1
733     6 -7.94       ((-717 -712):(-716 -714 717)) 822 -823  u=7  imp:n=1
734     4 -1.0        ((-717 -712):(-716 -714 717)) 823 -824  u=7  imp:n=1
735     6 -7.94       ((-717 -712):(-716 -714 717)) 824 -825  u=7  imp:n=1
736     4 -1.0        ((-717 -712):(-716 -714 717)) 825 -826  u=7  imp:n=1
737     6 -7.94       ((-717 -712):(-716 -714 717))      826  u=7  imp:n=1
c
750     6  -7.94      719 -720 -750            u=7  imp:n=1 $ screws in boral
751     6  -7.94      719 -720 -751            u=7  imp:n=1
752     6  -7.94      719 -720 -752            u=7  imp:n=1
753     6  -7.94      719 -720 -753            u=7  imp:n=1
754     6  -7.94      719 -720 -754            u=7  imp:n=1
755     6  -7.94      719 -720 -755            u=7  imp:n=1
756     6  -7.94      719 -720 -756            u=7  imp:n=1
757     6  -7.94      719 -720 -757            u=7  imp:n=1
758     6  -7.94      719 -720 -758            u=7  imp:n=1
759     6  -7.94      719 -720 -759            u=7  imp:n=1
760     6  -7.94      719 -720 -760            u=7  imp:n=1
761     6  -7.94      719 -720 -761            u=7  imp:n=1
762     6  -7.94      719 -720 -762            u=7  imp:n=1
763     6  -7.94      719 -720 -763            u=7  imp:n=1
764     6  -7.94      719 -720 -764            u=7  imp:n=1
765     6  -7.94      719 -720 -765            u=7  imp:n=1
766     6  -7.94      719 -720 -766            u=7  imp:n=1
767     6  -7.94      719 -720 -767            u=7  imp:n=1
c
770     6  -7.94      722 -723 -770            u=7  imp:n=1
771     6  -7.94      722 -723 -771            u=7  imp:n=1
772     6  -7.94      722 -723 -772            u=7  imp:n=1
773     6  -7.94      722 -723 -773            u=7  imp:n=1
774     6  -7.94      722 -723 -774            u=7  imp:n=1
775     6  -7.94      722 -723 -775            u=7  imp:n=1
776     6  -7.94      722 -723 -776            u=7  imp:n=1
777     6  -7.94      722 -723 -777            u=7  imp:n=1
778     6  -7.94      722 -723 -778            u=7  imp:n=1
779     6  -7.94      722 -723 -779            u=7  imp:n=1
780     6  -7.94      722 -723 -780            u=7  imp:n=1
781     6  -7.94      722 -723 -781            u=7  imp:n=1
782     6  -7.94      722 -723 -782            u=7  imp:n=1
783     6  -7.94      722 -723 -783            u=7  imp:n=1
784     6  -7.94      722 -723 -784            u=7  imp:n=1
785     6  -7.94      722 -723 -785            u=7  imp:n=1
786     6  -7.94      722 -723 -786            u=7  imp:n=1
787     6  -7.94      722 -723 -787            u=7  imp:n=1
c
790     6  -7.94      722 -723 -790            u=7  imp:n=1
791     6  -7.94      722 -723 -791            u=7  imp:n=1
792     6  -7.94      722 -723 -792            u=7  imp:n=1
793     6  -7.94      722 -723 -793            u=7  imp:n=1
794     6  -7.94      722 -723 -794            u=7  imp:n=1
795     6  -7.94      722 -723 -795            u=7  imp:n=1
796     6  -7.94      722 -723 -796            u=7  imp:n=1
797     6  -7.94      722 -723 -797            u=7  imp:n=1
798     6  -7.94      722 -723 -798            u=7  imp:n=1
799     6  -7.94      722 -723 -799            u=7  imp:n=1
800     6  -7.94      722 -723 -800            u=7  imp:n=1
801     6  -7.94      722 -723 -801            u=7  imp:n=1
802     6  -7.94      722 -723 -802            u=7  imp:n=1
803     6  -7.94      722 -723 -803            u=7  imp:n=1
804     6  -7.94      722 -723 -804            u=7  imp:n=1
805     6  -7.94      722 -723 -805            u=7  imp:n=1
806     6  -7.94      722 -723 -806            u=7  imp:n=1
807     6  -7.94      722 -723 -807            u=7  imp:n=1
c
810     6  -7.94      719 -720 -730            u=7  imp:n=1
811     6  -7.94      719 -720 -731            u=7  imp:n=1
812     6  -7.94      719 -720 -732            u=7  imp:n=1
813     6  -7.94      719 -720 -733            u=7  imp:n=1
```

```
814     6  -7.94       719 -720 -734              u=7  imp:n=1
815     6  -7.94       719 -720 -735              u=7  imp:n=1
816     6  -7.94       719 -720 -736              u=7  imp:n=1
817     6  -7.94       719 -720 -737              u=7  imp:n=1
818     6  -7.94       719 -720 -738              u=7  imp:n=1
819     6  -7.94       719 -720 -739              u=7  imp:n=1
820     6  -7.94       719 -720 -740              u=7  imp:n=1
821     6  -7.94       719 -720 -741              u=7  imp:n=1
822     6  -7.94       719 -720 -742              u=7  imp:n=1
823     6  -7.94       719 -720 -743              u=7  imp:n=1
824     6  -7.94       719 -720 -744              u=7  imp:n=1
825     6  -7.94       719 -720 -745              u=7  imp:n=1
826     6  -7.94       719 -720 -746              u=7  imp:n=1
827     6  -7.94       719 -720 -747              u=7  imp:n=1
c
c       Universe 30:  "box" around fuel
c
c 310     2   -2.713    -313  317     u=30 imp:n=1 $ radial left
c 311     2   -2.713     316 -310     u=30 imp:n=1 $ tangential bot
c 312     2   -2.713     314 -315 317 u=30 imp:n=1 $ radial right
c 315     2   -2.713     311 -312 316 u=30 imp:n=1 $ tangential top
316     6 -7.94         315  312     u=30 imp:n=1
317     4 -1.0        (312 -317 -315):(-316 -312) u=30 imp:n=1
c
320     4 -1.0             -315 317 -320      u=30 imp:n=1 $ radial water gap
321    21  9.2244E-02 313 -314 317  320 -321 u=30 imp:n=1 $ radial boral
322     4 -1.0             -315 317  321 -322 u=30 imp:n=1
323    21  9.2244E-02 313 -314 317  322 -323 u=30 imp:n=1
324     4 -1.0             -315 317  323 -324 u=30 imp:n=1
325    21  9.2244E-02 313 -314 317  324 -325 u=30 imp:n=1
326     4 -1.0             -315 317  325 -326 u=30 imp:n=1
327    21  9.2244E-02 313 -314 317  326 -327 u=30 imp:n=1
328     4 -1.0             -315 317  327 -328 u=30 imp:n=1
329    21  9.2244E-02 313 -314 317  328 -329 u=30 imp:n=1
330     4 -1.0             -315 317  329 -330 u=30 imp:n=1
331    21  9.2244E-02 313 -314 317  330 -331 u=30 imp:n=1
332     4 -1.0             -315 317  331 -332 u=30 imp:n=1
333    21  9.2244E-02 313 -314 317  332 -333 u=30 imp:n=1
334     4 -1.0             -315 317  333      u=30 imp:n=1
c
340     2   -2.713    -313  317  320 -321 u=30 imp:n=1  $ radial Al cladding
341     2   -2.713    -313  317  322 -323 u=30 imp:n=1
342     2   -2.713    -313  317  324 -325 u=30 imp:n=1
343     2   -2.713    -313  317  326 -327 u=30 imp:n=1
344     2   -2.713    -313  317  328 -329 u=30 imp:n=1
345     2   -2.713    -313  317  330 -331 u=30 imp:n=1
346     2   -2.713    -313  317  332 -333 u=30 imp:n=1
c
347     2   -2.713    314 -315 317 320 -321 u=30 imp:n=1 $ radial Al cladding
348     2   -2.713    314 -315 317 322 -323 u=30 imp:n=1
349     2   -2.713    314 -315 317 324 -325 u=30 imp:n=1
350     2   -2.713    314 -315 317 326 -327 u=30 imp:n=1
351     2   -2.713    314 -315 317 328 -329 u=30 imp:n=1
352     2   -2.713    314 -315 317 330 -331 u=30 imp:n=1
353     2   -2.713    314 -315 317 332 -333 u=30 imp:n=1
c
360     4 -1.0             -312 316 -320      u=30 imp:n=1 $ tangential water gap
361    21  9.2244E-02 310 -311 316  320 -321 u=30 imp:n=1 $ tangential boral
362     4 -1.0             -312 316  321 -322 u=30 imp:n=1
363    21  9.2244E-02 310 -311 316  322 -323 u=30 imp:n=1
364     4 -1.0             -312 316  323 -324 u=30 imp:n=1
365    21  9.2244E-02 310 -311 316  324 -325 u=30 imp:n=1
366     4 -1.0             -312 316  325 -326 u=30 imp:n=1
367    21  9.2244E-02 310 -311 316  326 -327 u=30 imp:n=1
368     4 -1.0             -312 316  327 -328 u=30 imp:n=1
369    21  9.2244E-02 310 -311 316  328 -329 u=30 imp:n=1
370     4 -1.0             -312 316  329 -330 u=30 imp:n=1
371    21  9.2244E-02 310 -311 316  330 -331 u=30 imp:n=1
372     4 -1.0             -312 316  331 -332 u=30 imp:n=1
373    21  9.2244E-02 310 -311 316  332 -333 u=30 imp:n=1
374     4 -1.0             -312 316  333      u=30 imp:n=1
c
380     2   -2.713    316 311 -312 320 -321 u=30 imp:n=1  $ horizontal Al cladding
381     2   -2.713    316 311 -312 322 -323 u=30 imp:n=1
382     2   -2.713    316 311 -312 324 -325 u=30 imp:n=1
```

```
383     2   -2.713     316 311 -312 326 -327 u=30 imp:n=1
384     2   -2.713     316 311 -312 328 -329 u=30 imp:n=1
385     2   -2.713     316 311 -312 330 -331 u=30 imp:n=1
386     2   -2.713     316 311 -312 332 -333 u=30 imp:n=1
c
387     2   -2.713     316 -310 320 -321 u=30 imp:n=1 $ horizontal Al cladding
388     2   -2.713     316 -310 322 -323 u=30 imp:n=1
389     2   -2.713     316 -310 324 -325 u=30 imp:n=1
390     2   -2.713     316 -310 326 -327 u=30 imp:n=1
391     2   -2.713     316 -310 328 -329 u=30 imp:n=1
392     2   -2.713     316 -310 330 -331 u=30 imp:n=1
393     2   -2.713     316 -310 332 -333 u=30 imp:n=1
c
c       Universe 51:  Dummy universe containing fuel
c
c       999     1 -10.31 -999 u=51    imp:n=1  $ for diagnostics only, not used
c       1000    1 -10.31  999 u=51    imp:n=1  $ for diagnostics only, not used

c       ******Fuel Assembly*************
c         fuel pin
1       cz     0.409575                 $ fuel radius
2       cz     0.41783                  $ radius inside clad
3       cz     0.47498                  $ radius outside clad
4       pz   182.88                     $ top of fuel
5       pz  -182.88                     $ bottom of fuel
6       pz   202.7555                   $ top of fuel pin
7       pz  -184.3405                   $ bottom of fuel pin
8       pz   201.4474                   $ bottom of top cap
11      px    -0.6688                   $ lattice definition
12      px     0.6688
13      py    -0.6688
14      py     0.6688
c       200     pz    -119.38
c         guide tube
18       cz     0.57150
19       cz     0.61214
c         perimeter of fuel assembly
21       px    10.2391 $ offset from surface 905
22       px   -12.1116 $
23       py    -6.6593 $ offset from surface 904
24       py   -29.0113 $
25       pz   226.466
26       pz -190.95720
126      pz -193.776
c       ******containment**************
61       cz     36.1950
62       cz     37.6174
63       pz   -197.5866  $ 1.5" thick
64       pz   -193.7766  $ 1.11" below bottom of fuel (strongback bottom not modeled)
65       pz    235.6866
66       pz    237.5916
c   67   pz   -203.0222
c   68   pz   -201.1172
69       pz    226.4664
70       pz    228.0666
c       ******outside of water refl****
72       cz     68.0974
73       pz   -228.0666  $ 1' water from 63
76       pz    268.0716  $ 1' water from 66
c
c  -- "box"
c
300     py -29.7925   $ defining box in u=0
301     py -29.0114
302     px -12.8928
303     px -12.1117
304     py -7.5675
305     px  9.9672
c
310     25 py 0.04445
311     25 py 0.2604
312     25 py 0.3048
313     25 px 0.04445
314     25 px 0.2604
315     25 px 0.3048
```

```
316     25 px 2.54
317     25 py 2.54
c
320      pz -171.049
321      pz -119.532
322      pz -109.758
323      pz -67.412
324      pz -57.638
325      pz -15.316
326      pz -5.542
327      pz 36.855
328      pz 46.629
329      pz 89.002
330      pz 98.776
331      pz 141.097
332      pz 150.871
333      pz 193.548
c
c       strongback surfaces
c
710     22 px 0
711     22 py 0
712     22 px 0.476
713     22 px 0.7808
714     22 py 0.476
715     22 py 0.7808
716     22 px -0.3114  $  0.43" less than surface 713
717     22 py -0.54
718     22 cz 0.7808
719     22 py 0.5205
720     22 py 0.7364
722     22 px 0.5205
723     22 px 0.7364
c
730     22 c/y -2.7752 -189.6872 0.47625
731     22 c/y -2.7752 -179.5526 0.47625
732     22 c/y -2.7752 -172.3187 0.47625
733     22 c/y -2.7752 -118.2624 0.47625
734     22 c/y -2.7752 -111.0285 0.47625
735     22 c/y -2.7752 -66.1416 0.47625
736     22 c/y -2.7752 -58.9077 0.47625
737     22 c/y -2.7752 -14.0462 0.47625
738     22 c/y -2.7752 -6.8123 0.47625
739     22 c/y -2.7752 38.1254 0.47625
740     22 c/y -2.7752 45.3593 0.47625
741     22 c/y -2.7752 90.2716 0.47625
742     22 c/y -2.7752 97.5055 0.47625
743     22 c/y -2.7752 142.3670 0.47625
744     22 c/y -2.7752 149.6009 0.47625
745     22 c/y -2.7752 194.8180 0.47625
746     22 c/y -2.7752 202.0519 0.47625
747     22 c/y -2.7752 213.8172 0.47625
c
750     22 c/y -16.7452 -189.6872 0.47625
751     22 c/y -16.7452 -179.5526 0.47625
752     22 c/y -16.7452 -172.3187 0.47625
753     22 c/y -16.7452 -118.2624 0.47625
754     22 c/y -16.7452 -111.0285 0.47625
755     22 c/y -16.7452 -66.1416 0.47625
756     22 c/y -16.7452 -58.9077 0.47625
757     22 c/y -16.7452 -14.0462 0.47625
758     22 c/y -16.7452 -6.8123 0.47625
759     22 c/y -16.7452 38.1254 0.47625
760     22 c/y -16.7452 45.3593 0.47625
761     22 c/y -16.7452 90.2716 0.47625
762     22 c/y -16.7452 97.5055 0.47625
763     22 c/y -16.7452 142.3670 0.47625
764     22 c/y -16.7452 149.6009 0.47625
765     22 c/y -16.7452 194.8180 0.47625
766     22 c/y -16.7452 202.0519 0.47625
767     22 c/y -16.7452 213.8172 0.47625
c
770     22 c/x -5.9248 -189.6872 0.47625
771     22 c/x -5.9248 -179.5526 0.47625
772     22 c/x -5.9248 -172.3187 0.47625
```

```
773     22 c/x -5.9248 -118.2624 0.47625
774     22 c/x -5.9248 -111.0285 0.47625
775     22 c/x -5.9248 -66.1416 0.47625
776     22 c/x -5.9248 -58.9077 0.47625
777     22 c/x -5.9248 -14.0462 0.47625
778     22 c/x -5.9248 -6.8123 0.47625
779     22 c/x -5.9248 38.1254 0.47625
780     22 c/x -5.9248 45.3593 0.47625
781     22 c/x -5.9248 90.2716 0.47625
782     22 c/x -5.9248 97.5055 0.47625
783     22 c/x -5.9248 142.3670 0.47625
784     22 c/x -5.9248 149.6009 0.47625
785     22 c/x -5.9248 194.8180 0.47625
786     22 c/x -5.9248 202.0519 0.47625
787     22 c/x -5.9248 213.8172 0.47625
c
790     22 c/x -16.9789 -189.6872 0.47625
791     22 c/x -16.9789 -179.5526 0.47625
792     22 c/x -16.9789 -172.3187 0.47625
793     22 c/x -16.9789 -118.2624 0.47625
794     22 c/x -16.9789 -111.0285 0.47625
795     22 c/x -16.9789 -66.1416 0.47625
796     22 c/x -16.9789 -58.9077 0.47625
797     22 c/x -16.9789 -14.0462 0.47625
798     22 c/x -16.9789 -6.8123 0.47625
799     22 c/x -16.9789 38.1254 0.47625
800     22 c/x -16.9789 45.3593 0.47625
801     22 c/x -16.9789 90.2716 0.47625
802     22 c/x -16.9789 97.5055 0.47625
803     22 c/x -16.9789 142.3670 0.47625
804     22 c/x -16.9789 149.6009 0.47625
805     22 c/x -16.9789 194.8180 0.47625
806     22 c/x -16.9789 202.0519 0.47625
807     22 c/x -16.9789 213.8172 0.47625
c
809      pz -188.417
810      pz -181.331  $ PH 1 (bottom)
811      pz -170.541  $ PH 1
812      pz -120.040  $ PH 2
813      pz -109.250
814      pz -67.920   $ PH 3
815      pz -57.130
816      pz -15.824   $ PH 4
817      pz -5.034
818      pz 36.347    $ PH 5
819      pz 47.137
820      pz 88.494    $ PH 6
821      pz 99.284
822      pz 140.589   $ PH 7
823      pz 151.379
824      pz 193.040   $ PH 8
825      pz 203.830   $ PH 8
826      pz 212.547
c
900      px 11.18006  $ FIXED for strongbacks touching
901      py -5.71956  $ FIXED for strongbacks touching
902      px -11.9593
903      py -28.7574  $ surface 901 minus 9.07"
c
c         904 is -7.1354 and 905 is 9.7633 for nominal case (with poison holders).
c         they are shifted to cut off poison holders to allow for
c         expansion for damaged cases.
c
c         To completely "slice off" the poison holders, set
c         904 to -6.6593 and 905 to 10.2392.
c
904      py -6.6593 $ tangential strongback lower bound, surface 901 minus total thickness
905      px 10.2392 $ radial strongback left bound, surface 901 minus total thickness
906      pz 215.7222
908      c/z 9.87856 -7.02106 1.3015
909      px -9.9019
910      py -6.35448
911      py -7.1344   $ fixed
912      px  9.7653   $ fixed
c
```

```
998      so  10000
999      pz  345.5565

mode     n
c        print
kcode  2000  1 30  530
ksrc    -16.08  10.4  0
         17.82   7.67 0
          0.55 -17.81 0
cut:n    j j 0 0
c
c      Materials
c
m1     92235     -0.249    $ fuel pellet
       92238    -82.615
       94239     -4.972
       94240     -0.264
       94241     -0.053
        8016    -11.847
m2     13027       1.0     $ aluminum cladding for BORAL
m4      1001       2       $ water
        8016       1
mt4     lwtr.01t
m5      6000     -0.06     $ XM-19
        7014     -0.4
       14000     -0.75
       15031     -0.04
       16032     -0.03
       23000     -0.3
       24000     -23.5
       25055     -6
       28000     -13.5
       41093     -0.3
       42000     -3
       26000     -52.12
m6      6000     -0.08     $ SS-304
       14000     -1.0
       15031     -0.045
       24000     -19.0
       25055     -2.0
       26000     -68.375
       28000     -9.5
m7     40000     -1.0    $ Cladding
c       41093     -0.030
m8     82000      1.0      $ lead
m9       6000     -25.1    $ water/steel mix, 5.8% steel by volume
        14000     -313.9
        15031     -14.1
        24000     -5964.9
        25055     -627.9
        26000     -21465.8
        28000     -2982.5
        1001     -7240.1
        8016     -57462.7
mt9     lwtr.01t
m21     5010     7.3123E-03 $ 35 mg/cm2 B-10, 75% credit
        5011     3.9244E-02
        6000     1.2248E-02
       13027     3.3439E-02
c          total 9.2244E-02
c
c          Translations
c
c          tr22 is the intersection of planes 904 and 905
c          when the poison holders are present (904 and 905 shift when it is
c          desired to "slice off" the poison holders).
c          Note that the origin of Universe 7 corresponds to the intersection
c          of these planes.
c
*tr22      9.7643 -7.1354 0.0
c
c          tr25 is the intersection of planes 300 and 302.  The origin of Universe 30
c          corresponds to the intersection of these planes.
c
*tr25     -12.8928 -29.7925 0.0
```

```
c
c         tr30 is computed by taking the coordinates of the intersection of planes
c         22 and 24 and adding half the pitch (note: can't be exact or else planes will
c         overlap, causing program termination.)
c
*tr30     -11.6368 -28.5365 0.0
c
c         tr53 and tr54 rotate the bottom assembly to create assemblies 2 and 3
c
*tr53     0 0 0                 120  30 90   150 120 90  90 90 0 $ +x+y
*tr54     0 0 0                 120 150 90    30 120 90  90 90 0 $ -x-y
```

This page left intentionally blank.

6.9.2 Infinite Array Model

The infinite array models are geometrically the same as the single package models, although small changes have been made to the outer boundary to simulate the infinite array. Additional cells and surfaces are listed below.

```
195    0          -881 882 -886 885 -883 884 -66 63  62  imp:n=1 $ w between packages
199    0          (881:-882:886:-885:883:-884:66:-63)    imp:n=0 $ outside world

c     hexagonal boundary of one unit lattice cell, close packed
 *881    px   37.6184
 *882    px  -37.6184
 *883     p  -0.5000000      0.866025404    0.0000000      37.6184
 *884     p  -0.5000000      0.866025404    0.0000000     -37.6184
 *885     p   0.5000000      0.866025404    0.0000000     -37.6184
 *886     p   0.5000000      0.866025404    0.0000000      37.6184
```

This page left intentionally blank.

7.0 PACKAGE OPERATIONS

This chapter delineates the procedures for loading a payload into the MOX Fresh Fuel Package (MFFP), and leakage rate testing of the containment boundary O-ring seals. The MFFP is designed such that both lid insertion/removal and strongback insertion/removal may be preformed either horizontally or vertically. The operational steps provided in this chapter address both loading/unloading options.

A variety of auxiliary equipment is utilized in the loading and unloading operations. While this equipment is not included in the transportation license for the package, a listing of the equipment and its function is provided below for clarity.

Air Pallet – Device used to move the MFFP when attached to the skid.

Package Connection Collar – Locating collar on the base of the insertion/extraction station. Package is aligned with and attached to the connection collar. (Used only for horizontal operations.)

Handling Lift Equipment – Equipment used to lift the MFFP (with attached transport skid).

Insertion/Extraction Station – Device used to insert and remove the strongback from the package. (Used only for horizontal operations.)

Lid Handling Fixture – Fixture that bolts to the package lid to assist in lid attachment/removal operations. (Used only for horizontal operations.)

Load/Unload Station – Device into which the strongback is installed when being loaded/unloaded with a fuel assembly.

Sealing Surface Protector – Device that attaches to the seal flange and protects the sealing surface during strongback loading/unloading operations.

Strongback Lift Tool – Tool that attaches to the top of the strongback for vertical transfer.

Top Plate Lifting Assembly – Lifting equipment used to remove the strongback top plate assembly.

Upending Frame – Device used to transfer the MFFP (with attached transport skid) between horizontal and vertical orientations. (Used only for vertical operations.)

Wall Mount Fixture – Fixture to which the upending frame attaches when the MFFP (with attached transport skid) is in the vertical orientation. (Used only for vertical operations.)

7.1 Package Loading

This section delineates the procedures for loading a payload into the MFFP. Hereafter, reference to specific MFFP components may be found in Appendix 1.4.2, *Packaging General Arrangement Drawings*. Note that the steps provided in the following sections may be performed in any logical sequence.

The loading operation shall be performed in a dry environment. If precipitation enters the cavity, the free-standing water shall be removed prior to loading the payload.

7.1.1 Preparation for Loading

7.1.1.1 Removal of MFFP from the Transport Conveyance

1. Disengage the tie-down devices from the shipping skid and the transport conveyance.

   CAUTION: Failure to disengage the tie-down devices may result in damage to the packaging, shipping skid, and/or the transport conveyance.

2. Using an air pallet or other lifting equipment, remove the MFFP/shipping skid from the transport conveyance and move to the loading area.
3. Remove the air pallet or other lifting equipment

7.1.1.2 Removal of the Closure Lid

7.1.1.2.1 Horizontal Operations

1. Remove the six (6) 1-inch socket head cap screws (SHCS) from the lid end impact limiter.
2. Utilizing appropriate lifting equipment, carefully lift and remove the lid end impact limiter and place in a secure area.
3. If necessary, repeat Steps 1 and 2 for the bottom end impact limiter.
4. Vent the interior of the MFFP through the lid end vent plug.
5. Loosen and / or remove the twenty-four (24) 3/4-inch SHCS attaching the lid to the package body. Ensure the lid remains in place on the body.
6. Utilizing four (4) 1/2-inch hex bolts, secure the lid handling fixture to the closure lid. Tighten the hex bolts to snug tight condition. Ensure any of the lid attachment fasteners that are covered by the lid handling fixture are removed prior to installing the lid handling fixture.
7. Connect appropriate lifting equipment to the lid handling fixture.
8. Remove any of the twenty-four (24) 3/4-inch SHCS not already removed in Steps 5 or 6 and carefully remove the closure lid with the lifting equipment and lid handling fixture. If necessary, the three T-handle assemblies on the lid handling fixture or three (3) 1/2-inch-13 x 2-inch bolts may be utilized in the three equally-spaced holes marked "for lid handling only" to assist in breaking the seal of the closure lid. Care shall be taken to not damage the MFFP containment seal surfaces.
9. Store the closure lid in a manner such that potential damage to the O-ring seals and sealing surfaces is minimized.

7.1.1.2.2 Vertical Operations

1. Attach the handling lift equipment, using the shackles on the support skid, in preparation for lifting the MFFP. Ensure the handling lift equipment "Lid End" is oriented toward the lid end of the MFFP.
2. Lift and place the MFFP with attached transport skid into the upending frame.
3. Secure the MFFP to the upending frame with both the ball lock pins and the tie-down straps.
4. Remove the six (6) 1-inch socket head cap screws (SHCS) from the lid end impact limiter.

5. Utilizing appropriate lifting equipment, carefully lift and remove the lid end impact limiter and place in a secure area. Optionally, the impact limiter may be removed prior to loading the MFFP into the upending frame (Step 2).
6. Vent the interior of the MFFP through the lid end vent plug.
7. Loosen the twenty-four (24), 3/4-inch SHCS attaching the lid to the package body. This step may also be performed following Step 8.
8. Ensure the upending frame lift arm is positioned with the lift point aligned with the approximate MFFP centerline and that attachment fasteners are snug tight. Using appropriate lifting equipment, rotate the upending frame with attached MFFP and skid to the vertical orientation. Transfer the upending frame to the location of the wall mount fixture and secure in place.
9. Rotate or remove the upending frame lift arm from the lifting position to the unloading (vertical) position.
10. Remove the twenty-four (24), 3/4-inch SHCS loosened in Step 7. If necessary, three (3) 1/2-inch-13 x 2 inch bolts may be utilized in the three equally-spaced holes marked "for lid handling only" to assist in breaking the seal of the closure lid.
11. Install three (3) swivel hoist rings with 1/2-inch-13 threads and rated load of at least 170 lb_f. into the three (3) equally spaced threaded holes labeled "For Lid Handling Only". Carefully remove the closure lid with the appropriate lifting equipment.
12. Store the closure lid in a manner such that potential damage to the O-ring seals and sealing surfaces is minimized.

7.1.1.3 Removal of the Strongback from the MFFP

7.1.1.3.1 Horizontal Operations

1. Install the sealing surface protector on the MFFP seal flange.

   NOTE: The sealing surface protector orientation is labeled along the edge. Correct orientation is required for correct interfacing with the insertion/extraction station.
2. Align the MFFP body and connect to the insertion/extraction station.
3. Insert the attachment bar of the insertion/extraction station into the center hole on the top plate of the strongback.
4. Remove the three (3) 1/2-inch SHCS that secure the strongback to the body.
5. Remove the strongback from the body using the insertion/extraction station. Care shall be taken to not damage the MFFP containment sealing surfaces.
6. Disconnect the MFFP body from the insertion/extraction station and move the MFFP body away from the insertion/extraction station.
7. Visually inspect the following components for wear or damage that could impair their function and, if necessary, replace or repair per the requirements of the drawings in Appendix 1.4.2, *Packaging General Arrangement Drawings*.

   a. Strongback

b. Fuel control structures (FCSs)
c. Neutron absorber plates on strongback and FCSs

8. Ensure the strongback restraint arms on the insertion/extraction station are closed and latched.
9. Use the insertion/extraction station to upend the strongback.
10. Lower the strongback and disconnect the insertion/extraction attachment bar from the strongback. Install the strongback lift tool into the center hole on the top plate of the strongback.
11. Connect appropriate lifting equipment to the strongback lift tool, unlatch the strongback restraint arms and swing into their full-open position. Lift and transport the strongback to the load/unload station.

7.1.1.3.2 Vertical Operations

1. Install the sealing surface protector on the MFFP seal flange.
2. Remove the three (3) 1/2-inch SHCS that secure the strongback to the body.
3. Attach the strongback lift tool to the center hole in the top plate assembly of the strongback.
4. Connect appropriate lifting equipment to the strongback lift tool. Lift and transport the strongback to the load/unload station.
5. Visually inspect the following components for wear or damage that could impair their function and, if necessary, replace or repair per the requirements of the drawings in Appendix 1.4.2, *Packaging General Arrangement Drawings*.

   a. Strongback
   b. Fuel control structures (FCSs)
   c. Neutron absorber plates on strongback and FCSs

7.1.2 Loading of Contents

7.1.2.1 Loading of Fuel Assemblies into Strongback

1. Close and latch the side restraints on the load/unload station and remove the strongback lift tool.
2. Remove the three (3) 3/8-inch SHCS attaching the BPRA restraint weldment to the top plate and remove the BPRA restraint weldment. Remove the three (3) 1/2-inch and three (3) 3/4-inch SHCS attaching the top plate to the strongback. Connect the top plate lifting assembly to the top plate. Lift the top plate clear of the strongback and place in a secure area.
3. Rotate the load/unload station top restraint into position and engage the strongback with the restraint pin.
4. Unlatch the load/unload station side restraints and swing into their full-open position.
5. Verify that the MOX fuel assemblies (FAs) to be loaded meet the payload requirements and limitations of the MFFP license.

6. Unlatch the eight (8) strongback clamp arms and the seven (7) fuel control structures (FCSs) for one of the strongback FA carrier sections by removing the appropriate quick-release pins and rotate each into the full-open position.
7. Ensure that the two fixed clamp pads on the bottom end plate are in their full open positions.
8. Utilizing appropriate lifting equipment, carefully place the FA, still vertically oriented, into the open section of the strongback.
9. Close each of the eight (8) clamp arms and the seven (7) FCSs. Secure each clamp arm and FCS in their closed position with the respective quick-release pin.
10. Using a manual or powered socket wrench, rotate the two tensioning SHCS located at each clamp arm and the bottom end plate clockwise to apply the clamping force to the FA grids. Once all control arms and FCSs are secured, disconnect and remove the lifting equipment from the FA.
11. Rotate the strongback approximately 120 degrees so that the next empty FA section in the strongback is accessible for loading.
12. Repeat Steps 6 through 11 for the second and third FAs (or dummy FAs), as necessary.
13. After the strongback is fully loaded with FAs, close and latch the load/unload station side restraints, and remove the load/unload station top restraint. Ensure the clamp pads on the top plate are fully retracted, and install the top end plate assembly.
14. Install the three (3) outer 3/4-inch SHCS that secure the top plate to the strongback. Tighten to 80 – 90 lb_f-ft torque, lubricated.
15. Install the three (3) inner 1/2-inch SHCS that secure the top plate to the strongback. Tighten to 23 – 27 lb_f-ft torque, lubricated.
16. Install the three (3) 3/8-inch SHCS that secure the BPRA restraint weldment to the strongback. Tighten to 23 – 27 lb_f-ft torque, lubricated.
17. Using a manual or powered socket wrench, rotate the two adjustment screws located at each top plate clamp pad clockwise to apply the clamping force to the FA top nozzle.
18. Tighten the four (4) 3/4-inch swivel clamp pads on the top plate until the screw pad contacts the FA top nozzle. Lock each swivel clamp pad in place with a hex nut.
19. Repeat Step 18 for the second and third FAs (or dummy FAs).

7.1.2.2 Loading of the Strongback into the MFFP

7.1.2.2.1 Horizontal Operations

1. Install the strongback lift tool into the receptacle in the center of the top plate of the strongback and connect appropriate lifting equipment. Unlatch the load/unload station side restraints and swing into their full-open position.
2. Lift and transport the strongback from the load/unload station to the insertion/extraction station. Place the strongback on the insertion/extraction station.

   CAUTION: The strongback must be properly oriented for the insertion operation before the strongback is placed on the insertion/extraction station.

3. Close and latch the strongback restraint arms on the insertion/extraction station. Disconnect from the lifting equipment and remove the strongback lift tool.
4. Connect the insertion/extraction attachment bar by engaging the receptacle in the center of the top plate and raise the strongback.
5. Deleted.
6. Use the insertion/extraction station to lower the strongback to a horizontal orientation.
7. Ensure that the MFFP interior is free of debris and/or damage that could prevent proper loading of the strongback.
8. If not already in position, install the sealing surface protector on the MFFP seal flange.

   NOTE: The sealing surface protector orientation is labeled along the edge. Correct orientation is required for correct interfacing with the insertion/extraction station.
9. Move and align the MFFP with the package connection collar on the insertion/extraction station.

   NOTE: Ensure that the azimuth orientation of the strongback and the lugs integral to the MFFP body are correctly aligned so that strongback insertion can be accomplished without interference.
10. Insert the strongback into the MFFP using the insertion/extraction station. Care shall be taken not to damage the MFFP containment seal surfaces.
11. Install the three (3) 1/2-inch SHCS that secure the strongback to the body. Tighten to 70 – 75 lb_f-ft torque, lubricated.
12. Disconnect the insertion/extraction station from the strongback.
13. Disconnect and move the MFFP body away from the insertion/extraction station.
14. Remove the sealing surface protector from the MFFP seal flange.

7.1.2.2.2 Vertical Operations

1. Install the strongback lift tool into the receptacle in the center of the top plate of the strongback and connect appropriate lifting equipment. Unlatch the load/unload station side restraints and swing into their full-open position.
2. Ensure that the MFFP interior is free of debris and/or damage that could prevent proper loading of the strongback.
3. Lift and transport the strongback from the load/unload station and lower into the MFFP. Care shall be taken not to damage the MFFP containment seal surfaces.

   NOTE: Ensure that the azimuth orientation of the strongback and the lugs integral to the MFFP body are correctly aligned so that strongback insertion can be accomplished without interference and be removed later using the insertion/extraction station, if desired.
4. Install the three (3) 1/2-inch SHCS that secure the strongback to the body. Tighten to 70 – 75 lbf-ft torque, lubricated.
5. Disconnect and remove the strongback lift tool from the strongback.

6. Remove the sealing surface protector from the MFFP seal flange.

7.1.2.3 Closure Lid Installation

7.1.2.3.1 Horizontal Operations

1. Visually inspect the following components for wear or damage that could impair their function and, if necessary, replace or repair per the requirements of the drawings in Appendix 1.4.2, *Packaging General Arrangement Drawings*.
   a. Vent port plug and accompanying O-ring seal
   b. Seal test port plug and accompanying O-ring seal
   c. Fill port plug and accompanying O-ring seal
   d. Closure lid bolts
   e. Impact limiters
   f. Impact limiter SHCS
2. Visually inspect the closure lid O-ring seals. If necessary, remove the O-ring seal(s) and clean the seal(s) and the sealing surface(s) on the closure lid and body to remove contamination. If, during the visual examination, it is determined that damage to the O-ring seal(s) and/or sealing surface(s) is sufficient to impair containment integrity, replace the damaged seal(s) and/or repair the damaged sealing surface(s) per Section 8.2.3.2.1, *Seal Area Routine Inspection and Repair*.
3. As an option, sparingly apply vacuum grease to the O-ring seals and install into the appropriate O-ring seal grooves in the closure lid, the vent port plug, the seal test port plug, and the fill port plug.
4. If the closure lid was removed from the lid handling fixture following removal from the package, secure the lid handling fixture to the closure lid utilizing four (4) 1/2-inch hex bolts. Tighten the hex bolts to snug tight condition. Ensure the vent port is open by loosening the vent port plug.
5. Install the closure lid on the MFFP body. Care shall be taken not to damage the sealing surfaces.
6. Remove the four (4) 1/2-inch hex bolts and the lid handling fixture. Ensure the lid remains in place on the body.
7. Install the twenty-four (24) 3/4-inch SHCS. Using a crossing pattern, tighten the SHCS to 175 – 220 lb_f-ft torque, lubricated.
8. Tighten the vent port, seal test port, and fill port plugs to 8 – 10 lb_f-ft torque.
9. Leakage rate test the vent port and closure lid containment O-ring seal in accordance with Section 7.4, *Preshipment Leakage Rate Test*.
10. Carefully lift and install the lid end impact limiter on the MFFP.
11. Install the six (6), 1-inch SHCS and tighten to 180 – 220 lb_f-ft torque, lubricated.
12. If not previously installed, install the bottom end impact limiter on the MFFP per Steps 10 and 11.
13. If previously installed, inspect the bottom end impact limiter to verify it is properly installed.
14. Install the tamper-indicating device on the appropriate lid end impact limiter bolts.

7.1.2.3.2 Vertical Operations

1. Visually inspect the following components for wear or damage that could impair their function and, if necessary, replace or repair per the requirements of the drawings in Appendix 1.4.2, *Packaging General Arrangement Drawings.*
   a. Vent port plug and accompanying O-ring seal
   b. Seal test port plug and accompanying O-ring seal
   c. Fill port plug and accompanying O-ring seal
   d. Closure lid bolts
   e. Impact limiters
   f. Impact limiter SHCS
2. Visually inspect the closure lid O-ring seals. If necessary, remove the O-ring seal(s) and clean the seal(s) and the sealing surface(s) on the closure lid and body to remove contamination. If, during the visual examination, it is determined that damage to the O-ring seal(s) and/or sealing surface(s) is sufficient to impair containment integrity, replace the damaged seal(s) and/or repair the damaged sealing surface(s) per Section 8.2.3.2.1, *Seal Area Routine Inspection and Repair.*
3. As an option, sparingly apply vacuum grease to the O-ring seals and install into the appropriate O-ring seal grooves in the closure lid, the vent port plug, the seal test port plug, and the fill port plug.
4. If not already installed, install three (3) swivel hoist rings with 1/2 inch-13 threads and rated load of at least 170 lb_f into the three (3) equally spaced threaded holes labeled "For Lid Handling Only". Ensure the vent port is open by loosening the vent port plug.
5. Install the closure lid on the MFFP body. Care shall be taken not to damage the sealing surfaces.

   NOTE: Ensure the lid is installed in the correct orientation, allowing the lid to be removed later in a horizontal orientation, if desired.
6. Remove the lifting equipment and three (3) swivel hoist rings.
7. Install the twenty-four (24), 3/4-inch SHCS. Using a crossing pattern, tighten the SHCS to 175 – 220 lb_f-ft torque, lubricated.
8. Tighten the vent port, seal test port, and fill port plugs to 8 – 10 lb_f-ft torque.
9. Leakage rate test the vent port and closure lid containment O-ring seal in accordance with Section 7.4, Preshipment Leakage Rate Test.
10. Position the upending fixture lift arm such that the lifting point is over the center of the MFFP.
11. Attach the appropriate lifting equipment to the upending frame and disconnect the upending frame from the wall mount fixture.
12. Lift and move the upending frame with the MFFP to a position appropriate for transitioning to the horizontal orientation.
13. Transition the upending frame with attached MFFP to the horizontal orientation.
14. Carefully lift and install the lid end impact limiter on the MFFP.

15. Install the six (6), 1-inch SHCS and tighten to 180 – 220 lb_f-ft torque, lubricated.
16. Inspect the bottom end impact limiter to verify it is properly installed.
17. Install the tamper-indicating device on the appropriate lid end impact limiter bolts.

7.1.3 Preparation for Transport (Loaded)

1. Using an air pallet or other lifting equipment, load the MFFP/shipping skid into the transport conveyance.
2. Remove the air pallet or other lifting equipment.
3. Install the tie-down devices to the shipping skid and the transport conveyance to secure the MFFP.
4. Install a one-inch cap screw and nut into each impact limiter lifting hole (4X).
5. Set the shock indicators affixed to the package shell, if required.
6. Monitor external radiation for each loaded MFFP per the guidelines of 49 CFR §173.441[1].
7. Determine that surface contamination levels for each loaded MFFP is per the guidelines of 49 CFR §173.443.
8. Determine the transport index for each loaded MFFP per the guidelines of 49 CFR §173.403.
9. Complete all necessary shipping papers in accordance with Subpart C of 49 CFR 172[2].
10. MFFP marking shall be in accordance with 10 CFR §71.85(c)[3] and Subpart D of 49 CFR 172. Package labeling shall be in accordance with Subpart E of 49 CFR 172. Package placarding shall be in accordance with Subpart F of 49 CFR 172.

---

[1] Title 49, Code of Federal Regulations, Part 173 (49 CFR 173), *Shippers–General Requirements for Shipments and Packagings*, Final Rule, 01-26-04.

[2] Title 49, Code of Federal Regulations, Part 172 (49 CFR 172), *Hazardous Materials Tables and Hazardous Communications Regulations*, Final Rule, 01-26-04.

[3] Title 10, Code of Federal Regulations, Part 71 (10 CFR 71), *Packaging and Transportation of Radioactive Material*, Final Rule, 01-26-04.

This page left intentionally blank.

7.2 Package Unloading

This section delineates the procedures for unloading a strongback from the MFFP. Hereafter, reference to specific MFFP components may be found in Appendix 1.4.2, *Packaging General Arrangement Drawings*. Note that the steps provided in the following sections may be performed in any logical sequence.

The unloading operation shall be performed in a dry environment. If precipitation enters the cavity, the free-standing water shall be removed prior to installing the closure lid.

7.2.1 Receipt of Package from Carrier

Prior to performing any unloading operations, the external surfaces of the MFFP shall be surveyed for potential radioactive contamination per the requirements of 10 CFR §20.1906[1]. In addition, inspect the tamper-indicating device on the lid end impact limiter bolts to verify that no unauthorized opening of the MFFP has occurred, and record the condition of the shock indicators.

7.2.2 Removal of Contents

7.2.2.1 Removal of MFFP from the Transport Conveyance

1. Disengage the tie-down devices from the shipping skid and the transport conveyance.

   CAUTION: Failure to disengage the tie-down devices may result in damage to the packaging, shipping skid, and/or the transport conveyance.

2. Using an air pallet or other lifting equipment, remove the MFFP/shipping skid from the transport conveyance and move to the loading area.
3. Remove the air pallet or other lifting equipment.

7.2.2.2 Removal of the Closure Lid

7.2.2.2.1 Horizontal Operations

1. Remove the tamper indicating device located between two of the lid end impact limiter bolts.
2. Remove the six (6) 1-inch socket head cap screws (SHCS) from the lid end impact limiter.
3. Utilizing appropriate lifting equipment, carefully lift and remove the lid end impact limiter and place in a secure area.
4. If necessary, repeat Steps 2 and 3 for the bottom end impact limiter.
5. Vent the interior of the MFFP through the lid end vent plug.
6. Loosen and / or remove the twenty-four (24), 3/4-inch SHCS attaching the lid to the package body. Ensure the lid remains in place on the body.

---

[1] Title 10, Code of Federal Regulations, Part 20 (10 CFR 20), *Standards for Protection of Radiation*, 01-01-03 Edition.

7. Utilizing four (4) 1/2-inch hex bolts, secure the lid handling fixture to the closure lid. Tighten the hex bolts to snug tight condition. Ensure any of the lid attachment fasteners that are covered by the lid handling fixture are removed prior to installing the lid handling fixture.
8. Connect appropriate lifting equipment to the lid handling fixture.
9. Remove any of the twenty-four (24), 3/4-inch SHCS not already removed in Steps 6 or 7 and carefully remove the closure lid with the lifting equipment and lid handling fixture. If necessary, the three T-handle assemblies on the lid handling fixture or three (3) 1/2-inch-13 x 2-inch bolts may be utilized in the three equally-spaced holes marked "for lid handling only" to assist in breaking the seal of the closure lid. Care shall be taken to not damage the MFFP containment seal surfaces.
10. Store the closure lid in a manner such that potential damage to the O-ring seals and sealing surfaces is minimized.

7.2.2.2.2 Vertical Operations

1. Remove the tamper indicating device located between two of the lid end impact limiter bolts.
2. Attach the handling lift equipment, using the shackles on the support skid, in preparation for lifting the MFFP. Ensure the handling lift equipment "Lid End" is oriented toward the lid end of the MFFP.
3. Lift and place the MFFP with attached transport skid into the upending frame.
4. Secure the MFFP to the upending frame with both the ball lock pins and the tie-down straps.
5. Remove the six (6) 1-inch socket head cap screws (SHCS) from the lid end impact limiter.
6. Utilizing appropriate lifting equipment, carefully lift and remove the lid end impact limiter and place in a secure area. Optionally, the impact limiter may be removed prior to loading the MFFP into the upending frame (Step 3).
7. Vent the interior of the MFFP through the lid end vent plug.
8. Loosen the twenty-four (24), 3/4-inch SHCS securing the closure lid. This step may also be performed following Step 10.
9. Ensure the upending frame lift arm is positioned with the lift point aligned with the approximate MFFP centerline and that attachment fasteners are snug tight. Using appropriate lifting equipment, rotate the upending frame with attached MFFP and skid to the vertical orientation. Transfer the upending frame to the location of the wall mount fixture and secure in place.
10. Rotate or remove the upending frame lift arm from the lifting position to the unloading position.
11. Remove the twenty-four (24), 3/4-inch SHCS loosened in Step 8. If necessary, three (3) 1/2-inch-13 x 2-inch bolts may be utilized in the three equally-spaced holes marked "for lid handling only" to assist in breaking the seal of the closure lid.
12. Install three (3) swivel hoist rings with 1/2-inch-13 threads and rated load of at least 170 lb_f into the three (3) equally spaced threaded holes labeled "For Lid Handling Only". Carefully remove the closure lid with the appropriate lifting equipment.

13. Store the closure lid in a manner such that potential damage to the O-ring seals and sealing surfaces is minimized.

7.2.2.3 Removal of the Strongback from the MFFP

7.2.2.3.1 Horizontal Operations

1. Install the sealing surface protector on the MFFP seal flange.

   NOTE: The sealing surface protector orientation is labeled along the edge. Correct orientation is required for correct interfacing with the insertion/extraction station.

2. Align the MFFP body and connect to the insertion/extraction station.
3. Insert the attachment bar of the insertion/extraction station into the center hole on the top plate of the strongback.
4. Remove the three (3) 1/2-inch SHCS that secure the strongback to the body.
5. Remove the strongback from the body using the insertion/extraction station. Care shall be taken to not damage the MFFP containment sealing surfaces.
6. Disconnect the MFFP body from the insertion/extraction station and move the MFFP body away from the insertion/extraction station.
7. Ensure the strongback restraint arms on the insertion/extraction station are closed and latched.
8. Use the insertion/extraction station to upend the strongback.
9. Lower the strongback and disconnect the insertion/extraction attachment bar from the strongback. Install the strongback lift tool into the center hole on the top plate of the strongback.
10. Connect appropriate lifting equipment to the strongback lift tool, unlatch the strongback restraint arms and swing into their full-open position. Lift and transport the strongback to the load/unload station.

7.2.2.3.2 Vertical Operations

1. Install the sealing surface protector on the MFFP seal flange.
2. Remove the three (3) 1/2-inch SHCS that secure the strongback to the body.
3. Attach the strongback lift tool to the center hole in the top plate assembly of the strongback.
4. Connect appropriate lifting equipment to the strongback lift tool. Lift and transport the strongback to the load/unload station.

7.2.2.4 Unloading of Fuel Assemblies from the Strongback

1. Close and latch the side restraints on the load/unload station and remove the strongback lift tool.

2. Remove the three (3) 3/8-inch SHCS attaching the BPRA restraint weldment to the top plate and remove the BPRA restraint weldment. Remove the three (3) 1/2-inch and three (3) 3/4-inch SHCS attaching the top plate to the strongback. Ensure that the two fixed clamp pads on the top plate are in their full open positions. Connect the top plate lifting assembly to the top plate. Lift the top plate clear of the strongback and place in a secure area.
3. Rotate the load/unload station top restraint into position and engage the strongback with the restraint pin.
4. Unlatch the load/unload station side restraints and swing into their full-open position.
5. Utilizing appropriate lifting equipment, attach the FA lifting equipment to the FA.
6. Using a manual or powered socket wrench, rotate the two adjustment screws located at each clamp arm counterclockwise to release the clamping force on the FA grids.
7. Unlatch the eight (8) strongback clamp arms and the seven (7) fuel control structures (FCSs) for one of the FA carrier sections by removing the appropriate quick-release pin and rotate each into the full-open position.
8. Ensure that the two fixed clamp pads on the bottom end plate are in their full open positions.
9. Utilizing appropriate lifting equipment, carefully remove the FA from the strongback.
10. Close each of the eight (8) clamp arms and the seven (7) FCSs. Secure each clamp arm and FCS in their closed position with the respective quick-release pin.
11. Rotate the strongback approximately 120 degrees so that the next FA is accessible for unloading.
12. Repeat Steps 5 through 11 for the second and third FAs (or dummy FAs, if removed).
13. After the strongback is fully unloaded, close and latch the load/unload station side restraints, and remove the load/unload station top restraint. Install the top plate assembly.
14. Install the three (3) outer 3/4-inch SHCS that secure the top plate to the strongback. Tighten to 80 – 90 lb_f-ft torque, lubricated.
15. Install the three (3) inner 1/2-inch SHCS that secure the top plate to the strongback. Tighten to 23 – 27 lb_f-ft torque, lubricated.
16. Install the three (3) 3/8-inch SHCS that secure the BPRA restraint weldment to the strongback. Tighten to 23 – 27 lb_f-ft torque, lubricated.

7.2.2.5 Loading of the Empty Strongback into the MFFP

7.2.2.5.1 Horizontal Operations

1. Install the strongback lift tool into the receptacle in the center of the top plate of the strongback and connect appropriate lifting equipment. Unlatch the load/unload station side restraints and swing into their full-open position.
2. Lift and transport the strongback from the load/unload station to the insertion/extraction station. Place the strongback on the insertion/extraction station.

CAUTION: The strongback must be properly oriented for the insertion operation before the strongback is placed on the insertion/extraction station.

3. Close and latch the strongback restraint arms on the insertion/extraction station. Disconnect from the lifting equipment and remove the strongback lift tool.
4. Connect the insertion/extraction attachment bar by engaging the receptacle in the center of the top plate and raise the strongback.
5. Deleted.
6. Use the insertion/extraction station to lower the strongback to a horizontal orientation.
7. Ensure that the MFFP interior is free of debris and/or damage that could prevent proper loading of the strongback.
8. If not already in position, install the sealing surface protector on the MFFP seal flange.

   NOTE: The sealing surface protector orientation is labeled along the edge. Correct orientation is required for correct interfacing with the insertion/extraction station.
9. Align the MFFP body and connect to the insertion/extraction station.

   NOTE: Ensure that the azimuth orientation of the strongback and the lugs integral to the MFFP body are correctly aligned so that strongback insertion can be accomplished without interference.
10. Insert the strongback into the MFFP using the insertion/extraction station. Care shall be taken to not damage the MFFP containment seal surfaces.
11. Install the three (3) 1/2-inch SHCS that secure the strongback to the body. Tighten to 70 – 75 lb_f-ft torque, lubricated.
12. Disconnect the insertion/extraction station from the strongback.
13. Disconnect and move the MFFP body away from the insertion/extraction station.
14. Remove the sealing surface protector from the MFFP seal flange.

7.2.2.5.2 Vertical Operations

1. Install the strongback lift tool into the receptacle in the center of the top plate of the strongback and connect appropriate lifting equipment. Unlatch the load/unload station side restraints and swing into their full-open position.
2. Ensure that the MFFP interior is free of debris and/or damage that could prevent proper loading of the strongback.
3. Install the sealing surface protector on the MFFP seal flange.
4. Lift and transport the strongback from the load/unload station and lower into the MFFP.

   NOTE: Ensure that the azimuth orientation of the strongback and the lugs integral to the MFFP body are correctly aligned so that strongback insertion can be accomplished without interference and be removed later using the insertion/extraction station, if desired.
5. Install the three (3) 1/2-inch SHCS that secure the strongback to the body. Tighten to 70 – 75 lb_f-ft torque, lubricated.

6. Disconnect from the lifting equipment and remove the strongback lift tool.
7. Remove the sealing surface protector from the MFFP seal flange.

7.2.2.6 Closure Lid Installation

7.2.2.6.1 Horizontal Operations

1. Visually inspect the following components for wear or damage that could impair their function and, if necessary, replace or repair per the requirements of the drawings in Appendix 1.4.2, *Packaging General Arrangement Drawings*.
   a. Vent port plug and accompanying O-ring seal
   b. Seal test port plug and accompanying O-ring seal
   c. Fill port plug and accompanying O-ring seal
   d. Closure lid bolts
   e. Impact limiters
   f. Impact limiters SHCS
2. Visually inspect the closure lid O-ring seals. If necessary, remove the O-ring seal(s) and clean the seal(s) and the sealing surface(s) on the closure lid and body to remove contamination. If, during the visual examination, it is determined that damage to the O-ring seal(s) and/or sealing surface(s) is sufficient to impair containment integrity, replace the damaged seal(s) and/or repair the damaged sealing surface(s) per Section 8.2.3.2.1, *Seal Area Routine Inspection and Repair*.
3. As an option, sparingly apply vacuum grease to the O-ring seals and install into the appropriate O-ring seal grooves in the closure lid, the vent port plug, the seal test port plug, and the fill port plug.
4. If the closure lid was removed from the lid handling fixture following removal, secure the lid handling fixture to the closure lid utilizing four (4) 1/2 hex bolts. Tighten the hex bolts to snug tight condition. Ensure the vent port is open by loosening the vent port plug.
5. Install the closure lid on the MFFP body. Care shall be taken to not damage the sealing surfaces.
6. Remove the four (4) 1/2-inch hex bolts and the lid handling fixture. Ensure the lid remains in place on the body.
7. Install the twenty-four (24), 3/4-inch SHCS. Using a crossing pattern, tighten the SHCS to 175 – 220 lb_f-ft torque, lubricated.
8. Tighten the vent port, seal test port, and fill port plugs to 8 – 10 lb_f-ft torque.
9. Carefully lift and install the lid end impact limiter on the MFFP.
10. Install the six (6), 1-inch SHCS and tighten to 180 – 220 lb_f-ft torque, lubricated.
11. If not previously installed, install the bottom end impact limiter on the MFFP per Steps 9 and 10.
12. If previously installed, inspect the bottom end impact limiter to verify it is properly installed.

7.2.2.6.2 Vertical Operations

1. Visually inspect the following components for wear or damage that could impair their function and, if necessary, replace or repair per the requirements of the drawings in Appendix 1.4.2, *Packaging General Arrangement Drawings*.
   a. Vent port plug and accompanying O-ring seal
   b. Seal test port plug and accompanying O-ring seal
   c. Fill port plug and accompanying O-ring seal
   d. Closure lid bolts
   e. Impact limiters
   f. Impact limiters SHCS
2. Visually inspect the closure lid O-ring seals. If necessary, remove the O-ring seal(s) and clean the seal(s) and the sealing surface(s) on the closure lid and body to remove contamination. If, during the visual examination, it is determined that damage to the O-ring seal(s) and/or sealing surface(s) is sufficient to impair containment integrity, replace the damaged seal(s) and/or repair the damaged sealing surface(s) per Section 8.2.3.2.1, *Seal Area Routine Inspection and Repair*.
3. As an option, sparingly apply vacuum grease to the O-ring seals and install into the appropriate O-ring seal grooves in the closure lid, the vent port plug, the seal test port plug, and the fill port plug.
4. If not already installed, install three (3) swivel hoist rings with 1/2 inch-13 threads and rated load of at least 170 lb_f into the three (3) equally spaced threaded holes labeled "For Lid Handling Only". Ensure the vent port is open by loosening the vent port plug.
5. Using appropriate lifting equipment, lift and install the closure lid on the MFFP body. Care shall be taken to not damage the sealing surfaces.

   NOTE: Ensure the lid is installed in the correct orientation, allowing the lid to be removed later in a horizontal orientation, if desired.
6. Remove the lifting equipment and three (3) swivel hoist rings.
7. Install the twenty-four (24), 3/4-inch SHCS. Using a crossing pattern, tighten the SHCS to 175 – 220 lb_f-ft torque, lubricated .
8. Tighten the vent port, seal test port, and fill port plugs to 8 – 10 lb_f-ft torque.
9. Position the upending fixture lift arm such that the lifting point is over the center of the MFFP.
10. Attach the appropriate lifting equipment to the upending frame and disconnect the upending frame from the wall mount fixture.
11. Lift and move the upending frame with the MFFP to a position appropriate for transitioning to the horizontal orientation.
12. Transition the upending frame with attached MFFP to the horizontal orientation.
13. Carefully lift and install the lid end impact limiter on the MFFP.
14. Install the six (6), 1-inch SHCS and tighten to 180 – 220 lb_f-ft torque, lubricated .

15. Inspect the bottom end impact limiter to verify it is properly installed.

7.2.2.7 Final Package Preparations for Transport (Unloaded)

1. Using an air pallet or other lifting equipment, load the MFFP into the transport conveyance.
2. Remove the air pallet or other lifting equipment.
3. Install the tie-down devices to the shipping skid and the transport conveyance to secure the MFFP.
4. Install a one-inch cap screw and nut into each impact limiter lifting hole (4X).
5. Transport the MFFP in accordance with Section 7.3, *Preparation of an Empty Package for Transport.*

7.3 Preparation of an Empty Package for Transport

Previously used and empty MFFPs shall be prepared and transported per the requirements of 49 CFR §173.428[1].

[1] Title 49, Code of Federal Regulations, Part 173 (49 CFR 173), *Shippers–General Requirements for Shipments and Packagings*, Final Rule, 01-26-04.

This page left intentionally blank.

7.4 Preshipment Leakage Rate Test

After the MFFP is assembled and prior to shipment, leakage rate testing shall be performed to confirm proper assembly of the package following the guidelines of Section 7.6, *Preshipment Leakage Rate Test*, and Appendix A.5.2, *Gas Pressure Rise*, of ANSI N14.5[1].

7.4.1 Gas Pressure Rise Leakage Rate Test Acceptance Criteria

In order to demonstrate containment integrity in preparation for shipment, no leakage shall be detected when tested to a sensitivity of 1×10^{-3} reference cubic centimeters per second (scc/sec) air, or less, per Section 7.6, *Preshipment Leakage Rate Test*, of ANSI N14.5.

7.4.2 Determining the Test Volume and Test Time

1. Assemble a leakage rate test apparatus that consists of, at a minimum, the components illustrated in Figure 7.4-1, using a calibrated volume with a range of 100 – 500 cubic centimeters, and a calibrated pressure transducer with a minimum sensitivity of 100 millitorr. Connect the test apparatus to the test volume (i.e., the seal test port, or the vent port, as appropriate).
2. Set the indicated sensitivity on the digital readout of the calibrated pressure transducer, ΔP, to, at a minimum, the resolution (i.e., sensitivity) of the calibrated pressure transducer (e.g., ΔP = 1, 10, or 100 millitorr sensitivity).
3. Open all valves (i.e., the vent valve, calibration valve, and vacuum pump isolation valve), and record ambient atmospheric pressure, P_{atm}.
4. Isolate the calibrated volume by closing the vent and calibration valves.
5. Evacuate the test volume to a pressure less than the indicated sensitivity on the digital readout of the calibrated pressure transducer or 0.76 torr, whichever is less.
6. Isolate the vacuum pump from the test volume by closing the vacuum pump isolation valve. Allow the test volume pressure to stabilize and record the test volume pressure, P_{test} (e.g., $P_{test} < 1$ millitorr for an indicated sensitivity of 1 millitorr).
7. Open the calibration valve and, after allowing the system to stabilize, record the total volume pressure, P_{total}.
8. Knowing the calibrated volume, V_c, calculate and record the test volume, V_t, using the following equation:

$$V_t = V_c\left(\frac{P_{atm} - P_{total}}{P_{total} - P_{test}}\right)$$

9. Knowing the indicated sensitivity on the digital readout of the calibrated pressure transducer, ΔP, calculate and record the test time, t, using the following equation (based on Equation B.14 of ANSI N14.5-1997):

$$t = \Delta P(1.32)V_t$$

[1] ANSI N14.5-1997, *American National Standard for Radioactive Materials - Leakage Tests on Packages for Shipment,* American National Standards Institute, Inc. (ANSI).

7.4.3 Performing the Gas Pressure Rise Leakage Rate Test

1. Isolate the calibrated volume by closing the calibration valve.
2. Open the vacuum pump isolation valve and evacuate the test volume to a pressure less than the test volume pressure, P_{test}, determined in Step 6 of Section 7.4.2, *Determining the Test Volume and Test Time*.
3. Isolate the vacuum pump from the test volume by closing the vacuum pump isolation valve. Allow the test volume pressure to stabilize and record the beginning test pressure, P_1. After a period of time equal to "t" seconds, determined in Step 9 of Section 7.4.2, *Determining the Test Volume and Test Time*, record the ending test pressure, P_2. To be acceptable, there shall be no difference between the final and initial pressures such that the requirements of Section 7.4.1, *Gas Pressure Rise Leakage Rate Test Acceptance Criteria*, are met.
4. If, after repeated attempts, the O-ring seal fails to pass the leakage rate test, replace the damaged seal and/or repair the damaged sealing surfaces per Section 8.2.3.2.1, *Sealing Area Routine Inspection and Repair*. Perform verification leakage rate test per the applicable procedure delineated in Section 8.2.2, *Maintenance/Periodic Leakage Rate Tests*.

7.4.4 Optional Preshipment Leakage Rate

As an option to Section 7.4.3, *Performing the Gas Pressure Rise Leakage Rate Test*, Section 8.2.2, *Maintenance/Periodic Leakage Rate Tests*, may be performed.

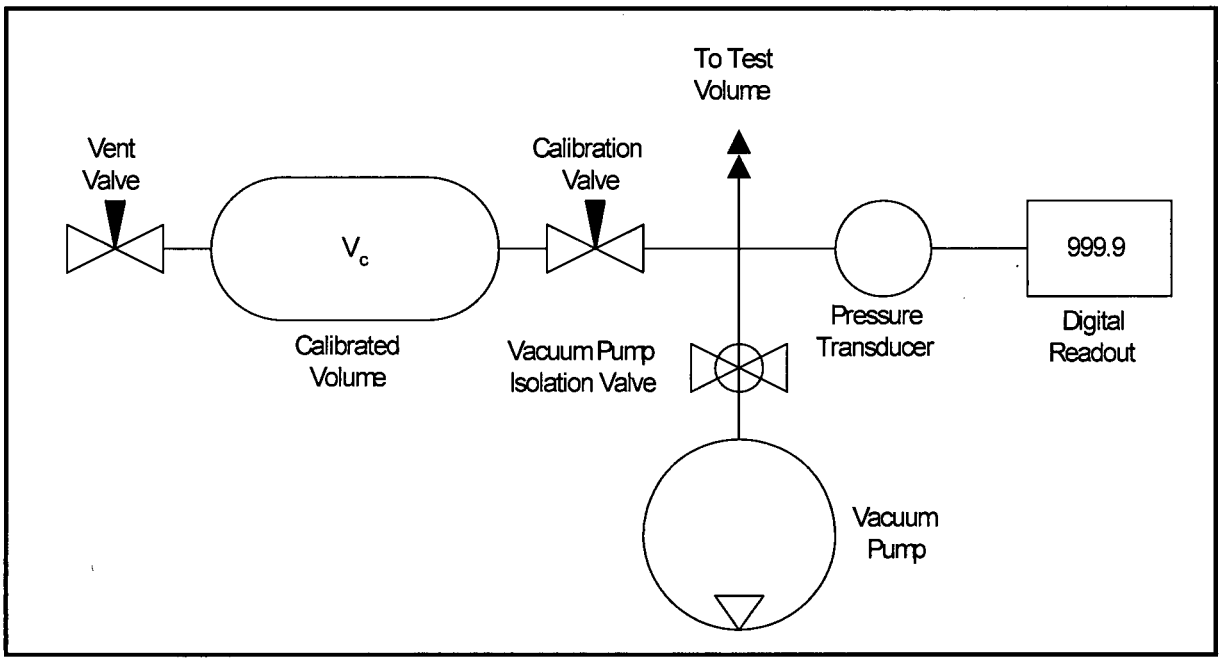

Figure 7.4-1 – Pressure Rise Leakage Rate Test Schematic

8.0 ACCEPTANCE TESTS AND MAINTENANCE PROGRAM

8.1 Acceptance Tests

Per the requirements of 10 CFR §71.85[1], this section discusses the inspections and tests to be performed prior to first use of the MFFP.

8.1.1 Visual Inspection and Measurements

All MFFP materials of construction and welds shall be examined in accordance with requirements delineated on the drawings in Appendix 1.4.2, *Packaging General Arrangement Drawings*, per the requirements of 10 CFR §71.85(a). Furthermore, the inspections of Section 8.2.3.2, *Seal Areas and Grooves*, shall be performed prior to pressure and leakage rate testing.

8.1.2 Weld Examinations

All welds are inspected per the requirements delineated on the drawings in Appendix 1.4.2, *Packaging General Arrangement Drawings*.

8.1.3 Structural and Pressure Tests

8.1.3.1 Lifting Device Load Testing

The MFFP does not contain any lifting devices requiring load testing.

8.1.3.2 Pressure Testing

Per the requirements of 10 CFR §71.85(b), the MFFP containment boundary shall be pressure tested to 150% of the maximum normal operating pressure (MNOP) to verify structural integrity. The MNOP of the MFFP is 10 psig. Thus, the MFFP containment vessel shall be pressure tested to $10 \times 1.5 = 15$ psig minimum.

Following pressure testing of the containment boundary, accessible base material and welds directly related to the pressure testing of the containment vessel shall be visually inspected for plastic deformation or cracking in accordance with AWS D.1.6[2], and liquid penetrant inspected per ASME Boiler and Pressure Vessel Code, Section V[3], Article 6, and ASME Boiler and Pressure Vessel Code, Section III[4], Division 1, Subsection NB, Article NB-5000, as delineated on the drawings in Appendix 1.4.2, *Packaging General Arrangement Drawings*. Indications of

---

[1] Title 10, Code of Federal Regulations, Part 71 (10 CFR 71), *Packaging and Transportation of Radioactive Material*, Final Rule, 01-26-04.

[2] ANSI/AWS D1.6:1999, *Structural Welding Code – Stainless Steel*, American Welding Society (AWS).

[3] American Society of Mechanical Engineers (ASME) Boiler and Pressure Vessel Code, Section V, *Nondestructive Examination*, 2001 Edition, 2002 and 2003 Addenda.

[4] American Society of Mechanical Engineers (ASME) Boiler and Pressure Vessel Code, Section III, *Rules for Construction of Nuclear Power Plant Components*, 2001 Edition, 2002 and 2003 Addenda.

cracking or distortion shall be recorded on a nonconformance report and dispositioned prior to final acceptance in accordance with the cognizant quality assurance program.

Leak testing per Section 8.1.4, *Fabrication Leakage Rate Tests*, shall be performed after completion of pressure testing to verify package configuration and performance to design criteria.

8.1.4 Fabrication Leakage Rate Tests

This section provides the generalized procedure for fabrication leakage rate testing of the containment vessel boundaries and penetrations following the completion of fabrication. Fabrication leakage rate testing shall follow the guidelines of Section 7.3, *Fabrication Leakage Rate Test*, of ANSI N14.5[5].

Prior to leakage rate testing, internal components that are not permanently affixed to the containment boundary, such as the strongback, shall be removed. For ease of leakage rate testing, the interior surfaces of the containment boundary should be thoroughly cleaned.

Fabrication leakage rate testing shall be performed on the containment boundary. Three separate tests comprise the series. Each test shall meet the acceptance criteria delineated in Section 8.1.4.1, *Fabrication Leakage Rate Test Acceptance Criteria.*

8.1.4.1 Fabrication Leakage Rate Test Acceptance Criteria

1. To be acceptable, each leakage rate test shall demonstrate a "leaktight" leakage rate of 1×10^{-7} reference cubic centimeters per second (scc/s), air, or less, per Section 6.3, *Application of Reference Air Leakage Rate (L_R)*, of ANSI N14.5.
2. In order to demonstrate the leaktight leakage rate, the sensitivity of the leakage rate test procedure shall be 5×10^{-8} cm^3/s, air, or less, per Section 8.4, *Sensitivity*, of ANSI N14.5.

8.1.4.2 Helium Leakage Rate Testing the Containment Structure Integrity

1. The fabrication leakage rate test of the MFFP cask shall be performed following the guidelines of Section A.5.3, *Gas Filled Envelope – Gas Detector*, of ANSI N14.5.
2. Assemble the MFFP with all three O-ring seals installed on the closure lid. Dunnage may be installed in the containment cavity for volume reduction. Assembly is as shown on the MFFP drawings in Appendix 1.4.2, *Packaging General Arrangement Drawings.* Optionally, the MFFP body may be tested using a test lid, and the MFFP closure lid may be tested using a test body. In that case, two separate leakage rate tests are performed.
3. Loosen and remove the vent port plug to allow gas flow from the cavity and install a test port tool.
4. Install a helium mass spectrometer leak detector (MSLD) to the test port tool. Evacuate through the vent port until the vacuum is sufficient to operate the MSLD. Optionally, install the test port tool to the test body or test lid, if used.

---

[5] ANSI N14.5-1997, *American National Standard for Radioactive Materials – Leakage Tests on Packages for Shipment,* American National Standards Institute, Inc. (ANSI).

5. Surround the assembled MFFP with an envelope filled with helium gas of 99% purity or better to a pressure slightly greater than atmospheric pressure.
6. Perform the helium leakage rate test to the requirements of Section 8.1.4.1, *Fabrication Leakage Rate Test Acceptance Criteria.* If, after repeated attempts, the containment structure fails to pass the leakage rate test, isolate the leak path and, prior to repairing the leak path and repeating the leakage rate test, record on a nonconformance report and disposition prior to final acceptance in accordance with the cognizant quality assurance program.
7. Remove the test port tool and re-install the vent port plug. Tighten to 8 – 10 lb_f-ft torque.

8.1.4.3 Helium Leakage Rate Testing the Main O-ring Seal

1. The fabrication leakage rate test of the MFFP containment O-ring seal integrity shall be performed following the guidelines of Section A.5.4, *Evacuated Envelope – Gas Detector*, of ANSI N14.5.
2. Assemble the MFFP with the three O-ring seals installed in the closure lid. Ensure the vent, seal test, and fill ports are installed with their associated O-ring seals. Assembly is as shown on the drawings in Appendix 1.4.2, *Packaging General Arrangement Drawings.*
3. Utilizing a test port tool, attach a vacuum pump and a source of helium gas, in parallel, to the fill port.
4. Close the valve to the source of helium gas and open the valve to the vacuum pump.
5. Utilizing a test port tool, rotate the fill port closure bolt to the open position.
6. Evacuate the system to a 90% vacuum or better (≤ 10% ambient atmospheric pressure). Isolate the vacuum pump from the system.
7. Provide a helium atmosphere inside the evacuated cavity by backfilling with helium gas (99% purity or better) to ambient atmospheric pressure (+1 psi, -0 psi).
8. Utilizing the test port tool, rotate the fill port plug to the closed position, and remove the helium-contaminated test port tool from the fill port.
9. Install a clean (helium-free) test port tool into the seal test port.
10. Utilizing appropriate fittings, attach a helium MSLD to the test port tool.
11. Utilizing the test port tool, rotate the seal test port closure bolt to the open position.
12. Evacuate the cavity above the lid containment O-ring seal until the vacuum is sufficient to operate the leak detector per the manufacturer's recommendations.
13. Perform the helium leakage rate test to the requirements of Section 8.1.4.1, *Fabrication Leakage Rate Test Acceptance Criteria.* If, after repeated attempts, the MFFP containment O-ring seal fails to pass the leak test, isolate the leak path and, prior to repairing the leak path and repeating the leak test, record on a nonconformance report and disposition prior to final acceptance in accordance with the cognizant quality assurance program.

8.1.4.4 Helium Leakage Rate Testing the Vent Port Plug O-ring Seal

1. The fabrication leakage rate test of the MFFP vent port plug O-ring containment seal integrity shall be performed following the guidelines of ANSI N14.5, Section A.5.4, *Evacuated Envelope – Gas Detector.*
2. The MFFP shall be assembled with all three O-ring seals installed on the closure lid. Ensure the vent, seal test, and fill port plugs are installed with their associated O-ring seals. Assembly is as shown on the MFFP drawings in Appendix 1.4.2, *Packaging General Arrangement Drawings.*
3. Verify the presence of a helium atmosphere below the vent port plug O-ring containment seal, as specified above in Steps 3 – 8 of Section 8.1.4.3, *Helium Leakage Rate Testing the Main O-ring Seal.*
4. Install a test port tool into the vent port.
5. Utilizing appropriate fittings, attach a helium MSLD to the test port tool.
6. Evacuate the cavity above the vent port plug O-ring containment seal until the vacuum is sufficient to operate the leak detector per the manufacturer's recommendations.
7. Perform the helium leakage rate test to the requirements of Section 8.1.4.1, *Fabrication Leakage Rate Test Acceptance Criteria.* If, after repeated attempts, the vent port plug O-ring containment seal fails to pass the leak test, isolate the leak path and, prior to repairing the leak path and repeating the leak test, record on a nonconformance report and disposition prior to final acceptance in accordance with the cognizant quality assurance program.

8.1.4.5 Helium Leakage Rate Testing the Fill Port Plug O-ring Seal

1. The fabrication leakage rate test of the MFFP fill port plug O-ring containment seal integrity shall be performed following the guidelines of Section A.5.4, *Evacuated Envelope – Gas Detector*, of ANSI N14.5.
2. The MFFP shall be assembled with all three O-ring seals installed on the closure lid. Ensure the vent, seal test, and fill port plugs are installed with their associated O-ring seals. Assembly is as shown on the MFFP drawings in Appendix 1.4.2, *Packaging General Arrangement Drawings.*
3. Verify the presence of a helium atmosphere below the fill port plug O-ring containment seal, as specified above in Steps 3 – 8 of Section 8.1.4.3, *Helium Leakage Rate Testing the Main O-ring Seal.*
4. Install a test port tool into the fill port.
5. Utilizing appropriate fittings, attach a helium MSLD to the test port tool.
6. Evacuate the cavity above the fill port plug O-ring containment seal until the vacuum is sufficient to operate the leak detector per the manufacturer's recommendations.
7. Perform the helium leakage rate test to the requirements of Section 8.1.4.1, *Fabrication Leakage Rate Test Acceptance Criteria.* If, after repeated attempts, the fill port plug O-ring containment seal fails to pass the leak test, isolate the leak path and, prior to repairing the leak path and repeating the leak test, record on a nonconformance report and disposition prior to final acceptance in accordance with the cognizant quality assurance program.

8.1.5 Component and Material Tests

8.1.5.1 Polyurethane Foam

This section establishes the requirements and acceptance criteria for installation, inspection, and testing of rigid, closed-cell, polyurethane foam utilized within the MFFP.

8.1.5.1.1 Introduction and General Requirements

The polyurethane foam used within the MFFP impact limiters is comprised of a specific "formulation" of foam constituents (i.e., mix of chemical constituents) that defines the foam's physical characteristics such as density, compressive stress, and specific heat. Based on the foam's physical requirements, chemical constituents are combined into batches containing multiple parts (e.g., parts A and B) for easier handling. Therefore, a foam "batch" is defined as mixing into vats a specific foam formulation for each part. Based on the foam's physical requirements, portions from each batch part are combined to produce the liquid foam material for pouring into the component to be foamed. Thus, a foam "pour" is defined as apportioning the batch parts into a desired quantity of liquid foam material for subsequent installation (pouring).

The following sections describe the general requirements for chemical composition, constituent storage, foamed component preparation, foam material installation, and foam pour and test data records.

8.1.5.1.1.1 Polyurethane Foam Chemical Composition

The foam supplier shall certify that the chemical composition of the polyurethane foam is as delineated below, with the chemical component weight percents falling within the specified ranges. In addition, the foam supplier shall certify that the finished (cured) polyurethane foam does not contain halogen-type flame retardants or trichloromonofluoromethane (Freon 11).

Carbon.....50% - 70%	Phosphorus.....≤ 2%
Oxygen.....14% - 34%	Silicon.....< 1%
Nitrogen.....4% - 12%	Chlorides.....< 1%
Hydrogen.....4% - 10%	Other.....< 1%

8.1.5.1.1.2 Polyurethane Foam Constituent Storage

The foam supplier shall certify that the polyurethane foam constituents have been properly stored prior to use, and that the polyurethane foam constituents have been used within their shelf life.

8.1.5.1.1.3 Foamed Component Preparation

Prior to polyurethane foam installation, the foam supplier shall verify that an anti-bond agent, such as automotive wax, has been applied to all of the component shell interior surfaces. In addition, due to the internal pressures generated during the foam pouring/curing process, the foam supplier shall visually verify that adequate bracing/shoring of the component shells is provided to maintain the dimensional configuration throughout the foam pouring/curing process.

8.1.5.1.1.4 Polyurethane Foam Installation

The direction of foam rise shall be vertically aligned with the impact limiter longitudinal axis. The surrounding walls of the component shell where the liquid foam material is to be installed shall be between 55 °F and 95 °F prior to foam installation. Measure and record the component shell temperature to an accuracy of ±2 °F prior to foam installation.

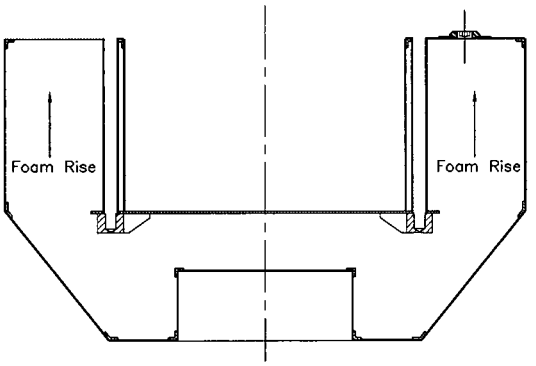

In the case of multiple pours into a single foamed component, the cured level of each pour shall be measured and recorded to an accuracy of ±1 inch.

Measure and record the weight of liquid foam material installed during each pour to an accuracy of ±10 pounds.

All test samples shall be poured into disposable containers at the same time as the actual pour it represents, clearly marking the test sample container with the pour date and a unique pour identification number. All test samples shall be cut from a larger block to obtain freshly cut faces. Prior to physical testing, each test sample shall be cleaned of superfluous foam dust.

8.1.5.1.1.5 Polyurethane Foam Pour and Test Data Records

A production pour and testing record shall be compiled by the foam supplier during the foam pouring operation and subsequent physical testing. Upon completion of production and testing, the foam supplier shall issue certification referencing the production record data and test data pertaining to each foamed component. At a minimum, relevant pour and test data shall include:

- formulation, batch, and pour numbers, with foam material traceability, and pour date,
- foamed component description, part number, and serial number,
- instrumentation description, serial number, and calibration due date,
- pour and test data (e.g., date, temperature, dimensional, and/or weight measurements, compressive modulus, thermal conductivity, compressive stress, etc., as applicable), and
- technician and Quality Assurance/Quality Control (QA/QC) sign-off.

8.1.5.1.2 Physical Characteristics

The following subsections define the required physical characteristics of the polyurethane foam material used for the MFFP impact limiter designs.

Testing for the various polyurethane foam physical characteristics is based on a "formulation", "batch", or "pour", as appropriate, as defined in Section 8.1.5.1.1, *Introduction and General Requirements*. The physical characteristics determined for a specific foam formulation are relatively insensitive to small variations in chemical constituents and/or environmental conditions, and therefore include physical testing for compressive modulus, Poisson's ratio, thermal expansion coefficient, thermal conductivity, specific heat, and leachable chlorides. Similarly, the physical characteristics determined for a batch are only slightly sensitive to small changes in formulation and/or environmental conditions during batch mixing, and therefore

include physical testing for flame retardancy, intumescence, and leachable chlorides. Finally, the physical characteristics determined for a pour are also only slightly sensitive to small changes in formulation and slightly more sensitive to variations in environmental conditions during pour mixing, and therefore include physical testing for density and compressive stress.

8.1.5.1.2.1 Physical Characteristics Determined for a Foam Formulation

Foam material physical characteristics for the following parameters shall be determined once for a particular foam formulation. If multiple components are to be foamed utilizing a specific foam formulation, then additional physical testing, as defined below, need not be performed.

8.1.5.1.2.1.1 Thermal Conductivity

1. The thermal conductivity test shall be performed using a heat flow meter (HFM) apparatus. The HFM establishes steady state unidirectional heat flux through a test specimen between two parallel plates at constant but different temperatures. By measurement of the plate temperatures and plate separation, Fourier's law of heat conduction is used by the HFM to automatically calculate thermal conductivity. Description of a typical HFM is provided in ASTM C518[6] . The HFM shall be calibrated against a traceable reference specimen per the HFM manufacturer's operating instructions.
2. Three (3) test samples shall be taken from the sample pour. Each test sample shall be of sufficient size to enable testing per the HFM manufacturer's operating instructions.
3. Place the test samples in a room (ambient) temperature environment (i.e., 65 °F to 85 °F) for sufficient time to thermally stabilize the test samples.
4. Measure and record the necessary test sample parameters as input data to the HFM per the HFM manufacturer's operating instructions.
5. Perform thermal conductivity testing and record the measured thermal conductivity for each test sample following the HFM manufacturer's operating instructions.
6. Determine and record the average thermal conductivity of the three test samples. The numerically averaged thermal conductivity of the three test samples shall nominally be 0.24 Btu-in/hr-ft^2-°F ±20% (i.e., within the range of 0.19 to 0.29 Btu-in/hr-ft^2-°F) for 10 pounds per cubic foot (pcf) density foam and 0.26 Btu-in/hr-ft^2-°F ±20% (i.e., within the range of 0.21 to 0.31 Btu-in/hr-ft^2-°F) for 11½ pcf density foam.

8.1.5.1.2.1.2 Specific Heat

1. The specific heat test shall be performed using a differential scanning calorimeter (DSC) apparatus. The DSC establishes a constant heating rate and measures the differential heat flow into both a test specimen and a reference specimen. Description of a typical DSC is

[6] ASTM C518, *Standard Test Method for Steady-State Heat Flux Measurements and Thermal Transmission Properties by Means of the Heat Flux Meter Apparatus*, American Society of Testing and Materials (ASTM).

provided in ASTM E1269[7]. The DSC shall be calibrated against a traceable reference specimen per the DSC manufacturer's operating instructions.

2. Three (3) test samples shall be taken from the sample pour. Each test sample shall be of sufficient size to enable testing per the DSC manufacturer's operating instructions.
3. Place the test samples in a room (ambient) temperature environment (i.e., 65 °F to 85 °F) for sufficient time to thermally stabilize the test samples.
4. Measure and record the necessary test sample parameters as input data to the DSC per the DSC manufacturer's operating instructions.
5. Perform specific heat testing and record the measured specific heat for each test sample following the DSC manufacturer's operating instructions.
6. Determine and record the average specific heat of the three test specimens. The numerically averaged specific heat at 75 °F of the three test samples shall be 0.35 Btu/lb_m-°F ±20% (i.e., within the range of 0.28 to 0.42 Btu/lb_m-°F).

8.1.5.1.2.1.3 Leachable Chlorides

1. The leachable chlorides test shall be performed using an ion chromatograph (IC) apparatus. The IC measures inorganic anions of interest (i.e., chlorides) in water. Description of a typical IC is provided in EPA Method 300.0[8]. The IC shall be calibrated against a traceable reference specimen per the IC manufacturer's operating instructions.
2. One (1) test sample shall be taken from a pour from each foam batch. The test sample shall be a cube with dimensions of 2.00 ±0.03 inches.
3. Place the test sample in a room (ambient) temperature environment (i.e., 65 °F to 85 °F) for sufficient time to thermally stabilize the test sample. Measure and record the room temperature to an accuracy of ±2 °F.
4. Obtain a minimum of 550 ml of distilled or de-ionized water for testing. The test water shall be from a single source to ensure consistent anionic properties for testing control.
5. Obtain a 400 ml, or larger, contaminant free container that is capable of being sealed. Fill the container with 262 ±3 ml of test water. Fully immerse the test sample inside the container for a duration of 72 ±3 hours. If necessary, use an inert standoff to ensure the test sample is completely immersed for the full test duration. Seal the container.
6. Obtain a second, identical container to use as a "control". Fill the control container with 262 ±3 ml of the same test water. Seal the control container.
7. At the end of the test period, measure and record the leachable chlorides in the test water per the IC manufacturer's operating instructions. The leachable chlorides in the test water shall not exceed one part per million (1 ppm).

---

[7] ASTM E1269, *Standard Test Method for Determining Specific Heat Capacity by Differential Scanning Calorimetry*, American Society of Testing and Materials (ASTM).

[8] EPA Method 300.0, *Determination of Inorganic Anions in Water by Ion Chromatography*, U.S. Environmental Protection Agency.

8. Should leachable chlorides in the test water exceed 1 ppm, measure and record the leachable chlorides in the test water from the "control" container. The difference in leachable chlorides from the test water and "control" water sample shall not exceed 1 ppm.

8.1.5.1.2.2 Physical Characteristics Determined for a Foam Batch

Foam material physical characteristics for the following parameters shall be determined once for a particular foam batch based on the formulation defined in Section 8.1.5.1.2.1, *Physical Characteristics Determined for a Foam Formulation.* If a single or multiple components are to be poured utilizing a single foam batch, then additional physical testing, as defined below, need not be performed for each foam pour. Foam used for the upper flange collar does not need to conform with this subsection.

8.1.5.1.2.2.1 Flame Retardancy

1. Three (3) test samples shall be taken from a pour from each foam batch. Each test sample shall be a rectangular prism with nominal dimensions of 0.5 inches thick, 3.0 inches wide, and a minimum length of 8.0 inches.
2. Place the test samples in a room (ambient) temperature environment (i.e., 65 °F to 85 °F) for sufficient time to thermally stabilize the test samples. Measure and record the room temperature to an accuracy of ±2 °F.
3. Install a ∅3/8 inches, or larger, Bunsen or Tirrill burner inside an enclosure of sufficient size to perform flame retardancy testing. Adjust the burner flame height to 1½ ±1/8 inches. Verify that the burner flame temperature is 1,550 °F, minimum.
4. Support the test sample with the long axis oriented vertically within the enclosure such that the test sample's bottom edge will be 3/4 ±1/16 inches above the top edge of the burner.
5. Move the burner flame under the test sample for an elapsed time of 60 ±2 seconds. As illustrated, align the burner flame with the front edge of the test sample thickness and the center of the test sample width.

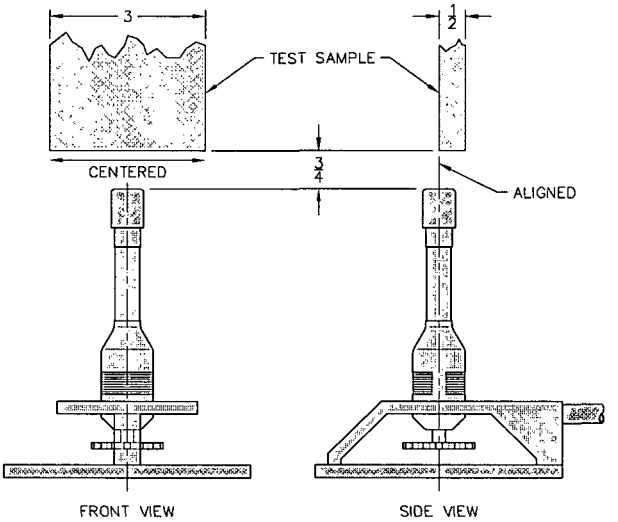

6. Immediately after removal of the test sample from the burner flame, measure and record the following data:
   a. Measure and record, to the nearest second, the elapsed time until flames from the test sample extinguish.
   b. Measure and record, to the nearest second, the elapsed time until drips from the test sample extinguish.
   c. Measure and record, to the nearest second, the burn length following cessation of all visible burning and smoking.
7. Flame retardancy testing acceptance is based on the following criteria:

a. The numerically averaged flame extinguishment time of each of the three test samples shall not exceed fifteen (15) seconds.

b. The numerically averaged flame extinguishment time of drips from each of the three test samples shall not exceed three (3) seconds.

c. The numerically averaged burn length of each of the three test samples shall not exceed six (6) inches.

8.1.5.1.2.2.2 Intumescence

1. Three (3) test samples shall be taken from a pour from each foam batch. Each test sample shall be a cube with nominal dimensions of 2.0 inches.
2. Place the test samples in a room (ambient) temperature environment (i.e., 65 °F to 85 °F) for sufficient time to thermally stabilize the test samples. Measure and record the room temperature to an accuracy of ±2 °F.
3. Preheat a furnace to 1,475 °F ±18 °F.
4. Identify two opposite faces on each test sample as the thickness direction. Measure and record the initial thickness (t_i) of each test sample to an accuracy of ±0.01 inches.

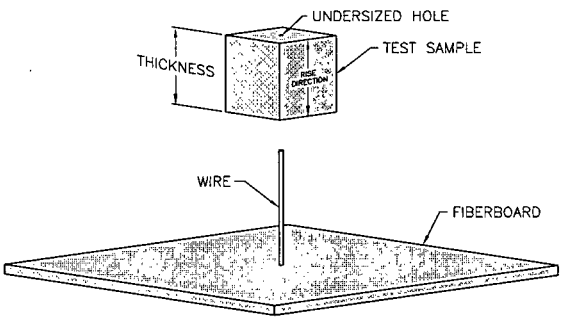

5. Mount a test sample onto a fire resistant fiberboard, with one face of the thickness direction contacting to the board. The direction of foam rise shall be normal to the fiberboard face. As illustrated above, the test samples may be mounted by installing onto a 12 to 16 gauge wire (Ø0.105 to Ø0.063 inches, respectively) of sufficient length, oriented perpendicular to the fiberboard face. The test samples may be pre-drilled with an undersized hole to allow installation onto the wire.
6. Locate the test sample/fiberboard assembly over the opening of the pre-heated furnace for a 90 ±3 second duration. After removal of the test sample/fiberboard assembly from the furnace, gently extinguish any remaining flames and allow the test sample to cool.
7. Remove the test sample from the fiberboard. Measure and record the final thickness (t_f) of the test sample to an accuracy of ±0.1 inches.
8. For each sample tested, determine and record the intumescence, I, as a percentage of the original sample length as follows:

$$I = \left(\frac{t_f - t_i}{t_i} \right) \times 100$$

9. Determine and record the average intumescence of the three test samples. The numerically averaged intumescence of the three test samples shall be a minimum of 50%.

8.1.5.1.2.3 Physical Characteristics Determined for a Foam Pour

Foam material physical characteristics for the following parameters shall be determined for each foam pour based on the formulation defined in Section 8.1.5.1.2.1, *Physical Characteristics Determined for a Foam Formulation.*

8.1.5.1.2.3.1 Density

1. Three (3) test samples shall be taken from the foam pour. Each test sample shall be a rectangular prism with nominal dimensions of 1.0 inch thick (T), minimum, × 2.0 inches wide (W) × 2.0 inches long (L).
2. Place the test samples in a room (ambient) temperature environment (i.e., 65 °F to 85 °F) for sufficient time to thermally stabilize the test samples. Measure and record the room temperature to an accuracy of ±2 °F.
3. Measure and record the weight of each test sample to an accuracy of ±0.01 grams.
4. Measure and record the thickness, width, and length of each test sample to an accuracy of ±0.001 inches.
5. Determine and record the room temperature density of each test sample utilizing the following formula:

$$\rho_{foam} = \frac{\text{Weight, g}}{453.6\ \text{g/lb}_m} \times \frac{1{,}728\ \text{in}^3/\text{ft}^3}{\text{T} \times \text{W} \times \text{L in}^3}, \text{pcf}$$

6. Determine and record the average density of the three test samples. The numerically averaged density of the three test samples shall nominally be within ±15% (i.e., within the range of 8.5 to 11.5 pcf for the nominal 10 pcf foam and 9.8 to 13.2 pcf for nominal 11½ pcf foam).

8.1.5.1.2.3.2 Parallel-to-Rise Compressive Stress

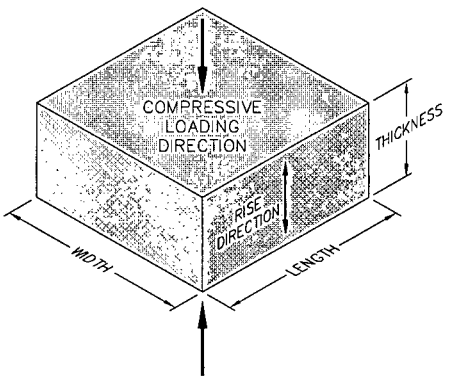

1. Three (3) test samples shall be taken from the foam pour. Each test sample shall be a rectangular prism with nominal dimensions of 1.0 inch thick (T) × 2.0 inches wide (W) × 2.0 inches long (L). The thickness dimension shall be the parallel-to-rise direction.
2. Place the test samples in a room (ambient) temperature environment (i.e., 65 °F to 85 °F) for sufficient time to thermally stabilize the test samples. Measure and record the room temperature to an accuracy of ±2 °F.
3. Measure and record the thickness, width, and length of each test sample to an accuracy of ±0.001 inches.
4. Compute and record the surface area of each test sample by multiplying the width by the length (i.e., W × L).
5. Place a test sample in a Universal Testing Machine. Lower the machine's crosshead until it touches the test sample. Set the machine's parameters for the thickness of the test sample.

6. Apply a compressive load to each test sample at a rate of 0.10 ±0.05 inches/minute until a strain of 70%, or greater, is achieved. For each test sample, plot the compressive stress versus strain and record the compressive stress at strains of 10%, 40%, and 70%.
7. Determine and record the average parallel-to-rise compressive stress of the three test samples from each batch pour. As delineated in Table 8.1-1, the average parallel-to-rise compressive stress for each batch pour shall be the nominal compressive stress ±20% at strains of 10%, 40%, and 70%.
8. Determine and record the average parallel-to-rise compressive stress of all test samples from each foamed component. As delineated in Table 8.1-1, the average parallel-to-rise compressive stress for a foamed component shall be the nominal compressive stress ±15% at strains of 10%, 40%, and 70%.

8.1.5.1.2.3.3 Perpendicular-to-Rise Compressive Stress

1. Three (3) test samples shall be taken from the foam pour. Each test sample shall be a rectangular prism with nominal dimensions of 1.0 inch thick (T) × 2.0 inches wide (W) × 2.0 inches long (L). The thickness dimension shall be the perpendicular-to-rise direction.

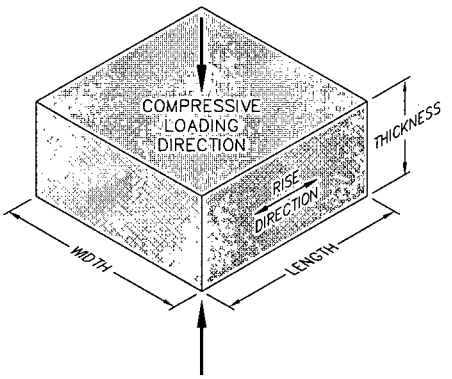

2. Place the test samples in a room (ambient) temperature environment (i.e., 65 °F to 85 °F) for sufficient time to thermally stabilize the test samples. Measure and record the room temperature to an accuracy of ±2 °F.
3. Measure and record the thickness, width, and length of each test sample to an accuracy of ±0.001 inches.
4. Compute and record the surface area of each test sample by multiplying the width by the length (i.e., W × L).
5. Place a test sample in a Universal Testing Machine. Lower the machine's crosshead until it touches the test sample. Set the machine's parameters for the thickness of the test sample.
6. Apply a compressive load to each test sample at a rate of 0.10 ±0.05 inches/minute until a strain of 70%, or greater, is achieved. For each test sample, plot the compressive stress versus strain and record the compressive stress at strains of 10%, 40%, and 70%.
7. Determine and record the average perpendicular-to-rise compressive stress of the three test samples from each batch pour. As delineated in Table 8.1-1, the average perpendicular-to-rise compressive stress for each batch pour shall be the nominal compressive stress ±20% at strains of 10%, 40%, and 70%.
8. Determine and record the average perpendicular-to-rise compressive stress of all test samples from each foamed component. As delineated in Table 8.1-1, the average perpendicular-to-rise compressive stress for a foamed component shall be the nominal compressive stress ±15% at strains of 10%, 40%, and 70%.

8.1.5.2 Neutron Poison Plates

8.1.5.2.1 Visual Examinations

The neutron poison plates specified on the drawings in Appendix 1.4.2, *Packaging General Arrangement Drawings* shall be visually examined for defects and cracks prior to being installed on the strongback.

8.1.5.2.2 Dimensional Inspections

The neutron poison plates shall be verified to meet the dimensional requirements specified on the drawings in Appendix 1.4.2, *Packaging General Arrangement Drawings* prior to being installed on the strongback.

8.1.5.2.3 Boron Areal Density

The neutron poison plates (i.e., boral) specified on the drawings in Appendix 1.4.2, *Packaging General Arrangement Drawings* shall be verified to have a minimum total boron per unit area of the sandwiched material. Samples from each sheet pour of the neutron absorber are to be retained for testing and record purposes. The boron-10 (^{10}B) areal density within a panel shall be verified by wet chemical analysis and/or neutron attenuation testing to be 0.035 gram/cm^2 or greater. The acceptance standards shall be controlled by statistical data to ensure the minimum requirements are achieved with a 95% probability at a 95% confidence level. The maximum variations in the manufacturing processes (statistical tolerance interval) over a significantly large sample size shall be the basis of the acceptance criteria. All material certifications, lot control records, and test records are to be maintained to ensure material traceability.

Table 8.1-1 – Acceptable Compressive Stress Ranges for Foam (psi)

Sample Range	Parallel-to-Rise at Strain, $\varepsilon_{\|\|}$						Perpendicular-to-Rise at Strain, $\varepsilon_{\perp}$					
	ε = 10%		ε = 40%		ε = 70%		ε = 10%		ε = 40%		ε = 70%	
Foam Density (pcf)	10	11½	10	11½	10	11½	10	11½	10	11½	10	11½
Nominal -20%	286	376	333	444	899	1328	264	348	318	432	892	1380
Nominal -15%	304	400	354	472	955	1411	281	370	338	459	948	1466
Nominal	358	470	416	555	1124	1660	330	435	398	540	1115	1725
Nominal +15%	412	541	478	638	1293	1909	380	500	458	621	1282	1984
Nominal +20%	430	564	499	666	1349	1992	396	522	478	648	1338	2070

8.1.6 Shielding Tests

The MFFP does not contain any biological shielding.

8.1.7 Thermal Tests

Material properties utilized in Chapter 3.0, *Thermal Evaluation*, are consistently conservative for the normal conditions of transport (NCT) and hypothetical accident condition (HAC) thermal analyses performed. As such, with the exception of the tests required for polyurethane foam, as shown in Section 8.1.5, *Component and Material Tests*, specific acceptance tests for material thermal properties are not performed.

This page left intentionally blank.

8.2 Maintenance Program

This section describes the maintenance program used to ensure continued performance of the MFFP.

8.2.1 Structural and Pressure Tests

No structural or pressure tests are necessary to ensure continued performance of the MFFP.

8.2.2 Maintenance/Periodic Leakage Rate Tests

This section provides the generalized procedure for maintenance and periodic leakage rate testing of the containment vessel penetrations during routine maintenance, or at the time of seal replacement or seal area repair. Verification leakage rate testing shall follow the guidelines of Section 7.4, *Maintenance Leakage Rate Test*, and Section 7.5, *Periodic Leakage Rate Test*, of ANSI N14.5[1].

Maintenance and periodic leakage rate testing shall be performed on the main O-ring seal, vent port seal, and fill port seal in accordance with Section 8.2.2.2, *Helium Leakage Rate Testing the Main O-ring Seal*, Section 8.2.2.3, *Helium Leak Testing the Vent Port Plug O-ring Seal*, and Section 8.2.2.4, *Helium Leakage Rate Testing the Fill Port Plug O-ring Seal*, respectively.

8.2.2.1 Maintenance/Periodic Verification Leakage Rate Test Acceptance Criteria

Maintenance and periodic verification leak testing acceptance criteria are identical to the criteria delineated in Section 8.1.4.1, *Fabrication Leakage Rate Test Acceptance Criteria.*

8.2.2.2 Helium Leakage Rate Testing the Main O-ring Seal

1. The maintenance/periodic verification leak test of the MFFP containment O-ring seal integrity shall be performed following the guidelines of Section A.5.4, *Evacuated Envelope – Gas Detector*, of ANSI N14.5.
2. Assemble the MFFP with the three O-ring seals installed in the closure lid. Ensure the vent, seal test, and fill port plugs are installed with their associated O-ring seals. Assembly is as shown on the drawings in Appendix 1.4.2, *Packaging General Arrangement Drawings.*
3. Utilizing a test port tool, attach a vacuum pump and a source of helium gas, in parallel, to the fill port.
4. Close the valve to the source of helium gas and open the valve to the vacuum pump.
5. Utilizing a test port tool, rotate the fill port plug to the open position.
6. Evacuate the system to a 90% vacuum or better ($\leq$ 10% ambient atmospheric pressure). Isolate the vacuum pump from the system.
7. Provide a helium atmosphere inside the evacuated cavity by backfilling with helium gas (99% purity or better) to ambient atmospheric pressure (+1 psi, -0 psi).

---

[1] ANSI N14.5-1997, *American National Standard for Radioactive Materials – Leakage Tests on Packages for Shipment,* American National Standards Institute, Inc. (ANSI).

8. Utilizing a test port tool, rotate the fill port plug to the closed position, and remove the helium-contaminated test port tool from the fill port.
9. Install a clean (helium-free) test port tool into the seal test port.
10. Utilizing appropriate fittings, attach a helium mass spectrometer leak detector (MSLD) to the test port tool.
11. Utilizing the test port tool, rotate the seal test port plug to the open position.
12. Evacuate the cavity above the lid containment O-ring seal until the vacuum is sufficient to operate the leak detector per the manufacturer's recommendations.
13. Perform the helium leakage rate test to the requirements of Section 8.2.2.1, *Maintenance/Periodic Leakage Rate Test Acceptance Criteria.* If, after repeated attempts, the MFFP containment O-ring seal fails to pass the leak test, isolate the leak path and, prior to repairing the leak path and repeating the leak test, record on a nonconformance report and disposition prior to final acceptance in accordance with the cognizant quality assurance program.

8.2.2.3 Helium Leakage Rate Testing the Vent Port Plug O-ring Seal

1. The maintenance/periodic verification leak test of the MFFP vent port plug O-ring containment seal integrity shall be performed following the guidelines of ANSI N14.5, Section A.5.4, *Evacuated Envelope – Gas Detector.*
2. The MFFP shall be assembled with all three O-ring seals installed on the closure lid. Ensure the vent, seal test, and fill port plugs are installed with their associated O-ring seals. Assembly is as shown on the MFFP drawings in Appendix 1.4.2, *Packaging General Arrangement Drawings.*
3. Verify the presence of a helium atmosphere below the vent port plug O-ring containment seal, as specified above in Steps 3 – 8 of Section 8.2.2.2, *Helium Leakage Rate Testing the Main O-ring Seal.*
4. Install a test port tool into the vent port.
5. Utilizing appropriate fittings, attach a helium MSLD to the test port tool.
6. Evacuate the cavity above the vent port plug O-ring containment seal until the vacuum is sufficient to operate the leak detector per the manufacturer's recommendations.
7. Perform the helium leakage rate test to the requirements of Section 8.2.2.1, *Maintenance/Periodic Leakage Rate Test Acceptance Criteria.* If, after repeated attempts, the vent port plug O-ring containment seal fails to pass the leak test, isolate the leak path and, prior to repairing the leak path and repeating the leak test, record on a nonconformance report and disposition prior to final acceptance in accordance with the cognizant quality assurance program.

8.2.2.4 Helium Leakage Rate Testing the Fill Port Plug O-ring Seal

1. The maintenance/periodic verification leak test of the MFFP fill port closure bolt O-ring containment seal integrity shall be performed following the guidelines of Section A.5.4, *Evacuated Envelope – Gas Detector*, of ANSI N14.5.

2. The MFFP shall be assembled with all three O-ring seals installed on the lid. Ensure the vent, seal test, and fill ports are installed with their associated O-ring seals. Assembly is as shown on the MFFP drawings in Appendix 1.4.2, *Packaging General Arrangement Drawings.*
3. Verify the presence of a helium atmosphere below the fill port plug O-ring containment seal, as specified above in Steps 3 – 8 of Section 8.2.2.2, *Helium Leakage Rate Testing the Main O-ring Seal.*
4. Install a test port tool into the fill port.
5. Utilizing appropriate fittings, attach a helium MSLD to the test port tool.
6. Evacuate the cavity above the fill port closure bolt O-ring containment seal until the vacuum is sufficient to operate the leak detector per the manufacturer's recommendations.
7. Perform the helium leakage rate test to the requirements of Section 8.2.2.1, *Maintenance/Periodic Leakage Rate Test Acceptance Criteria.* If, after repeated attempts, the MFFP fill port closure bolt O-ring containment seal fails to pass the leak test, isolate the leak path and, prior to repairing the leak path and repeating the leak test, record on a nonconformance report and disposition prior to final acceptance in accordance with the cognizant quality assurance program.

8.2.3 Component and Material Tests

8.2.3.1 Fasteners

All threaded components shall be visually inspected annually for deformed or stripped threads. Damaged threaded components shall be repaired or replaced prior to further use. The threaded components to be visually inspected include the containment lid bolts, vent port closure bolt, fill port closure bolt, seal test port closure bolt, strongback/neutron plate fasteners, fuel channel support fasteners, and impact limiter bolts.

All quick-release pins shall be visually inspected annually for proper operation and damage. Inoperable or damaged pins shall be repaired or replaced prior to further use.

8.2.3.2 Seal Areas and Grooves

8.2.3.2.1 Seal Area Routine Inspection and Repair

Before each use and at the time of seal replacement, the sealing surfaces on the closure lid and body shall be visually inspected for damage that could impair the sealing capabilities of the MFFP. Perform surface finish inspections for the body upper forging, and the O-ring grooves and sealing surfaces on the closure lid. Damage shall be repaired prior to further use (e.g., using emery cloth or other surface finishing techniques) to restore the sealing surfaces to the surface finish specified in Section 8.2.3.2.2, *Surface Finish of Sealing Areas.*

Upon completion of containment seal area repairs, perform a leakage rate test per the applicable section of Section 8.2.2, *Maintenance/Periodic Leakage Rate Tests.*

8.2.3.2.2 Surface Finish of Sealing Areas

The surface finish for the main O-ring sealing regions shall be a 125 micro-inch finish, or better, to maintain package configuration and performance to design criteria. If the surface condition is

determined to exceed 125 micro-inch, repair the surface per the requirements of Section 8.2.3.2.1, *Seal Area Routine Inspection and Repair*.

8.2.3.3 Impact Limiters

Before each use, the impact limiters shall be inspected for tears or perforations in the stainless steel sheets, and for the presence of the fire-consumable plastic plugs. Any damage shall be repaired prior to further use.

8.2.3.4 Strongback

Before each use, the strongback (including neutron poison plates) shall be inspected for missing or damaged components. Any damage shall be repaired prior to further use.

8.2.3.5 Fuel Control Structures

Before each use, the fuel control structures (FCSs), including neutron poison plates, shall be inspected for missing or damaged components. Any damage shall be repaired prior to further use.

8.2.3.6 Seals

All containment O-ring seals shall be replaced annually (or when damaged) per the specifications as delineated on the drawings in Appendix 1.4.2, *Packaging General Arrangement Drawings*. Following seal replacement and prior to a loaded shipment, the seal(s) shall be leakage rate tested to the requirements of Section 8.2.2, *Maintenance/Periodic Verification Leak Tests*.

8.2.4 Thermal Tests

No thermal tests are necessary to ensure continued performance of the MFFP.

8.2.5 Miscellaneous Tests

No miscellaneous tests are necessary to ensure continued performance of the MFFP.